AN INVESTIGATION OF FLUORINE OVERVOLTAGE

AT CARBON ANODES

by

Martyn J. Wilmott

A Thesis submitted to the
University of Newcastle upon Tyne
for the Degree of Doctor of Philosophy

August 1987

ACKNOWLEDGEMENTS

I would like to thank my supervisor, Dr Ray Brown, for his help, guidance and friendship throughout the course of this study, and for his patience during the writing of this thesis.

I would also like to thank SERC and British Nuclear Fuels Plc for providing the funds for this project and I would like to thank Drs Ellis, May and Marshall of British Nuclear Fuels for all their help during this project.

I would like to thank Dr Bevan Price of the UKAEA, Risley who carried out the XPS and SIMS analysis.

I would also like to thank the many members of the School of Chemistry Workshop and Technical Staff for their assistance throughout this project.

I would like to express my sincere thanks to John Whitley and all those members of Dr Armstrong's research group especially Drs Moore, Evans and Churchouse and Mr K. Airey and Mr M. Todd who all made the time at Newcastle extremely enjoyable both socially and academically.

Finally I would like to thank Elaine Hills for her patience and continued encouragement and her skilful assistance in the preparation of this thesis.

ABSTRACT

The high anode overvoltage exhibited by fluorine cells has been variously attributed to bubble overvoltage and to inhibition of the electron transfer process by a layer of insulating carbon fluoride on the surface of the electrode. This thesis presents the results of various experiments which attempt to assess the contribution of the carbon fluoride film to the anode overvoltage in the absence of bubble overvoltage.

Fluorine evolution from the molten salt KF.2HF at 85°C was studied at vertical carbon anodes. The techniques employed to study the kinetics and mechanism of this reaction included cyclic voltammetry, steady state potentiostatic polarisation, A.C. impedance, potential pulse and constant current electrolysis. Such measurements indicated that several types of carbon fluoride can be produced on the anode evolving fluorine, depending on the potential of electrolysis. These measurements also show the difficulty in obtaining kinetic parameters for the fluorine evolution reaction.

The nature of the fluoride film produced on the carbon anode was investigated using XPS and SIMS analysis of electrodes polarised in the KF.2HF melt at 5V and 9V. These measurements indicated that the film is not one single carbon fluoride but more of a graded nature becoming more heavily fluorinated at higher potentials.

The inhibiting effect of the solid film was studied by transfering carbon electrodes, following fluorine evolution in the KF.2HF melt under well defined

conditions, to other electrochemical systems using aqueous or organic electrolytes at room temperature, where electrode kinetic studies were made of redox reactions. Kinetic data were compared with those obtained with unfluorinated carbon surfaces.

Observations obtained by the above methods have been related to estimates of the thickness of the carbon fluoride film as determined by measurements of the double layer capacitance in the KF.2HF melt and in other solvent systems.

Both capacitance measurements and kinetic studies of redox reactions indicate that the film became progresively thicker as the potential of the fluorine anode was raised. Rates of redox reactions fell by at least two orders of magnitude in the presence of a film formed by polarising the carbon at 6.0V in the KF.2HF melt.

Attempts were made to overcome the inhibiting effect of the fluoride films by incorporating transition metals in the carbon anodes. The last section of this thesis explains the manufacture of doped carbon samples and presents results obtained in the KF.2HF melt using such anode materials.

Chapter 1

INTRODUCTION

Chapter 2

THEORY AND INSTRUMENTATION

Chapter 3

EXPERIMENTAL

Chapter 6

ELECTRON TRANSFER REACTIONS AT ELECTRODES SUBJECTED TO FLUORINE EVOLUTION

Chapter 7

GENERAL DISCUSSION OF THE FLUORINE EVOLUTION REACTION AT COMMERCIAL ELECTRODES

Chapter 8

NOVEL CARBON ELECTRODES FOR FLUORINE EVOLUTION

CHAPTER 1

INTRODUCTION

1.1 INTRODUCTION

Fluorine is produced by the electrolysis of the molten salt KF.2HF at a temperature of 85 to 100°C. Whilst the theoretical decomposition potential for HF in KF.2HF is 2.9V[1,2] industrial cells operate with voltages in the range 10 to 14V. The power efficiency of the process has been calculated to be about 26%.[3]

Total world production of fluorine is in the region 10,000 to 20,000 ton per year.[4] The production of UF_6 for uranium isotope enrichment requires 55% of the fluorine produced whilst production of the dielectric SF_6 accounts for 40% of the market.

The historical development of fluorine cell technology has been discussed in several reviews, notably those of Cady,[6] Rudge,[7] and Leech[8] whilst Ikeda[9] and several other reviewers[10-14] give descriptions of the cells currently in use.

The first authentic fluorine cell of Moissan[15] used liquid anhydrous HF containing a potassium fluoride support electrolyte, at a temperature less than 0°C. Cady[16] carried out a phase study of the system HF/KF in 1934. He also measured the partial pressure of HF over the KF/HF system and its variation with temperature. He showed the existence of several HF-rich compounds in the system. The melting points of KF/HF systems varied from 70°C to 240°C as the composition varied from KF.4HF to KF.HF.

In the 1940s cells of three different types were developed based on KF.xHF electrolytes. The cells are classified according to their temperature of operation.

Low temperature cells used a solution of KF in liquid HF operating at a temperature in the range 15 to 50°C. Medium temperature cells used KF.2HF operating in the range 70 to 130°C and high temperature cells used KF.HF at a temperature from 245 to 310°C. All modern fluorine cells use a melt of composition KF.2HF, as this composition provides conditions in which melting point, conductivity, vapour pressure of HF above the melt and melt density are all optimal from an operational point of view. Also with this composition relatively low rates of corrosion of all components occur and variations in the electrolyte composition can be tolerated without too much change in the operating temperature of the cell.

Early fluorine cells used nickel anodes but these suffered from corrosion problems and so all industrial cells now use carbon anodes. These anodes are subject to bubble overvoltage as is the case with all gas evolution processes where gas bubbles decrease the active surface area of the working electrode. In the case of carbon anodes used in fluorine evolution this bubble overvoltage is especially severe because the carbon surface becomes fluorinated and, as a result, the anode is not wetted by the electrolyte, thereby making release of fluorine bubbles more difficult. The bubbles become flattened and as a result more of the anode surface is blocked off to current flow. Such flattened bubbles are said to be "lenticular". As more of the anode surface becomes blocked by gas bubbles a phenomenon known as "polarisation" can occur. This is an increase in cell voltage at a given current density. Under extreme

conditions the whole anode surface can become covered by a fluorine gas film. Under these circumstances a phenomenon known as "anode effect" can occur. This is a process associated with cell voltages in excess of 30V where the anode is seen to emit bluish arcs similar to a glow discharge in order that the applied current can be maintained.

Such polarisation problems can be overcome by using anodes of porous carbon which allow fluorine to escape to the electrolyte surface through the interconnected pores of the anode. Certain additives to the melt such as nickel,[17] are said to alleviate the problem of polarisation by decreasing the electrode/electrolyte contact angle thereby facilitating bubble release. Addition of lithium fluoride[18] to the molten salt is also said to diminish anode polarisation. The mechanism by which such additives work is not clearly understood, but it is believed that the active nickel depolariser is a Ni(IV) species.

Rudge proposed that non wetting of the carbon anode was a result of the formation of a surface layer of carbon monofluoride $(CF)_n$.[17] Watanabe[19] later confirmed the existence of this surface film by XPS spectroscopy.

Watanabe has tried to elucidate both the kinetics and mechanism of fluorine evolution[20] in KF.2HF at temperatures in the region of 90°C. Arvia and Bebczuk de Cusminsky[21] have carried out studies in KF.HF at temperatures in the range 251-256°C. Both sets of authors proposed similar mechanisms for fluorine evolution:

$$HF_2^- + C \longrightarrow HF + C\cdots\cdots F + e^- \qquad 1.1$$

followed by either

$$C\cdots\cdots F + C\cdots\cdots F \longrightarrow C + F_2 \qquad 1.2$$

or

$$C\cdots\cdots F + F^- \longrightarrow C + F_2 + e^- \qquad 1.3$$

Step 1.2 can be discounted on consideration of the bond energies of the C-F (441 $kJmol^{-1}$) and F-F (153 $kJmol^{-1}$) bonds. The mechanism involves the breaking of two C-F bonds in the course of formation of a single F-F bond. More generally, all mechanisms involving fluorine adsorbed on carbon can be discounted whereas $(C-F)_n$ is unlikely to be an intermediate in the formation of fluorine.

More recently, the following has been proposed to occur as a side reaction[22]

$$C + HF_2^- \longrightarrow 1/n(CF)_n + HF + e^- \qquad 1.4$$

$$(CF)_n \longrightarrow C + C_2F_6 + CF_4 + \text{etc.} \qquad 1.5$$

The presence of a carbon monofluoride film as a result of fluorine electrolysis was demonstrated using XPS.[19]

Examination of the formation of $(CF)_n$ on pyrolytic graphite revealed that under polarised conditions, the layer plane had about five times more CF than had the

edge plane. Using the results of Cadman et al.[23] a film thickness of about 5.8nm was observed on the layer plane and about 1.9nm on the edge plane. This is directly opposite to results obtained from gas phase fluorination where atomic fluorine attacks the edge plane more rapidly than the layer plane.[23,24,25] This must show the role of electrode potential on $(CF)_n$ formation.

Cyclic voltammetry of various carbons in KF.2HF showed at least three electrochemical processes occurring between 0 and 7V (vs. a Pt rod).[22,26] The first anodic peak was observed at about 1.6V. Addition of water to the electrolyte resulted in an increase in the height of this peak, but unequivocal demonstration that this peak was due to water oxidation was not performed. The peak appeared to be present only on the first sweep. A second peak was observed at 3.5 to 4.0V with clearest definition on layer plane graphite.

The third anodic peak was observed at 6V (vs. Pt) and was the largest peak. The peak potential varied for different carbon materials (5V on layer-plane graphite, 6V on edge-plane graphite). In general this peak decreased with successive scanning. The dependence of peak height on sweep rate was investigated.[22] The edge plane of pyrolytic graphite showed a linear increase in peak height with the logarithm of the sweep rate. The film formed on layer-plane graphite was found to be thermally more stable than that produced on the edge of pyrolytic graphite.

It is clear that the fluorine evolution reaction has received comparatively little academic investigation.

All reports lead to the conclusion that the fluorine evolution reaction is inhibited in some manner, as a result of either the $(CF)_n$ film *per se* or the fluorine gas film which it supports. The relative contributions to the anode overvoltage made by the insulating polymer film and the gas film which results from the non-wetting properties of the polymer are not known.

1.2 REFERENCES

1. O.R. Brown, Electrochimica.Acta. 25, 367, (1980).
2. D. Devilliers, F. Lantelme and M. Chemla, J.Chim.Phys.Phys.Chim.Bio. 76, 428, (1979).
3. J.F. Ellis and G.F. May, J.Fluorine.Chem. 33, 133, (1986).
4. D. Pletcher, Industrial Electrochemistry, Chapman and Hall, London Ch. 5, p132, (1982).
5. R. Papp, Centenary of the Discovery of Fluorine, International Symposium Abstracts, Abstract A1 p193, Paris, (1986).
6. G.H. Cady, Fluorine Chemistry, Vol.1, J.H. Simons (ed.), Academic Press, N.Y. p293, (1950).
7. A.J. Rudge, Chem.Ind. 247, (1949).
8. H.R. Leech, in Supplement to Mellor's Comprehensive Treatise on Inorganic and Theoretical Chemistry, Volume 1, Supplement 1, The Halogens, J.W. Mellor (ed) Longmans, Green and Co. Ltd., London, p15 et seq (1962).
9. B.M. Ikeda, Ph.D. Thesis, University of Newcastle upon Tyne, (1982).
10. A.J. Rudge, in Industrial Electrochemical Processes, A.T. Kuhn (ed) Elsevier Publishing Co., London, Ch1, (1971).
11. W.E. Kwasnik, Fort.Chem.Fors. 8, 309, (1967).
12. A.T. Kuhn, in Enycylopedia of the Electrochemistry of the Elements, A.J. Bard (ed) Vol IV, Dekker Publishing Co., N.Y., Chapter IV-2, (1975).
13. R.J. Ring and D. Royston, Australian Atomic Energy Commission AAEC/E281, (1973).

14. H.R. Neumark and J.M. Siegmund in Encyclopedia of Chemical Technology, R.E. Kirk and D.F. Othmer, (eds) Vol IX, Interscience Encyclopedia Inc 2nd Edn., N.Y., p506, (1966).
15. R. Moissan, Compt.Rendu. 102, 1543, (1886).
16. G.H. Cady, J.Am.Chem.Soc. 56, 1431, (1934).
17. A.J. Rudge, Chem.Ind. (London) 482, (1966).
18. N. Watanabe, M. Ishii, and S. Yoshizawa, J.Electrochem.Soc.Jpn. 29, 177, (1961).
19. H. Imoto, T. Nakajima and N. Watanabe, Bull.Chem.Soc.Jpn. 48, 1963, (1975).
20. N. Watanabe, M. Inoue and S. Yoshizawa, J.Electrochem.Soc.Jpn. 31, 168, (1963).
21. A.J. Arvia and J.B. de Cusminsky, Trans.Faraday.Soc. 58, 1019, (1962).
22. N. Watanabe and K. Ueno, Bull.Chem.Soc.Jpn. 49, 1736, (1976).
23. P. Cadman, J.D. Scott and J.M. Thomas, Carbon 15, 75, (1977).
24. N. Watanabe, Y. Koyama, A. Shibuya and K. Kumon, Mem.Fac.Eng. Kyoto University 33, 15, (1971).
25. M.L. Bernard, A. Hardy, P. Hobbies, R. Lucas and M. Roux, Bull.Soc.Chim.France 6, 2192, (1972).
26. M. Nishimara, A. Tasaka, K. Nakanishi and N. Watanabe, Denki Kagaku 38, 294, (1970).

CHAPTER 2

THEORY AND INSTRUMENTATION

2.1.1 A.C. IMPEDANCE

The use of impedance measurements has become increasingly popular as a means of investigating electrochemical systems. The method was first used by Dolin and Ershler,[1] in 1940, and the theory of the technique has been developed by Randles,[2] Gerischer,[3] Grahame,[4] Sluyters,[5] and de Levie.[6]

An electrochemical interphase can be envisaged as a combination of resistances and capacitors (the so called equivalent circuit) Figure 2.1.

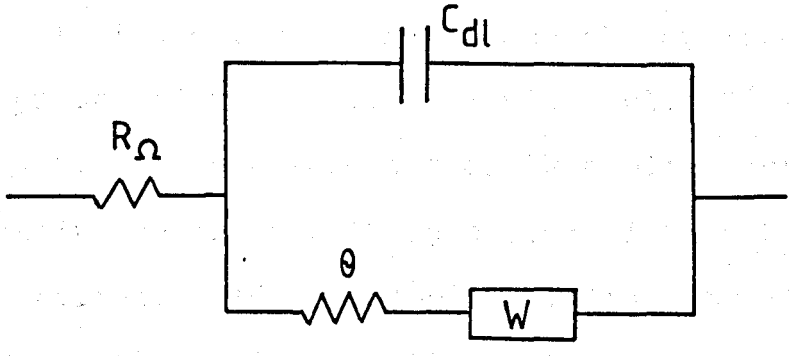

Figure 2.1

In this R_Ω represents the effective ohmic resistance of the electrolyte between the working electrode and the tip of the reference electrode probe together with the bulk resistance of the electrode and the resistance of the connector leads to the electrodes, C_{dl} represents the double layer capacitance and θ represents the resistance to charge transfer. The impedance due to diffusional processes is known as the Warburg impedance, and is represented by W.

Before discussing the impedance of the circuit shown in Figure 2.1, the impedances of passive electrical components and their combinations will be considered.

When a small amplitude potential difference

$E = E_o \sin\omega t$ is applied to an electrochemical system the resulting current is given by $I = I_o \sin(\omega t + \phi)$. This current has the vector properties of magnitude and direction. The magnitude is given by E_o/I_o and the direction by the phase angle ϕ.

Impedance can be represented in terms of complex plane impedances with an in-phase component Z' and a quadrature component Z''. In a complex plane plot Z' is plotted as abscissa and Z'' as ordinate.

When a signal $E = E_o \sin(\omega t)$ is applied across a pure resistance, the resulting current is $I = E_o/R \sin \omega t = I_o \sin(\omega t)$. The current and the applied voltage are in phase and in the complex plane plot $Z' = R$ and $Z'' = 0$. When the same signal is applied across a pure capacitance the resulting current is $I = E_o \omega C \cos(\omega t)$. The current leads the applied voltage by 90° and in the complex plane plot $Z' = 0$ and $Z'' = 1/\omega C$.

For a series combination of resistance and capacitance the impedance Z is given by $Z = Z_R + Z_C$, which in this case is $Z = R + 1/j\omega C$. The real part of Z, (Z'), is thus R and the imaginary part Z'' is $-1/\omega C$. For a parallel combination of resistance and capacitance the impedance is given by :

$$1/Z = 1/Z_R + 1/Z_C = 1/R + j\omega C \qquad 2.1$$

These simple networks are represented in the complex plane as shown in Figure 2.2 Addition of a resistance in series with the parallel resistance/capacitance network merely translates the impedance along the Z' axis by the

value of R.

The impedance of the cell represented by Figure 2.1 is[5]

$$Z = R_{\Omega} + \left[\frac{1}{j\omega C + 1/\theta + \sigma\omega^{-\frac{1}{2}} - j\sigma\omega^{-\frac{1}{2}}} \right] \qquad 2.2$$

$$Z = Z' - jZ'' \qquad 2.3$$

Separation of the real and imaginary parts of Z in equation 2.2 results in

$$Z' - jZ'' = R_{\Omega} + \left[\frac{\theta + \sigma\omega^{-\frac{1}{2}}}{(C\sigma\omega^{\frac{1}{2}} + 1)^2 + \omega^2 C^2 (\theta + \sigma\omega^{-\frac{1}{2}})^2} \right] \qquad 2.4$$

$$- j \left[\frac{\omega C(\theta + \sigma\omega^{-\frac{1}{2}})^2 + \sigma\omega^{-\frac{1}{2}}(\omega^{\frac{1}{2}} C\sigma + 1)}{(C\sigma\omega^{\frac{1}{2}} + 1)^2 + \omega^2 C^2 (\theta + \sigma\omega^{-\frac{1}{2}})^2} \right]$$

This complicated formula has two extreme cases of interest.

At low frequencies 2.4 reduces to

$$Z' - jZ'' = R_{\Omega} + \theta + \sigma\omega^{-\frac{1}{2}} - j(\sigma\omega^{-\frac{1}{2}} + 2\sigma^2 C) \qquad 2.5$$

When plotting Z'' against Z' a straight line of slope 45° is obtained Figure 2.3.

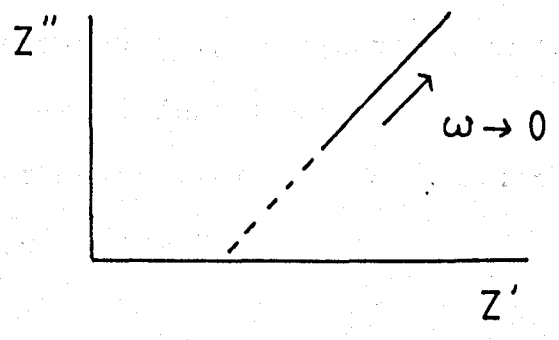

Figure 2.3

At high frequencies diffusional resistance can be neglected and equation 2.4 reduces to

$$Z' - jZ'' = R_\Omega + \frac{\theta}{1 + \omega^2 C^2 \theta^2} - j\left[\frac{\omega C \theta^2}{1 + \omega^2 C^2 \theta^2}\right] \qquad 2.6$$

Elimination of ω between Z' and Z'' leads to

$$(Z'')^2 = \left(\frac{\theta}{2}\right)^2 - \left[Z' - R_\Omega - \frac{\theta}{2}\right]^2 \qquad 2.7$$

which is the equation for a semicircle (Figure 2.4) with maximum Z'' at a frequency given by

$$\omega_{max} = \frac{1}{C\theta} \qquad 2.8$$

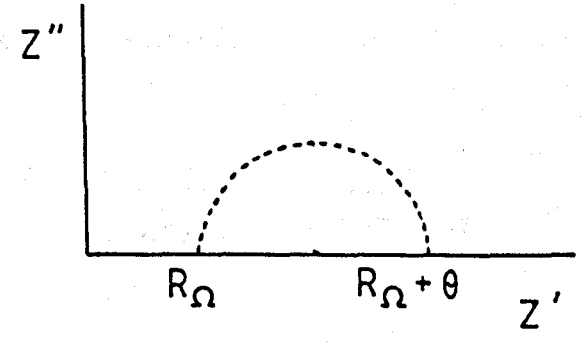

Figure 2.4

The charge transfer resistance can be obtained directly from the diameter of the semicircle and the value of capacitance from the frequency corresponding to the top of the semicircle (equation 2.8).

Quasi-reversible charge transfer processes show a mixture of diffusion control as $\omega \longrightarrow 0$ and charge transfer control as $\omega \longrightarrow \infty$ and the complex plane plot is as in Figure 2.5

2.1.2 Evaluation of Kinetic Parameters

The method used in this work for evaluation of rate constants and diffusion coefficients is that outlined by Macdonald and McKubre.[7] For a quasi-reversible reaction as $\omega \rightarrow \infty$:

$$Z' = \theta + R_\Omega + \sigma\omega^{-\frac{1}{2}} \qquad 2.9$$

$$Z'' = 2\sigma^2 C + \sigma\omega^{-\frac{1}{2}} . \qquad 2.10$$

Therefore plots of Z' ($\omega \longrightarrow 0$) and Z'' ($\omega \longrightarrow 0$) against $\omega^{-\frac{1}{2}}$ will yield straight lines of slope σ and intercepts of $R_\Omega + \theta$ and $2\sigma^2 C$ respectively. The values of R_Ω and C were evaluated at high frequencies or in the absence of the electroactive species and hence σ and θ could be determined. From θ it is possible to determine the apparent standard rate constant k_{sh} using :

$$k_{sh} = \frac{RT}{n^2F^2AC_o^{\alpha} C_R^{(1-\alpha)} \theta} \qquad 2.11$$

For $\alpha = 0.5$ and $C_o = C_R = \frac{1}{2}C_B$

where C_B = Bulk concentration and A is the electrode area.

Hence 2.11 becomes

$$k_{sh} = \frac{2RT}{n^2F^2A\, C_B \theta} \qquad 2.12$$

Mean diffusion coefficients for oxidised and reduced

species were obtained using the equation

$$\sigma = \frac{4RT}{2^{\frac{1}{2}} n^2 F^2 C_B D^{\frac{1}{2}} A} \qquad 2.13$$

2.1.3 The Effect of Porosity on Electrode Impedance

The random structure of a real porous electrode is complex. The simplest theoretical models involve simple non-connecting pores.[6]

The simplest treatment of a porous surface assumes that the planar portion of the electrode is small in comparison with the porous area, and therefore, the influence of the planar surface on the total impedance can be ignored. It is also assumed that the pore is parrallel-sided and the equipotential surfaces within the pore are flat and perpendicular to the pore axis. The neglect of curvature for the equipotential surfaces can be justified for a pore of length greater than its diameter. With these assumptions, the pore can be considered as semi-infinite. The resultant impedance spectrum can be represented by Figure 2.6. It is linear with a slope unity. When the pore lengths are varied the behaviour exhibited is shown in Figure 2.7. At high frequencies even shallow pores behave as semi infinite, but at low frequencies only the deepest pores are semi infinite. Then, the electrode behaves in a more planar fashion i.e. the pores have finite depth.

2.2 CYCLIC VOLTAMMETRY

This is a non-steady state polarisation method whereby the potential is swept linearly with time, and the current vs. voltage response is recorded. The technique has many variables which are preset by the operator e.g. starting potential, reverse potential and sweep rate. Usually a symmetrical triangular waveform is used in which case the forward and reverse sweep rates are identical. The technique has been developed theoretically by Randles, Sevcik, Nicholson and Shain and by Saveant.[8-11]

In this work the technique was initially used in order to characterise redox reactions for use at fluorinated electrodes. Using this method the reversible potential for a simple redox process :

$$O + ne \rightleftharpoons R$$

could be quickly determined.

The early work in this project used a Bryans X-Y recorder to record the cyclic voltammograms. This was not suitable for fast scan work and subsequently a computerised system was used.

The current vs. potential response for a simple redox reaction is shown in Figure 2.8.

It is noted that the current response is peaked which is a result of reaching a maximum in the rate of mass transfer to the electrode. Diagnostic criteria for various cases are outlined below.

For a reversible process there are two peaks : one on each scan

1) The ratio of the peak currents ($i_p^a/i_p^c=1$).

2) The peak potentials E_p^a, E_p^c and the half peak potential $E_{p/2}$ are independent of the scan rate.

3) $E_p^c - E_p^a = -56/n$ mV at 25 C. This difference is independent of the sweep rate. (Where n is the number of electrons transfered.)

4) $i_p \propto \nu^{\frac{1}{2}}$ (where ν is the sweep rate.)

The reversible potential E_r was taken as $(E_p^a + E_p^c)/2$. For a quasi-reversible process two peaks are again obtained

1) $E_p^a - E_p^c$ may approach 56/n mV at low sweep rates (ν) but increases as ν increases.

2) E_p shifts as the sweep rate is changed.

3) $i_p^a/i_p^c = 1$ only when $\alpha = 0.5$.

For an irreversible process there is no peak on the reverse scan.

1) $i_p \propto \nu^{\frac{1}{2}}$

2) E_{pc} shifts negative by $30/\alpha n$ mV for a ten-fold increase in sweep rate.

If the electrode process involved is an adsorption, and both the oxidised and reduced species are electroactive in the potential range under investigation, then mass transport effects can be ignored. If the electron transfer is reversible then both the anodic and cathodic peaks are sharp and symmetrical, and there is little or no peak separation. The charges associated with the anodic and cathodic processes are equal.

For irreversible adsorption the forward peak is no longer symmetrical, and there is no reverse peak. For quasi-reversible systems there are again two peaks but they are not symmetrical and the peak potentials are not coincident.

2.3 ELECTROCHEMICAL INSTRUMENTATION

The potentiostat used in this study was designed and constructed in these laboratories.[12] It has a 50V output capability with a maximum current output of 1.8Å. The amplifier inputs allowed a working potential range of 5V although only 3V was available on the bias control. In order to obtain high electrode potentials (up to 9V), a floating d.c. voltage source, powered by a 9V pp9 battery, was inserted between the reference electrode and the reference electrode terminal of the potentiostat (Figure 2.9a). This floating d.c supply was switchable in one volt increments (Figure 2.9b).

The current-measuring unit was designed and built in these laboratories.[13] The unit enabled the ohmic error introduced by placing the current-measuring resistor into the working electrode lead to be compensated by feedback. The unit also had an integrator circuit which was used to determine the amount of charge passed during an electrolysis.

The potentiostat could be employed as a galvanostat (Figure 2.10) by providing a fixed resistance betweeen the reference electrode terminal and earth. In this mode the reference electrode terminal was connected to the working electrode and the electrode potential between

the working and reference electrodes was measured on a digital voltmeter or on a Y/t chart recorder (Chessel BD8 flat bed strip recorder).

For cyclic voltammetry measurements a function generator designed and constructed in these laboratories[12] was used. It has a 3V maximum output capability, as either square wave or ramped potential programmes. Sweep rates could be selected in the range $10^{-4}Vs^{-1}$ up to $10^{3}Vs^{-1}$. Forward and reverse scan rates were adjustable and continuous cycling was possible. Voltammograms were recorded on Bryans 26000 or 29000 series A4xy chart recorders.

Subsequently cyclic voltammetry was performed using a system under the control of an Apple II Plus Microcomputer in conjunction with the potentiostat and current-measuring unit already described. This system could also be used for potential pulse measurements.[14]

A.C. impedance measurements were made using a Solartron 1174 frequency response analyser (FRA) and a Solartron 1186 electrochemical interface (ECI) under the control of an Apple II plus microcomputer (Figure 2.11). Alternatively a Solartron 1172 FRA was used in conjunction with the potentiostat and current measuring unit already described, under the control of an Apple II plus computer. Software developed in these laboratories allowed control of the equipment and subsequent data analysis.[15]

2.4 ESCA AND SIMS

Electron Spectroscopy for Chemical Analysis (ESCA) and Secondary Ion Mass Spectrometry (SIMS) were carried out at the analytical section of the UKAEA at Risley.

The ESCA technique uses either ultraviolet or x-ray sources to bombard samples to produce the photoelectric effect. In this case Al Kα x radiation ($h\nu$ = 1486eV) was used resulting in x-ray induced photoelectron emission (x-ray photoelectron spectroscopy or XPS).

The atoms in a molecule are bound by the valence electrons which are described by molecular orbitals. Core electrons, however, are described by atomic-like orbitals.[16]

The binding energies, B, of the electrons in the valence orbitals are small, normally $0 \longrightarrow 50$eV. Those of the core electrons are >200eV. The XPS examinations in this work involved only core electrons.

The photoelectric effect is described by the equation :

$$\text{K.E. (ejected electrons)} = h\nu - B$$

K.E. = Kinetic Energy

$h\nu$ = energy of incident radiation

Chemical information is obtained from the binding energy values as this varies according to the chemical environment of the atom in the molecule. Thus the binding energies of the core electrons give rise to chemical shifts (binding energies are increased when the

atom concerned is bonded to eletronegative groups).

The XPS examination was performed using a KRATOS LTD ES300 electron spectrometer, with PMI (Physical Electronics) argon ion etchers used for sputtering. The vacuum obtained was 10^{-7} - 10^{-8} mbar. During ion etching, pressures of 10^{-4}mbar were used.

Secondary Ion Mass Spectrometry (SIMS) involves bombardment of the sample surface with a high energy primary ion beam (in this case Ar^{+}) which etches the surface and produces secondary ions derived from the surface constituents. These ions are detected spectrometrically. Depth profiles can be obtained by monitoring a single ion intensity as a function of sputtering time.

The SIMS exmination was performed on a modified VG Scientific Ltd ESCA LAB spectrometer at a vacuum of 10^{-7}mbar.

Samples for ESCA and SIMS examination were mounted on metal sample holders using a small quantity of colloidal silver adhesive.

2.5 SCANNING ELECTRON MICROSCOPY AND EDAX

SEM and EDAX were used to analyse the surface of electrodes, especially those containing transition metal additives. EDAX analysis gave information about the elemental composition of electrodes.

The instrument used was a Cambridge Stereoscan MK IIA, with an EDAX 707 analyser attachment.

2.6 OTHER TECHNIQUES

Infrared analysis of certain compounds and electrodes was performed using a Nicolet FTIR instrument.

Figure 2.2

IMPEDANCE SPECTRA FOR VARIOUS ELEMENTARY CIRCUITS

a) A discrete resistance R

b) A Capacitor C

c) A Resistor and Capacitor in series $R_s + C_s$

d) A resistor R_p in Parallel with a Capacitor C_p

a)

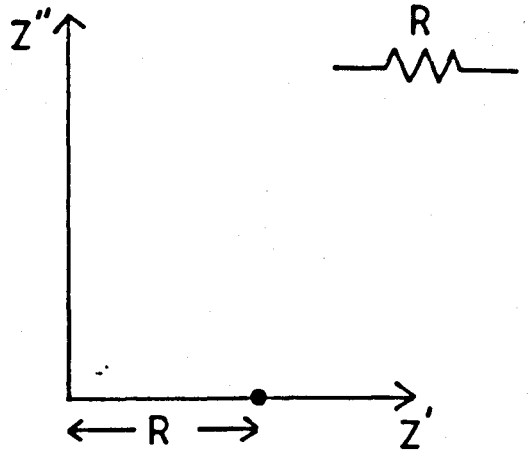

b)

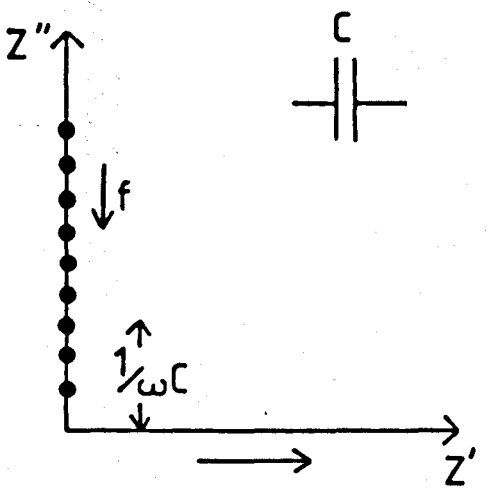

c)

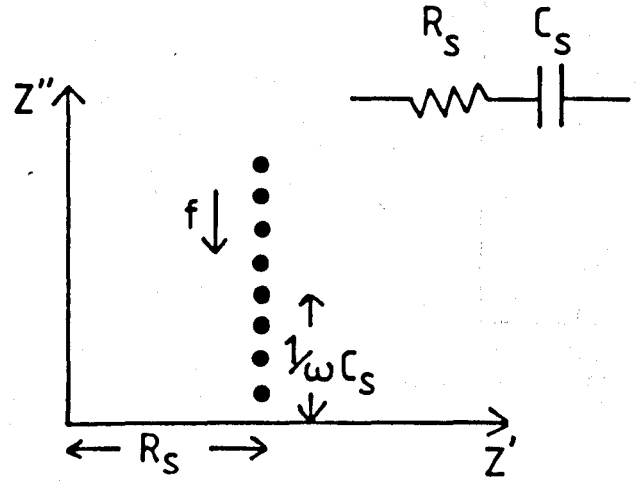

d)

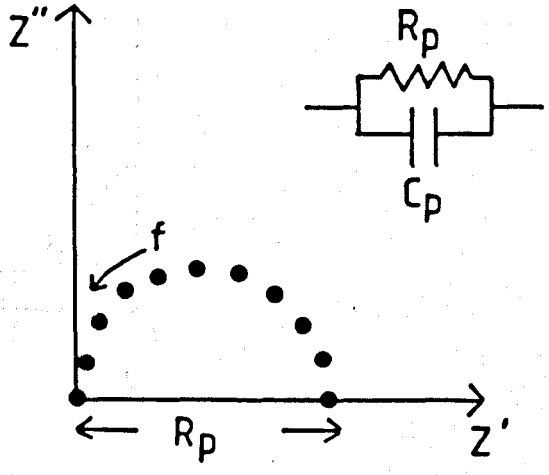

Figure 2.5

Typical impedance spectrum, and equivalent circuit for an electrochemical reaction where θ is the charge transfer resistance and W is the Warburg (Diffusion) impedance

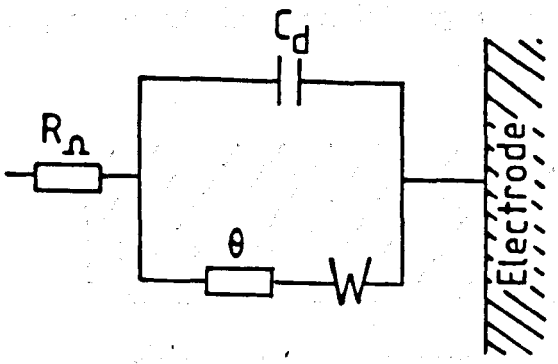

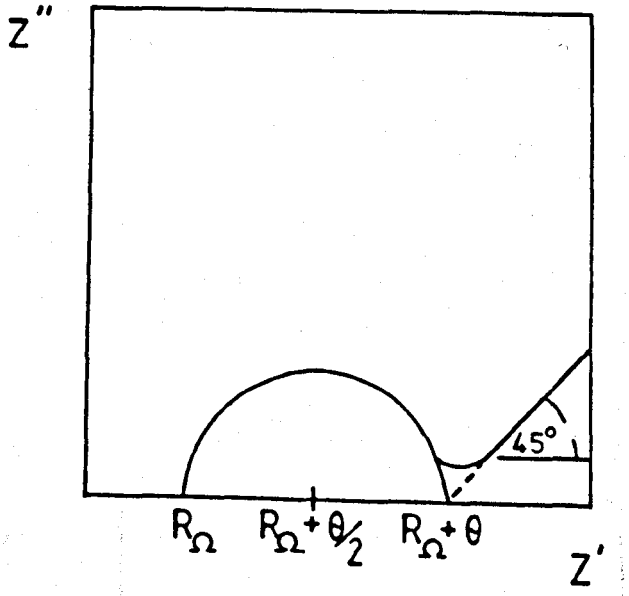

Figure 2.6

Typical impedance spectrum for a semi-infinite porous electrode in the absence of any Faradaic process. Z is the douple layer capacitance per unit length and R is the resistance per unit length along the pore.

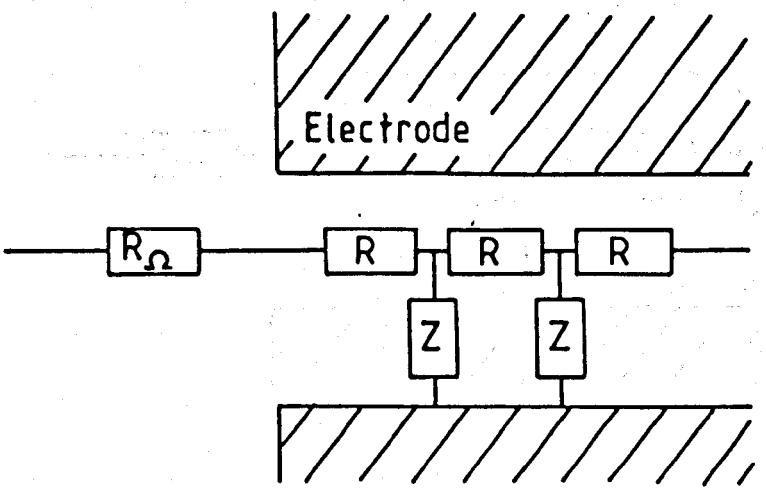

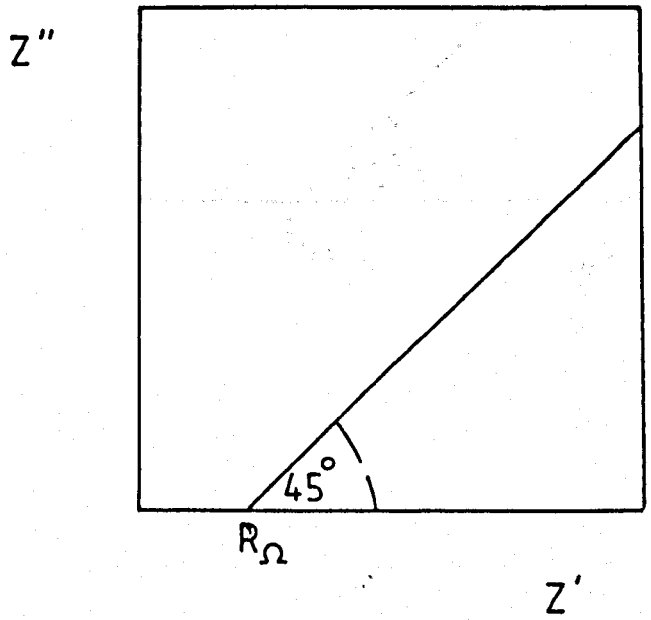

Figure 2.7

Typical impedance spectrum for a porous electrode where the pores have a finite depth.

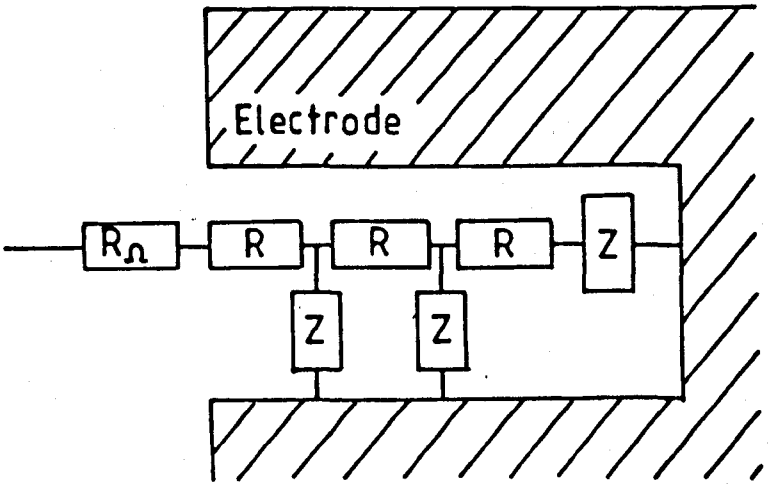

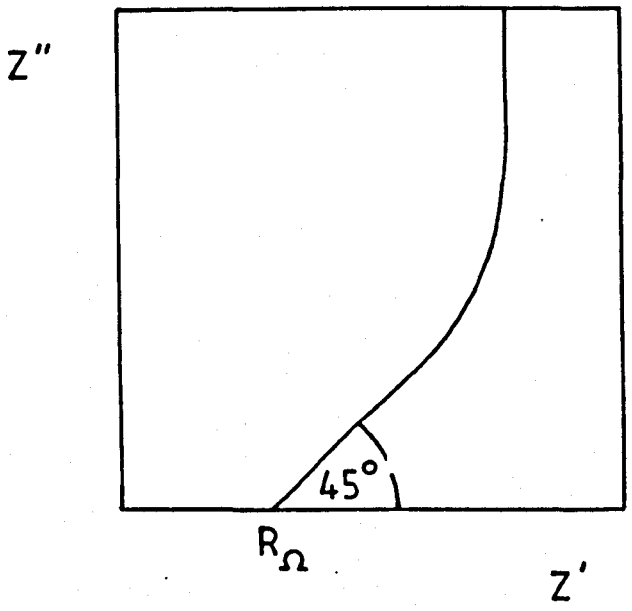

Figure 2.8

The upper diagram shows the potential programm applied in cyclic voltammetry.

The lower diagram shows the current vs. potential response for a simple reversible redox reaction.

E_{pa} and E_{pc} are the anodic and cathodic peak potentials; i_{pa} and i_{pc} are the anodic and cathodic peak currents.

The dashed line is the current transient obtained if the potential is held at the negative limit. Here the potential axis is treated as a time axis, with reversal of direction at the negative sweep limit.

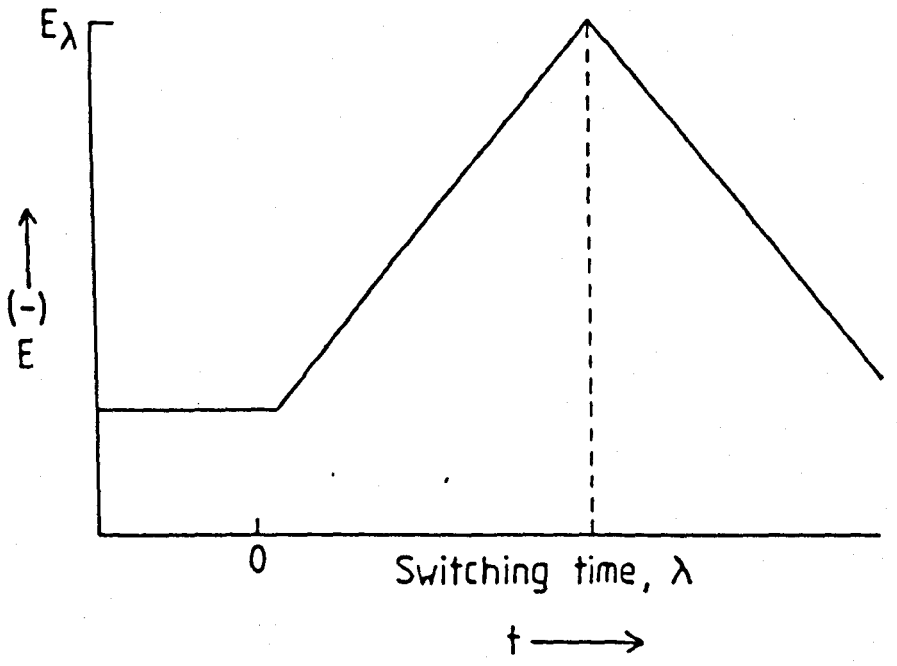
E_λ
(-)
E
0
Switching time, λ
t ⟶

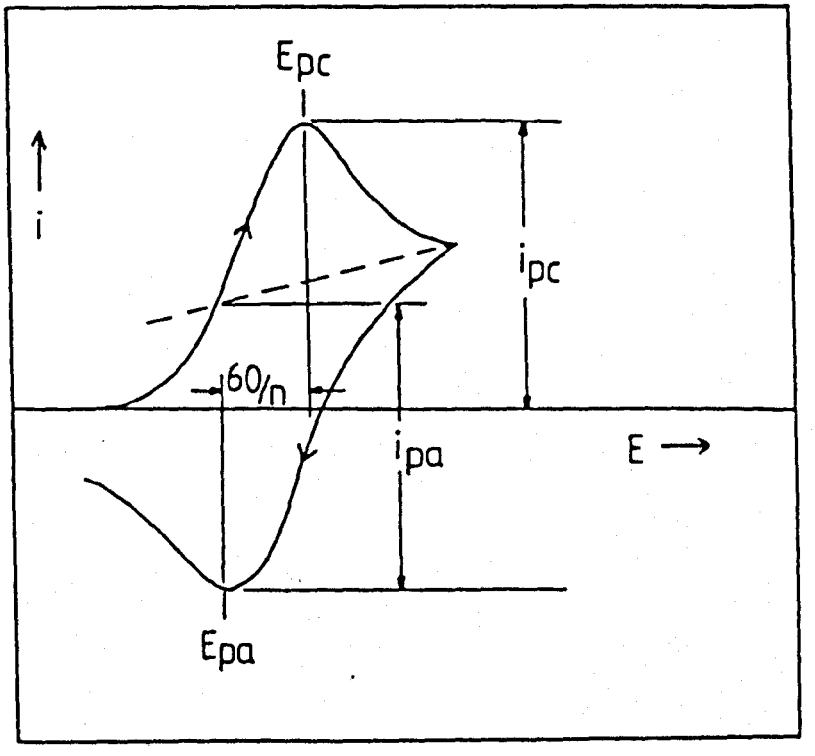
E_{pc}
i
i_{pc}
60/n
i_{pa}
E ⟶
E_{pa}

Figure 2.9

FLOATING D.C. SUPPLY

A) The configuration used to bias the reference electrode in order to achieve the desired working potential :

B PP9, 9V Battery

C Counter Electrode

CMR Current Measuring Resistor

FG Function Generator

PS Potentiostat

RE Reference Electrode

W Working Electrode

B) The circuit diagram for the D.C. supply.

A

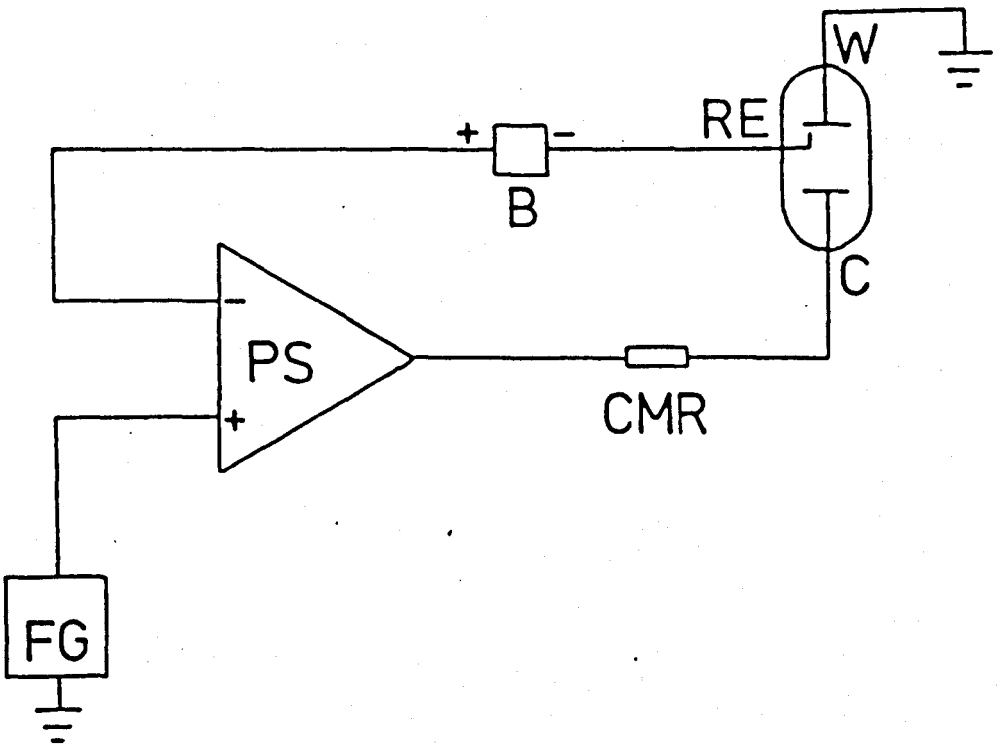
W
RE
+
B
−
C
PS
CMR
FG

B

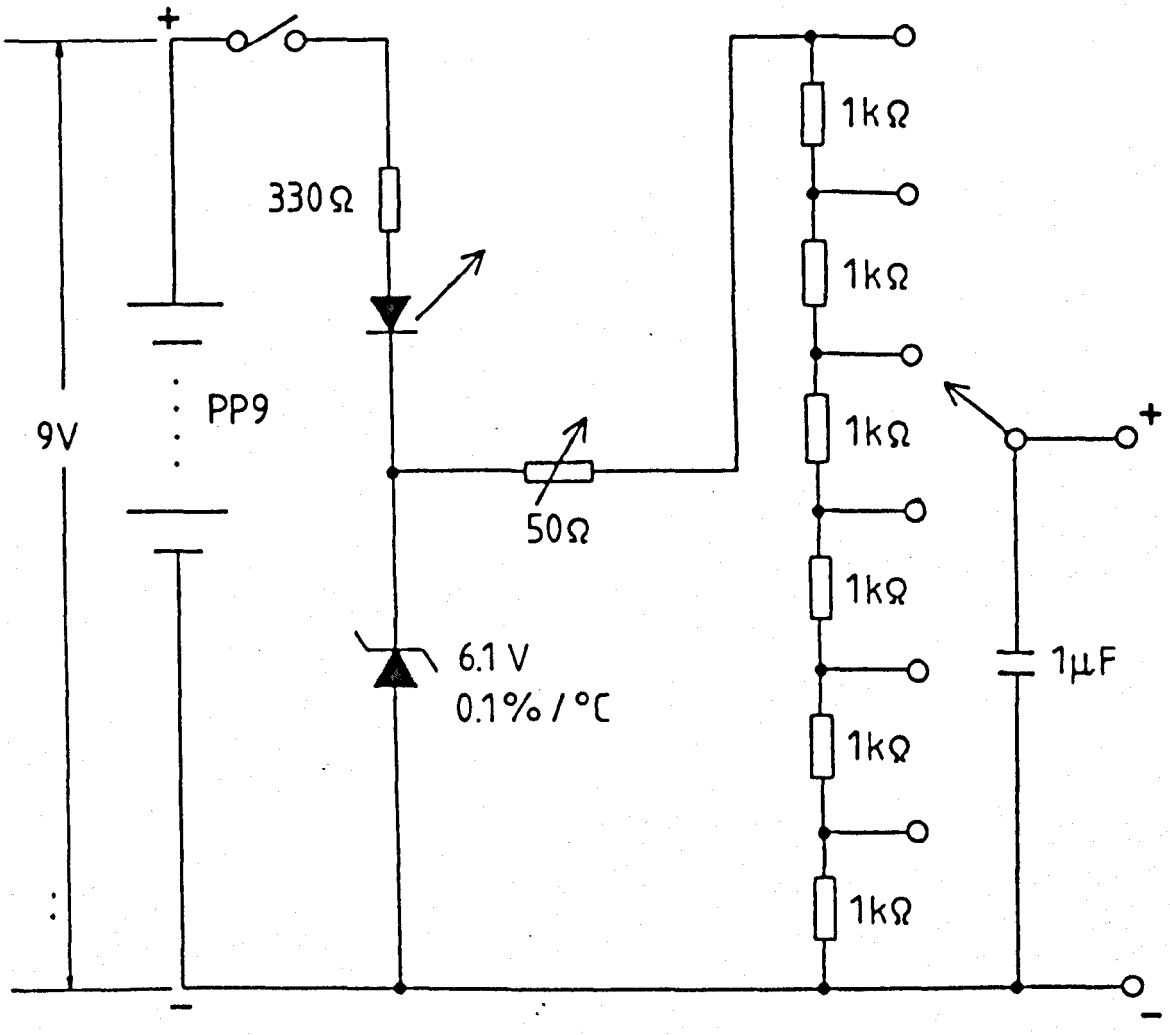
+
330Ω
9V
PP9
50Ω
6.1 V
0.1% / °C
1kΩ
1kΩ
1kΩ
1kΩ
1kΩ
1kΩ
1µF
+
−
−

Figure 2.10

CIRCUIT USED IN GALVANOSTATIC MEASUREMENTS

CET Counter Electrode Terminal of Potentiostat

RET Reference Electrode Terminal of Potentiostat

WET Working Electrode Terminal of Potentiostat

B Bias Potential Control

CE Counter Electrode

RE Reference Electrode

WE Working Electrode

DVM Digital Voltmeter

CR Chart Recorder

BA Buffer Amplifier (voltage follower)

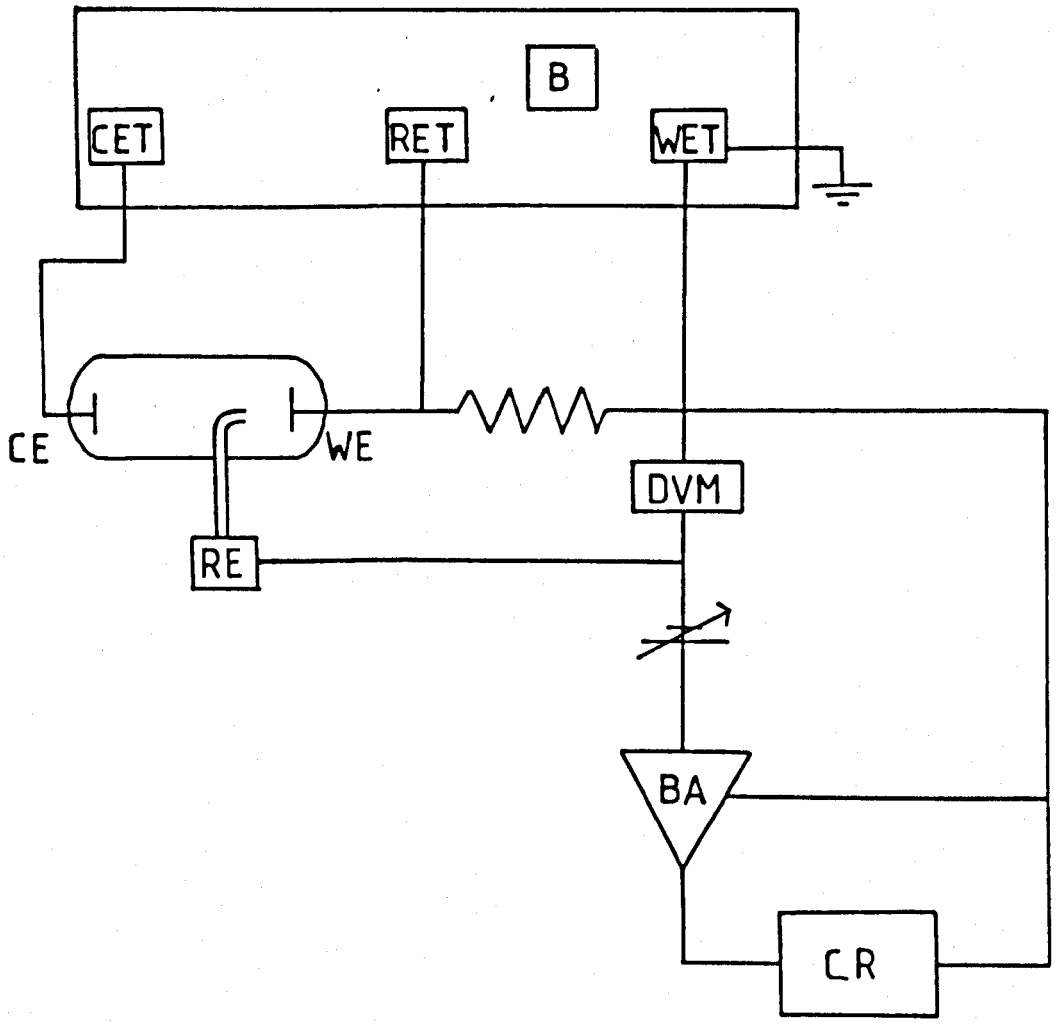
B
CET
RET
WET
CE
WE
RE
DVM
BA
CR

Figure 2.11

A.C. IMPEDANCE EXPERIMENTAL ARRANGEMENT

FRA Frequency Response Analyser

ECI Electrochemical Interface (Potentiostat)

RE1 Reference Electrode 1

RE2 Reference Electrode 2

WE Working Electrode

CE Counter Electrode

X_{out} X output of ECI to FRA X_{in}

Y_{out} Y output of ECI to FRA Y_{in}

FRA_{out} Output from Frequency Response Analyser into ECI input

When using a three electrode cell RE2 is connected to the working electrode.

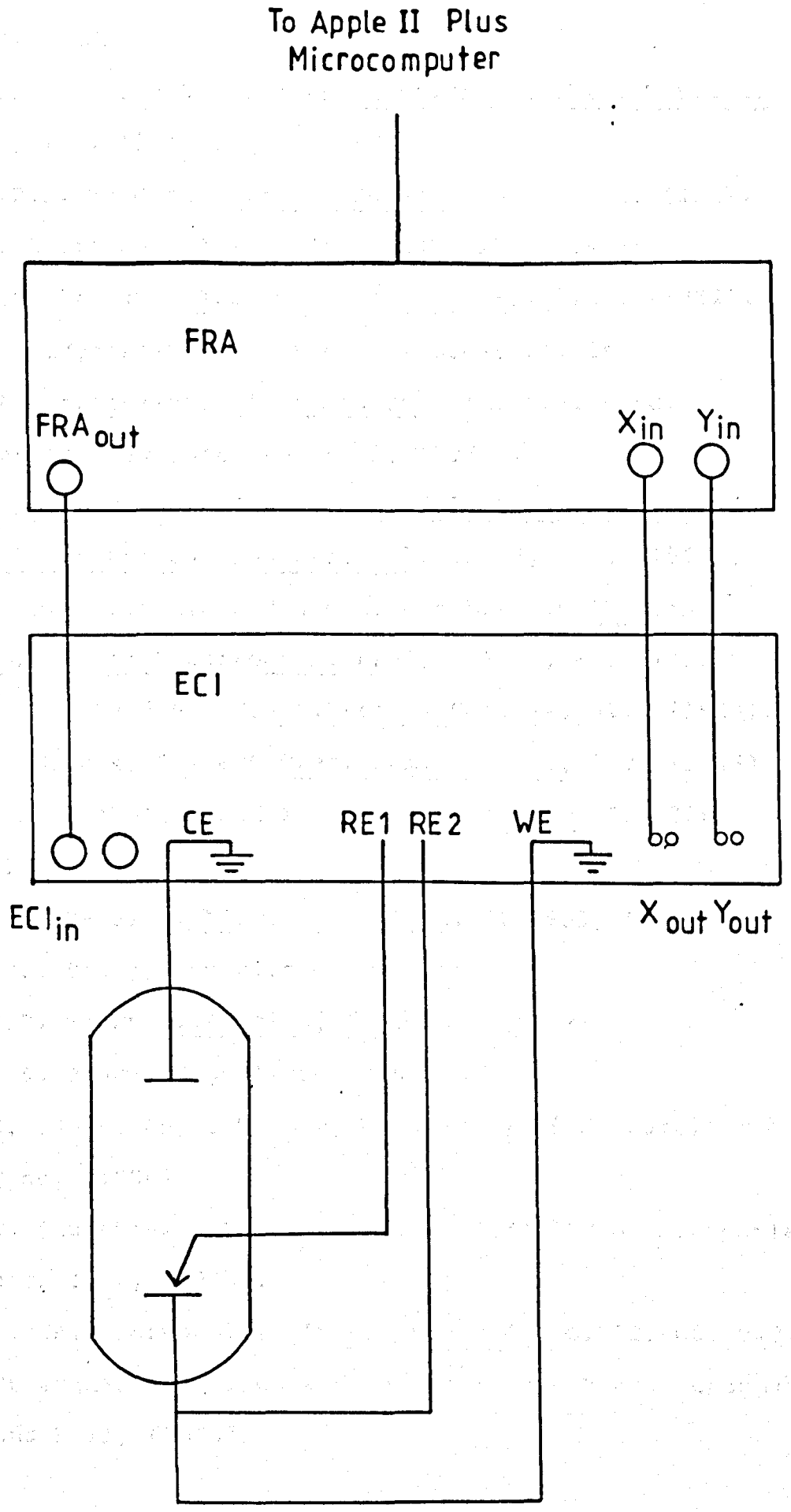
To Apple II Plus
Microcomputer
FRA
FRA out
X in
Y in
ECI
CE
RE1
RE2
WE
ECI in
X out
Y out

2.7 REFERENCES

1. P. Dolin and D. Ershler, Acta.Physicochim. U.R.S.S. 13, 747, (1940).
2. J.E.B. Randles, Discuss.Faraday Soc. 1, 11, (1947).
3. M. Gerischer, Z.Phys.Chem. 198, 286, (195)1.
4. D.C. Grahame, J.Electrochem.Soc. 99, 370C, (1952).
5. M. Sluyters-Rehbach and J.H. Sluyters, in "Electroanalytical Chemistry", ed. A.J. Bard, Dekker, New York, Vol 4, 1, (1970).
6. R. De Levie, in "Advances in Electrochemistry and Electrochemical Engineering", Vol 6, 329, (1967).
7. D. D. MacDonald and M.C.H. Mckubre, in "Modern Aspects of Electrochemistry", Vol 14, 61, (1982).
8. J.E.B. Randles, Trans.Faraday Soc. 44, 327, (1948).
9. A. Sevcik, Collect.Czec.Chem.Comm. 13, 349, (1948).
10. R.S. Nicholson and I. Shain, Anal.Chem. 36, 706, (1964).
11. J.M. Saveant, Electrochim.Acta. 12, 999, (1967).
12. O.R. Brown, Unpublished results.
13. O.R. Brown, J.Physics(E) 5, 365, (1972).
14. O.R. Brown, Unpublished results.
15. G. Evans, Ph.D. Thesis, University of Newcastle upon Tyne, (1986).
    S. Churchouse, Ph.D. Thesis, University of Newcastle upon Tyne, (1985).
16. P.M.A. Sherwood, in "Spectroscopy", Vol 13, ed. B.P. Straughan and S. Walker, Science Paperbacks, Chapman and Hall, (1976).

CHAPTER 3

EXPERIMENTAL

3.1 MOLTEN SALT EQUIPMENT

3.1.1 The Fluorine Cell

Previous studies in these laboratories[1,2] have resulted in the production of a non-metallic system in which it is possible to make measurements on the fluorine evolution reaction.

Fluorocarbon plastics were used throughout the study due to their stability towards molecular fluorine. Cell components were machined from either Kel-F^{R} (polychlorotrifluoroethylene) or PTFE (polytetrafluoroethylene). The cell body, however, was a commercially available polymethylpentane beaker (Azlon Labplex, England) of 250ml capacity. The beaker was transparent and had a rim which allowed for fitting of a cell top. The cell top was constructed from PTFE (Figure 3.1) and all cell components were inserted through this top. The top was sealed to the body using a silicone rubber sealant, and all components were similarly sealed into the top.

3.1.2 Working Electrodes

Working electrodes used throughout this study were all discs and include vitreous carbon (ϕ8mm, 2mm thick) (Le Carbone Lorraine), Union Carbide hard carbon (YBD ϕ 8mm) supplied by BNFL, pyrolytic graphites with edge orientation and basal plane orientation (Le Carbone ϕ 8mm) and doped electrodes prepared in these laboratories (Chapter 8).

The main problem encountered using disc electrodes is effecting a good seal between the electrode holder

and the electrode disc so that only a planar surface is presented and the edges of the disc are not active towards electrode reactions.

In order to produce a good seal the carbon discs were embedded into molten Kel-F under pressure.

The mold, originally designed as a press for the production of KBr discs for infrared spectroscopy, was adapted to accommodate Kel-F.

Before molding, the Kel-F was prepared in the form of a cylinder (ϕ= 13mm, height 15mm) which contained a shallow concentric hole (depth 1mm, ϕ 8mm) in one end to locate the carbon disc during the molding process.

The assembled press, with carbon disc and Kel-F in place, was evacuated for 1 hour in order to avoid trapping air bubbles in the plastic during the molding process. The assembly was then heated in an oven at 200°C for two hours. Only then was the pressure applied ($2000 kgcm^{-2}$) to effect the compression molding process. This was performed in an hydraulic press (Specac) immediately after the mold had been removed from the oven. The vacuum was maintained whilst the apparatus cooled to room temperature. Finally the Kel-F piece, containing the embedded disc, was machined to the dimensions of Figure 3.2.

All carbon electrodes, whether commercial or produced in these laboratories, were prepared in this way.

The electrode assemblies were dsigned to screw into the working electrode holder shown in Figure 3.3. The Viton^{R} 'O' ring prevented leakage of electrolyte

solutions to the back of the electrode.

Electrical contact was made using a spring, which abutted onto a platinum disc attached to a nickel wire.

3.1.3 Reference Electrode

The reference electrode used in this study was the Pd/H_2 electrode. It has the advantage over the Pt/H_2 electrode that bubbling hydrogen over the palladium is unnecessary. The palladium lattice expands to accommodate molecular hydrogen.

The reference electrode compartment was constructed of Kel-F, Figure 3.4, and consisted of two parts, the compartment itself, and the Pd wire holder.

A small ball of palladium was formed by melting at the end of the palladium wire (0.5mm diameter, 99.99% purity, Johnson Matthey Ltd.). Whenever the electrode had been used the ball was reformed. Formation of the ball was achieved by careful heating of the wire in a non oxidising flame.

The electrode was filled with hydrogen by cathodic charging in the KF.2HF electrolyte. Charging was performed with a DC power pack (Solartron, D.C. Power supply type AS757.4) set so that the initial charging current was 5mA. Charging was performed for six hours and the electrode was then allowed to stabilise for twelve hours before it was used. The anode used during the charging process was a porous carbon rod.

3.1.4 Counter Electrode

The counter electrodes were simply porous carbon rods of large surface area. The length of the rod was 11cm and the diameter 9mm.

3.1.5 Electrode Shrouds

The electrode shrouds (Figure 3.5 and 3.6) were of PTFE. The purpose of the shrouds was to allow the fluorine produced at the working electrode and hydrogen at the cathode to escape during electrolysis, without mixing.

3.1.6 Other Components

The cell top was fitted with a PTFE nitrogen bubbler and nitrogen purger. There were outlets for the electrolysis products which were vented as near as possible to the fume cupboard exit.

To minimise atmospheric contamination through leaks into the cell, a small nitrogen overpressure was applied to the cell.

The cell top was fitted with a Kel-F tube which allowed for admission of gaseous HF when necessary so that the HF content of the electrolyte was kept in the range 43±1%.

The HF content of the electrolyte was monitored by measuring the density of the electrolyte with a "home made" hydrometer, made from Kel-F and weighted with mercury. The hydrometer is shown in Figure 3.7.

3.1.7 Preparation of the Hydrometer

Kel-F tubing (ϕ=6mm) was heated in a hot air stream until it became clear in the middle. At this point it was pulled at both ends so that it became narrow in the middle. This was then cut in the centre and the thin end sealed in a hot air stream. A bubble was then blown in the tube resulting in the shape shown in Figure 3.7. The tube was then filled with mercury and the thicker end was sealed.

Calibration of the hydrometer was performed by using solutions of known density in the range 1.8 to 1.9gcm^{-3}. Such solutions were prepared by the addition of iodoform (ρ = 4gcm^{-3}) to 1-iodopropane (ρ = 1.74gcm^{-3}) the densities being measured with a standard hydrometer. Densities of 1.8 to 1.9gcm^{-3} could be monitored using the hydrometer corresponding to electrolyte compositions in the range 40 to 46% of HF by weight.

3.1.8 Handling of HF

99.8% HF (BDH or Air Products) was admitted to the melt, without further purification, directly from the cylinder using a gas line produced from Kel-F tubing (ϕ=6mm). Before HF was added to the electrolyte it was 'diluted' with nitrogen to prevent too vigorous a reaction between the KF.HF and HF.

3.1.9 The Cell Heater

The cell was heated by means of an air stream under thermostatic control. The fan heater assembly is shown in Figure 3.8. To safeguard against overheating the

maximum power to the heater was controlled by a variable autotransformer adjusted so that in the event of failure of the thermostat the temperature could not rise to above 100°C. Another safety device was also used to avoid fire hazard in the event of failure of the fan. This was a thermal fuse opening at 141°C (RS 413 175) which was placed between the heating element and the fan.

3.1.10 Operation of the Cell

Each time a new melt was prepared a new polymethylpentane beaker was used for the cell body. This was a necessary precaution, as prolonged exposure to KF.2HF had a deleterious effect on the beaker, often resulting in cracking.

All components that had been exposed to silicone rubber were immersed in alcoholic KOH to remove any organic residues. This was followed by an acid wash using concentrated sulphuric acid. Thrice distilled water was used to rinse the cell before drying it at 100°C.

Early work used industrially supplied electrolytes (BNFL). These varied in composition (Table 3.1) and were used without further purification. When such electrolytes were used they were placed in the beaker which was then covered with a simple PTFE lid and sealed with silicone rubber. This was then placed in the heating assembly and allowed to melt (4-5 hours). When the electrolyte was molten the PTFE lid was replaced with the preassembled cell top. The whole cell was then

sealed with silicone rubber and the gas tubes connected.

Subsequently a purer electrolyte was used which was made by the addition of HF to KF.HF (BDH GPR). In this case a known weight of KF.HF was placed in the beaker and HF slowly admitted using the gas handling line. The formation of KF.2HF would usually take three or four hours. The composition of the electrolyte is also shown in Table 3.1.

A large porous carbon electrode was inserted as a working electrode and used to charge the Pd/H_2 reference electrode. This was performed using a Solartron D.C. power supply set so that the initial charging current was 5mA.

3.1.11 Pre-electrolysis

Electrolytes were only pre-electrolysed to remove water. This was performed by evolving fluorine for at least 12 hours at the porous electrode used to charge the Pd/H_2 reference electrode. The HF content was then replenished using anhydrous HF. The fluorine produced reacted with any water to produce F_2O, which passed from the cell.

Potentiostatic pre-electrolysis at potentials below the flurorine evolution potential is slow. It has been claimed[3] that pulsed pre-electrolysis can be effective in drying HF. In such a drying procedure the active pulse (with respect to water electrolysis) was of 45s duration at 4V with the inactive part of the cycle being 8s at 1V. Pulsed electrolysis lasted for 24 to 48 hours. Such a technique probably relies on the generation of

active fluorine atoms/radicals which react with water to produce F_2O. However during this study it was found to be unsuitable for drying KF.2HF. Analysis of the melt supplied by BNFL showed a water content of 0.75g/100g (≈0.8M). The average melt consisted of 150ml of KF.2HF (0.12 moles of water). In order to electrolyse all this water during a pulsed pre-electrolysis a charge of at least 23000 coulombs needs to be passed. The actual charge passed in a pulsed pre-electrolysis was 7000C, obviously not enough to electrolyse all of the water.

This observation appears to indicate that pulsed pre-electrolysis is not effective in drying KF.2HF. Another fresh melt was pre-electrolysed using the pulsed technique. After 280 minutes a charge of 1445C had been passed. Currents fell with time. Interruption of the pulsed electrolysis followed by a 1 minute delay and restart of the electrolysis had no effect on the electrolysis currents. The charge of 1445C is equivalent to 7.5×10^{-3} moles of water (≈0.1cm^3). The pulsed pre-electrolysis was again interrupted and 0.1cm^3 of water was added. Again there was no effect on the pulsed pre-electrolysis currents. (A rise in current would be expected if the pre-electrolysis were electrolysing water). After 3525C of charge had passed 0.3cm^3 of water was added to the melt. Again there was no effect on the pre-electrolysis currents.

These measurements indicate that pulsed pre-electrolysis is not effective in drying of KF.2HF. For this reason all melts were dried by potentiostatic evolution of fluorine at +6V for at least 12 hours.

3.2 THE KINETIC CELL

After electrodes were fluorinated in KF.2HF they were removed from the melt, rinsed with thrice distilled water and transferred to a two compartment glass cell where kinetic measurements of model redox systems were made. The main compartment contained the carbon working electrode and a platinum counter electrode positioned opposite the working electrode. The reference electrode was separated from the Luggin capillary by a closed liquid-seal tap which prevented mixing of the reference aqueous electrolyte with the electrolytic solutions in the main body.Liquid junction potentials generated by such a reference electrode arrangement were ignored. In order to reduce the high-frequency noise generated across the large impedance imposed by the closed tap, a 0.1 or 1μF by-pass capacitor was connected between the reference electrode terminal and a platinum wire sealed into the Luggin capillary.

3.3 SOLVENT PURIFICATION

3.3.1 Acetonitrile

Procedures for purification of acetonitrile have been reviewed by Mann.[4] That adopted here has been reported by Walters and Ramely.[5] The purification procedure is outlined below :

1. AnalaR grade acetonitrile (BDH) was refluxed with anhydrous aluminium chloride ($15 gdm^{-3}$) for one hour, followed by distillation. This is reported to remove acrylonitrile.

2. The distillate is refluxed with potassium permanganate ($10gdm^{-3}$) for 15 minutes followed by distillation. This removes any oxidisable material and also any HCl developed in step 1.
3. The distillate is refluxed with potassium bicarbonate ($15gdm^{-3}$) for one hour followed by distillation. This is reported to remove amines generated in step 2.
4. The solvent is percolated through a column of dry molecular sieves, type 4A, and then refluxed with calcium hydride for 1 hour. The solvent was then fractionally distilled at atmospheric pressure and at a temperature of 80°C using the apparatus shown in Figure 3.9.

3.3.2 Water

Water used for cleaning glassware and in the preparation of all aqueous solutions was thrice distilled using an all glass apparatus.

3.3.3 Mercury

Mercury, used in electrode preparations and as a working electrode, was twice distilled. The mercury was cleaned by agitation with dilute nitric acid and then washed with thrice distilled water. The mercury was dried by washing with acetone and by passing the mercury through a small pin hole in the tip of a filter cone. The mercury was then vacuum distilled twice in separate all-glass stills.

3.4 CHEMICALS

Sodium perchlorate (BDH AnalaR) was recrystallised

times from thrice distilled water, and dried in a vacuum oven at 60°C for twelve hours. The anhydrous solid was stored over P_2O_5 in vacuo.

Other chemicals used, such as ammonium sulphate, potassium chloride and potassium sulphate, were all BDH AnalaR grade and were recrystallised from thrice distilled water and dried in an oven at 120°C.

Copper amine solutions were prepared by the addition of AnalaR copper sulphate (BDH) to ammonia solutions prepared by dilution of analytical grade ammonia 0.88 (BDH). The ammonia concentration was determined by titration against 0.1M HCl before and after each experiment.

Copper sulphate, potassium hexacyanoferrate(II) and potassium hexacyanoferrate(III) were BDH AnalaR and used without further purification.

Ferrocene was supplied by Aldrich and was used without further purification.

Potassium hexachloroiridate (Johnson Matthey) was used without further purification.

3.5 REFERENCE ELECTRODES IN AQUEOUS AND ORGANIC ELECTROLYTES

In the study of redox kinetic measurements various reference electrodes were used. For the measurements made in acetonitrile/$NaClO_4$ a saturated NaCl/calomel electrode was used. In aqueous chloride solutions a saturated KCl/calomel electrode was used whilst in solutions containing sulphate support electrolytes a mercury/mercurous sulphate reference was used.

All electrodes were made by the batch method whereby several of the same electrode were prepared at one time and compared against one another.

3.6 PREPARATION OF CARBON WORKING ELECTRODES

3.6.1 Vitreous Carbon

Various methods of preparation of vitreous carbon electrodes were investigated. However, one method was used more than most and is described here; other methods, where relevant, will be outlined elsewhere in this thesis.

Vitreous carbon discs (Le Carbone, Great Britain, J. Tipple, London, or made in this laboratory) were first abraded with 100 grit carborundum followed by smoothing with 5/0, 4/0 and 3/0 wet and dry paper. After each stage the electrodes were ultrasonically cleaned in thrice distilled water. This procedure was followed by polishing to a mirror finish with diamond lapping compounds (Hyprez Spray Diamond, Engis Ltd., Maidstone, Kent) dispersed on foam fabric (Hyprocel Pelion self-adhesive polishing discs, Engis Ltd.). The series 45μ, 14μ, 3μ, 1μ and ¼μ grade diamond lap was used. After each stage the electrodes were ultrasonically cleaned in acetone. Finally the electrodes were ultrasonically cleaned in thrice distilled water. Excess water was removed with a filter paper or clean lens tissue, before drying in an oven at 100°C.

3.6.2 Pyrolytic Graphites

Pyrolytic graphite discs with face orientation were

cleaned by removing the surface layers with 'Sellotape'. They were then ultrasonically cleaned in acetone followed by water. Excess water was removed before drying in an oven at 100°C.

Discs with edge orientation were lightly polished with 4/0 and 3/0 dry paper before ultrasonic cleaning in water, and drying at 100°C.

3.6.3 Hard Carbon

Hard Carbons (Union Carbide YBD, BNFL) were lightly abraded to remove rough edges and finished with 4/0; 3/0 dry papers. They were then ultrasonically cleaned in water followed by drying at 100°C in an oven.

3.7 CLEANING OF GLASSWARE AND GLASS CELLS

The procedure adopted for cleaning the fluorine cell was described earlier.

All glass cells and flasks were cleaned before each experiment. This involved a preliminary wash with water followed by complete immersion in an acid cleaning mixture comprising 50% by volume concentrated nitric acid and 50% by volume concentrated sulphuric acid. Generally glassware was allowed to soak for 24 hours before being thoroughly washed with thrice distilled water and dried in an oven at 120°C.

On other occasions glassware was cleaned using alcoholic KOH solution in which case glassware was only allowed to soak for two to three hours before being rinsed thoroughly with thrice distilled water.

TABLE 3.1

Composition of electrolytes used for fluorine evolution.

ELECTROLYTE	HF %wt	H_2O %wt	Fe	Ni	Cu	Pb	Cr	Co	V
					ppm				
Typical Industrial Unconditioned Electrolyte (BNFL)	40.5	0.23	280	10	5	310	ND	ND	ND
Pure Electrolyte Prepared from Addition of HF to KF.HF	43	0.1	12	10	5	20	ND	ND	ND

ND = Not Determined

Figure 3.1

THE FLUORINE CELL TOP

The drawings are to scale and dimensions are in mm. The upper drawing is a plan view of the cell top, showing the entry points for the various components of the cell, whilst the lower is a cross-sectional view.

C Counter Electrode

E Gas Exhaust

G Gas Bubbler

P Gas Purger

R Reference Electrode

S Bubble Scraper

W Working Electrode

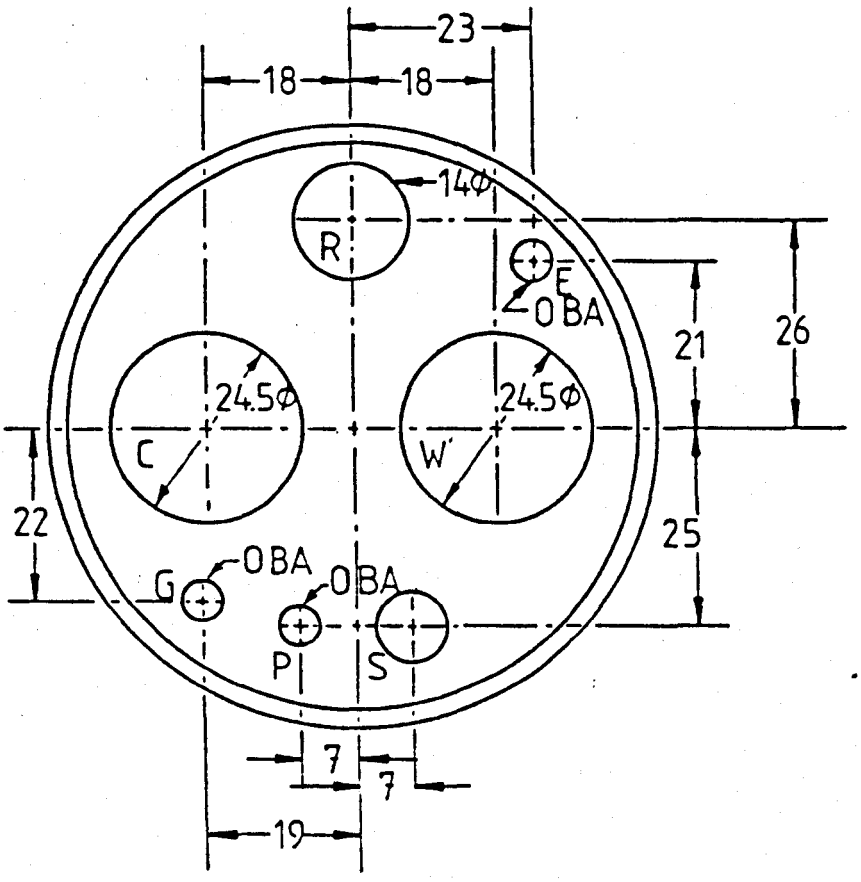
23
18
18
14Φ
R
E
OBA
21
26
24.5Φ
24.5Φ
C
W
22
25
G
OBA
OBA
P
S
7
7
19

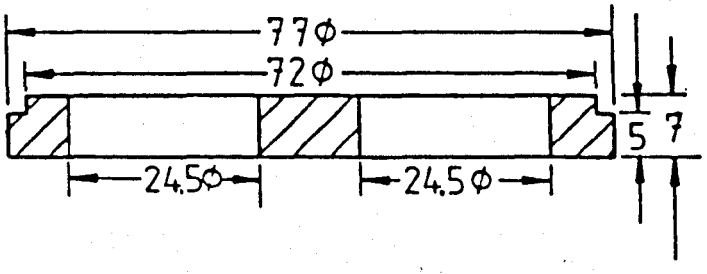
77Φ
72Φ
5
7
24.5Φ
24.5Φ

Figure 3.2

FLUORINE CELL WORKING ELECTRODE

Cross sectional view of an embedded carbon disc working electrode.

The drawing is 7x actual size and dimensions are in mm.

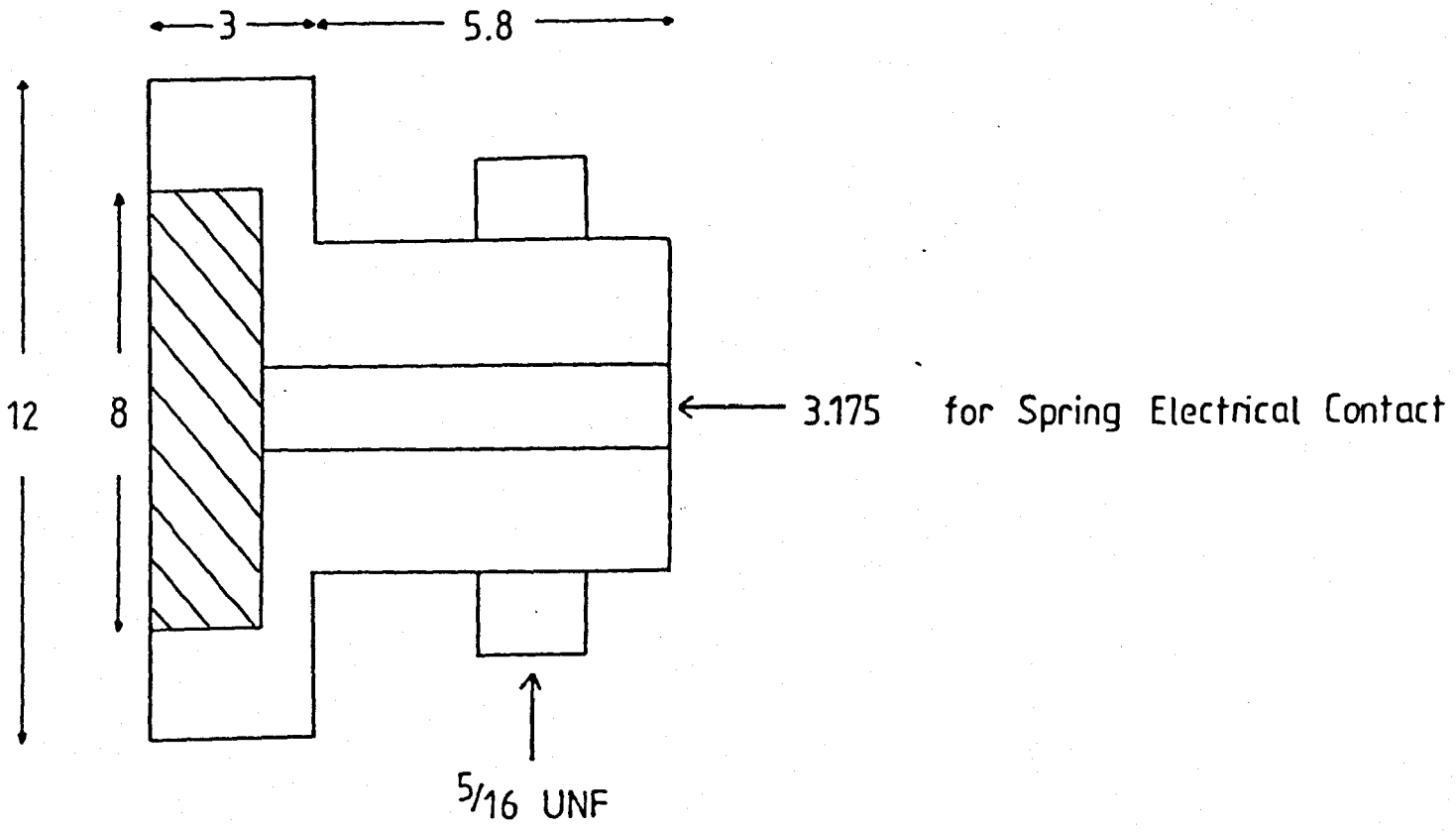
3
5.8
12
8
3.175
for Spring Electrical Contact
5/16 UNF

Figure 3.3

FLUORINE CELL WORKING ELECTRODE HOLDER

A. Cross sectional view, dimensions are in mm and drawing is twice scale.

B. Isometric view of the assembled working electrode.

A

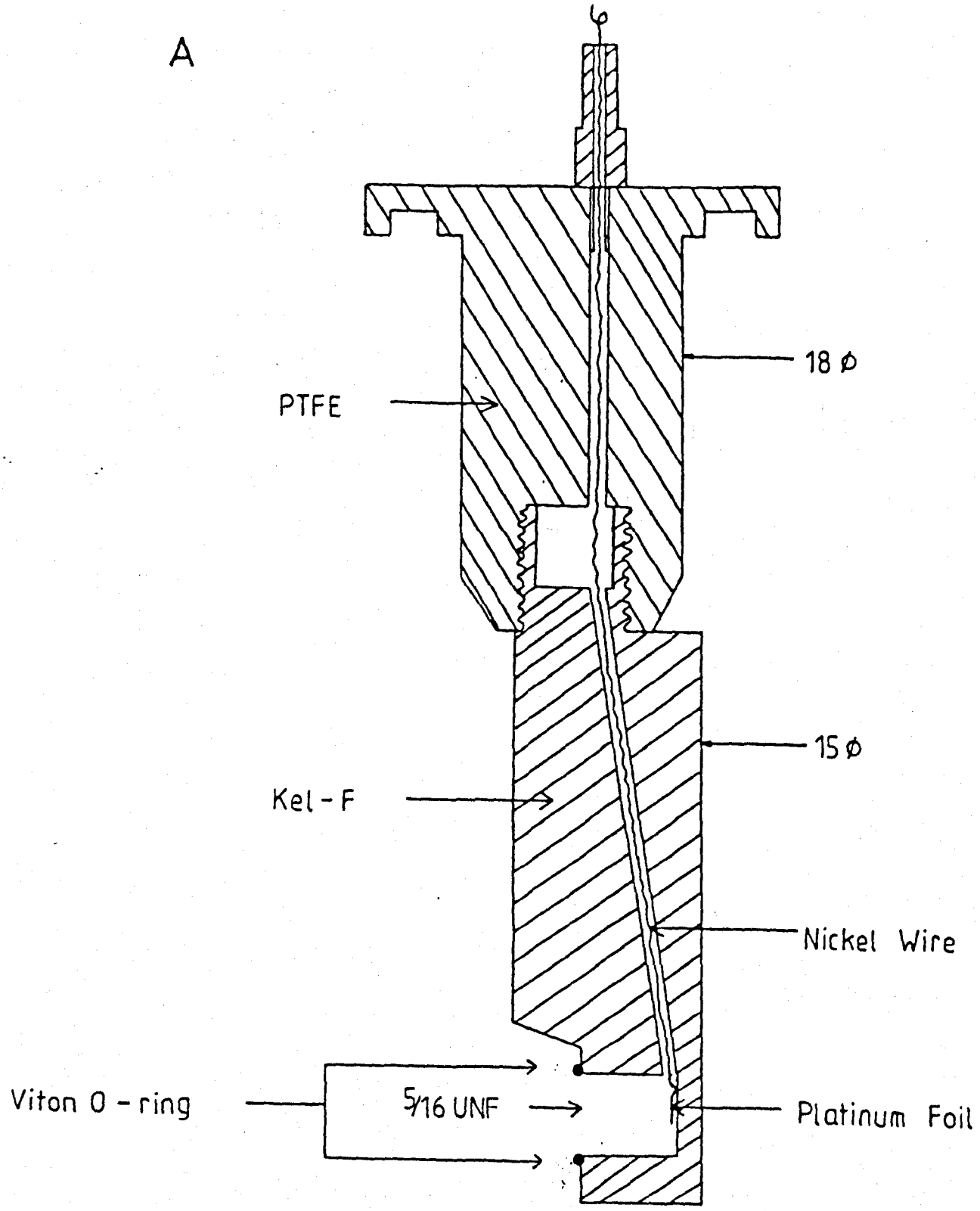
18 ø
PTFE
15 ø
Kel - F
Nickel Wire
Viton O - ring
5/16 UNF
Platinum Foil

B

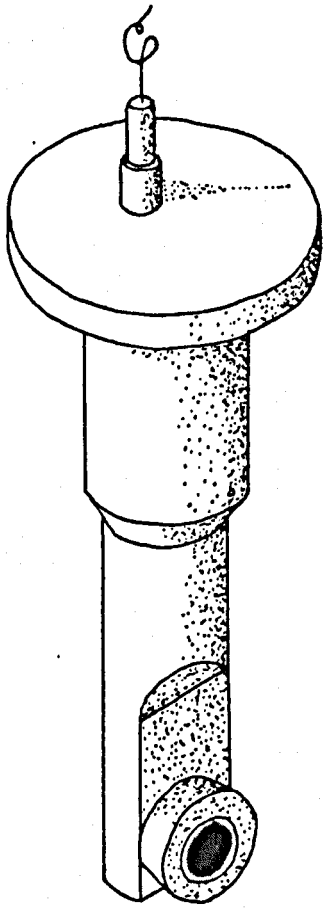

Figure 3.4

FLUORINE CELL REFERENCE ELECTRODE

On the right is an isometric (partial section) view.

On the left is a cross-section view.

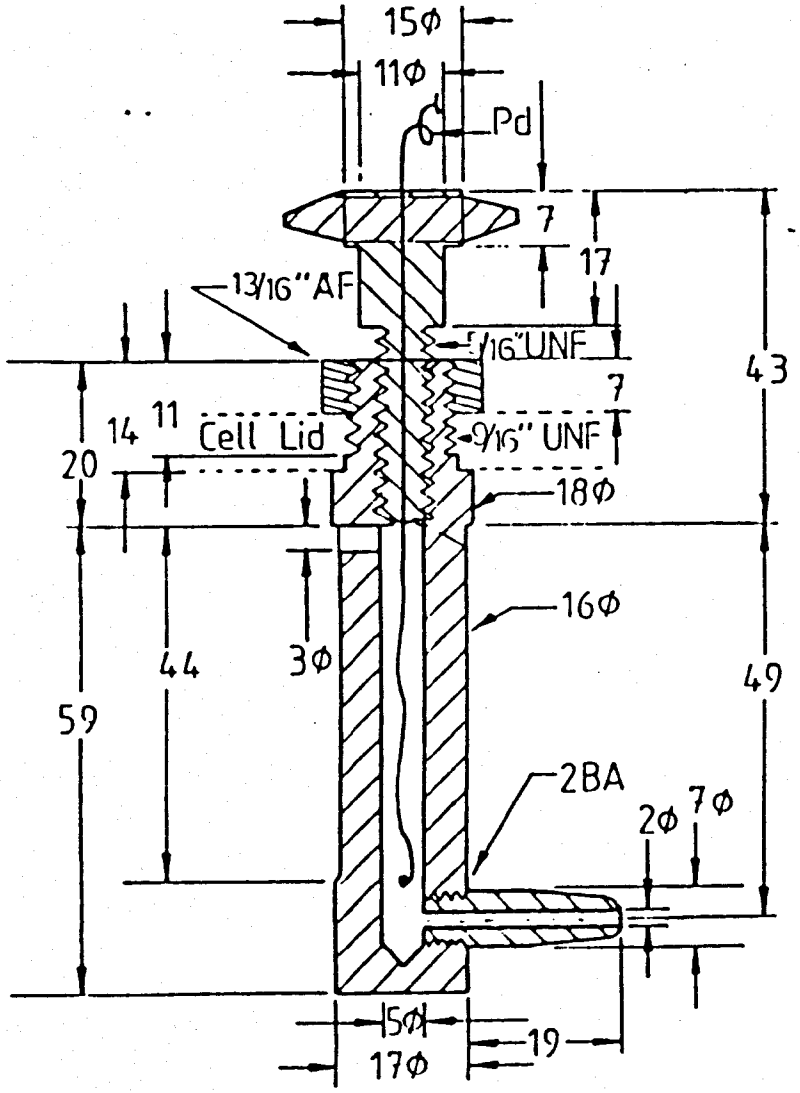
15Φ
11Φ
Pd
7
17
13/16" AF
5/16" UNF
7
43
14
11
Cell Lid
9/16" UNF
20
18Φ
16Φ
44
3Φ
49
59
2BA
2Φ
7Φ
5Φ
19
17Φ

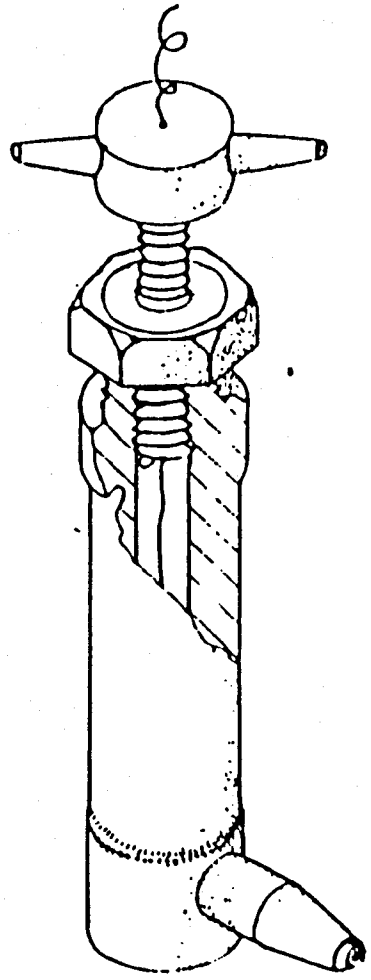

Figure 3.5

FLUORINE CELL WORKING ELECTRODE SHROUD

Upper drawing is a cross-sectional view. The lower drawing is an isometric view. Dimensions are in mm.

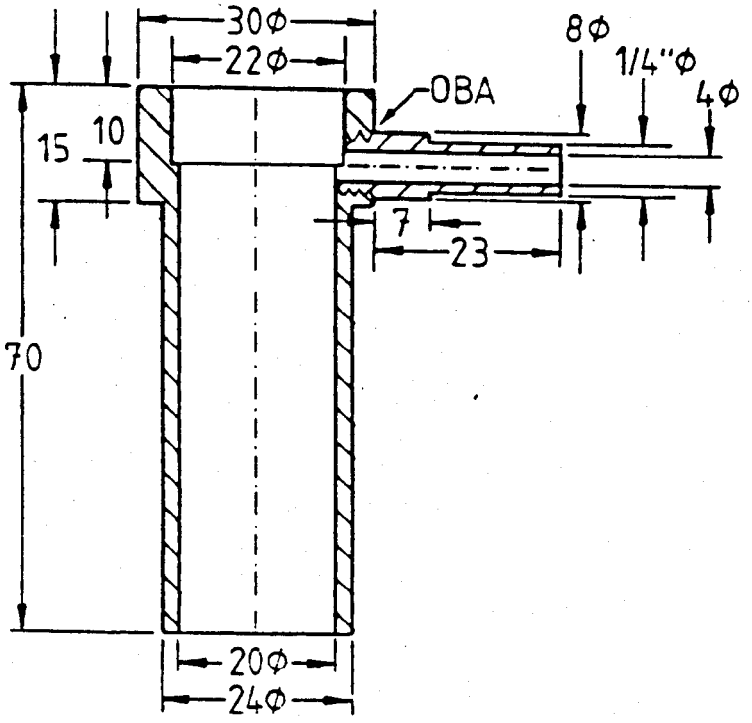
30Φ
22Φ
OBA
8Φ
1/4"Φ
4Φ
15
10
7
23
70
20Φ
24Φ

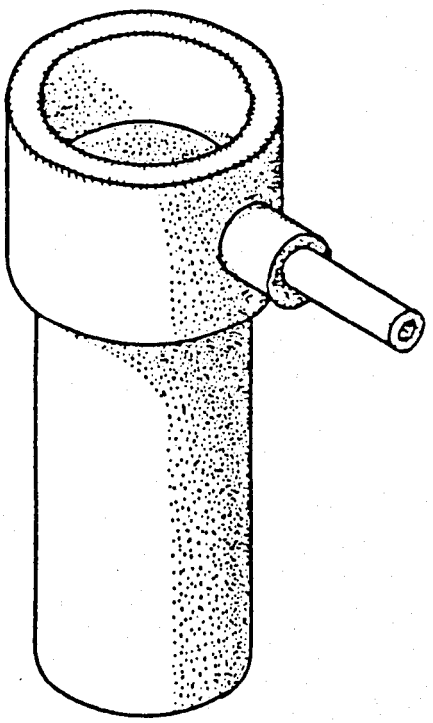

Figure 3.6

FLUORINE CELL COUNTER ELECTRODE SHROUD

The upper drawing is a cross-sectional view. The lower drawing is an isometric view. Dimensions are in mm.

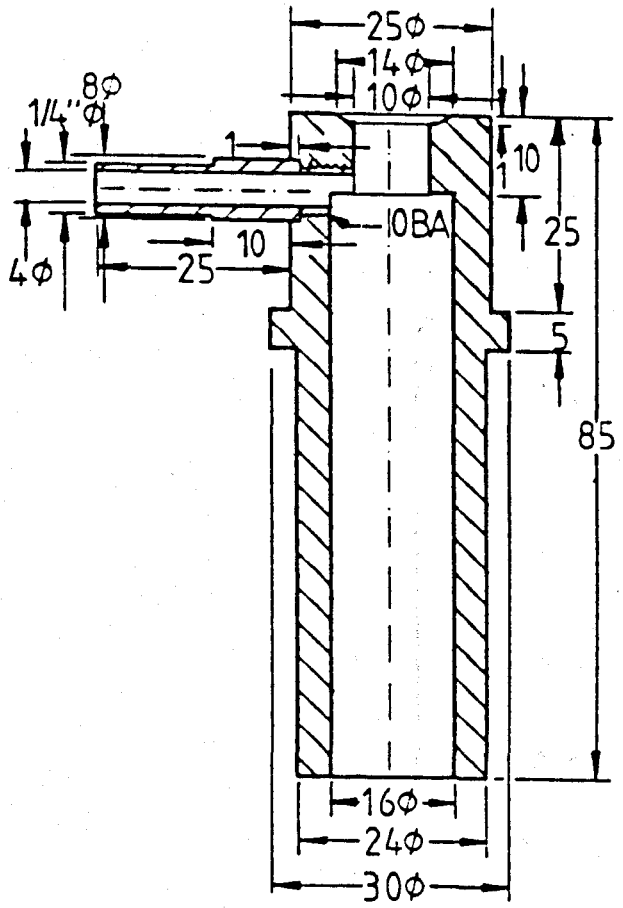
25Φ
14Φ
10Φ
1/4"
8Φ
1
10
1
10BA
25
10
25
4Φ
5
85
16Φ
24Φ
30Φ

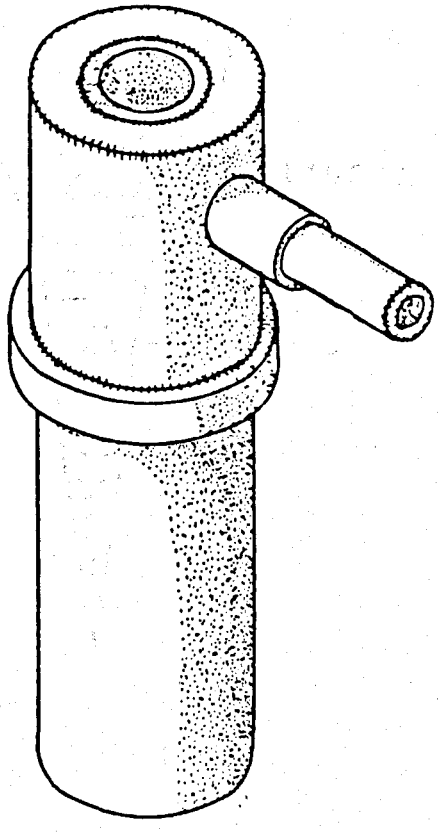

Figure 3.7

Fluorine Cell Hydrometer

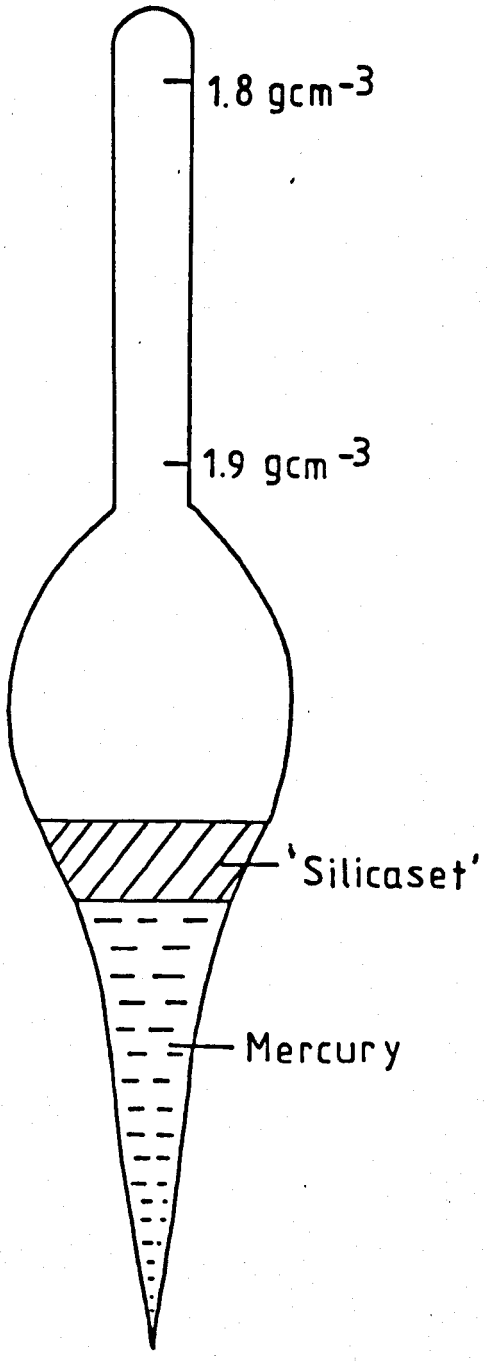

Figure 3.8

THE FLUORINE CELL HEATER

An isometric view of the cell heating assembly.

Materials of Construction :

A) Aluminium

B) Brass

C) Tubular Steel

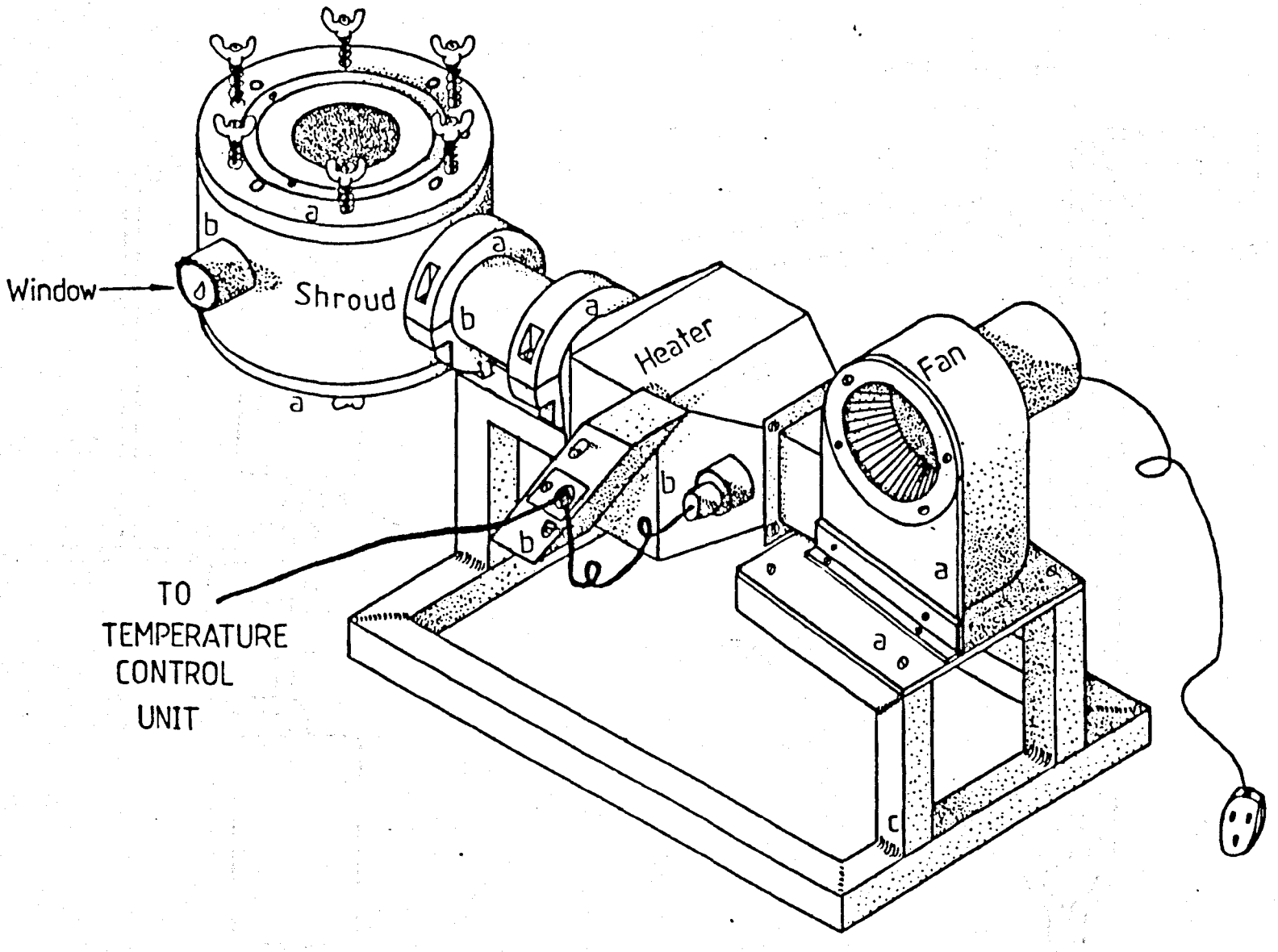
Window
Shroud
Heater
Fan
TO
TEMPERATURE
CONTROL
UNIT
a
b
c

Figure 3.9

Distillation Apparatus for Solvent Purification.

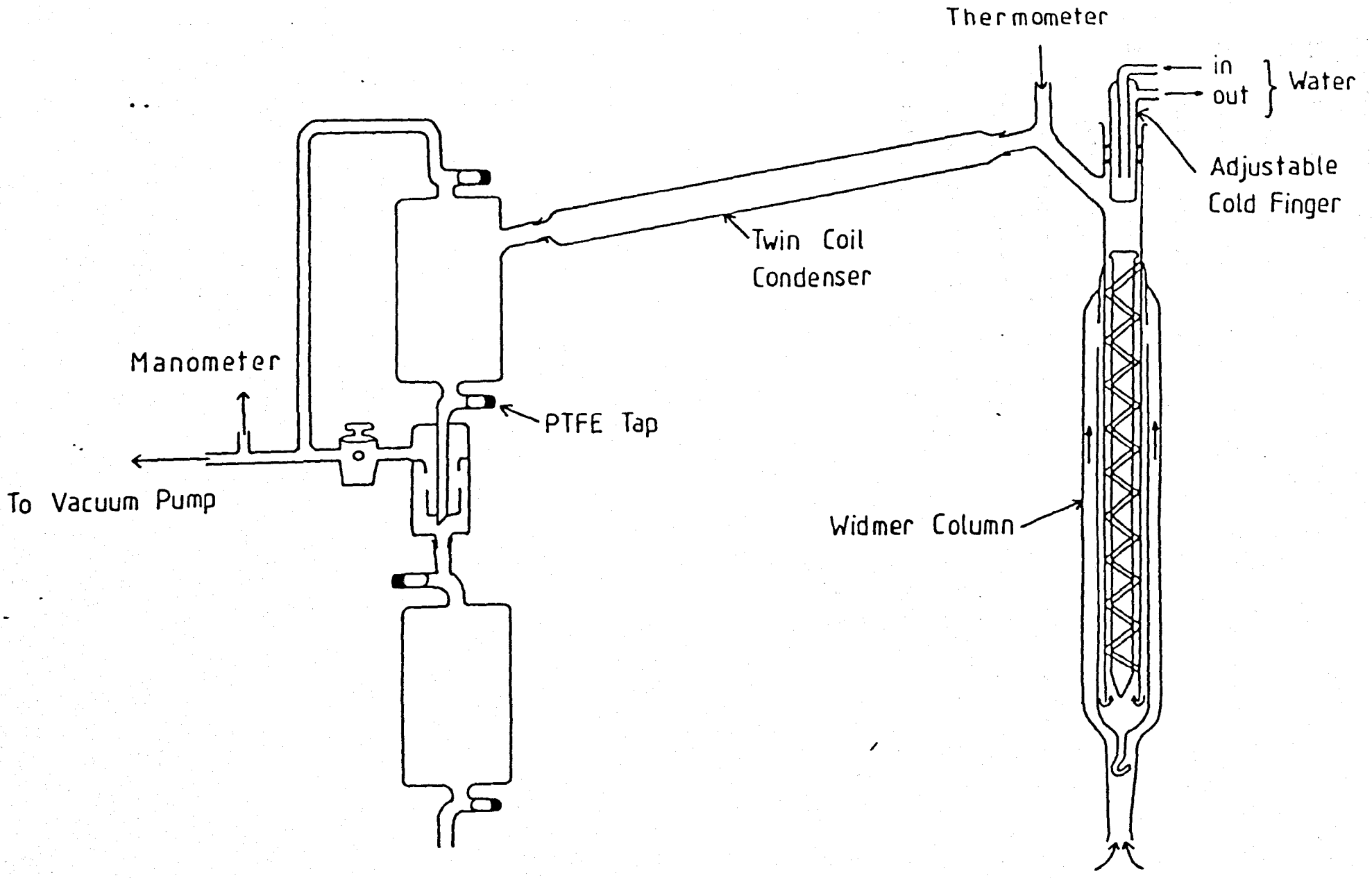

3.8 REFERENCES

1. B.M Ikeda, Ph.D. Thesis, University of Newcastle upon Tyne, (1982).
2. M.J. Wilmott, M.Sc. Thesis, University of Newcastle upon Tyne, (1983).
3. H.H. Rogers, S. Evans and J.H. Johnson, J.Electrochem.Soc. 111, 701, (1964).
4. C.K. Mann in "Electroanalytical Chemistry", ed. A.J. Bard, Dekker Publishing Co., N.Y. 3, 57, (1967).
5. M. Walters and L. Ramely, Anal.Chem. 45, 165, (1973).

CHAPTER 4

STUDIES IN KF.2HF ELECTROLYTE AT 85°C

4.1 INTRODUCTION

The experiments described in this chapter investigate the kinetics and mechanism of fluorine evolution at carbon anodes. In particular an attempt is made to account for the large overvoltage observed with fluorine cells.

The techniques used have included cyclic voltammetry, a.c. impedance, potential step and steady state electrolysis.

Unless otherwise stated, results presented were obtained in a pure electrolyte prepared in these laboratories, having a composition shown in Table 3.1. Other results were obtained using industrial electrolytes, but features were often obscured by the presence of metal impurities.

4.2 CYCLIC VOLTAMMETRY

Cyclic voltammograms were recorded at vitreous carbon, pyrolytic graphite and Union Carbide YBD carbon electrodes. The effects of sweep rate and potential range were investigated.

4.2.1 Vitreous Carbon Anodes

Voltammograms were recorded over the range -1.0V to 3.5V. Voltammograms recorded at $1Vs^{-1}$ are shown in Figure 4.1. The first cycle and steady state voltammograms are presented.

Using a fresh electrode the voltammogram currents were always highest on the first scan. An anodic peak was observed on the positive-going sweep at 2.0V and a

cathodic peak on the negative-going sweep was observed at -0.5V.

If the potential limits were set between 0V and 3.5V an anodic peak was obtained at 2.0V on the first sweep, but on the second sweep no peak was obtained (Figure 4.2). Similarly, if the potential limits were -1.0V and 0.5V no cathodic peak was observed, Figure 4.3.This seems to indicate that the peaks at 2.0V and -0.5V are electrochemically coupled, i.e. are the anodic and cathodic peaks for a single surface process.

The effect of sweep rate was examined over the range -1.0V to 3.5V. Sweep rates were varied between $0.1Vs^{-1}$ and $10Vs^{-1}$. The results of these measurements are shown in Table 4.1.

The charge, Q_a associated with the anodic peak was found to increase with decreasing sweep rate. At a given sweep rate the cathodic charge was similar to the anodic charge. Variations between vitreous carbon electrodes were found especially at slow sweep rates. In some cases at $0.1Vs^{-1}$ Q_a could be as high as $10mCcm^{-2}$. The results shown in Table 4.1 all refer to the same electrode.

Plots of I_{pa} against ν and $\nu^{\frac{1}{2}}$ are shown in Figure 4.4, and show that I_{pa} is proportional neither to ν nor $\nu^{\frac{1}{2}}$, both plots being non-linear.

4.2.2 Effect of Fluorine Evolution Pretreatment

The effect of previous fluorine evolution on the cyclic voltammograms was examined. In this case the voltammograms were recorded over the range 3.5V to -1.0V

i.e. starting at the positive limit to prevent reduction of any fluoride films formed during fluorine evolution.

The effect of holding the potential at 3.5V between sweeps was also investigated. It was found that with increasing time at 3.5V the anodic peak current at 2.0V increased on the subsequent scan. These results are shown in Table 4.2.

This increase in peak current was attributed to a surface roughening due to fluorine evolution at 3.5V. The cathodic currents were also observed to increase relative to the fresh electrode surface.

Vitreous carbon electrodes were subjected to electrolyses at electrode potentials in the sequence 4V, 5V, 6V, 7V and 8V for thirty minutes in each case.

After each electrolysis the scan behaviour was recorded over the range 3.5V to -1.0V. Two experiments were performed in each case. The first was to record the scan behaviour immediately after fluorine evolution; the second was to record after removal of the gas film by disturbing the electrode.

After evolution of fluorine at 4V the original cathodic peak at -0.5V was seen to move more positive to -0.1V. No new peaks developed, and the charges under the anodic and cathodic peaks were equal. Repeating the voltammetric experiment after removal of the electrode and immediate replacement showed a slight increase in both the anodic and cathodic peak currents, and is attributed to removal of residual fluorine from the electrode surface, Figure 4.5.

The voltammogram recorded immediately after

evolution of fluorine at 5V is shown in Figure 4.6. On the first sweep a large cathodic peak was observed at -0.75V; this peak was not observed on subsequent scans, but a cathodic peak at -0.2V was apparent. After removal of the fluorine gas film the first scan showed peaks at -0.75V and -0.2V. Only the peak at -0.2V was seen on subsequent scans, Figure 4.7. Removal of the electrode a second time did not result in the reappearance of the peak at -0.75V. It was noted however, that fluorine currents at 3.5V had increased (Figure 4.8) probably due to surface roughening.

Immediately after evolution of fluorine at 6V the scan recorded over the range 3.5V to -1.0V appeared as shown in Figure 4.9. The anodic peak at 2.0V was small and no cathodic peak was observed. After removal of the gas film the voltammogram appeared as in Figure 4.10. The anodic peak current had increased and an ill-defined cathodic peak at -0.5V was observed.

The scan recorded immediately after fluorine evolution at 7V is shown in Figure 4.11. No peaks, anodic or cathodic, were observed. Removal of the gas film resulted in only a slight increase in currents, the peak at 2.0V reappearing, Figure 4.12.

The scan recorded immediately after evolution of fluorine at 8V is shown in Figure 4.13. The electrode is very inactive. Removal of the fluorine gas layer resulted in a slight increase in the currents (Figure 4.14).

It was noted that, after removal of the gas film from electrodes which had been exposed to fluorine at

potentials of 6V or less, both hydrogen evolution and fluorine evolution currents were larger than on a fresh electrode, and indeed increased with increasing potential of electrolysis. However at potentials of 7 and 8V both the FER and HER currents were lower than on a fresh electrode.

Following electrolysis at 8V it was found that the sweep over the range 3.5 to -1.0V was as shown in Figure 4.14. If the electrode was then held at -1.0V for 30 minutes, and the sweep recorded after this period over the range -1.0V to 3.5V (Figure 4.15) the anodic peak at 2.0V was again seen, and a cathodic peak was observed at -0.5V.

The voltammogram recorded at fresh vitreous carbon over the range -1.0V to 3.5V is shown in Figure 4.1. The addition of water to the electrolyte, so that the melt was 1.0M in water, had no effect on the voltammogram obtained. The addition of nickel to the melt as NiF_2 ($1x10^{-2}M$) also had no effect on the voltammogram.

4.2.3 Other Electrode Materials

Sweep results were also obtained on pyrolytic graphites, both basal plane and edge orientation, and on Union Carbide YBD hard carbons.

Figure 4.16 shows the steady state voltammogram obtained with pyrolytic graphite of basal plane orientation. A pair of coupled peaks are obtained. The anodic peak was observed at 2.5V whilst the cathodic peak was found at 1.7V. Evidence for the coupling of

these peaks was obtained by limiting the scan range. On scanning from 1.8V to 3.5V an anodic peak was observed on the first positive sweep but not on the second. Using the scan range -0.5V to 1.75V at a fresh electrode no cathodic reducion peak was observed. Voltammograms always showed highest currents on the first sweep with a fresh electrode. This was true for all electrode materials.

Pyrolytic graphites with edge orientation gave a steady state voltammogram as shown in Figure 4.17. The anodic peak appeared at 2.2V but no significant cathodic peak is obtained.

Union Carbide YBD anodes gave an anodic peak on the positive scan at 2.1V with a cathodic peak on the negative scan at -0.4V (Figure 4.18).

Addition of lithium fluoride (0.29M) had no effect on the scan behaviour over the range -1.0V to 2.6V.

4.2.4 Discussion of Cyclic Voltammetric Results.

The peak observed at 2.0V has been attributed to the decomposition of water.[3] However, it appears from this work that this explanation is unsatisfactory, as addition of water to the molten KF.2HF had no effect on the observed voltammetric behaviour. Also, all melts were pre-electrolysed for 24hrs by evolution of fluorine at ~6V before measurements were made. It is therefore unlikely that this peak is due to decomposition of water.

On limiting the scan range between 0.5 and 3.5V for vitreous carbon electrodes an anodic peak was only

obtained on the first scan and no peak was obtained on subsequent scans. This points towards formation of an anodic film at the electrode surface on the forward scan which cannot be reduced above 0.5V. Table 4.3 indicates the thermodynamic formation potentials for various carbon fluorides at 85°C in KF.2HF.[4]

Currents on the first sweep at a fresh carbon electrode were always higher than on subsequent sweeps. It is likely that the number of favourable sites for fluorination is highest at the fresh electrode surface and the fall in current on subsequent scans indicates a fall in the number of available sites for fluorination. On examination of the thermodynamic formation potentials for various fluorocarbons it is also likely that carbon tetrafluoride is also produced on the first sweep, a peak in current being observed as a result of the simultaneous formation of an inhibiting CF_x compound at the electrode surface. The stationary voltammogram shows that the process occurring at 2.0V is coupled to a cathodic process between 0 and -0.5V. The cathodic process could therefore be reduction of the CF_x species formed anodically at 2.0V.

Adsorption of fluoride ion may also result in a peak at 2.0V but such a process is likely to be more reversible than is observed, with desorption occurring before 0V.

In the stationary state the possibility of intercalation of K^+ into $(CF_x)_n$ exists. K^+ could be intercalated on the negative sweeps with the reverse process occurring on the anodic sweep. Intercalation of

K^+ into graphite to produce C_8K is known.[5] Intercalation of lithium into graphite fluoride should be easier than intercalation of potassium. For this reason lithium fluoride was added to the melt to investigate whether new peaks occurred in the cyclic voltammogram in the presence of lithium. No difference was observed when pyrolytic graphite (basal plane orientation) was cycled in the presence of lithium, the voltammograms being the same as in the absence of lithium. However, it was noted that with basal plane orientation a peak which was very small was obtained at about 1.8V. This peak was never observed on the first scan, but was always present on subsequent scans. It was only observed with pyrolytic graphite of basal plane orientation. This peak could be due to intercalation of K^+ into the $(CF_x)_n$ produced on the first positive sweep. Addition of lithium did not show any effect on the voltammogram, however, and it is difficult to draw mechanistic conclusions from the cyclic voltammetric data.

It was noted that in the region 2.5V to 3.0V the anodic current never falls to zero, indicating that the electrode is not totally passivated. The current at 2.5V increases with increasing sweep rate indicating that a faradaic process is occurring on the "passivated" electrode: most probably fluorine evolution. It is unlikely that these currents are due to a thermal or chemical decomposition of the "passivating" layer as such processes would not be expected to increase with increasing sweep rate.

From a thermodynamic viewpoint free fluorine cannot

coexist in contact with a carbon electrode. Even at electrode potentials negative to fluorine evolution it is probable that a film of $(CF_x)_n$ forms on the anode surface. It may be easier to intercalate K^+ into the $(CF_x)_n$ polymer than into a free carbon surface but these cyclic voltammetric results have not presented evidence for K^+ intercalation into $(CF_x)_n$. The peaks observed on negative sweeps are therefore attributed to reduction of the $(CF_x)_n$ formed on the positive sweeps.

Comparison of the results obtained on basal plane orientation graphite with those obtained on edge orientation graphite indicate that the $(CF_x)_n$ polymer produced on the basal plane is easier to reduce than that obtained with edge orientation material. This is consistent with the results of Watanabe.[6] This difference in activity can be explained in terms of the number of sites available for fluorination with each material, and indeed Cadman et al.[7] showed that the edge orientation of graphite is fluorinated three times faster than the plane orientaton. The basal plane presents an ordered array of aromatic rings with few C-H bonds whereas the edge orientation presents a surface with many more C-H bonds which will be easily fluorinated. Therefore, the edge orientation becomes more heavily fluorinated and the $(CF_x)_n$ is more difficult to reduce than with the basal plane orientation.

The effect of evolution of fluorine on the sweep behaviour observed over the range -1.0V to 3.5V was examined. As the potential of fluorination was made more

positive the electrodes became less active over the range -1.0V to 3.5V. The $-(CF_x)_n-$ polymer became more difficult to reduce and indeed the results indicate more than one type of $(CF_x)_n$ is produced, consistant with XPS and SIMS studies (Chapter 5). It is not possible from these sweep results to identify potential regions where a specific carbon fluoride is produced. It is probable that the reason why the carbon fluoride becomes more difficult to reduce is not only due to formation of a new material (more intensive fluorination) but also to more extensive fluorination at higher potentials.

The theoretical formation potential of F_2 from HF is 2.89V.[1,2] The mechanism for fluorine evolution can be divided into two regions.

Potentials less than 3.0V

Processes occurring below 3.0V might include

i) $C + 4HF \longrightarrow CF_4 + 2H_2 \quad E^o = 1.27V$

ii) $C + xHF \rightleftharpoons CF_x + x/2\ H_2 \quad E^o = = 1.4V$

The reversibility of reaction ii) decreases as the value of x approaches 1.

Potentials greater than 3.0V

$$HF_2^- \longrightarrow HF + F^\cdot + e^-$$

$$2F^\cdot \longrightarrow F_2$$

$$nC + nF^\cdot \longrightarrow (CF)_n$$

$$(CF)_n + F^\cdot \longrightarrow CF_2 + CF_4$$

$$CF_{0.5} + \tfrac{1}{2}F^\cdot \longrightarrow CF_{1.0}$$

etc.

4.2.5 Fast Scan Cyclic Voltammetry

Using a stationary electrode poses problems when investigating the kinetics of the fluorine evolution reaction. As fluorine is not easily released from the anode surface, the electrode area continuously changes. As already stated, a film, the nature of which is potential-dependent, is also formed on the electrode surface during fluorine evolution. It was hoped that, by utilising fast potential scans, the electrode surface would be only minimally altered during the course of the experiment, and also that fluorine bubbles would not have sufficient time to form to alter the accessible surface area of the electrode.

Cyclic voltammetry was performed over the range 0 to 5V at $10Vs^{-1}$ and $50Vs^{-1}$. Such measurements were performed using all forms of commercial carbon:

vitreous, pyrolytic graphites and YBD hard carbon.

Hysteresis was obtained in the fluorine evolution region with all types of carbon material. Figure 4.19 shows voltammograms at $10Vs^{-1}$ for various anode materials. A Tafel plot for a pyrolytic graphite anode with face orientation is shown in Figure 4.20. It is not possible to obtain kinetic information from such a plot, which merely indicates the difficulty in studying kinetics of the fluorine evolution reaction. Similar plots were obtained at all anode materials.

The fact that linear Tafel plots are not obtained highlights that, even on fast scan, the electrode surface is continually changing. Kinetic studies using sweep voltammetry of the fluorine evolution reaction are unsuccessful using a stationary electrode.

4.3 IMPEDANCE STUDIES

4.3.1 Introduction

In the absence of any electrode reaction, the interface between an electrolyte solution and a smooth, non-porous electrode gives an impedance spectrum consisting of a vertical line, corresponding to the double layer capacitance in series with the ohmic resistance of the layer of electrolyte between the electrode surface and the tip of the reference electrode probe. The double-layer capacitance can be evaluated from the high-frequency part of the spectrum, using the relation

$$C_{dl} = (2\pi f Z'')^{-1}$$

where f = frequency, Z" = imaginary part of the impedance and C_{dl} is the capacitance of the double layer.

Double layer capacitance studies have been made by various workers using vitreous carbon electrodes,[8,9,10] and it has been found that at no potential is such an electrode ideally polarizable. In this study electrodes were examined in sulphuric acid solutions in order to characterise them before studies were performed in KF.2HF molten salt electrolyte.

4.3.2 Capacitance Studies in Sulphuric Acid Solution

Double layer capacitance studies were made over the range -0.9V to +0.6V (vs Hg/Hg_2SO_4) in 0.5M sulphuric acid. Vitreous carbon electrodes were cleaned in the

usual way with diamond polishing compounds. Electrodes were allowed to equilibrate at each measurement potential for five minutes before measurements were made. Impedance plots were taken over the range 100kHz to 1Hz and capacitance values were calculated at the high frequency end of the spectrum. A typical impedance plot for a vitreous carbon anode in 0.5M H_2SO_4 at 0.2V (vs Hg_2SO_4) is shown in Figure 4.21. Typical values for the double layer capacitance on edge orientation graphite and YBD hard carbon electrodes were found to be 100μFcm^{-2} and 80μFcm^{-2} respectively. The geometric area for these electrodes was 0.5cm^2. A planar electrode would be expected to give rise to a double layer capacitance of 10-20μFcm^{-2}. This indicates that the actual area of such electrodes is at least five times larger than the geometric area.

Pyrolytic graphite face orientation and vitreous carbon electrodes were examined over the range -900mV to +600mV (vs Hg/Hg_2SO_4) at 100mV intervals. Capacitance results are displayed in Figures 4.22 and 4.23 respectively.

4.3.3 Measurements in KF.2HF

Interfacial impedance measurements were made using vitreous carbon and face orientation pyrolytic graphite electrodes, in KF.2HF at potentials from 0V to 2.6V (vs Pd/H_2). Above 1V a semicircle was obtained, the diameter of which did not change significantly on increasing the potential (Figure 4.24). On returning the potential from 2.6V to 0V in 0.2V increments the diameter of this

semicircle increased as 1V was approached (Figure 4.25). Below 1V a semicircle was not obtained.

Analysis of the raw impedance data afforded the parallel capacitance, C_p. Plots of C_p as a function of potential for vitreous carbon and face orientation graphites are shown in Figures 4.26 and 4.27 respectively. A peak in capacitance was observed at a potential in the region 0.4V - 0.6V, on both types of material. Above these potentials the capacitance was seen to fall dramatically. In the case of vitreous carbon the fall is from above $35\mu Fcm^{-2}$ at 0.5V to $3\mu Fcm^{-2}$ by 1.3V and to $0.3\mu Fcm^{-2}$ at 2.0V. This seems to indicate that an insulating film is formed well before significant steady state fluorine evolution occurs. As the potential is made more negative from 2.6V to 0V, the capacitance remains very low all the way to 0V using a vitreous carbon electrode. Holding such an electrode at 0V for ten minutes did not result in any significant recovery with vitreous carbon electrodes and the capacitance remains very low as the potential is made more positive from 0V to 1.0V. However, when the electrode used was face orientation pyrolytic graphite a capacitance increase was observed from about 0.6V as the potential was made more negative. Holding the potential at 0V for ten minutes resulted in a further increase and a capacitance peak was again observed as the potential was made more positive from 0V to 1.0V.

The face orientation of pyrolytic graphite was used to examine the time dependent impedances at various potentials between 0 and 2.4V.

At 2.4V a semicircle was obtained. The time dependences of the parallel capacitance and of R_{ct}, the diameter of the semicircle, are shown in Figure 4.28. There is an increase in R_{ct} and a decrease in capacitance, again further evidence for formation of a resistive film on the anode surface before fluorine evolution has occurred. Having held the electrode at 2.4V for 16 hours the potential was returned to 0V and the impedance monitored with time (Figure 4.29). The capacitance recovered to the original value exhibited at 0V before treatment at 2.4V.

Time-dependent measurements of capacitance values were also made at 0.6, 1.0 1.2, 1.3 and 1.4V. At potentials above 1.0V the capacitance fell with time (Figure 4.30), whereas at 0.6V the capacitance increased with time (Figure 4.31). This indicates that the film formed on the pyrolytic graphite face anode is stable to reduction above 0.8±0.2V. The recovery of capacitance was also monitored as a function of time at -0.5V and was found to be similar to that measured at 0V (Figure 4.29).

These measurements indicate that there is an insulating film produced on carbon anodes in KF.2HF melts well below the potential at which fluorine is evolved. This film can be reduced in the molten salt at potentials below 0.6V.

Interfacial capacitance measurements were made at 0.7V in KF.2HF following polarisation of vitreous carbon and face orientation graphites at various potentials in the range 3.5V to 8.0V where fluorine evolution occurs.

The potential 0.7V was chosen as a point at which little reduction of the fluoride film would be expected on the timescale of the impedance measurement. Electrodes were polarised at a given potential for thirty minutes. Fluorine gas was removed from the electrode surface by disturbing the electrode, and then an impedance plot was recorded at 0.7V. The results are shown in Table 4.4. The table contains values for film thicknesses obtained using the equation

$$d = \frac{\varepsilon\varepsilon_o}{C_d}$$

d = film thickness
ε = relative permittivity of the film
ε_o = permittivity of free space
C_d = double layer capacitance/area

The assumed model treats the interphase as a parallel plate capacitor. A value of the dielectric constant for $(CF_x)_n$ was assumed similar to that of PTFE and taken as 2.1.

It is to be noted that extremely large resistance values and large film thicknesses were obtained when pyrolytic graphite was used as an anode. This can be attributed to incomplete removal of the fluorine gas film before the impedance was recorded.

Redox kinetic measurements made in aqueous and non-aqueous solvents (Chapter 6) showed an increase in ohmic resistance after fluorination of an anode at about 7V to 8V. These impedance measurements made in the KF.2HF melt show an increase in the resistance after treatment at a potential of 5V to 6V. The conductivity

of carbon fluorides is known to decrease on increasing the fluorine content[11] and from these measurements it appears that a higher fluoride is produced above 5V.

It was found that, at a given time, the higher the potential of fluorination the larger was the resistive component of the impedance measured at 0.7V (Figure 4.32). The effect of time of fluorination was examined using vitreous carbon electrodes. At any one potential there was variation in the resistive component with time. Time-dependent measurements were therefore repeated and electrolysis was stopped at well defined points on the current-time curve. For this measurement comparison was made between the impedance obtained on stopping the electrolysis at a peak in current on the current-time trace (i.e. when fluorine was released from the electrode surface) with that obtained when the electrolysis was stopped at a trough in the current (i.e. the steady state fluorine evolution current). The results for vitreous carbons subjected to electrolysis at 5.0V and 8.0V were compared and are shown in Table 4.5.

It is seen that for a series of measurements made when the electrolysis was stopped after a current peak there is a general increase in resistance and decrease in capacitance with time at both 5.0V and 8.0V, the effect being more pronounced at 8.0V. There was more variation when measurements were made after the electrolysis at 5.0V was stopped in a current trough but the impedance appeared to be independent of the point at which the electrolysis at 8.0V was halted.

4.3.4 Capacitance Measurements in Other Solvents

In the course of redox kinetic measurements (Chapter 6) double layer capacitance values were determined in solvents other than KF.2HF for electrodes pretreated by fluorine evolution in KF.2HF. Both aqueous and non-aqueous electrolyte solutions were used.

Capacitance values for electrodes fluorinated at various potentials in KF.2HF were determined in aqueous potassium chloride electrolyte solutions and in acetonitrile/sodium perchlorate solutions. The results obtained were evaluated from high frequency impedance data at potentials of +300mV (vs saturated NaCl/Calomel) in acetonitrile and +230mV (vs saturated KCl/Calomel) in aqueous solutions. The capacitance values obtained are shown in Table 4.6. These capacitance results again indicate that there is a change in the nature of the film at 5 to 6V.

Capacitance values obtained in solvents other than KF.2HF were always higher than in KF.2HF itself. This indicated a change in the film on removal from the KF.2HF system.

The effect of immersion of fluorinated anodes in water and acetonitrile on the capacitance obtained at 0.7V in KF.2HF was studied.

Electrodes were fluorinated at 6V in KF.2HF for thirty minutes. The gas film was removed and the capacitance at 0.7V was determined in KF.2HF. Each anode was left at open circuit for ten minutes in the melt and a further measurement was then made at 0.7V in KF.2HF. The anode was then removed and kept in a desiccator for

ten minutes before being replaced in the KF.2HF melt where a further measurement was made at 0.7V. Following this the electrode was removed and immersed for ten minutes in either acetonitrile or water. Each electrode was then dried and a capacitance result obtained at 0.7V in the KF.2HF melt. The results are presented in Table 4.7.

The table shows that both water and acetonitrile do alter the nature of the film on the anode surface. For this reason the results obtained for the redox systems discussed in Chapter 6 were obtained as quickly as possible after transfer of the electrode.

Simple removal of the electrode from the system does not have any effect on the capacitance at 0.7V. However, if the electrode is left at open circuit in the melt a slight increase in the capacitance is obtained. This may be indicative of some thermal decomposition of the film at 90°C in KF.2HF.

4.4 POLARISATION MEASUREMENTS

4.4.1 Steady State Electrolysis in KF.2HF

Steady state currents were measured at vitreous carbon electrodes between -1.0V and 5.0V (vs Pd/H_2) in KF.2HF. The currents were recorded on a Chessel flat-bed recorder as a function of time and the mean steady currents were determined from these traces. The steady-state current-voltage curve is shown in Figure 4.33. The plot is quite featureless. Hydrogen evolution commences at -0.75V, whilst fluorine evolution starts above 3.25V. Currents measured above 3.0V will be

subject to bubble overvoltage and as such will not be a true representation of the steady-state current, as part of the electrode surface will be blocked by fluorine gas bubbles. A plot of log i against potential over the range 4.0V to 5.0V is shown in Figure 4.34. The Tafel slope of this plot is $0.69 V dec^{-1}$. This value has no significance because of the presence of increasingly severe bubble overvoltage.

Vitreous carbon electrodes were subjected to electrolysis in KF.2HF at potentials between 3V and 9V. The cell used allowed observation of the anodes as fluorine was being evolved at the electrode surface. The size of bubbles and coverage of the anode surface by bubbles was examined as a function of potential and the results are shown in Table 4.8. Bubbles were not produced until the potential was 4V. At 4V 70% of the electrode surface was covered by small spherical bubbles which easily detached from the electrode surface. As the potential was made more positive the extent of bubble coverage increased. At potentials between 5V and 9V at least 50% of the surface was covered by one bubble, which was lenticular. At 9V 80% of the electrode surface was covered by one bubble, and 15% was covered by smaller bubbles which detached from the surface easily resulting in fluctuations in the current-time trace. These results indicate that bubble overvoltage becomes more severe as the potential of electrolysis becomes more positive.

It is obvious from these results that in American fluorine cells where non-porous hard carbons are used as

anodes bubble overvoltages must be severe. The problem will not be so severe in UK fluorine cells where porous electrodes are used.

4.4.2 Potential Step Measurements

In an attempt to obtain polarisation data for the fluorine evolution reaction, potential step measurements were performed. In doing this it was hoped that bubble formation would not occur over the timescale of the experiment and so measured currents would correspond to a bubble-free surface.

Pulse measurements were carried out using a computer-controlled apparatus. Initially step measurements were of the form :

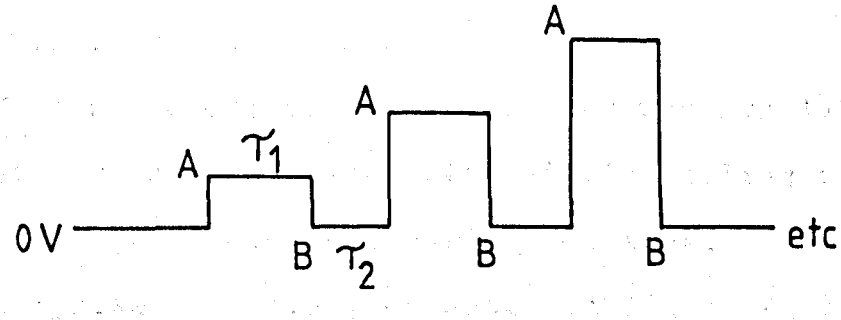

The B pulse was always to 0V and the time duration was 75s. It was intended that 75s was enough to reduce any species produced on the electrode surface after the A pulse which was 50ms at potentials between 3.7V and 5.1V. Currents were recorded during the A pulse. A falling transient was observed as shown in Figure 4.35 when the electrode used was either vitreous carbon, YBD or face-orientation graphite. A steady-state current was attained after 10ms. The steady state current was plotted against pulse potential and the results for

vitreous carbon, face-orientation graphite and YBD hard carbon are shown in Figure 4.36. None of these three types of electrode material gives rise to an exponential curve predicted from Tafel's Law. Currents are much larger when YBD or face orientation graphite is used. In the case of YBD electrodes the large currents are due to the larger surface area (relative to the geometric area) of the electrodes. In the case of the pyrolytic graphite electrodes the large currents obtained probably contain a significant contribution from the process of surface oxidation that occurs at 2.0V as shown by cyclic voltammetry; i.e. the currents are not solely fluorine evolution currents. Indeed with all types of electrode material, using this single pulse method gives rise to currents which include contributions due to surface oxidation.

When the electrode material used was pyrolytic graphite with edge orientation simple falling transients were not obtained. The transient obtained was dependent on the pulse potential, as shown in Figure 4.37. Steady-state currents were not obtained and the shape of the transient at higher potentials indicated that a gradual surface oxidation was occurring.

In order to obtain information about the fluorine evolution process alone, separate from the surface oxidation contribution, a double pulse method was used as outlined below.

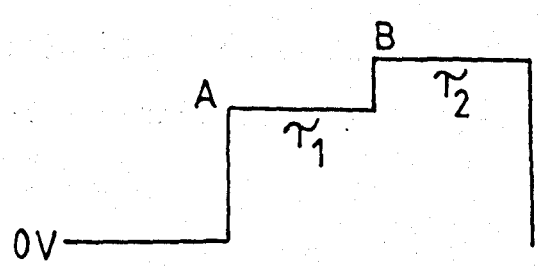

The A pulse was always to a potential of 3.0V for 5s (τ_1). The B pulse was to potentials in the region 4.0V to 5.2V for 200ms (τ_2). The duration of the A pulse was sufficient to cause complete surface oxidation due to the process occurring at 2.0V as observed by cyclic voltammetry; a subsequent pulse to 3.0V resulted in negligible currents. The potential was returned to the baseline value of 0V after each B pulse.

With all the electrode materials examined by this method falling transients were observed. At longer times the fall can be attributed to blockage of the electrode by fluorine gas bubbles. For each type of material the currents were measured at 1ms, 10ms and 100ms after the pulse and plotted as a function of pulse potential (Figures 4.38, 4.39, and 4.40). At all times with all materials the current-voltage relations were almost linear.

The effect of fluorine evolution was examined by comparing the currents obtained on pulsing from 3.0 to 5.0V at a fresh carbon surface and at one previously exposed to fluorine at 6V for 30 minutes. It was found that for all electrode materials the currents measured were significantly lower after the electrodes had been subjected to fluorine evolution (Figure 4.41).

Pulse measurements proved unsuccessful in determining kinetic parameters for the fluorine evolution reaction but again show the significance of the barrier to electron transfer presented by the formation of a carbon fluoride layer on the electrode surface.

4.4.2.1 Pulse Results in the Region 1.8V to 2.8V

The results presented in the section on cyclic voltammetry showed an anodic peak at 2.0V for all electrode materials on the positive-going scan.

To investigate the process occurring at 2.0V, single step potential pulse measurements were made over the range 1.8V to 2.8V. The baseline potential was 1V and a single step of 1.0s duration was made to the measurement potential. Instead of recording currents the amount of charge was recorded for each pulse (Figure 4.42). The charge was plotted as a function of potential. Both edge and face pyrolytic graphites showed a peak in the charge-potential curve at 2.3V, whereas the peak for vitreous carbon was at 2.6V (Figures 4.43 and 4.44). The charges for all materials are similar and correspond to formation of a surface film of several layers thickness (monolayer coverage would represent $0.3mCcm^{-2}$). It is probable that the process occurring at 2.0V is formation of a surface film, but formation of gaseous fluorocarbons such as CF_4 will also occur.

Another series of pulse measurements took the form :

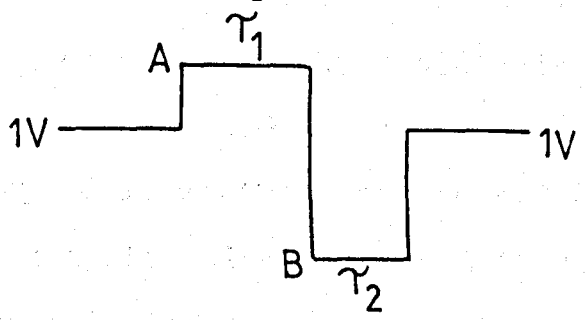

The A pulse was to a potential in the region 1.8V to 2.8V whilst the B pulse was always to 0V. The duration of each pulse was 100ms. The charge obtained in each pulse was recorded. The charge recorded on the negative

pulse was only 50% of the charge recorded on the positive pulse. Three explanations can be given for this. In the first the process occurring on the positive scan is due to fluoride film formation only, and only partial reduction of this film occurs on the negative pulse. In the second, the process occurring on the positive pulse is due to both surface oxidation and formation of gaseous fluorocarbon products and hence the cathodic charge due to surface reduction is less. In the third the fluoride film formed on the positive pulse decomposes thermally resulting in a decrease in the amount of cathodic charge obtained on pulsing to 0V.

4.4.3 Bubble Release Analysis

An alternative method for acquiring polarisation data was attempted. This involved recording the current transient immediately after the current had exceeded a pre-selected threshold value. When a bubble was released from the electrode surface the current rose initially; but decayed as a fresh bubble grew. Release of a bubble from the electrode surface would cause the current to exceed the pre-selected threshold value and thus a current transient would be recorded. Such measurements were attempted at vitreous carbon and at both types of pyrolytic graphite electrode at 6.0V in KF.2HF. When a bubble was released from the electrode surface the current peak observed was found to vary, indicating that variation in the amount of surface coverage occurred and that bubble release did not actually clear the whole electrode surface. After a bubble was released the

duration of the recorded transient was 1s. The variation in peak currents is shown in Table 4.9. The peak currents recorded never exceeded the current values obtained for the same electrodes by the double pulse technique, indicating again that the surface was still partially blocked by bubbles. Such measurements have proved of no use as a means of acquiring polarisation data corresponding to a bubble-free surface.

The mean steady-state currents at 6.0V for vitreous carbon and pyrolytic graphite are in the range 1 to 3mAcm^{-2}. Potential-pulse currents at 6.0V often exceeded 100mAcm^{-2}, indicating that during steady-state electrolysis only 1% or less of the electrode surface is actually not covered by bubbles. This is consistent with the visual observations of fluorine evolution discussed earlier in this chapter.

4.5 DISCUSSION OF RESULTS OBTAINED IN KF.2HF

The aim of this work was to distinguish between bubble overvoltage and overvoltage due to a fluoride film on the anode surface and to obtain polarisation data free from the former.

Visual observation of the electrode surface during fluorine evolution has shown that, at potentials greater than 5V (vs Pd/H_2) the electrode surface is more than 90% covered by fluorine gas bubbles. Evidently these bubbles will make a significant contribution to the cell voltage in an operating fluorine cell by causing a physical decrease in the operating surface area of the anode.

However, the results presented in this chapter show that an insulating film is produced on the anode surface at lower potentials than those required for fluorine evolution. In chapter 6 it will be shown that this film presents a significant barrier to electron transfer.

Cyclic voltammetry in the potential range preceding fluorine evolution has shown that an inhibiting surface film is formed on all carbon materials at potentials in the region of 2.0V (vs Pd/H_2). The anodic peak observed in the cyclic voltammetric experiments was shown not to be due to water electrolysis; added water had no effect on the observed currents. All melts were, in fact, pre-electrolysed at 6V for 24 hours in order to dry them by evolved fluorine. The cathodic processes which occurred during cyclic voltammetry experiments depended on the type of anode carbon used. However, the area under the cathodic portion of the steady state voltammograms was always similar to the area under the anodic part of the voltammogram, indicating that the cathodic process probably clears the surface of the carbon fluoride film formed in the anodic process. The peak observed at 2.0V was always largest when a fresh electrode was used and this fact was attributed to the formation of gaseous fluorocarbon products such as CF_4, C_2F_6 etc. The fluoride film formed on the anodic scans was shown to be stable against reduction above 0V for vitreous carbons and above 1.8V for face-orientation graphites. This was shown by limiting the potential range of the scan experiment.

If the scan range for vitreous carbon electrodes was limited to between 0 and 3.5V the peak in the region of 2.0V was only observed on the first positive sweep. Similarly, limiting the potential range to between 1.8V and 3.5V for face-orientation graphite resulted in an anodic peak on only the first positive scan.

Devilliers et al. have shown,[11] by mass spectroscopic analysis, that solid carbon fluorides produced during fluorine evolution are thermally decomposed at potentials in the region 85°C to 100°C to produce gaseous carbon fluorides such as CF_4. In the region 2.5V to 3.0V the anodic current never falls to zero. The current in this region increases with increasing sweep rate indicating that a non steady-state process is occurring.

Intercalation of cations into the anode during cyclic voltammetry should eventually disrupt the surface causing it to break up. Continued cyclic voltammetry had no effect on the anode surface and addition of lithium fluoride to the electrolyte also had no effect. It is unlikely, then, that the peaks observed in the voltammograms are due to intercalation and removal of ions.

Reduction of the carbon fluoride could simply be the reverse of its anodic formation from carbon and HF_2^- ions or alternatively a hydrogenation to partially-fluorinated hydrocarbons. In the latter case; continued cycling of the electrode would result in erosion of the anode. As no evidence was found for this it is likely that the cyclic voltammetric peaks are due

to the kinetically irreversible reaction:

$$nC + mF^- \longrightarrow me^- + C_nF_m$$

Voltammograms were found to vary depending on the anodic treatment of the carbons before cycling. It is likely that there are different degrees of fluorination of the carbon surface and there is no one single stoichiometric carbon fluoride on the anode surface at any given potential.

Tafel plots obtained from fast-scan voltammetry were non linear, indicating that the surface of the electrode is continually changing. It was impossible to extract kinetic information from such plots.

Interfacial impedance measurements also showed that a resistive film is produced on the anode surface long before fluorine evolution occurs. There is a large fall in the interfacial capacitance above 0.5V. This surface film was found to be reducible by holding the anode at a potential of 0V for ten minutes. The surface film on pyrolytic graphite face electrodes was found to be stable to reduction above 0.8 ± 0.2V.

Anodic treatment of the electrodes in KF.2HF followed by subsequent interfacial impedance measurements at 0.7V indicated that as the potential of electrolysis increased the thickness of the fluoride film on the anode surface increased or the relative permittivity falls. There was also an increase in the resistive component of the impedance as the potential of electrolysis increased. It appears from these

measurements that the film is not simple and the operating fluorine anode can be represented by the model shown in Figure 7.2.

Impedance measurements of fluorinated anodes in solvents other than KF.2HF showed that the fluoride film was unstable, both chemically and electrochemically. Simple immersion in the solvent resulted in a capacitance increase whilst polarisation at negative potentials could restore capacitance values to the original values obtained on fresh carbon anodes.

Impedance measurements in the KF.2HF melt indicate that a simple equivalent circuit can be drawn for the system:

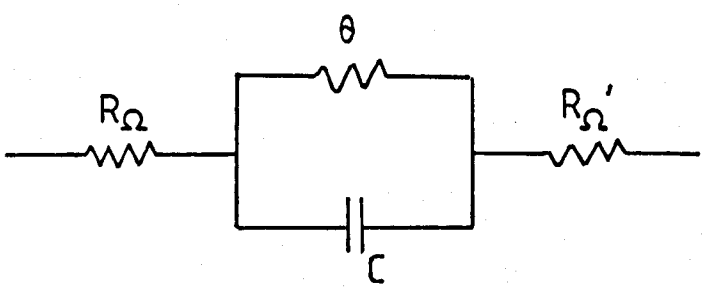

where R_Ω is the ohmic resistance between the Luggin probe and the electrode surface, θ is the charge transfer resistance, C the capacitance of the double layer and R_Ω' is the resistance of the fluoride film on the electrode surface. R_Ω', C and θ all depend on electrode potential.

As mentioned earlier, at least 90% of the electrode surface is covered by fluorine bubbles during steady-state electrolysis. Attempts to obtain polarisation data by a single potential step method were unsatisfactory due to contributions to measured currents from the surface process occurring at 2.0V. Using a

double step method resulted in linear I/E plots and hence no kinetic data could be extracted from them. The effect of fluorine evolution was shown, however, by pulsing to 5.0V after polarisation at a potential of 6V for 30 minutes, in which case the currents were some 50% smaller than on a fresh anode, indicating that a surface film had been produced on the anode surface.

Use of a suitable rotating electrode[12] would enable measurements to be made in the abscence of the fluorine gas layer and would perhaps enable determination of kinetic parameters for the fluorine evolution reaction.

TABLE 4.1

Cyclic voltammetry in KF.2HF. The effect of sweep rate.

ν Vs^{-1}	E_{pa} V	E_{pc} V	I_{pa} $mAcm^{-2}$	I_{pc} $mAcm^{-2}$	Q_a $mCcm^{-2}$
10	2.1	-0.5	8.6	-10.1	0.7
3	2.1	-0.4	3.4	-4.0	0.85
1	2.1	-0.25	1.7	-1.6	1.2
0.1	2.0	0.0	0.3	-0.25	3

TABLE 4.2

Cyclic voltammetry in KF.2HF. The effect of time spent at 3.5V.

TIME AT 3.5V mins	I_{pa} $mAcm^{-2}$	Q_a $mCcm^{-2}$
0	1.38	0.96
1	1.42	0.99
2	1.64	1.15
3	2.00	1.40
4	2.21	1.55
9	2.33	1.75
14	2.67	2.00
19	2.75	2.06
24	2.92	2.19
54	3.20	2.88
84	3.20	2.88
114	3.20	2.88
144	3.20	2.88

TABLE 4.3

Thermodynamic formation potentials for various carbon fluorides at 85°C in KF.2HF.

FLUORIDE	E/V (358K)
F_2	2.89
$CF_4(g)$	1.27
$CF_{1.125}(s)$	1.44
$CF_{0.597}(s)$	1.45
$C_4F(s)$	2.07

TABLE 4.4

The effect of potential of electrolysis on the impedance measured in KF.2HF at 0.7V (vs. Pd/H_2)

ELECTRODE MATERIAL	TREATMENT POTENTIAL/V	C μFcm^{-2}	R_Ω Ωcm^2	d nm
Vitreous Carbon	None	15.0	2.5	-
	3.5	1.2	6.0	1.5
	4.0	1.5	4.45	1.2
	5.0	1.0	5.15	1.8
	6.0	0.66	8.15	2.8
	7.0	0.26	11.35	7.1
	8.0	0.33	12.25	5.6
	-1.0	7.42	1.4	-
Pyrolytic Graphite	None	11.06	2.39	-
Face	+5	0.44	8.2	4.2
	+6	0.16	19.15	11.6
	+7	0.04	74.5	46.2
	+8	0.03	81	61.6

TABLE 4.5

Impedance results obtained at 0.7V in KF.2HF after treatment at 5.0V or 8.0V. The effect of stopping the electrolysis at a current peak or in a current trough is shown.

5.0V	PEAKS			TROUGHS	
TIME mins	R Ωcm^2	C μFcm^{-2}	TIME mins	R Ωcm^2	C μFcm^{-2}
*3	5.1	0.82	7	8.2	0.52
18	5.75	0.62	100	5.65	0.72
239	5.6	0.52	187	5.45	0.72
367	6.6	0.38	332	6.65	0.46
416	7.3	0.36	399	6.10	0.44

* FRESH ELECTRODE R = 2.44μcm^2 C = 9.94μFcm^{-2}

8.0V	PEAKS			TROUGHS	
TIME mins	R Ωcm	C μFcm^{-2}	TIME mins	R Ωcm	C μFcm^{-2}
$2	8.4	0.36	7	8.9	0.32
24	11.05	0.22	56	10.95	0.24
127	16.55	0.14	141	12.55	0.24
203	26.8	0.08	244	31	0.06
276	25.65	0.08	302	29	0.06

$ FRESH ELECTRODE R = 2.31μcm^2 C = 9.74μFcm^{-2}

TABLE 4.6

Capacitance values and estimated film thicknesses, measured in the stated solvent, for vitreous carbon electrodes subjected to fluorine evolution in KF.2HF.

ACETONITRILE/SODIUM PERCHLORATE +300mV

Fluorination Potential/V	C_d μFcm^{-2}	Film Thickness/nm
None	24.5	-
+2	23.7	-
+4	20.7	-
+6	3.4	0.54
+9	2.1	0.88

AQUEOUS POTASSIUM CHLORIDE +230mV

Fluorination Potential/V	C_d μFcm^{-2}	Film Thickness/nm
None	25.1	-
+4	24.6	-
+6	5.6	0.33
+8	0.85	2.2

TABLE 4.7

The effect of solvents on the capacitance values of fluorinated electrodes measured at 0.7V in KF.2HF.

CONDITION	CAPACITANCE AT 0.7V IN KF.2HF μFcm^{-2}
Fresh Electrode	15
+6V for 30 minutes	2.4
O/C in melt for 10 minutes	3.75
Removed from melt and stored in desiccator for 10 minutes	2
Immersed in water for 10 minutes	6
Immersed in Acetonitrile for 10 minutes	7.6

TABLE 4.8

Steady-state electrolysis in KF.2HF at vitreous carbon electrodes. Determination of fluorine bubble size and the extent of surface bubble coverage.

POTENTIAL V	TIME INTO ELECTROLYSIS	COVERAGE	BUBBLE SIZE
+3	30S	zero	
	5 minutes	zero	
	10 minutes	zero	
+4	30s	60%	V. small
	5 minutes	70%	V. small
	10 minutes	70%	V. small
+5	30s	80-85%	Large[#]
	5 minutes	90-95%	Large[$]
+6V	30s	95%	Large[&]
+7, +8, +9	30s	95%	Large[*]

[#] At 5V coalescence of bubbles starts. Bubbles are lenticular covering large area of the electrode.

[$] 50% of the electrode is covered by one bubble.

[&] 70% of the electrode is covered by one bubble.

[*] 80% of the electrode is covered by one bubble.

TABLE 4.9

Variation in peak currents obtained at different electrode materials at 6.0V in KF.2HF using the bubble release technique described in the text.

ELECTRODE MATERIAL	RANGE VALUES OF PEAK CURRENT BY TRANSIENT MEASUREMENTS /$mAcm^{-2}$
Vitreous Carbon	12.5-38.3
Pyrolytic Graphite (Face)	21-95
Pyrolytic Graphite (Edge)	24-172

Figure 4.1

Cyclic voltammetry in KF.2HF at $1.0Vs^{-1}$ at polished vitreous carbon A = $0.5cm^2$.

——— First sweep.

------ Steady state.

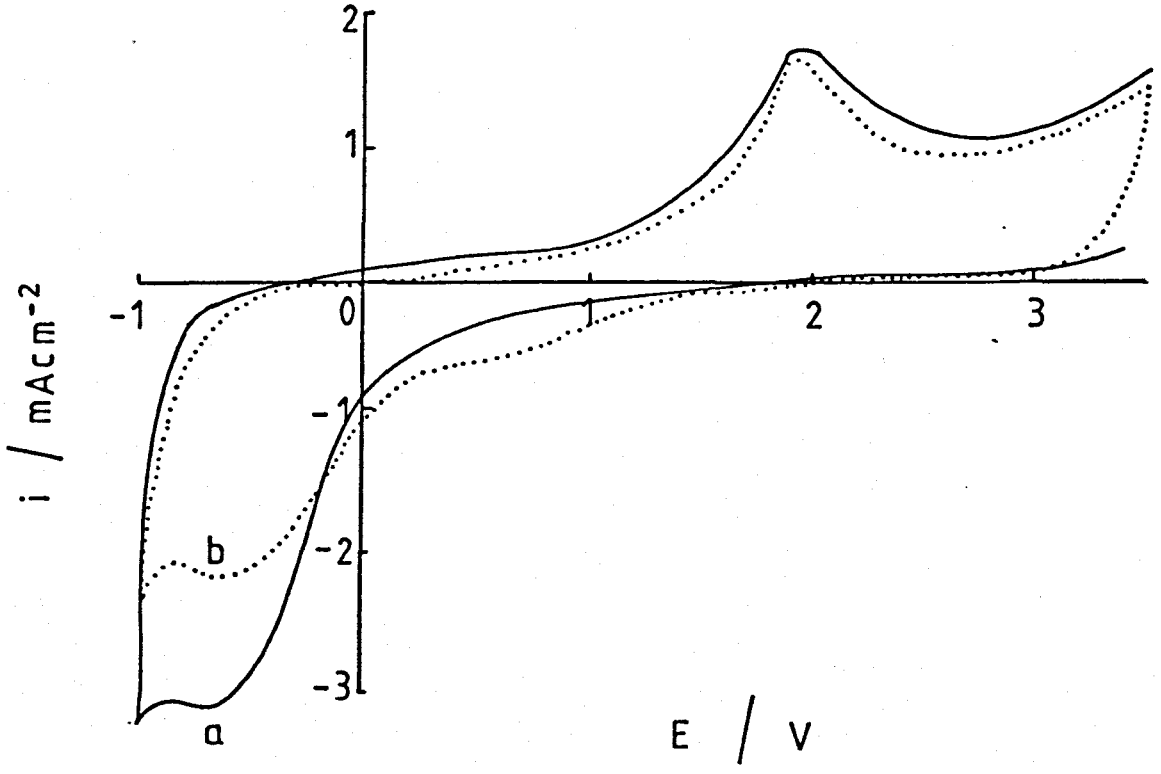
2
1
-1
0
1
2
3
-1
-2
-3
i / mAcm^{-2}
b
a
E / V

Figure 4.2

Cyclic voltammetry in KF.2HF at $1.0Vs^{-1}$ at polished vitreous carbon A = $0.5cm^2$.

a) First sweep.

b) Second sweep.

a)

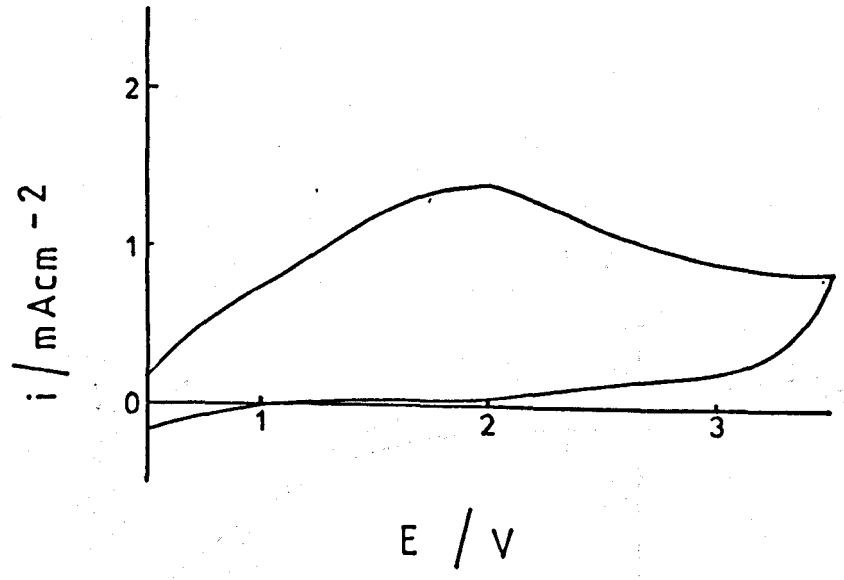

b)

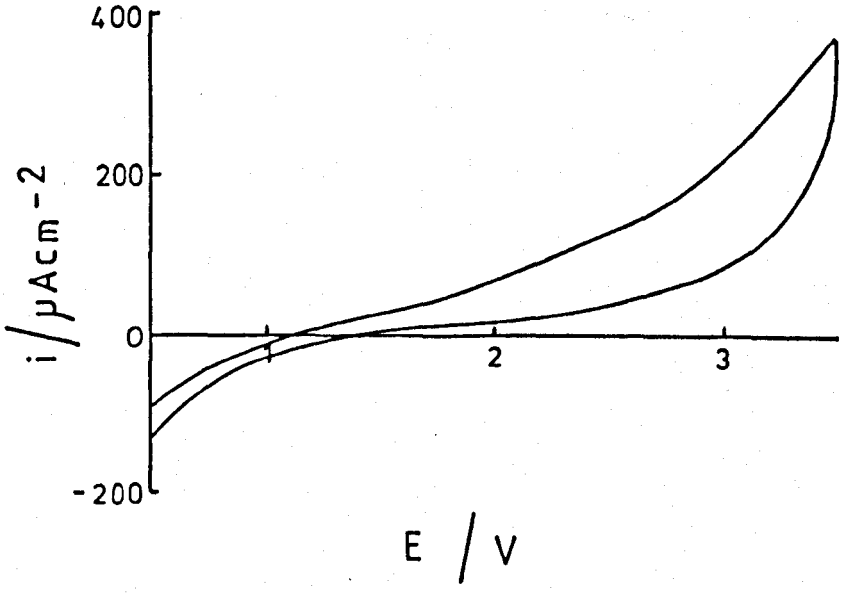

Figure 4.3

Cyclic voltammetry in KF.2HF at $1.0Vs^{-1}$ at polished vitreous carbon A = $0.5cm^2$. Limits restricted between -1.0V and +0.5V. Steady-state trace.

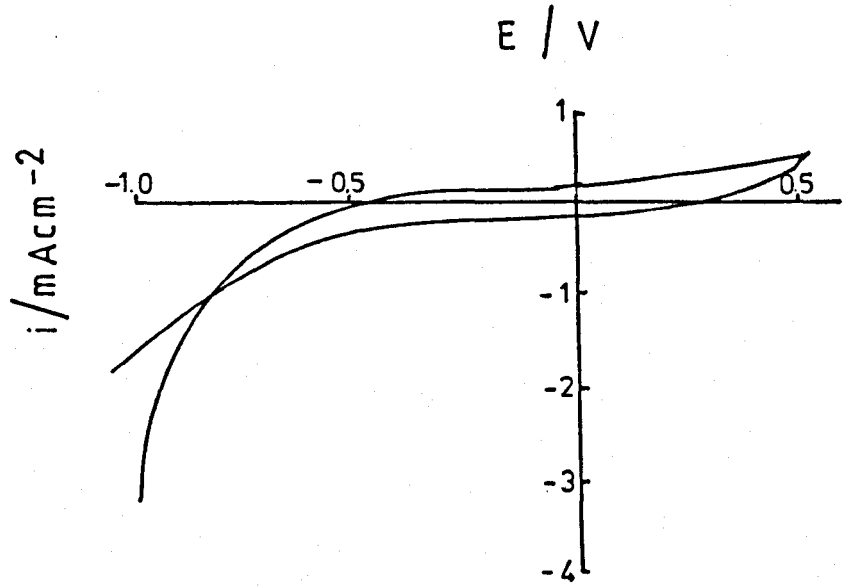

Figure 4.4

Plots of I_{pa} against ν and $\nu^{\frac{1}{2}}$ from the cyclic voltammetry data of table 4.1.

a) I_{pa} vs. ν

b) I_{pa} vs. $\nu^{\frac{1}{2}}$

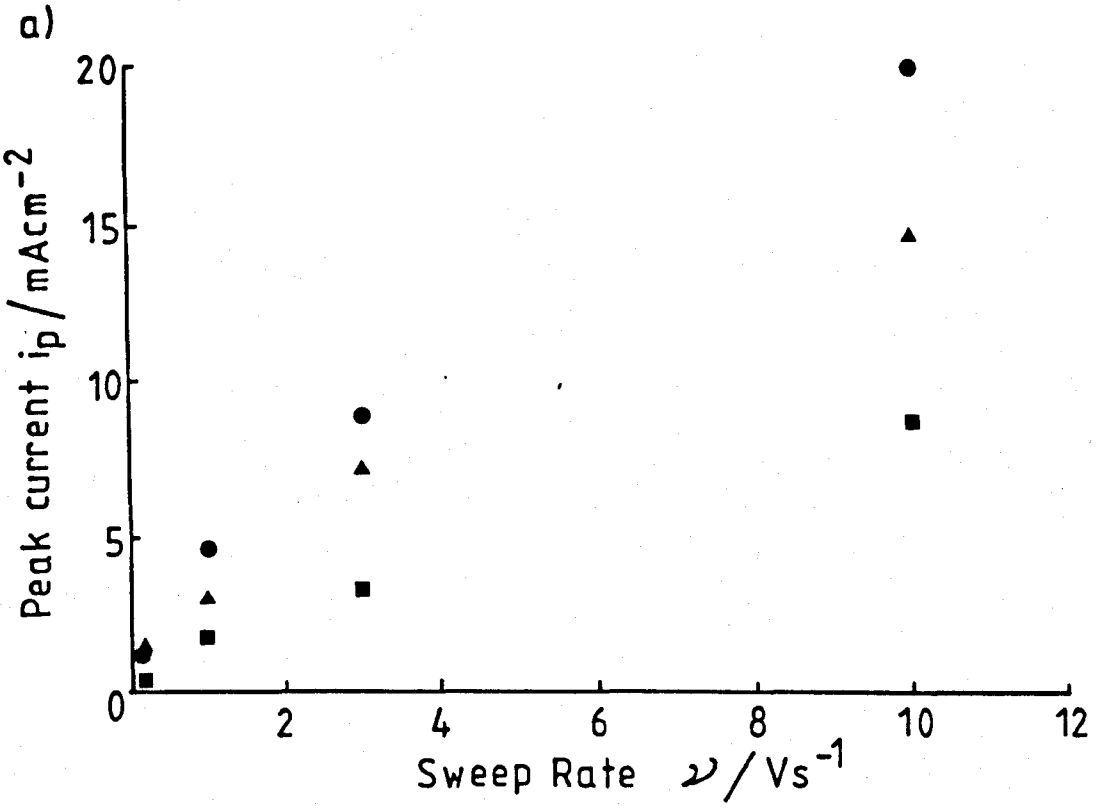
a)
Peak current i_p / mAcm^{-2}
20
15
10
5
0
2
4
6
8
10
12
Sweep Rate ν / Vs^{-1}

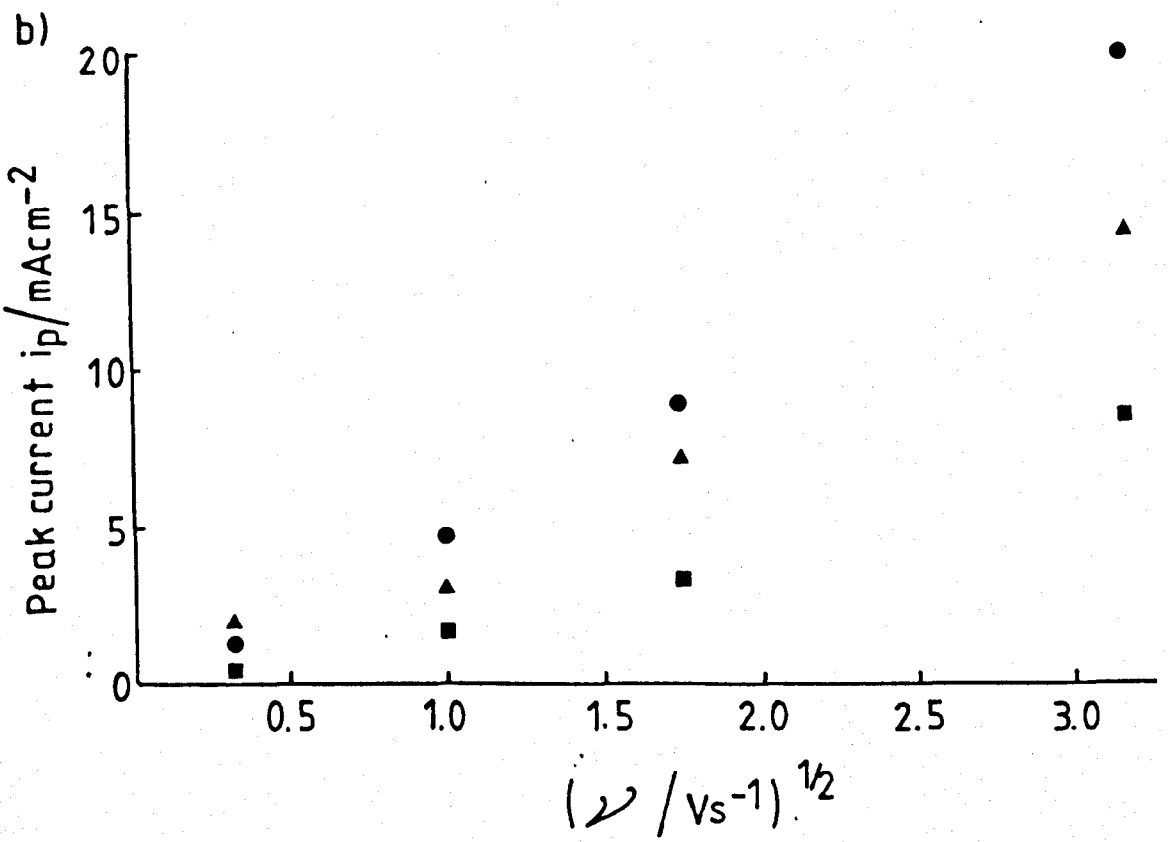
b)
Peak current i_p / mAcm^{-2}
20
15
10
5
0
0.5
1.0
1.5
2.0
2.5
3.0
$(\nu$ / Vs$^{-1})^{1/2}$

Figure 4.5

Cyclic voltammetry in KF.2HF at $1.0Vs^{-1}$ at polished vitreous carbon A = $0.5cm^2$. Electrode has evolved fluorine for 30 minutes at 4V. Upper plot, scan before removal of the gas film. Lower plot, scan after removal of the gas film.

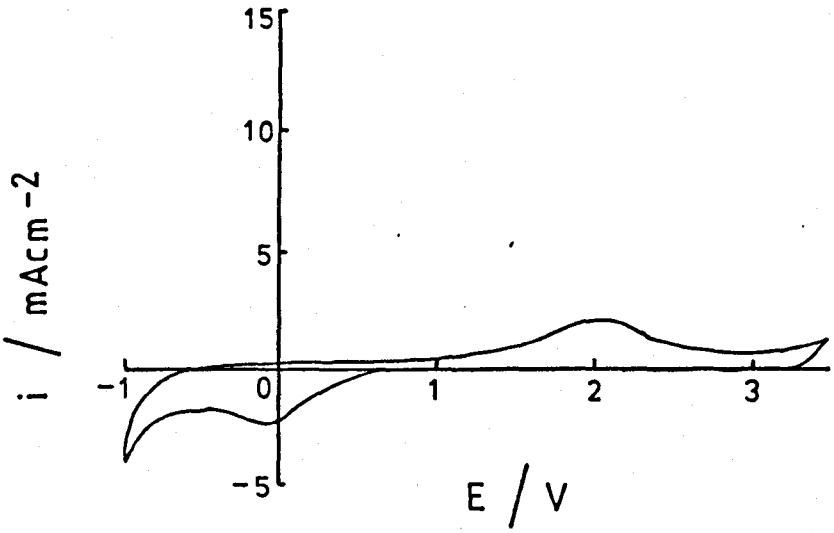
15
10
5
-5
-1
0
1
2
3
i / mAcm-2
E / V

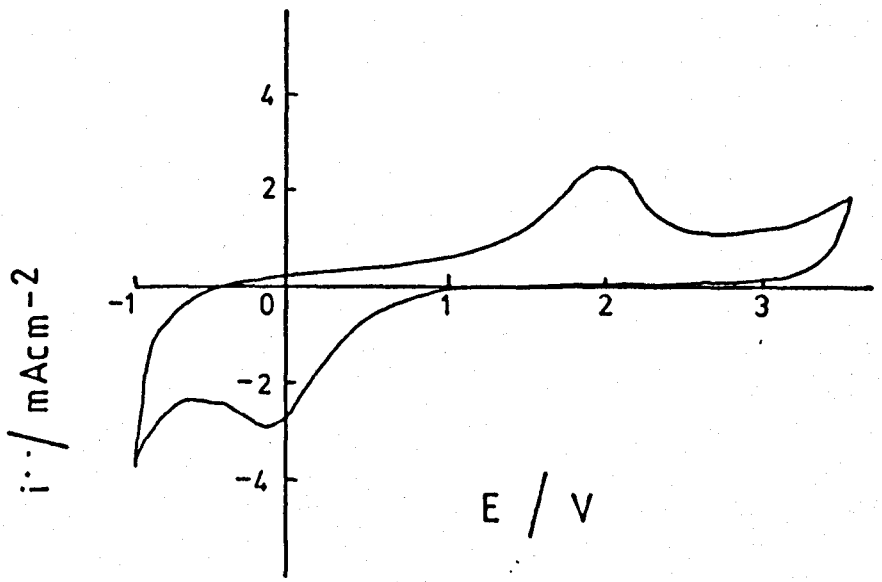
4
2
-2
-4
-1
0
1
2
3
i / mAcm-2
E / V

Figure 4.6

Cyclic voltammetry in KF.2HF at $1.0Vs^{-1}$ at polished vitreous carbon A = $0.5cm^2$. Electrode has evolved fluorine for 30 minutes at +5V. Scans before removal of the gas film.

——— First scan.

····· Steady state scan.

Figure 4.7

Cyclic voltammetry in KF.2HF at $1.0Vs^{-1}$ at polished vitreous carbon A = $0.5cm^2$. Electrode has evolved fluorine for 30 minutes at +5V. Scans after removal of the gas film.

——— First scan.

····· Steady state scan.

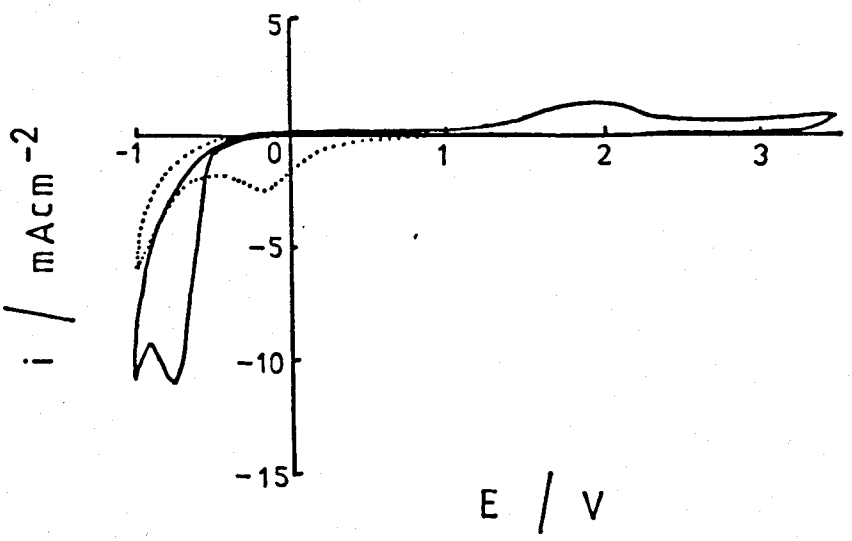
5
-1
0
1
2
3
-5
-10
-15
i / mAcm-2
E / V

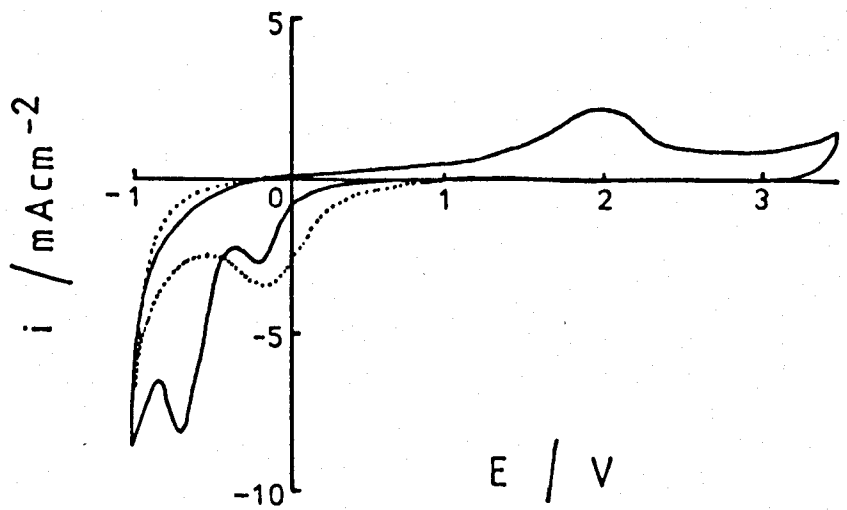
5
-1
0
1
2
3
-5
-10
i / mAcm-2
E / V

Figure 4.8

Cyclic voltammetry in KF.2HF at $1.0Vs^{-1}$ at polished vitreous carbon A = $0.5cm^2$. Electrode has evolved fluorine for 30 minutes at 5V. Scan after removal of the electrode from the melt a second time.

——— First scan

····· Steady-state scan.

Figure 4.9

Cyclic voltammetry in KF.2HF at $1.0Vs^{-1}$ at polished vitreous carbon A = $0.5cm^2$. Electrode has evolved fluorine for 30 minutes at 6V. Scan before removal of the gas film.

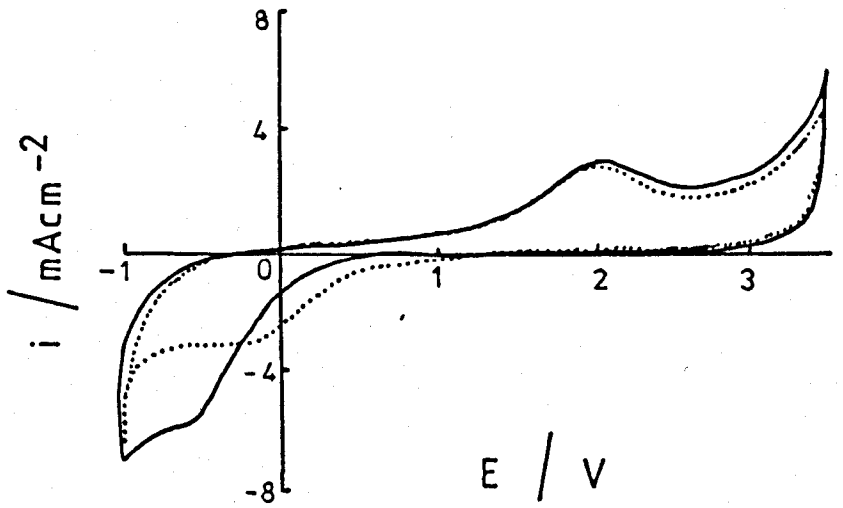
8
4
-1
0
1
2
3
-4
-8
i / mAcm -2
E / V

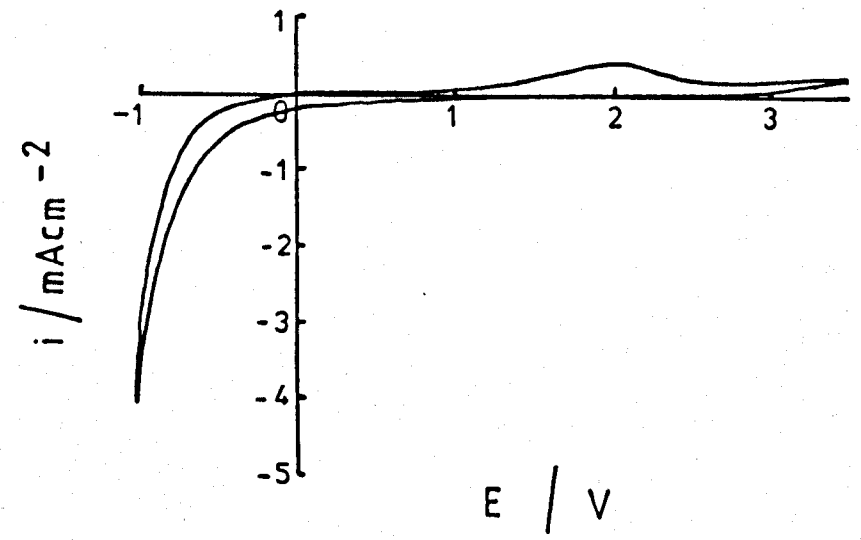
1
-1
0
1
2
3
-1
-2
-3
-4
-5
i / mAcm -2
E / V

Figure 4.10

Cyclic voltammetry in KF.2HF at $1.0Vs^{-1}$ at polished vitreous carbon A = $0.5cm^2$. Electrode has evolved fluorine for 30 minutes at +6V. Scan after removal of the gas film.

Figure 4.11

Cyclic voltammetry in KF.2HF at $1.0Vs^{-1}$ at polished vitreous carbon A = $0.5cm^2$. Electrode has evolved fluorine for 30 minutes at +7V. Scan before removal of the gas film.

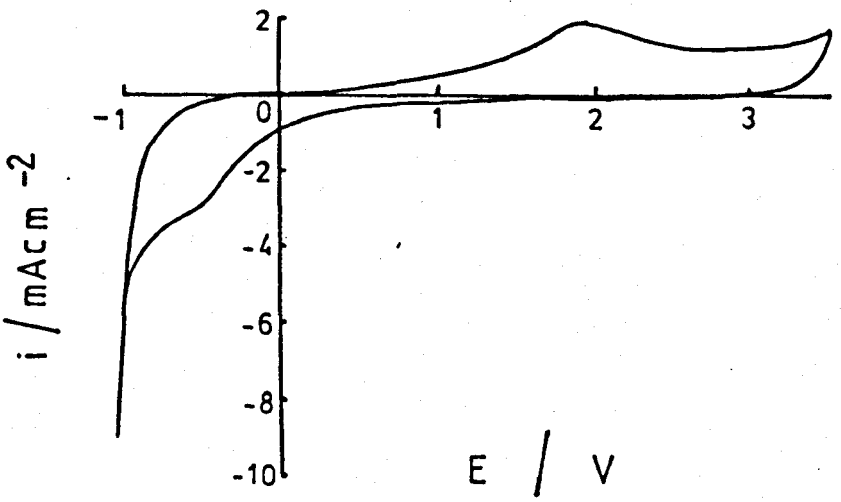
2
-1
0
1
2
3
-2
-4
-6
-8
-10
i / mAcm -2
E / V

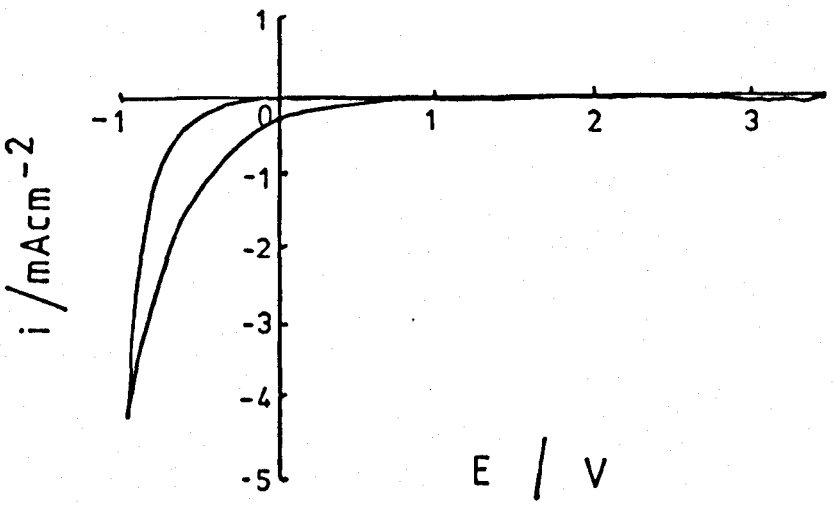
1
-1
0
1
2
3
-1
-2
-3
-4
-5
i /mAcm-2
E / V

Figure 4.12

Cyclic voltammetry in KF.2HF at $1.0Vs^{-1}$ at polished vitreous carbon A = $0.5cm^2$. Electrode has evolved fluorine for 30 minutes at +7V. Scan after removal of the gas film.

Figure 4.13

Cyclic voltammetry in KF.2HF at $1.0Vs^{-1}$ at polished vitreous carbon A = $0.5cm^2$. Electrode has evolved fluorine for 30 minutes at +8V. Scan before removal of the gas film.

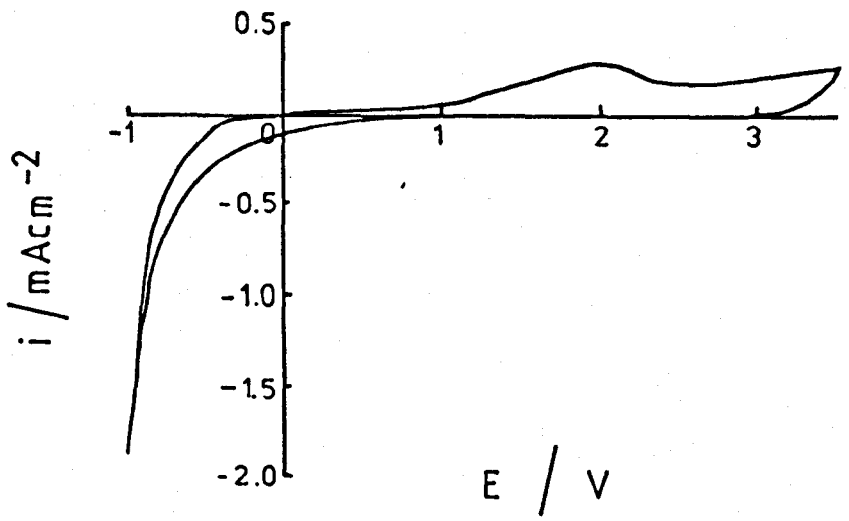
0.5
-1
0
1
2
3
-0.5
-1.0
-1.5
-2.0
i / mAcm-2
E / V

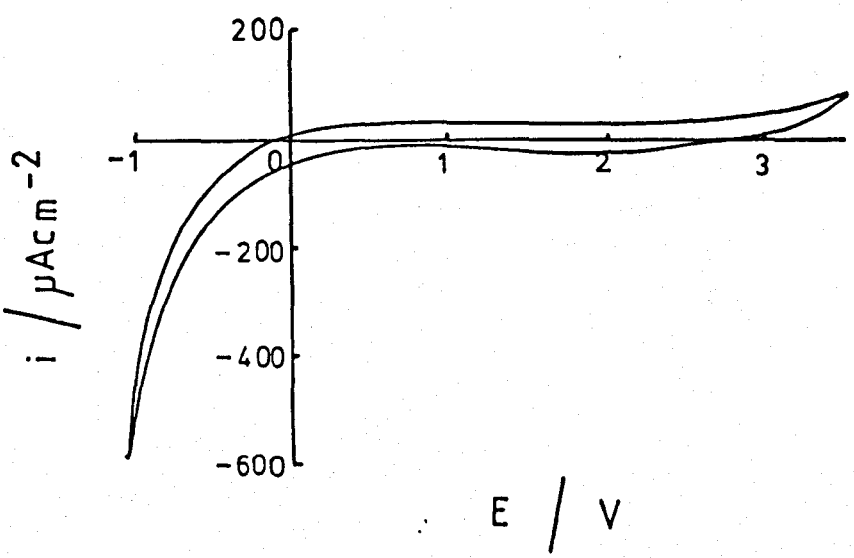
200
-1
0
1
2
3
-200
-400
-600
i / μAcm-2
E / V

Figure 4.14

Cyclic voltammetry in KF.2HF at $1.0Vs^{-1}$ at polished vitreous carbon A = $0.5cm^2$. Electrode has evolved fluorine for 30 minutes at +8V. Scan after removal of the gas film.

Figure 4.15

Cyclic voltammetry in KF.2HF at $1.0Vs^{-1}$ at polished vitreous carbon A = $0.5cm^2$. The electrode has been held at -1.0V for 30 minutes after electrolysis at +8V for 30 minutes.

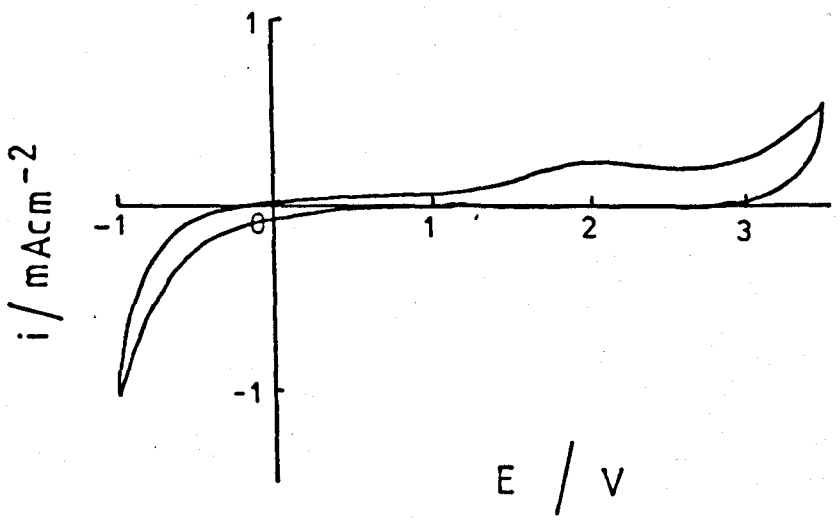
i / mAcm^{-2}
1
-1
0
1
2
3
-1
E / V

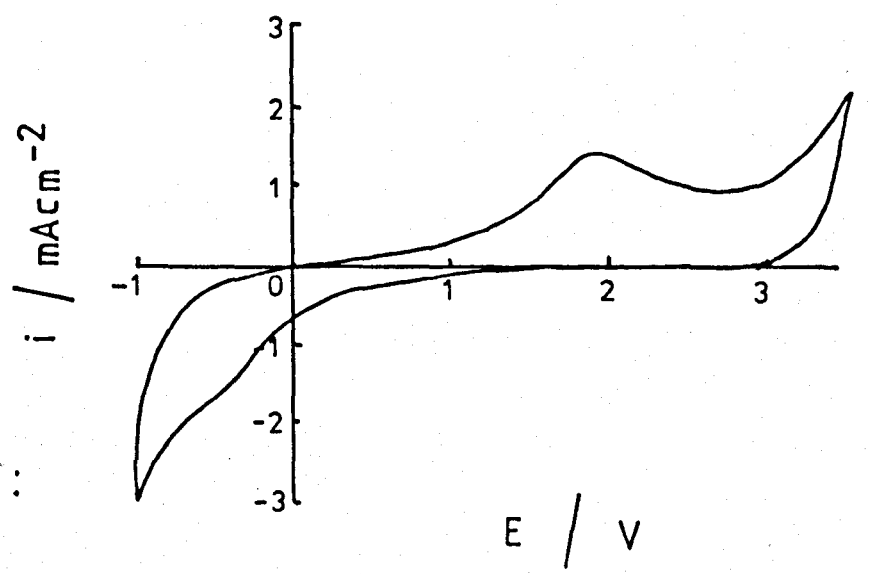
i / mAcm^{-2}
3
2
1
-1
0
1
2
3
-1
-2
-3
E / V

Figure 4.16

Steady state voltammogram at pyrolytic graphite with face orientation in KF.2HF at $10Vs^{-1}$.

Figure 4.17

Steady state voltammogram at pyrolytic graphite with edge orientation in KF.2HF at $10Vs^{-1}$.

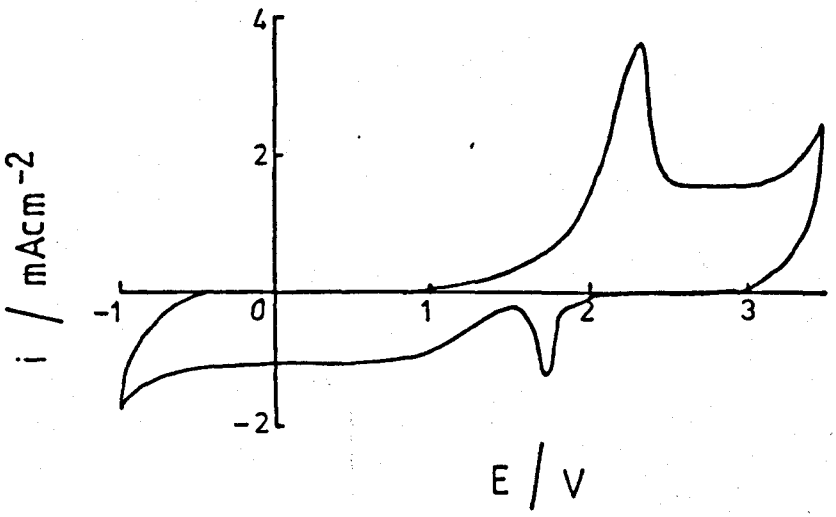
4
2
-1
0
1
2
3
-2
i / mAcm-2
E / V

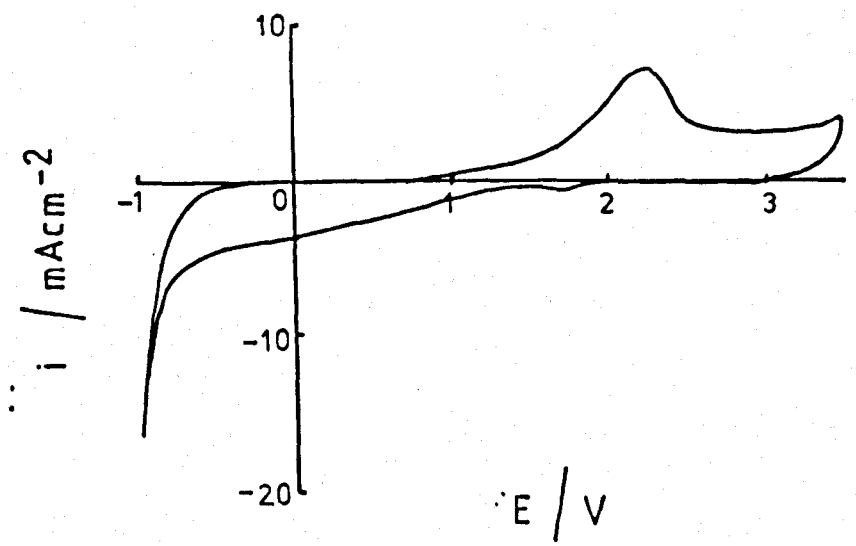
10
-1
0
1
2
3
-10
-20
i / mAcm-2
E / V

Figure 4.18

Steady state voltammogram at YBD porous carbon in KF.2HF at $10Vs^{-1}$.

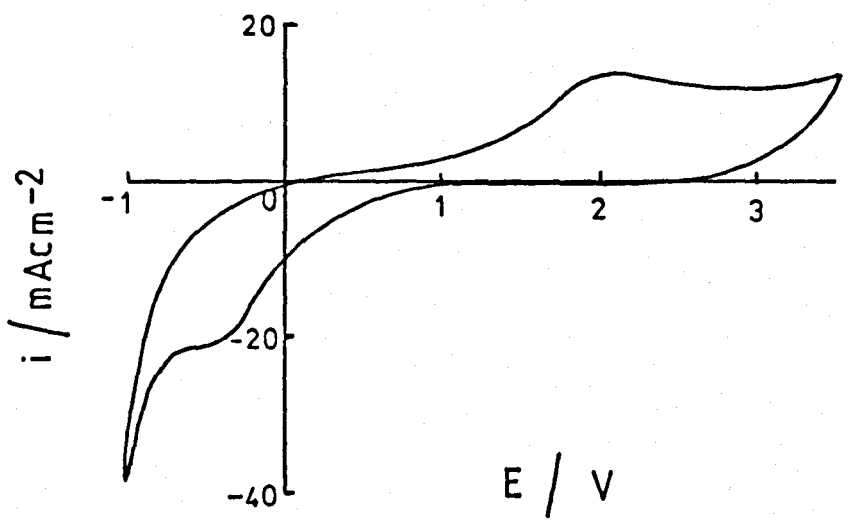

Figure 4.19

Cyclic voltammetry in KF.2HF over the range 0V to 5.0V at $10Vs^{-1}$.

a) Vitreous carbon.

b) YBD porous carbon.

c) Pyrolytic graphite with face orientation.

a)

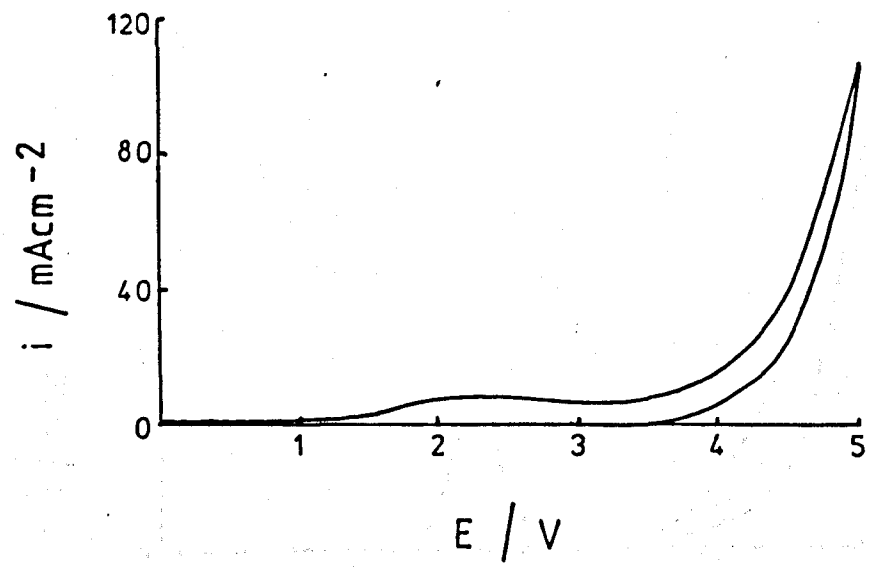

b)

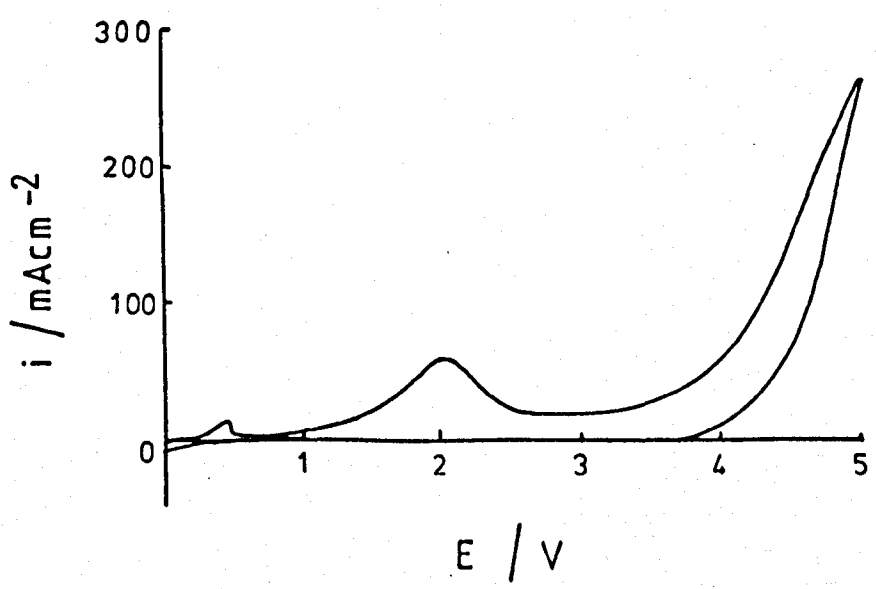

c)

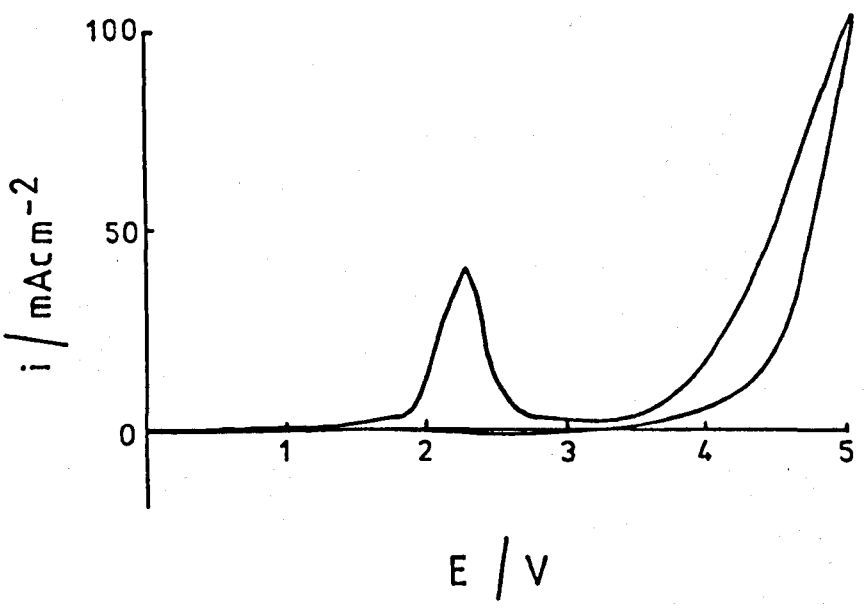

Figure 4.20

Tafel plot obtained from fast scan ($10Vs^{-1}$) voltammetry at vitreous carbon in KF.2HF.

——— Positive scan.

– – – – Negative scan.

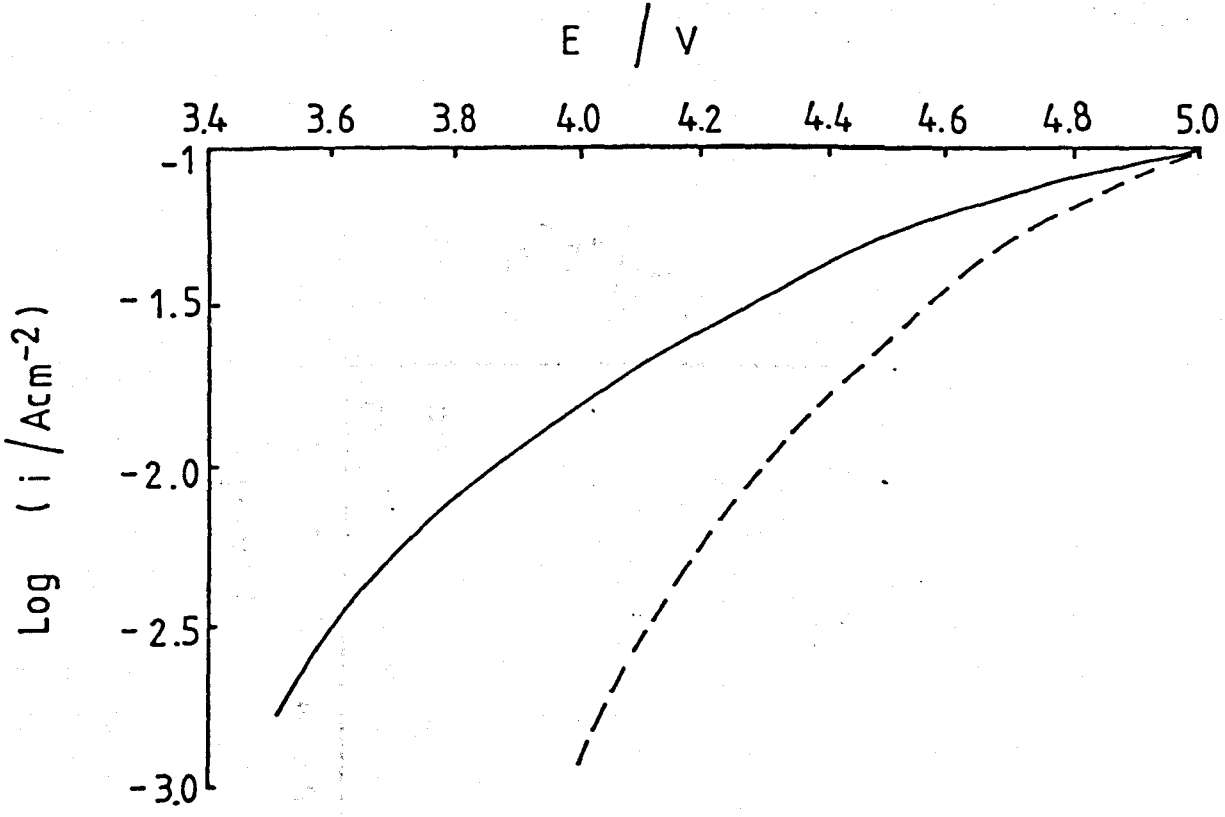
E / V
3.4
3.6
3.8
4.0
4.2
4.4
4.6
4.8
5.0
-1
-1.5
-2.0
-2.5
-3.0
Log (i /Acm-2)

Figure 4.21

Impedance plot for vitreous carbon A = 0.5cm^2 in 0·5M H_2SO_4 at 0.2V (vs. Hg_2SO_4). Frequencies in Hz.

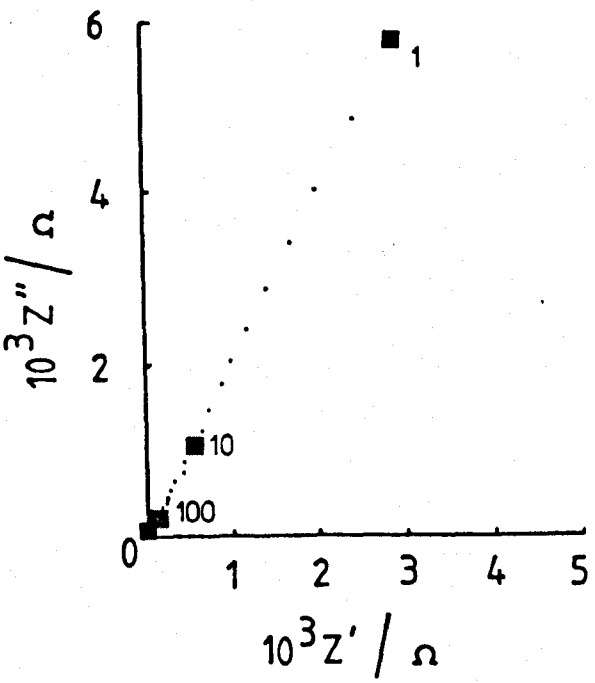

Figure 4.22

Capacitance data as a function of potential obtained from impedance measurements in 0.5M H_2SO_4. Results for pyrolytic graphite with face orientation. A = $0.5cm^2$

(●) Forward scan

(■) Negative scan

(X) Results obtained after cycling of the electrode between -0.9 and +0.7V (vs. Hg/Hg_2SO_4).

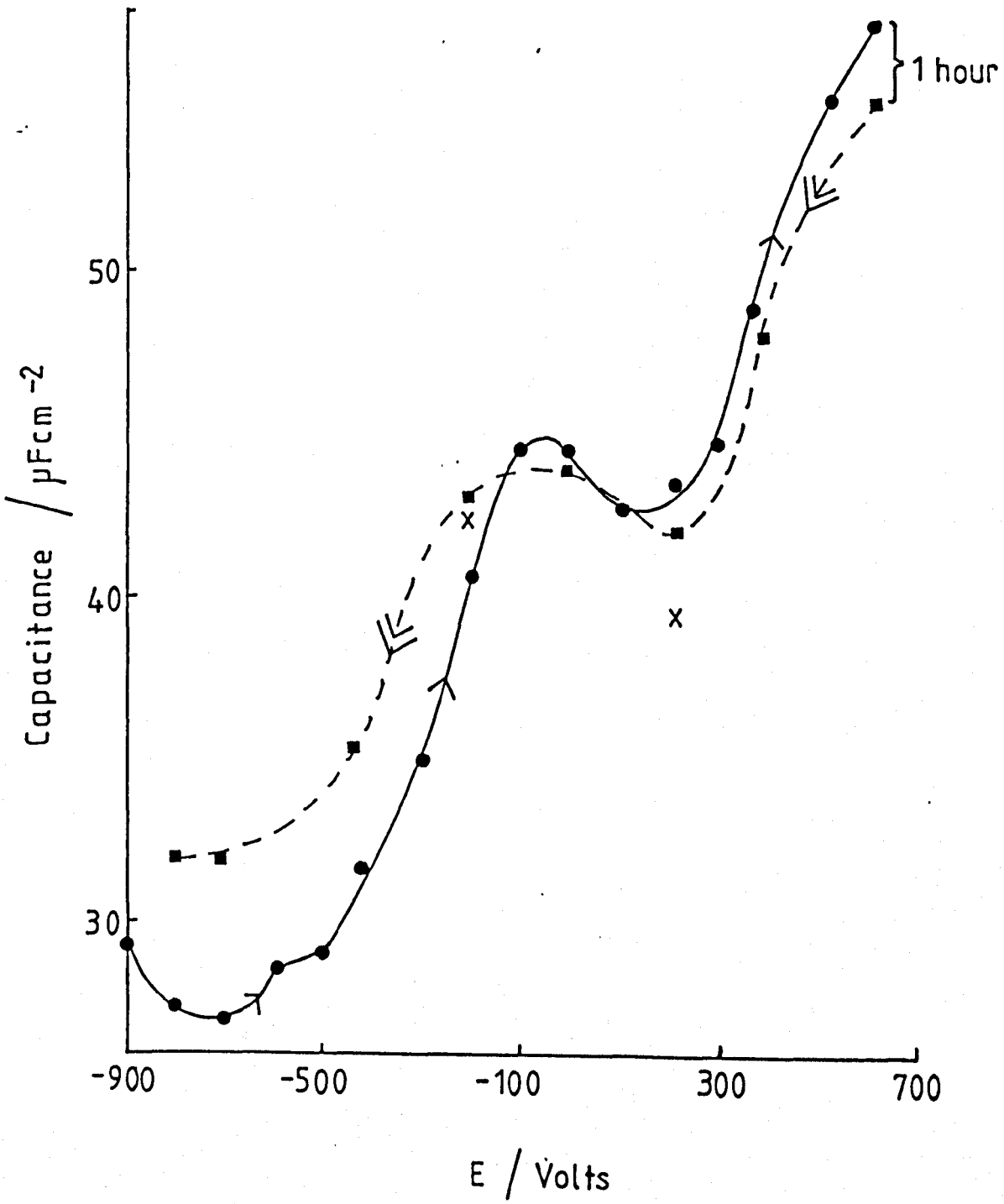
1 hour
50
40
30
Capacitance / μFcm -2
-900
-500
-100
300
700
E / Volts

Figure 4.23

Capacitance potential data obtained from impedance measurements in 0.5M H_2SO_4 at vitreous carbon.

(■) Forward scan.

(●) Reverse scan.

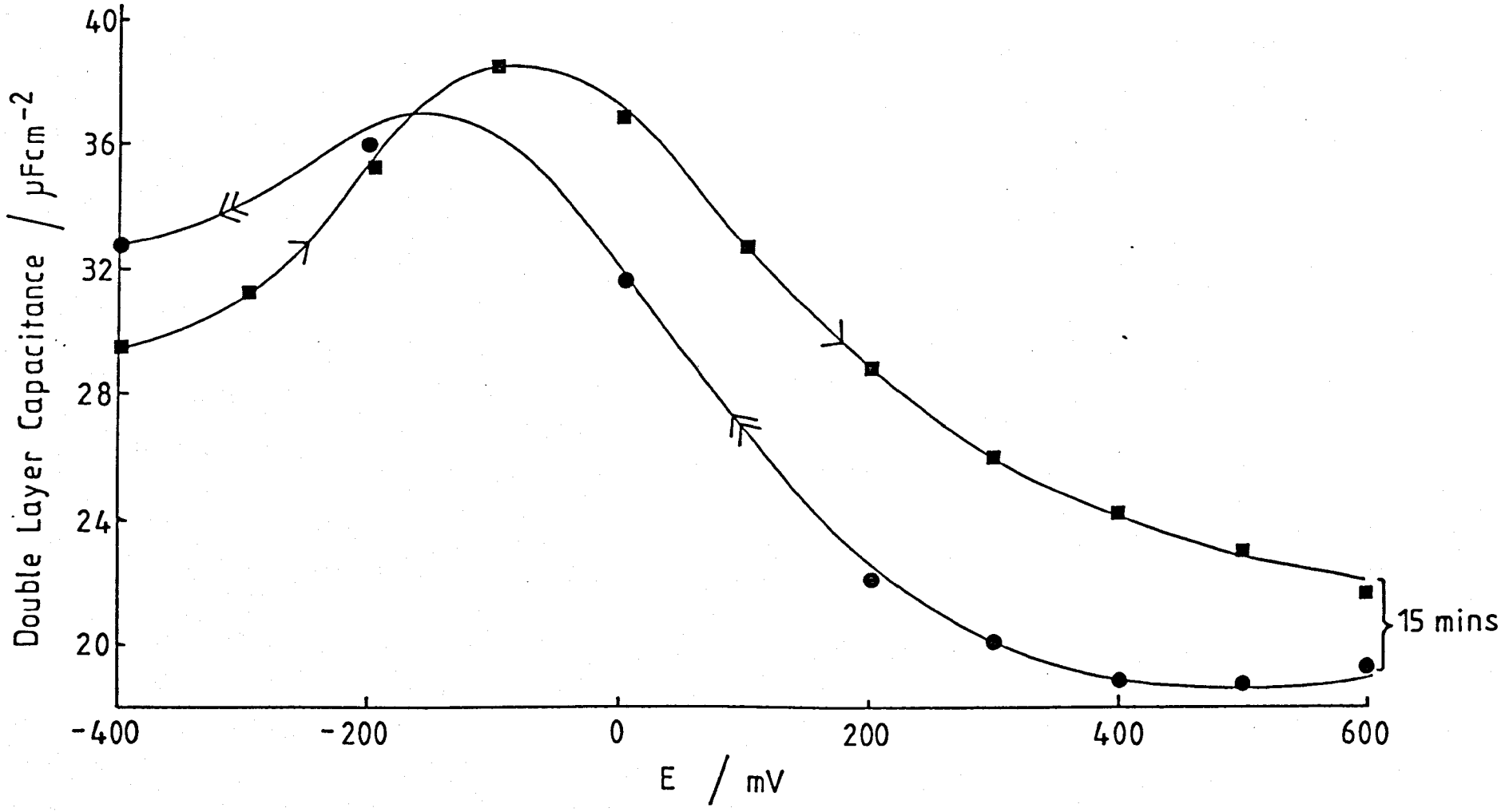
40
36
32
28
24
20
Double Layer Capacitance / μFcm⁻²
-400
-200
0
200
400
600
E / mV
15 mins

Figure 4.24

Impedance measurements in KF.2HF at vitreous carbon ($A=0.5cm^2$). Results obtained on increasing the positive potential. Frequencies in Hz.

(◇) = 1.4V.

(■) = 2.6V.

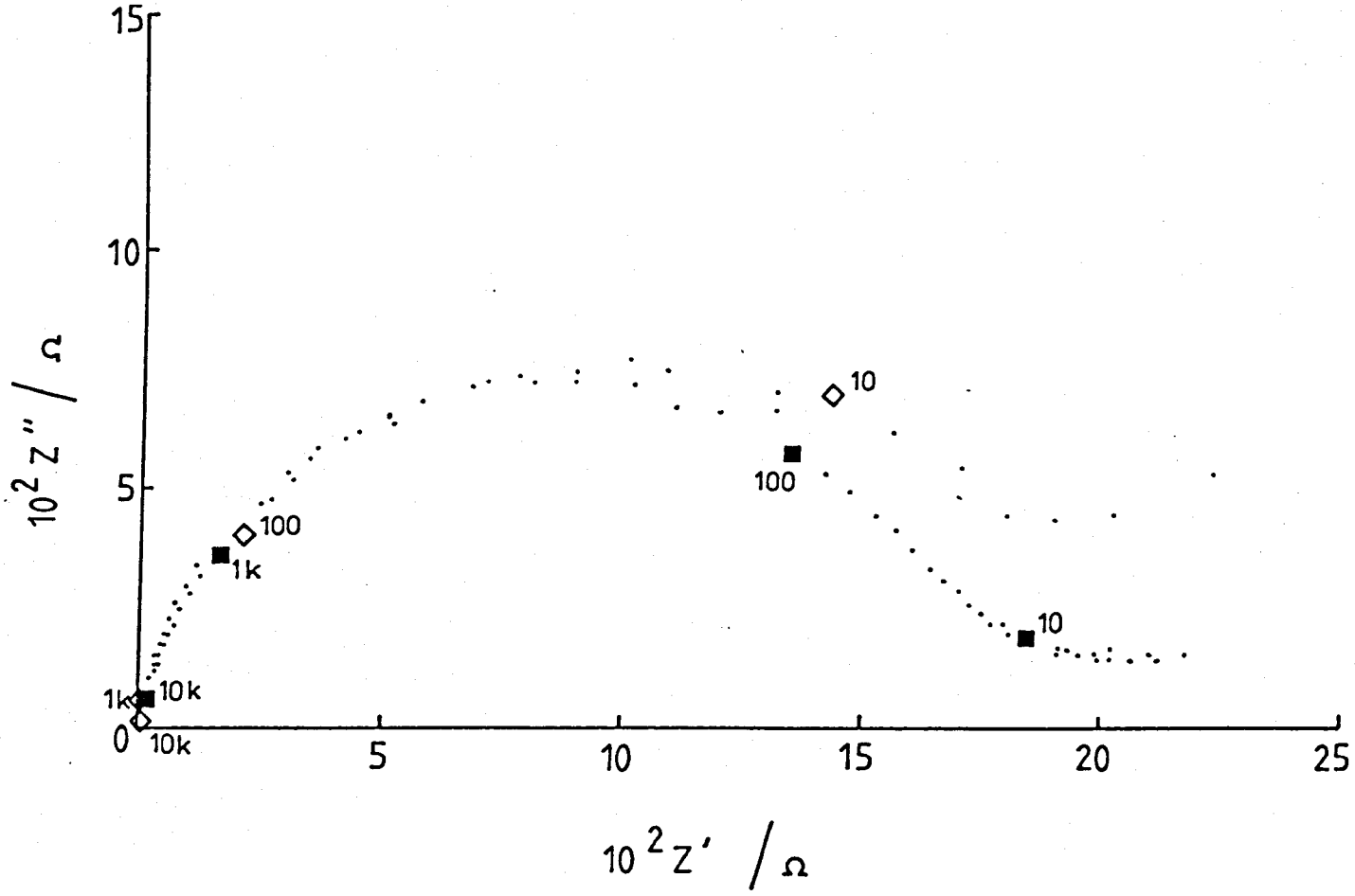
15
10
5
0
$10^2 Z'' / \Omega$
10
100
1k
10k
1k
10k
100
10
5
10
15
20
25
$10^2 Z' / \Omega$

Figure 4.25

Impedance measurements in KF.2HF at vitreous carbon ($A=0.5cm^2$). Results obtained on decreasing the positive potential. Frequencies in Hz.

(○) = 2.6V.

(◇) = 2.2V.

(●) = 1.8V.

(◆) = 1.4V.

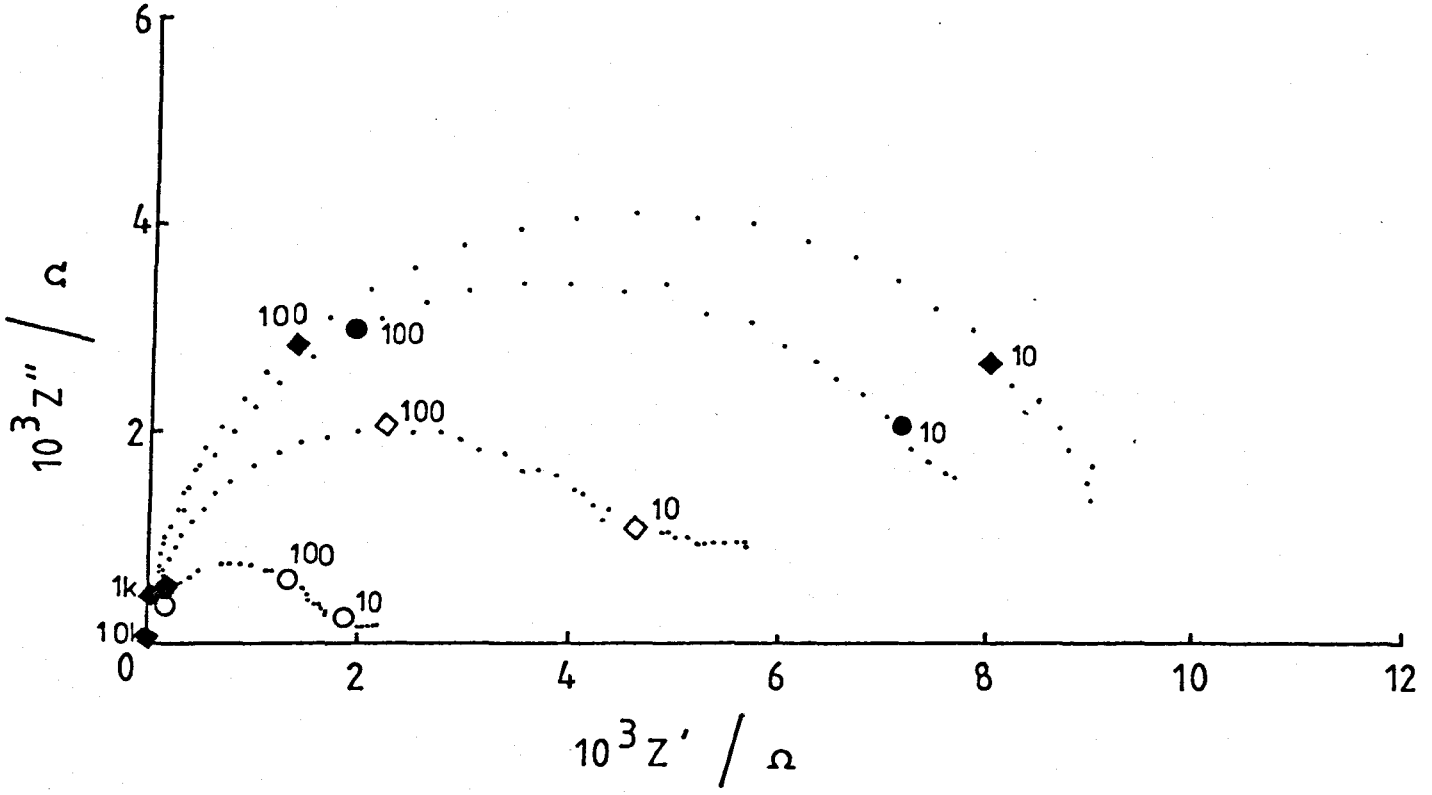
6
4
2
0
2
4
6
8
10
12
$10^3 Z'' / \Omega$
$10^3 Z' / \Omega$
100
100
100
10
10
10
100
10
1k
10k

Figure 4.26

Capacitance potential data obtained from impedance measurements in KF.2HF at vitreous carbon.

a) Whole plot.

b) Expanded section of high potential region.

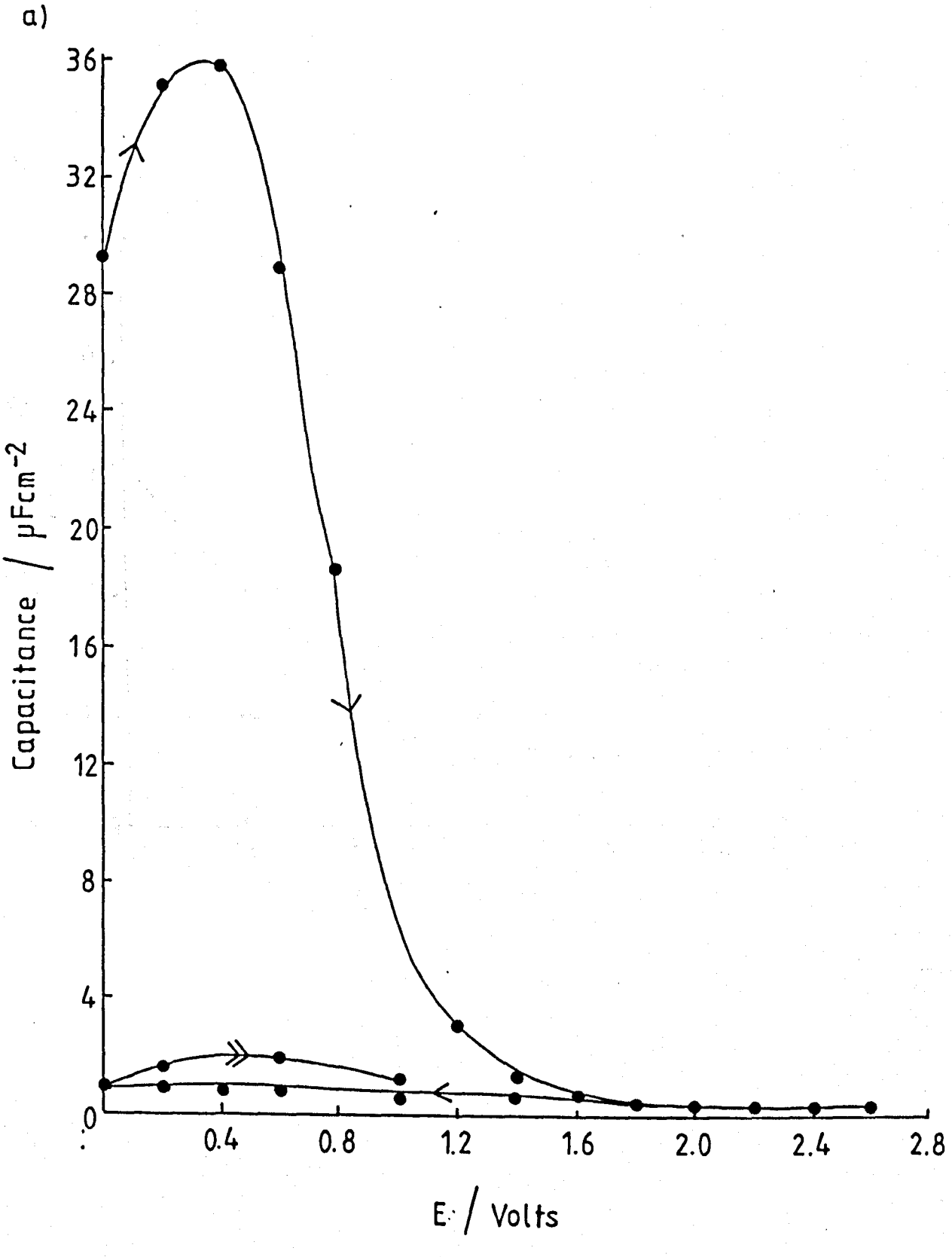
a)
36
32
28
24
20
16
12
8
4
0
Capacitance / μFcm⁻²
0.4
0.8
1.2
1.6
2.0
2.4
2.8
E / Volts

b)

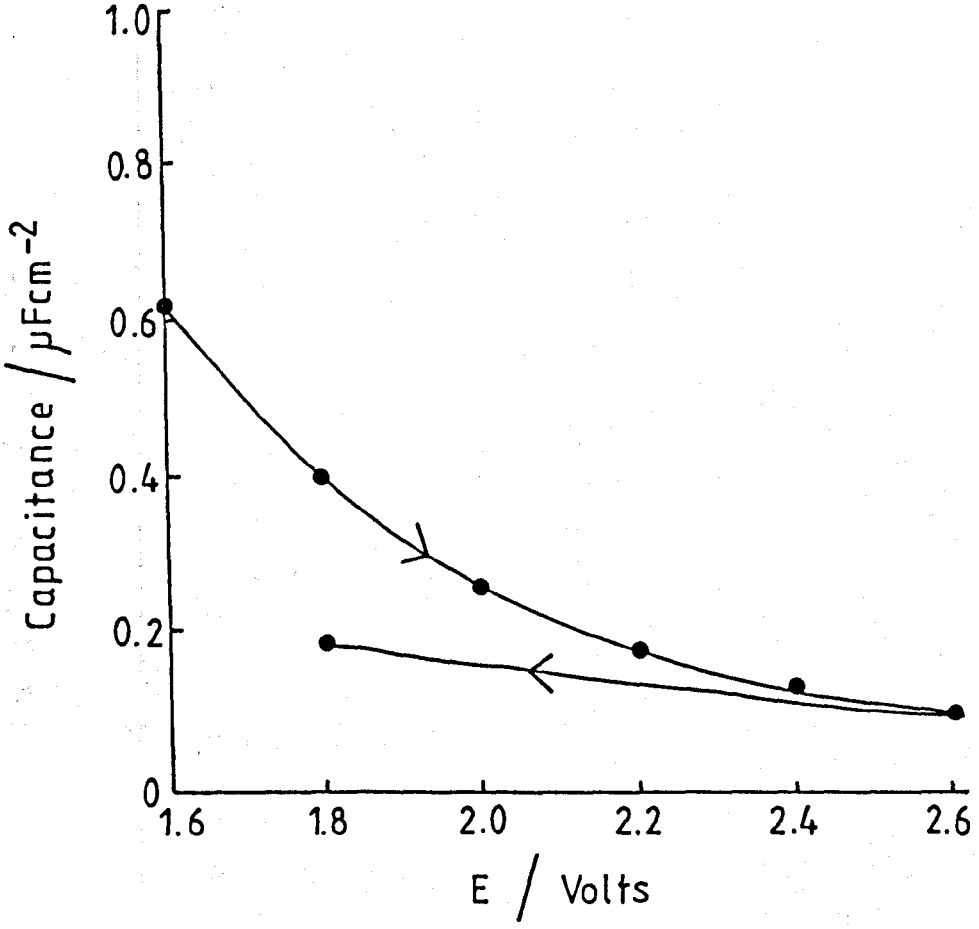

Figure 4.27

Capacitance potential data obtained from impedance measurements in KF.2HF at pyrolytic graphite with face orientation.

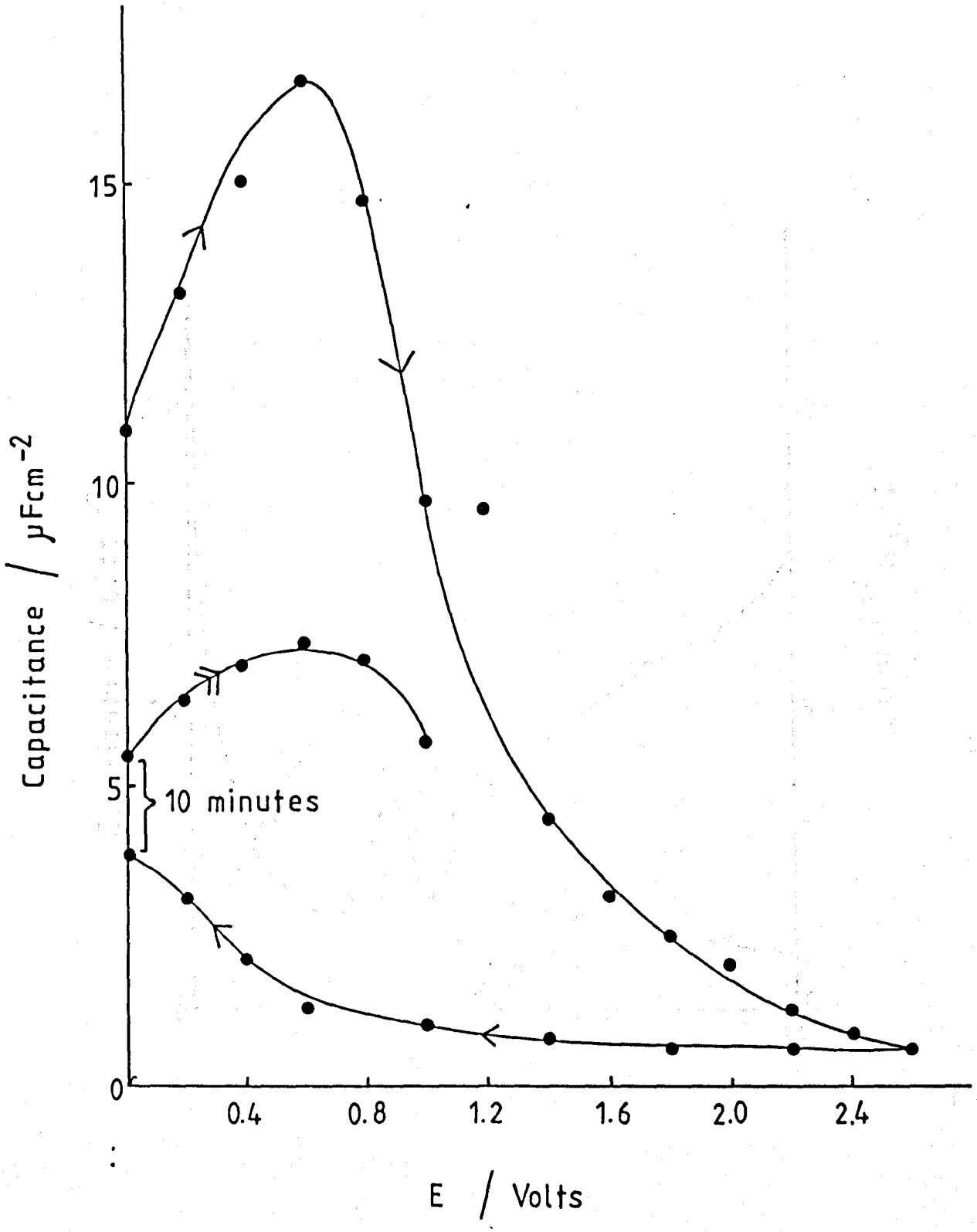

Figure 4.28

Time dependance data obtained at pyrolytic graphite with face orientation in KF.2HF at 2.4V.

(X) = Capacitance/Time data.

(●) = Resistance/Time data.

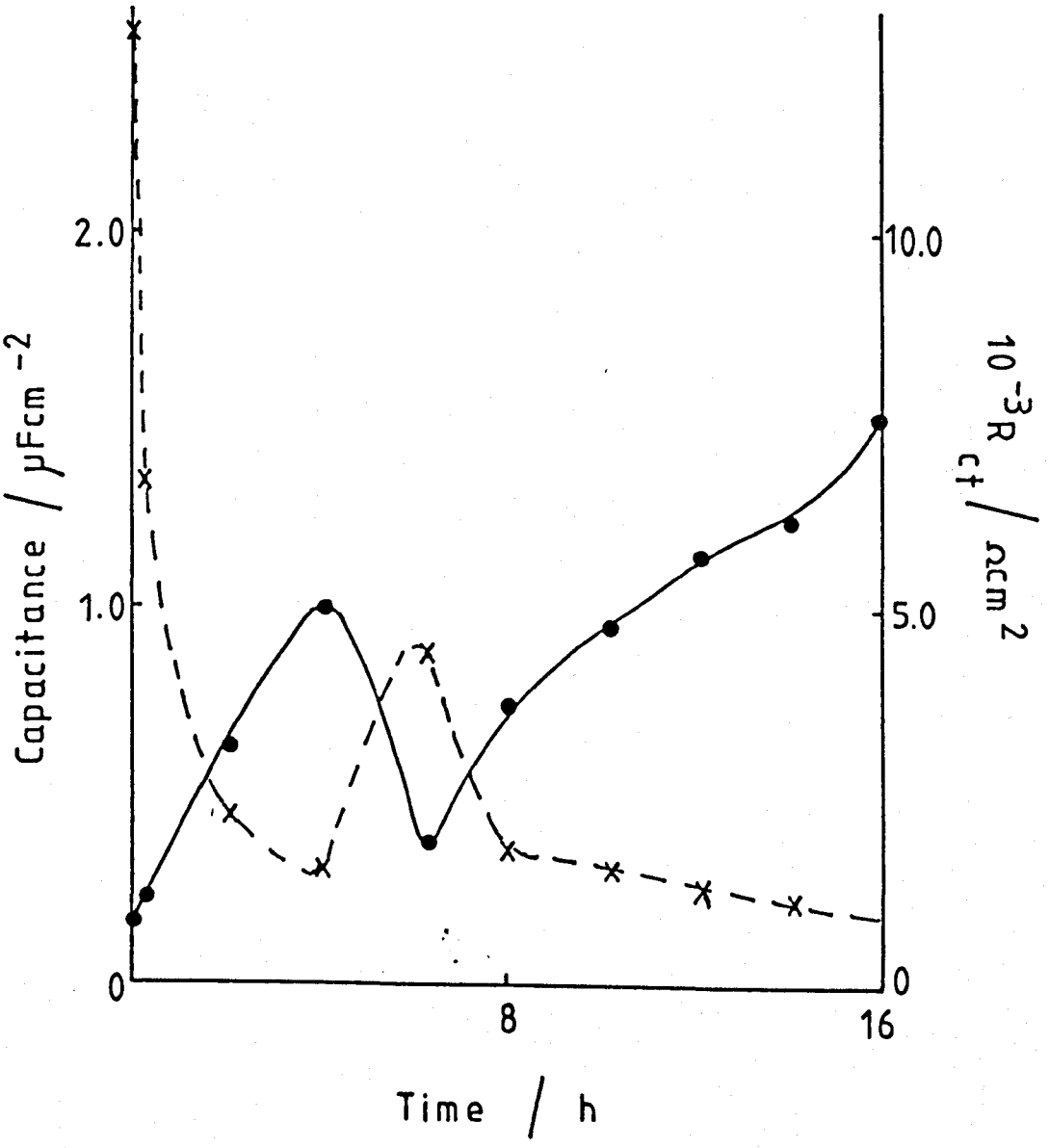

Figure 4.29

Time dependence studies of the interfacial capacitance of pyrolytic graphite with face orientation in KF.2HF at (●) 0V and (□) -0.5V after previous treatment of the electrode at 2.4V for 16hrs. (·····) capacitance of a fresh electrode.

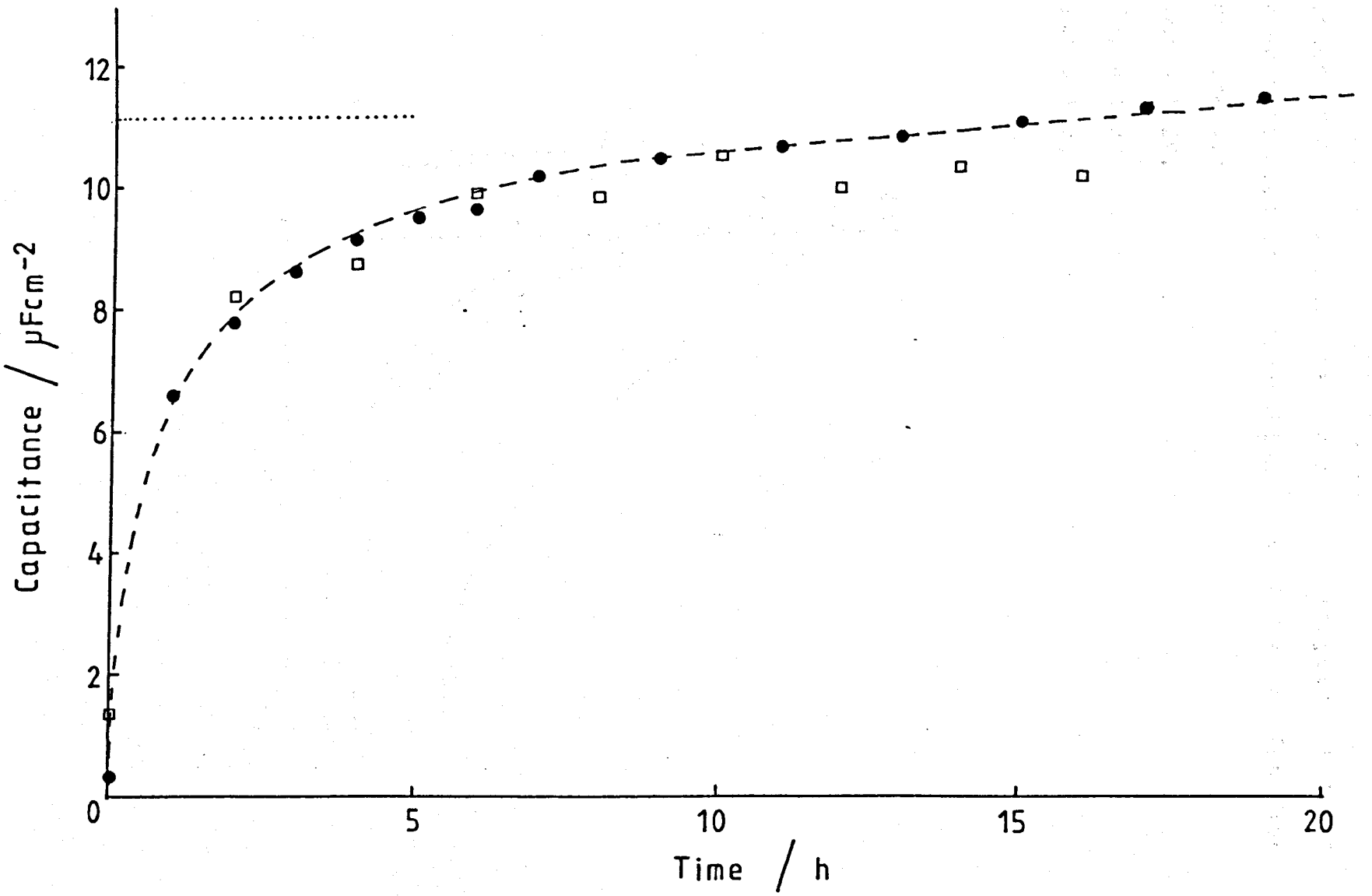
12
10
8
6
4
2
0
Capacitance / μFcm-2
5
10
15
20
Time / h

Figure 4.30

Interfacial capacitance for a pyrolytic graphite electrode with face orientation in KF.2HF as a function of time at:

(●) = 1.2V.

(■) = 1.3V.

(▲) = 1.4V.

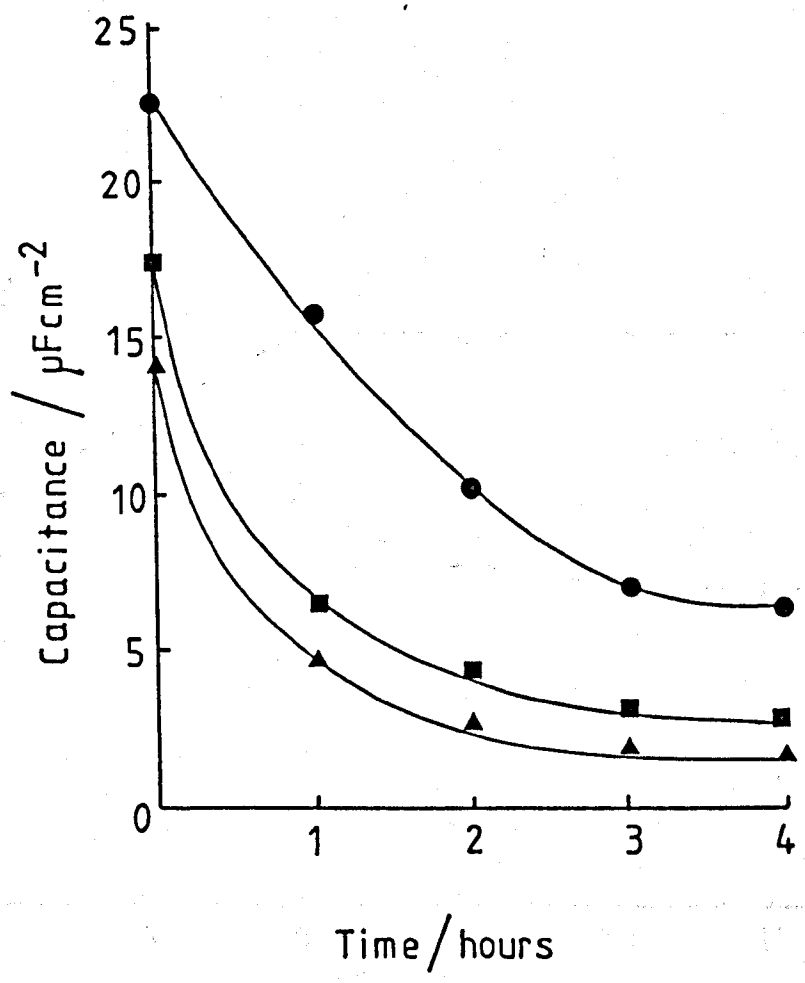

Figure 4.31

Interfacial capacitance for a pyrolytic graphite electrode with face orientation in KF.2HF as a function of time at:

(■) = 1.0V.

(●) = 0.6V.

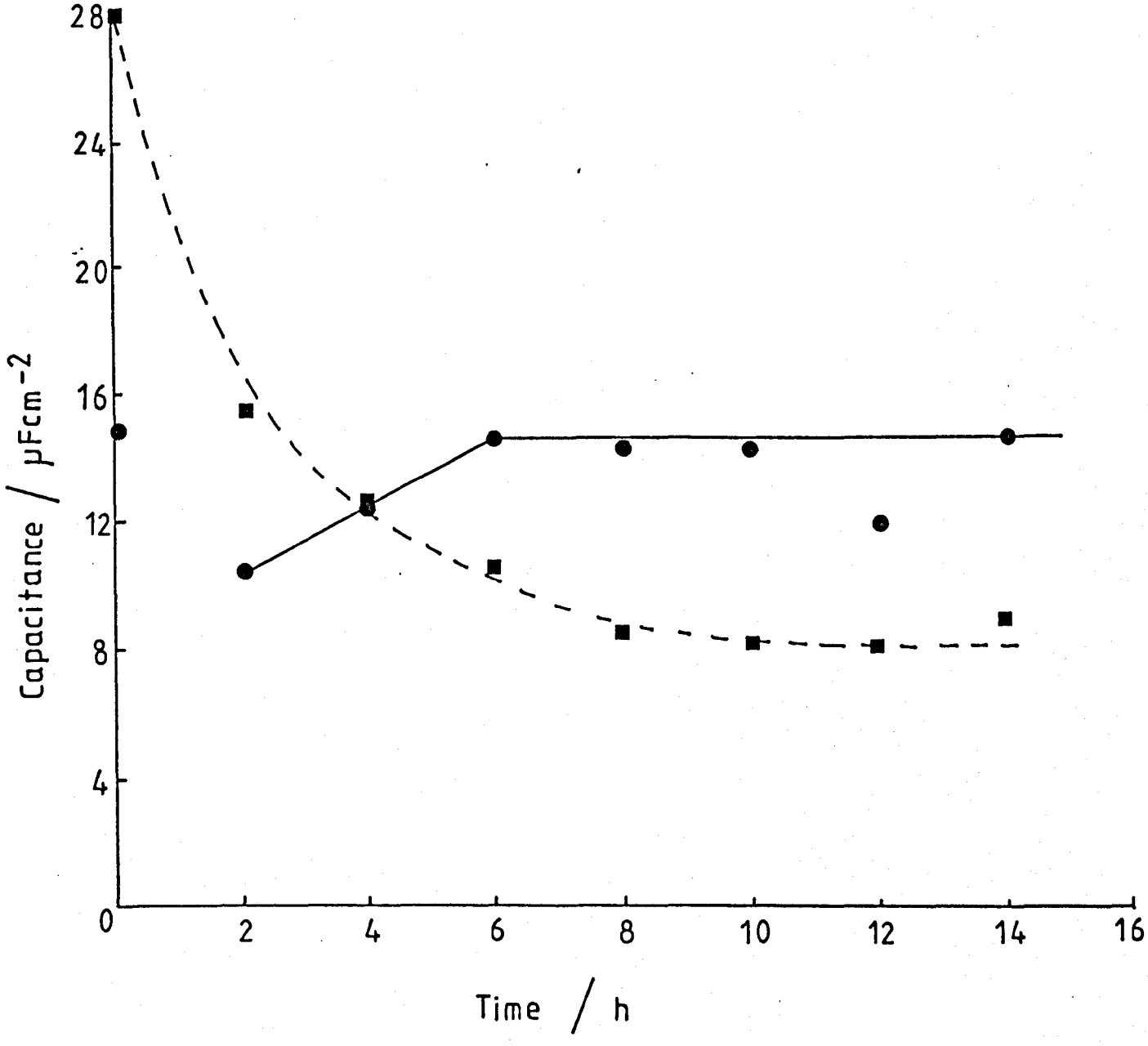

Figure 4.32

Resistance data obtained at vitreous carbon at 0.7V in KF.2HF after treatments of the electrode at various positive potentials for varying lengths of time. Electrode area = $0.5cm^2$

a) After treatment at 5V

b) After treatment at 6V

c) After treatment at 7V

d) After treatment at 8V

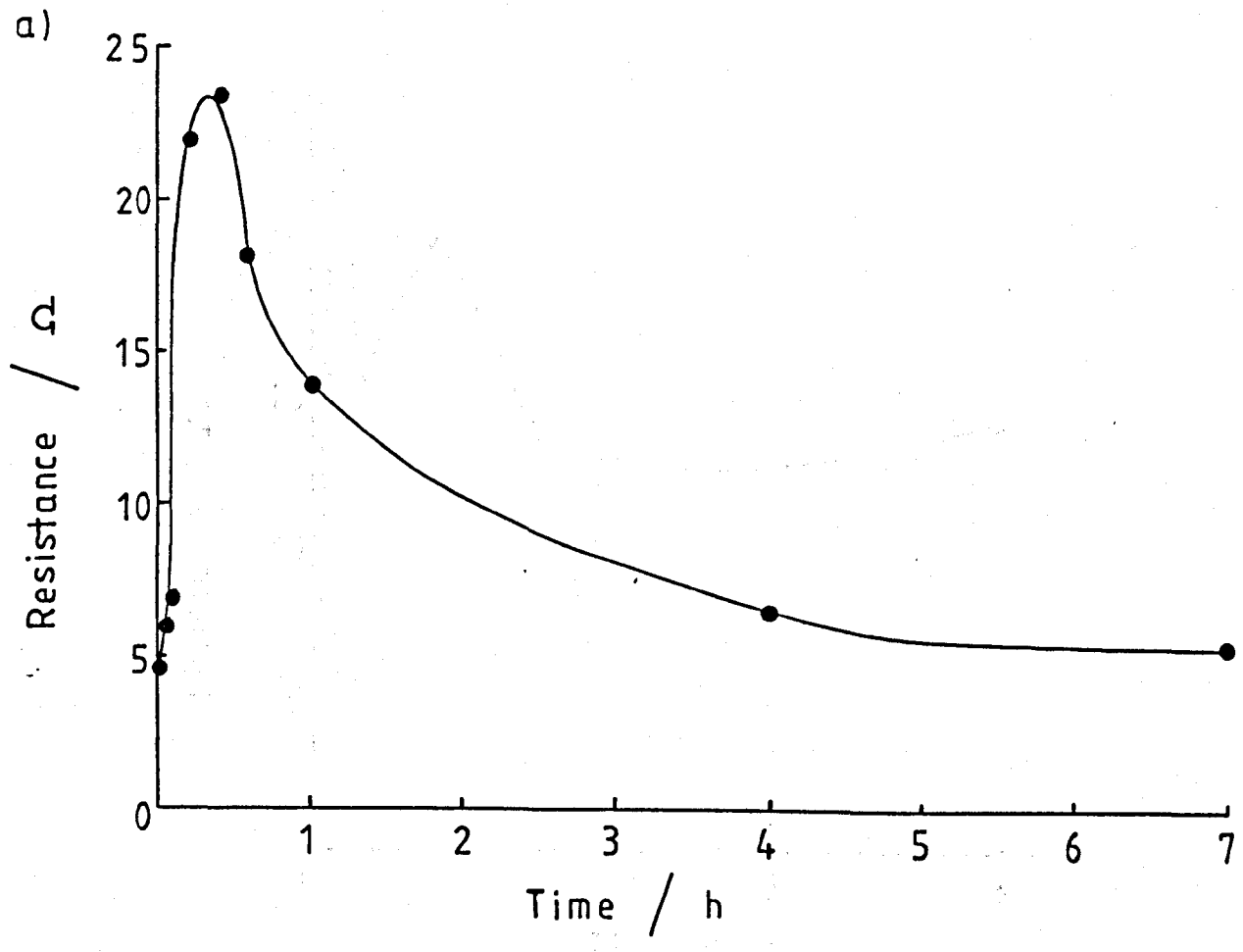
a)
25
20
15
10
5
0
Resistance / Ω
1
2
3
4
5
6
7
Time / h

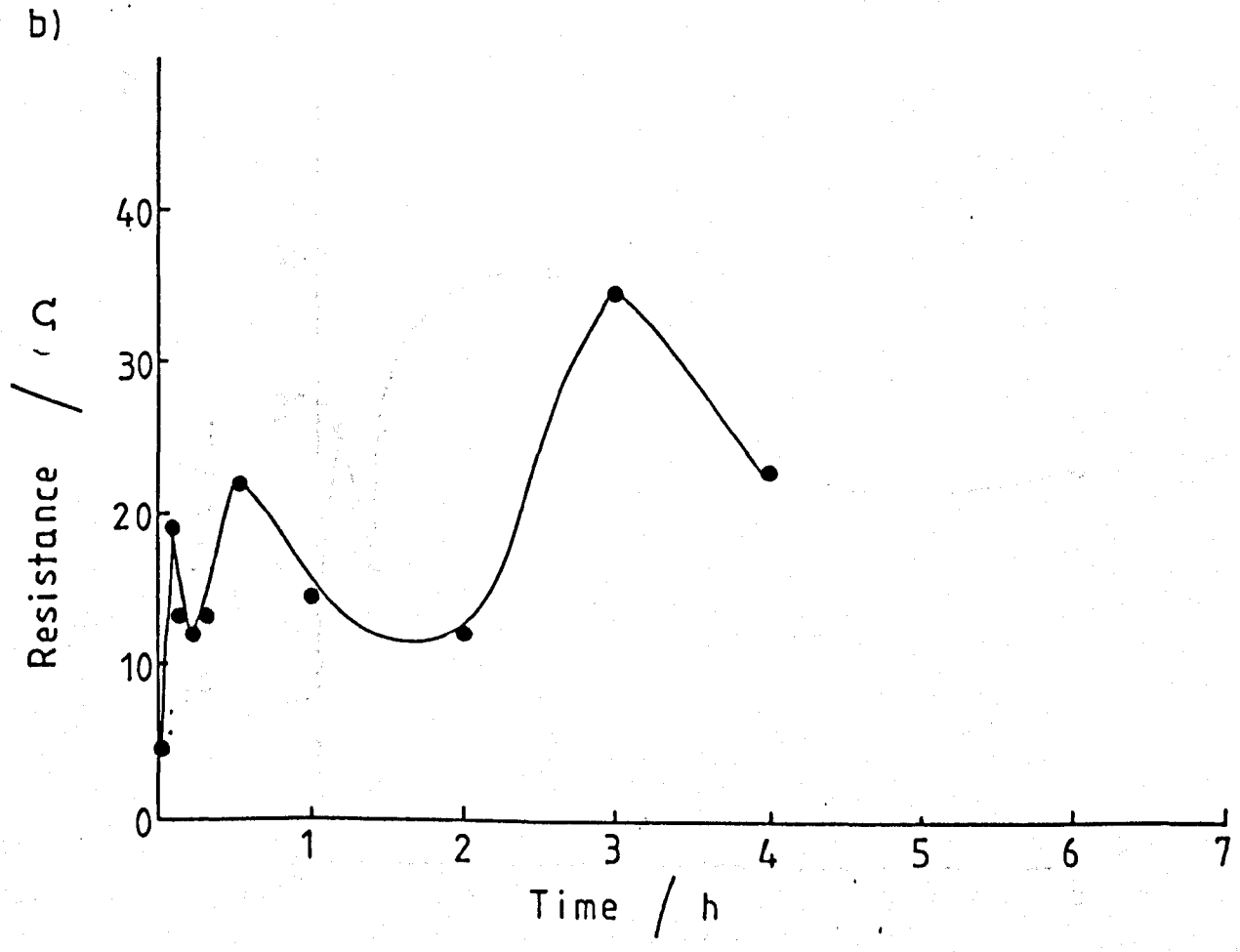
b)
40
30
20
10
0
Resistance / Ω
1
2
3
4
5
6
7
Time / h

c)

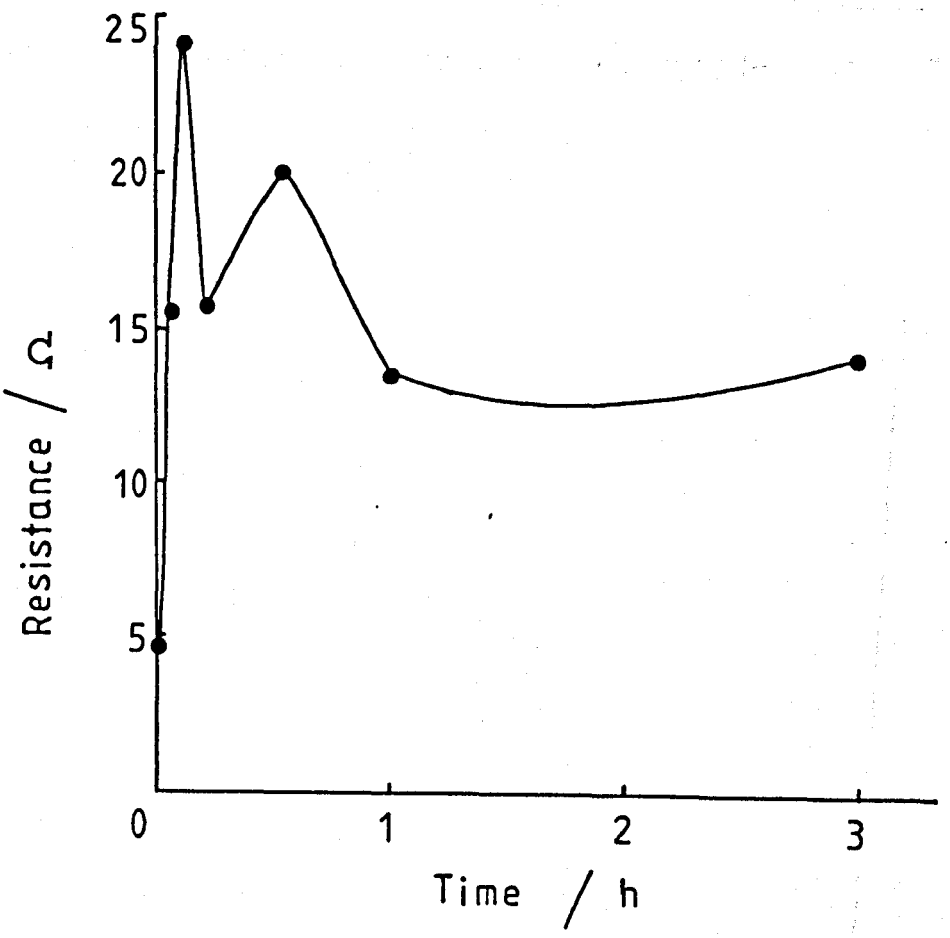
25
20
15
10
5
0
Resistance / Ω
1
2
3
Time / h

d)

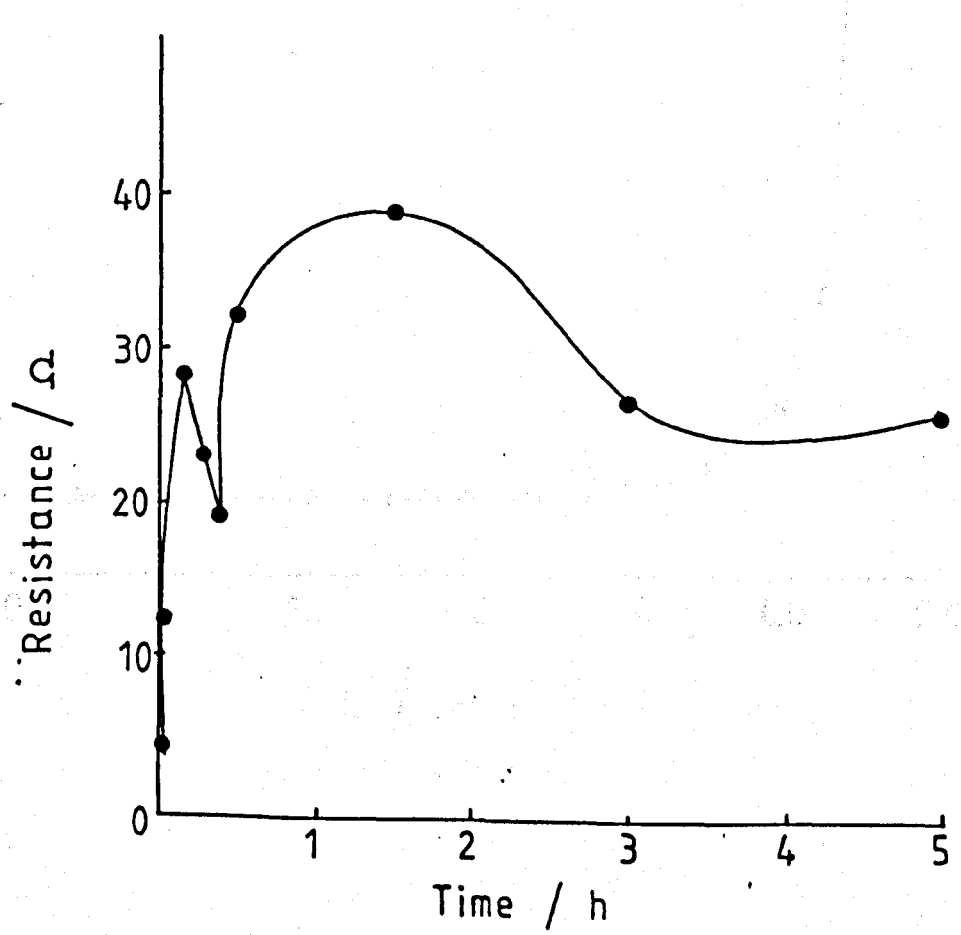
40
30
20
10
0
Resistance / Ω
1
2
3
4
5
Time / h

Figure 4.34

Tafel plot of data from figure 4.33 in the region 4.0V to 5.0V. Area = $0.5cm^2$.

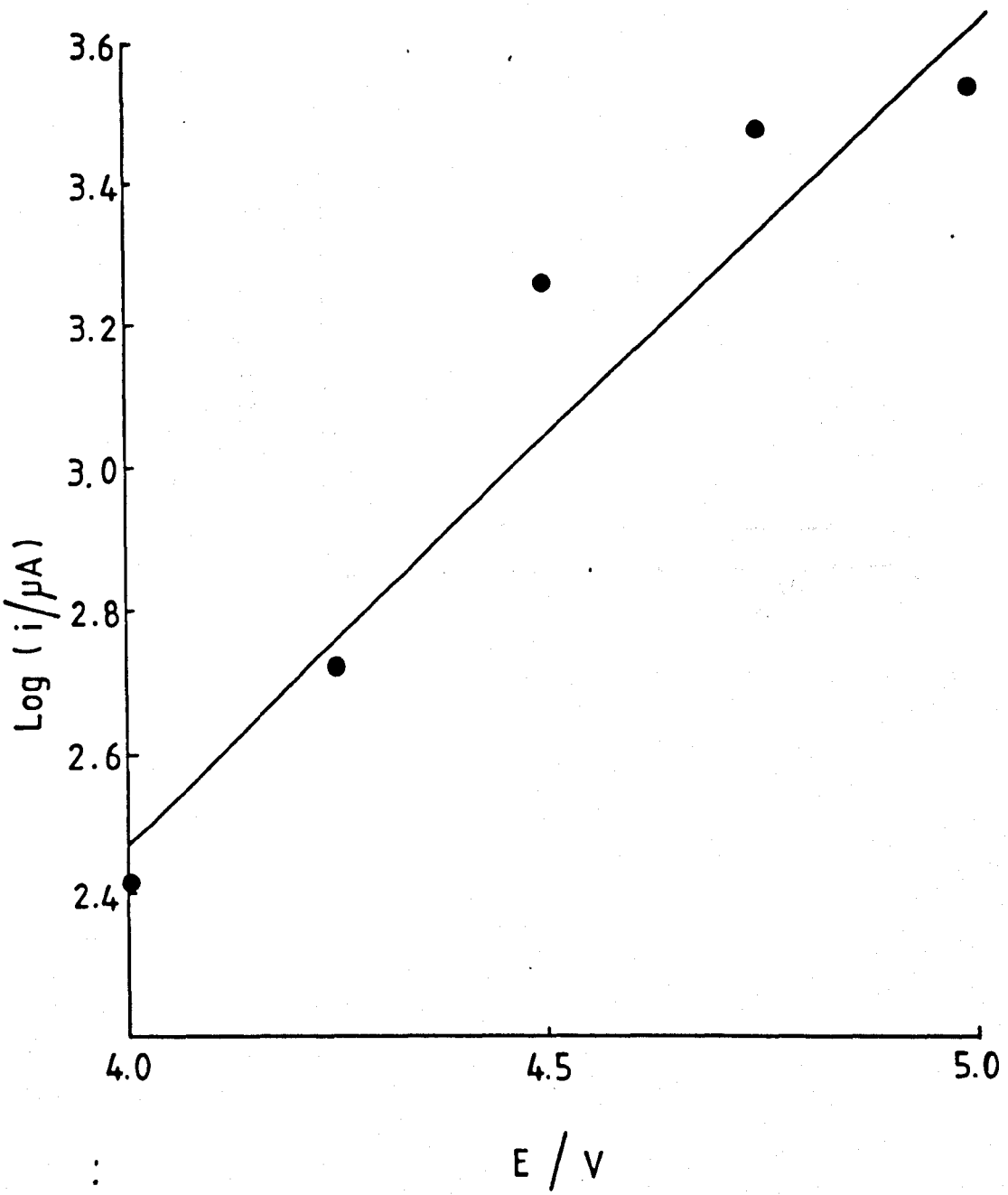

Figure 4.35

Typical falling transient obtained during a potential pulse experiment in KF.2HF from a base potential of 0V to potential in the region 3.7V to 5.1V, using either vitreous carbon, face orientation graphite or YBD carbon. The plot shown is for a pulse to 4.9V using a vitreous carbon electrode.

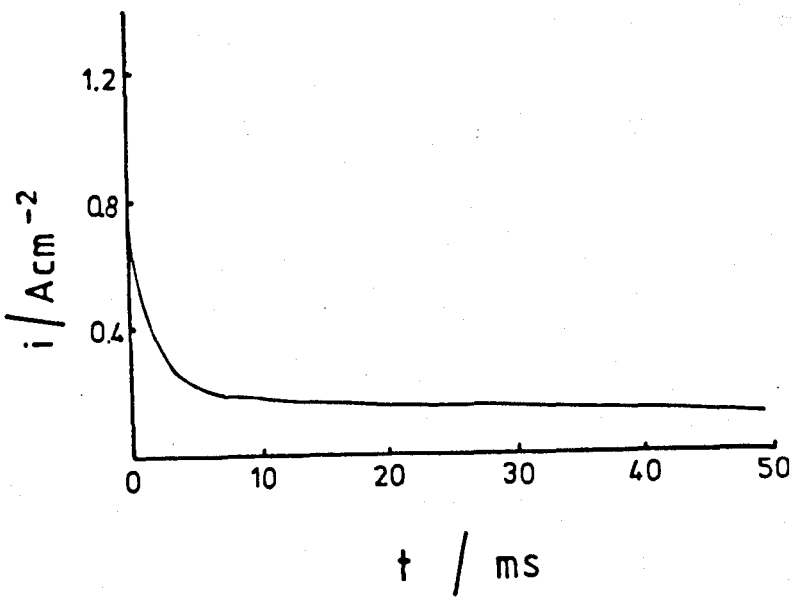

Figure 4.36

Polarisation data obtained during single pulse measurements in KF.2HF.

(■) Pyrolytic graphite with face orientation.

(●) YBD carbon.

(▲) Vitreous carbon.

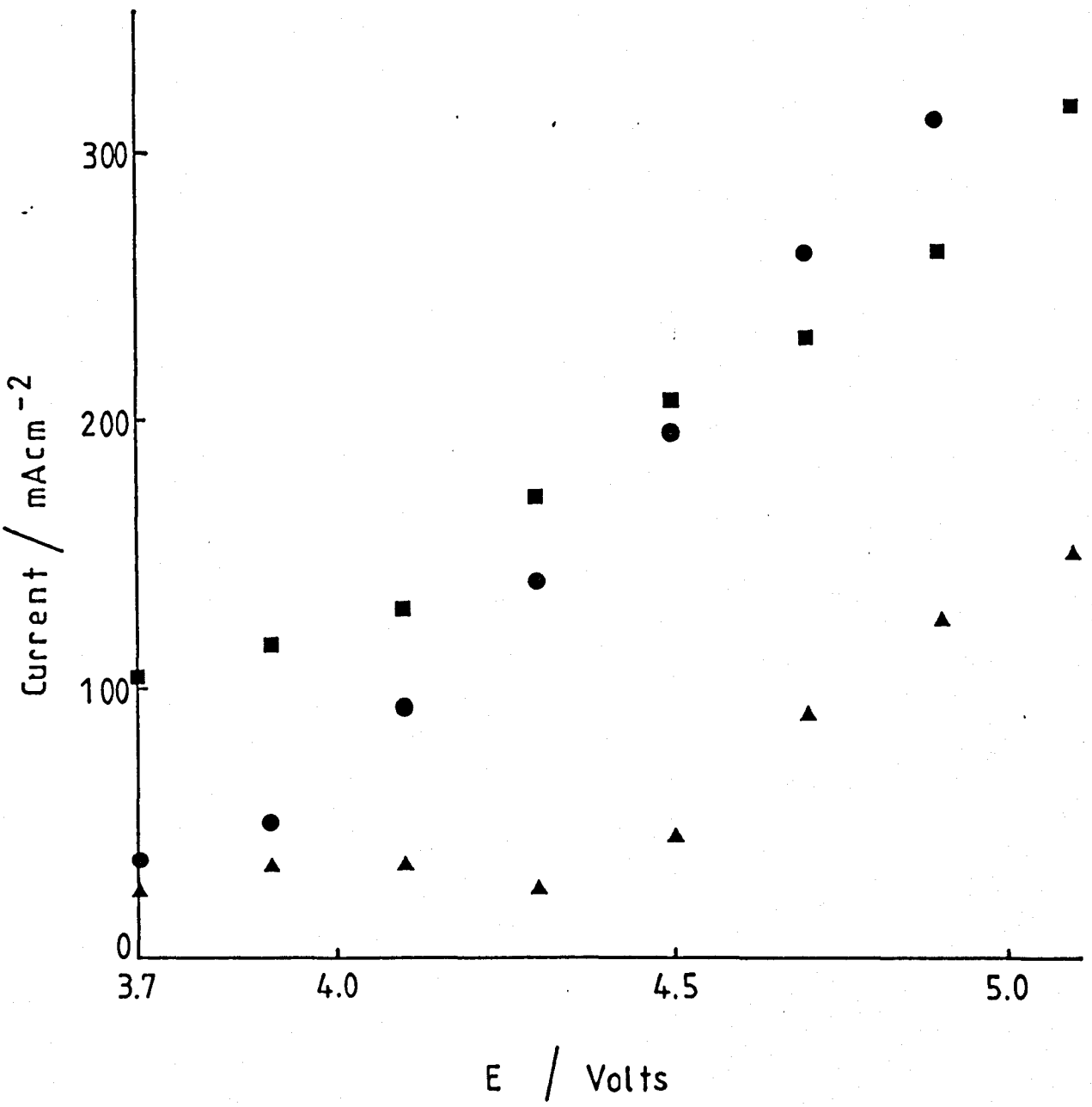

Figure 4.37

Potential pulse measurements in KF.2HF at pyrolytic graphite with edge orientation.

a) 3.7V

b) 3.9V

c) 4.1V

d) 4.3V

e) 4.5V

f) 4.7V

g) 4.9V

h) 5.1V

a)

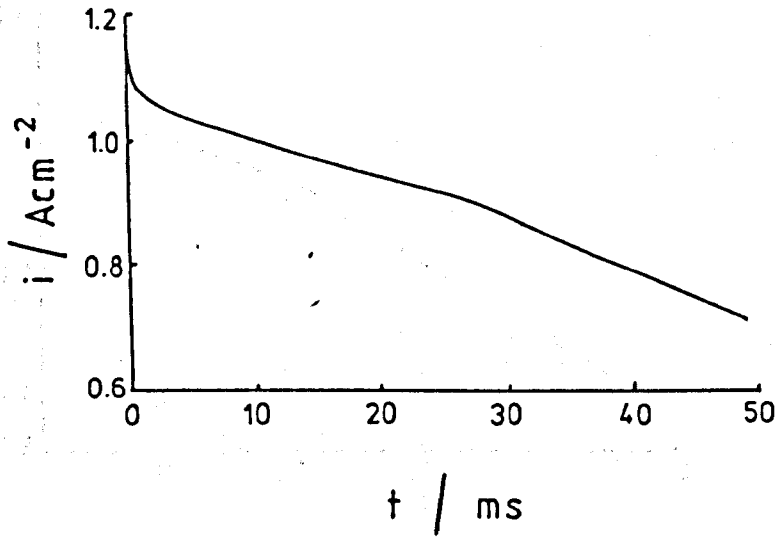
1.2
1.0
0.8
0.6
i / Acm^{-2}
0
10
20
30
40
50
t / ms

b)

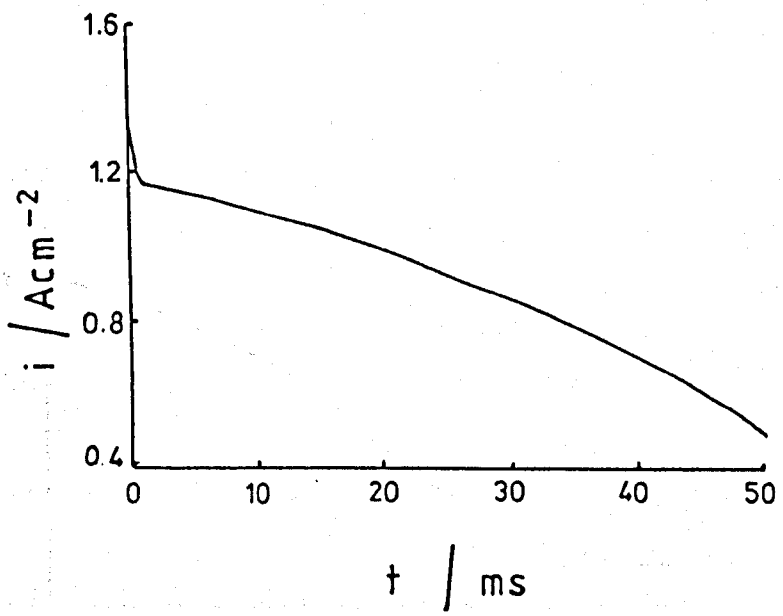
1.6
1.2
0.8
0.4
i / Acm^{-2}
0
10
20
30
40
50
t / ms

c)

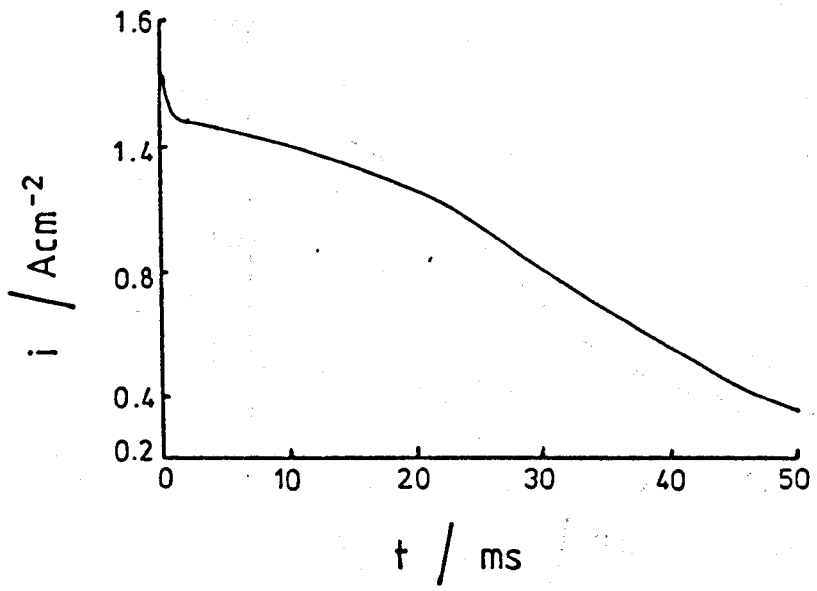
1.6
1.4
0.8
0.4
0.2
i / Acm-2
0
10
20
30
40
50
t / ms

d)

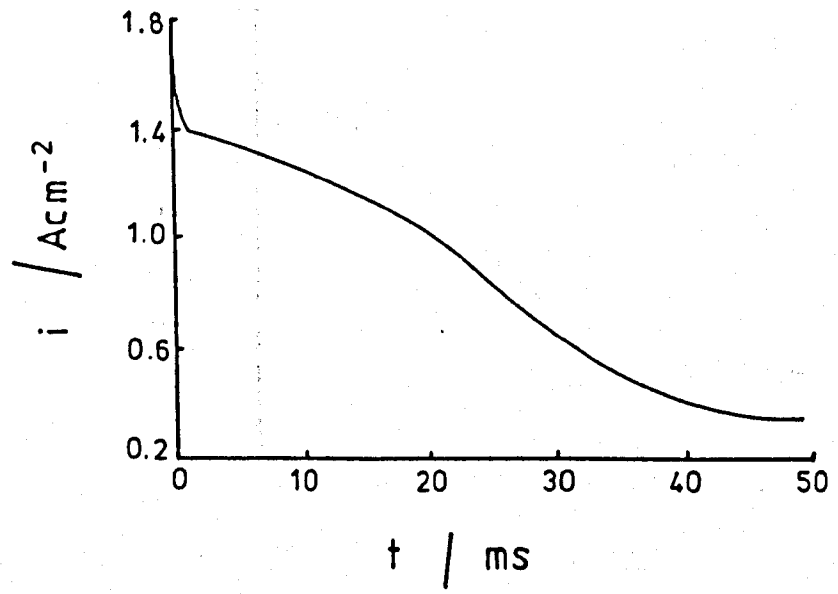
1.8
1.4
1.0
0.6
0.2
i / Acm-2
0
10
20
30
40
50
t / ms

e)

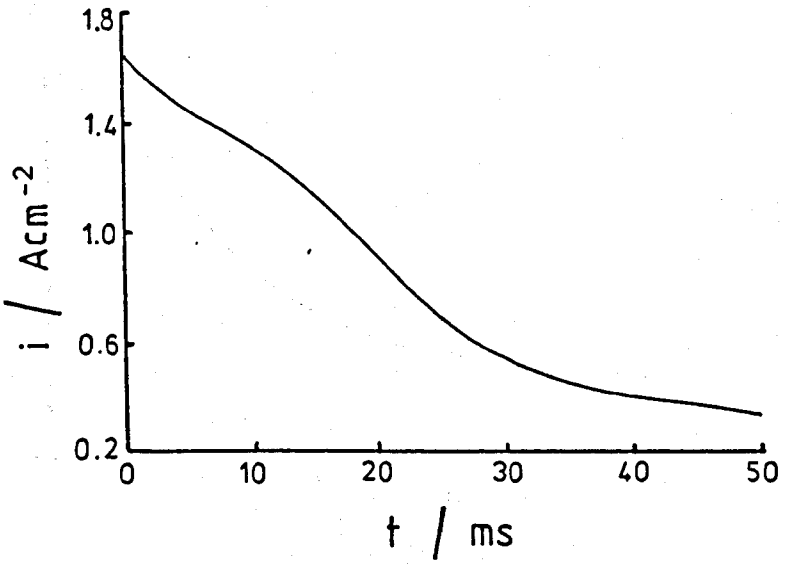
1.8
1.4
1.0
0.6
0.2
i / Acm^{-2}
0
10
20
30
40
50
t / ms

f)

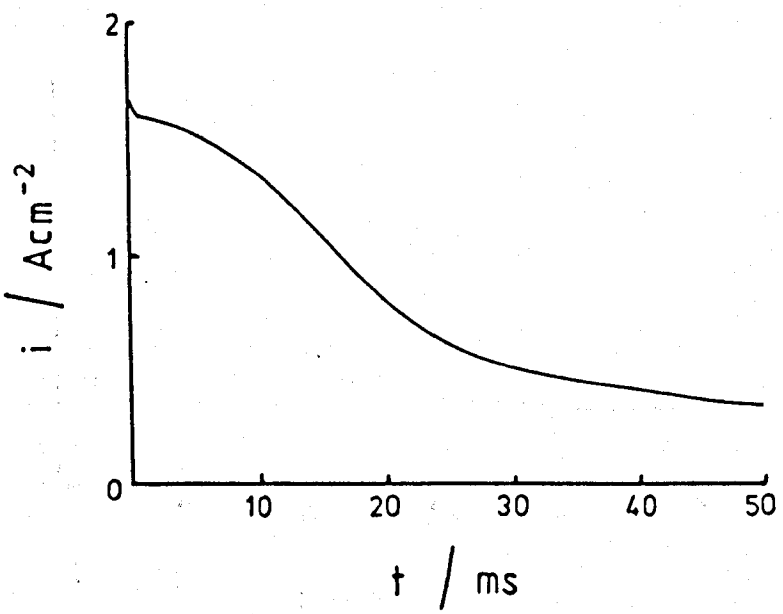
2
1
0
i / Acm^{-2}
10
20
30
40
50
t / ms

g)

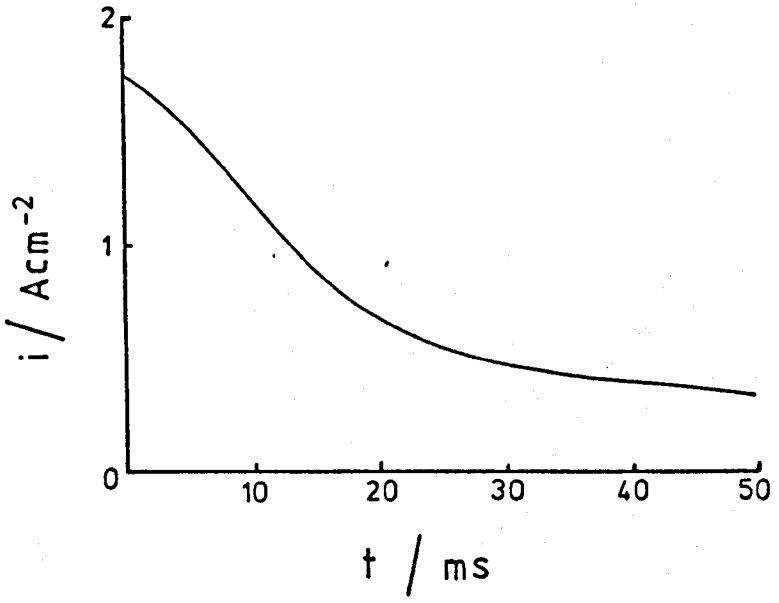

h)

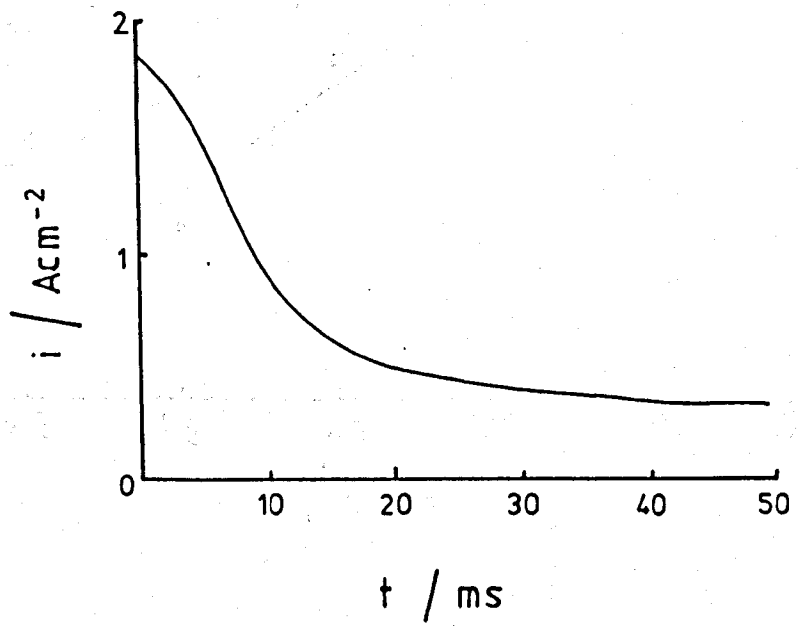

Figure 4.38

Polarisation data obtained in KF.2HF at a vitreous carbon electrode using a double pulse method.

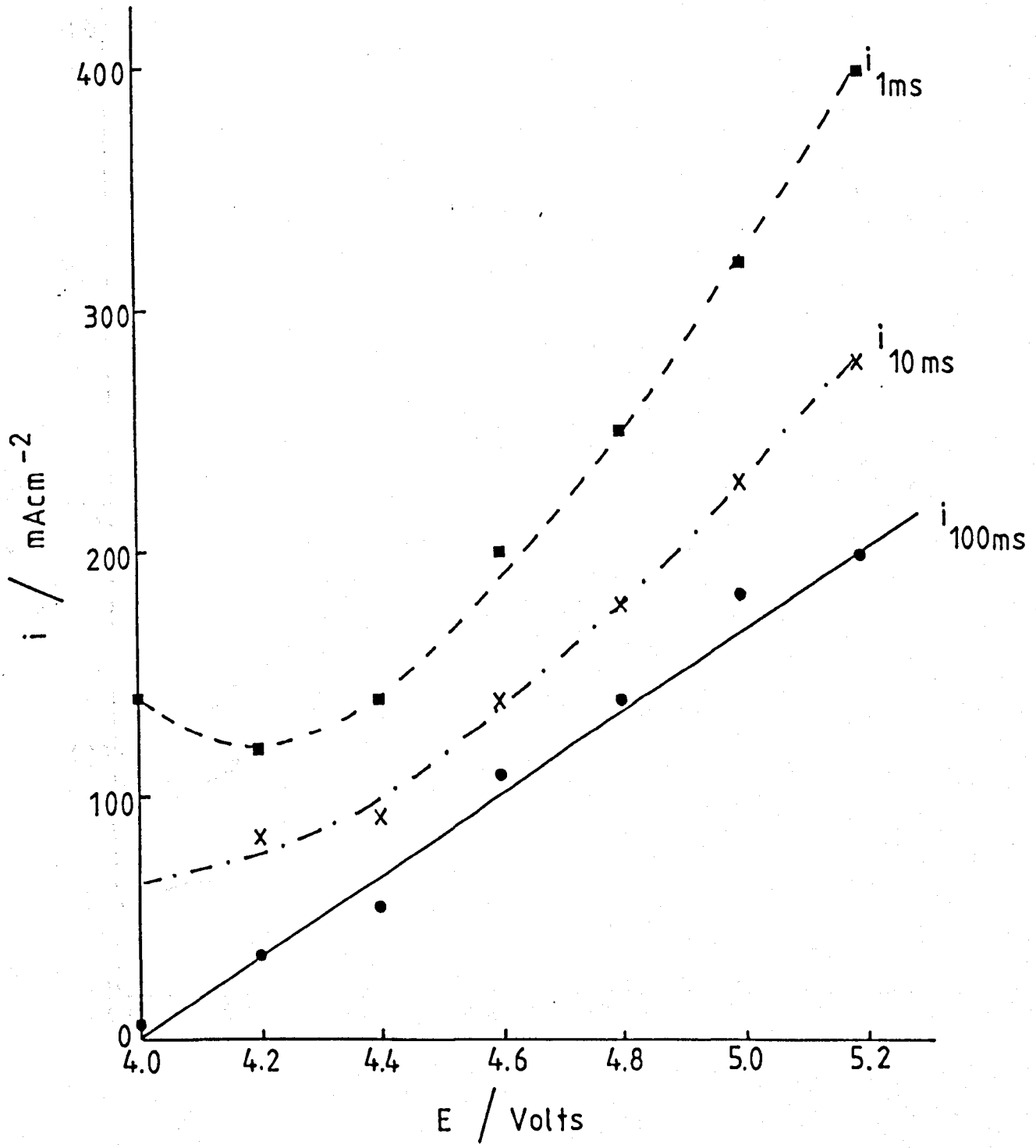

Figure 4.39

Polarisation data obtained in KF.2HF at a pyrolytic graphite electrode with face orientation using a double pulse method.

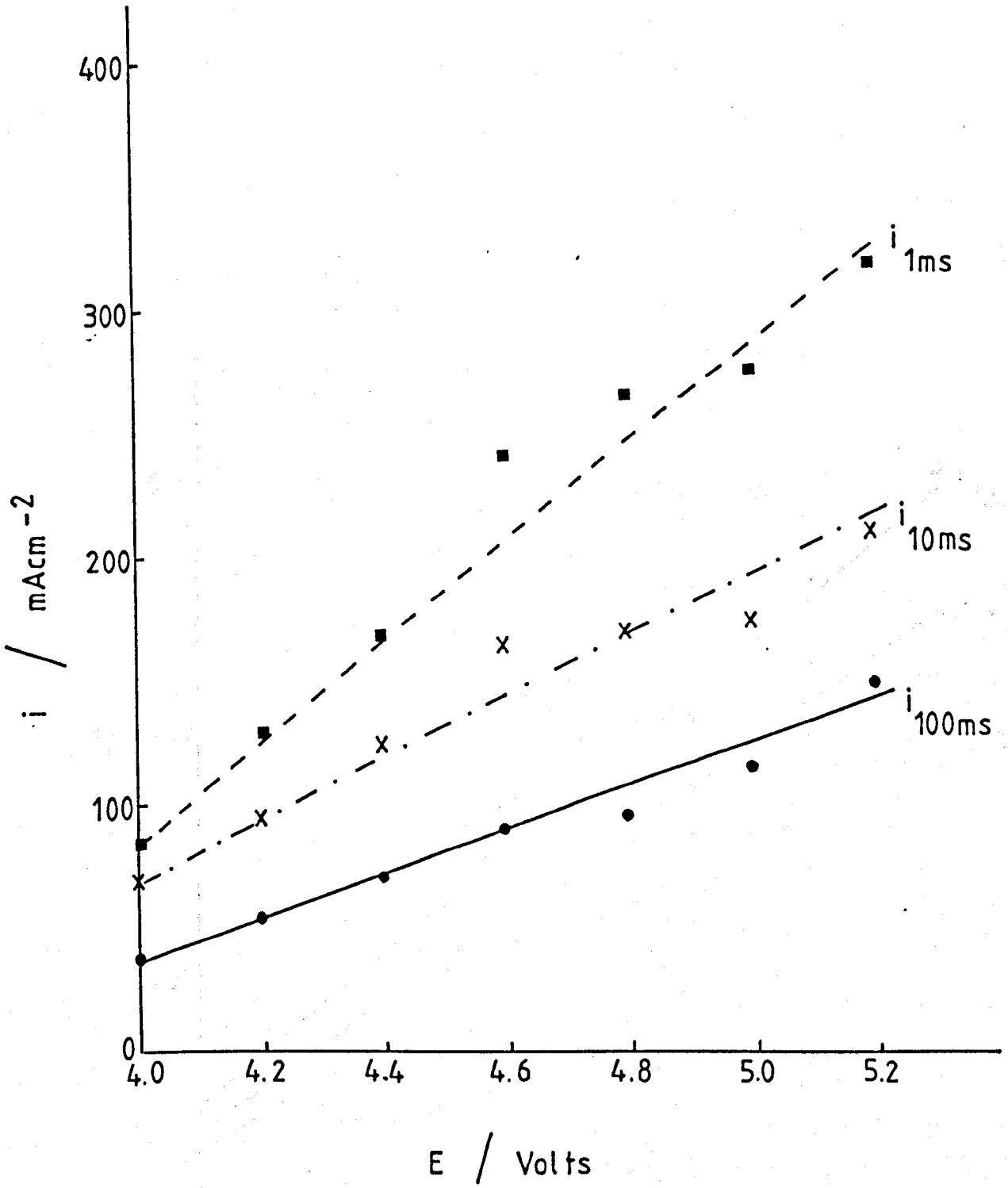

Figure 4.40

Polarisation data obtained in KF.2HF at a pyrolytic graphite electrode with edge orientation using a double pulse method.

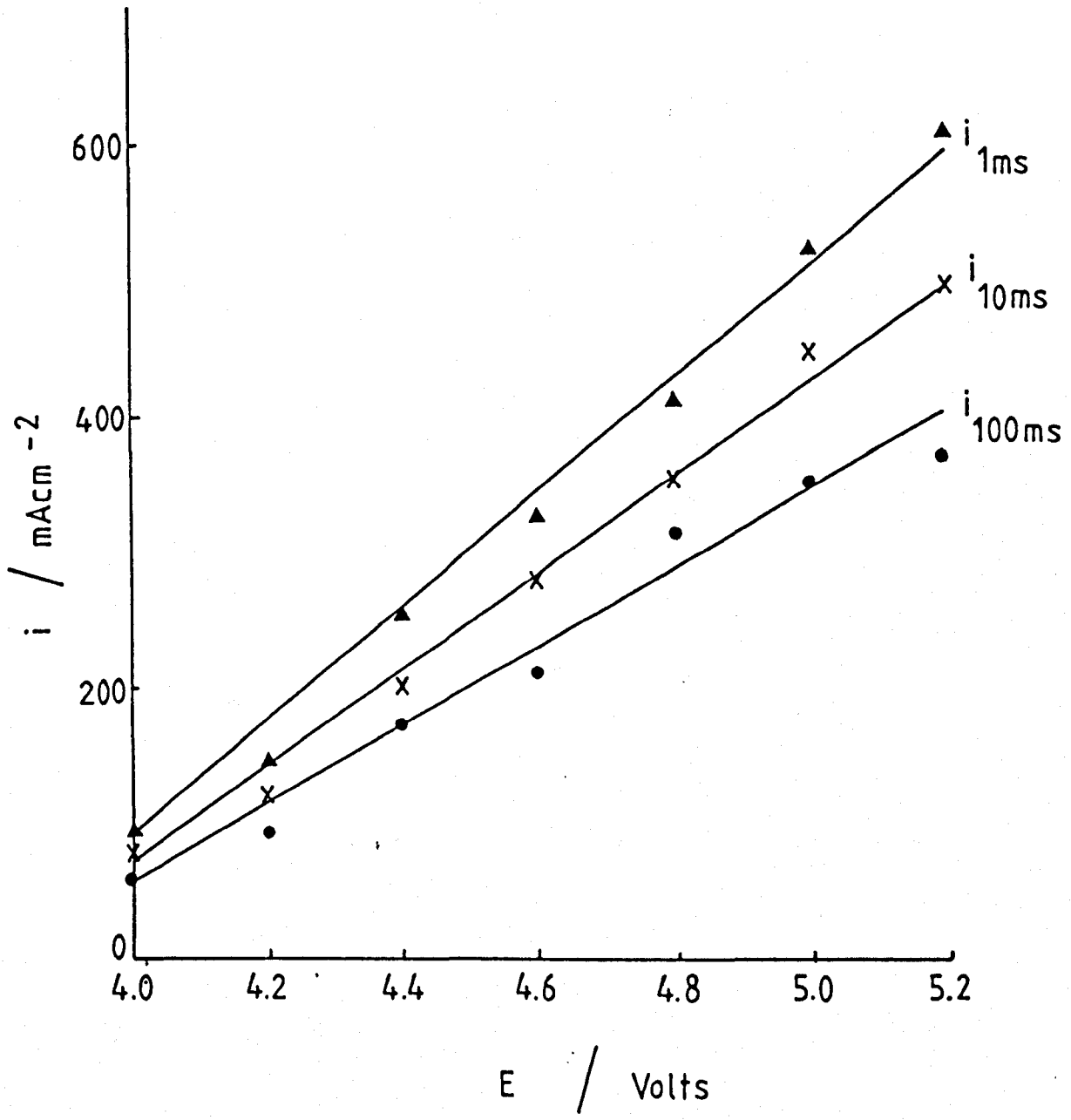

Figure 4.41

Polarisation data obtained at various anode materials in KF.2HF. The current 100ms after the pulse is plotted against potential. The diagram also shows the effect of fluorine evolution at 6.0V for 30 minutes on the currents measured at 5.0V.

(●) Pyrolytic graphite with edge orientation

(○) Pyrolytic graphite with edge orientation after fluorine evolution at 6V for 30 mins.

(▲) Vitreous carbon

(△) Vitreous carbon after fluorine evolution at 6V for 30 mins.

(■) Pyrolytic graphite with face orientation

(□) Pyrolytic graphite with face orientation after fluorine evolution at 6V for 30 minutes.

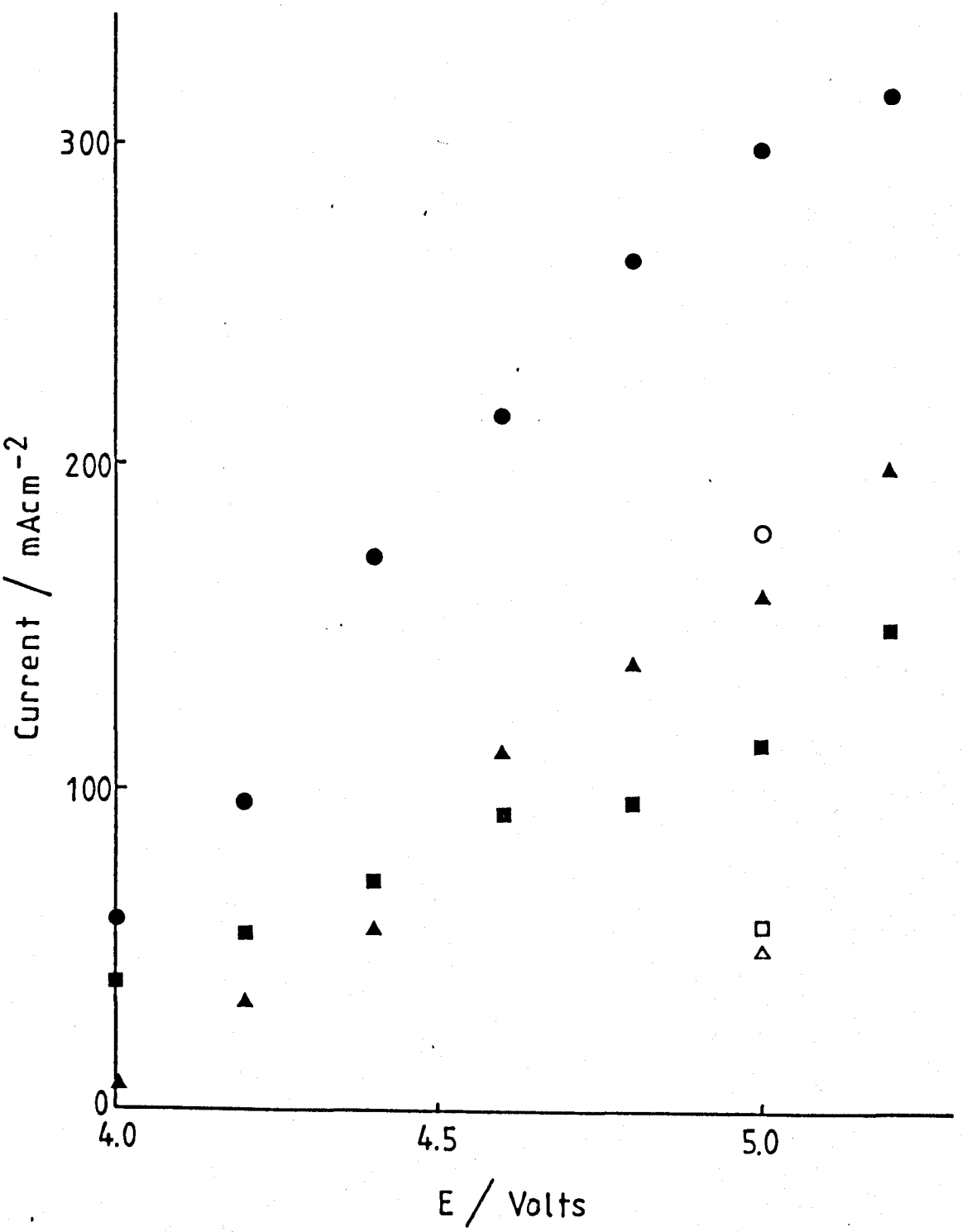
300
200
100
0
Current / mAcm^{-2}
4.0
4.5
5.0
E / Volts

Figure 4.42

Charge transient obtained during potential pulse measurements in KF.2HF in the region 1.8V to 2.8V.

a) Face orientation pyrolytic graphite.

b) Edge orientation pyrolytic graphite.

c) Vitreous carbon.

a)

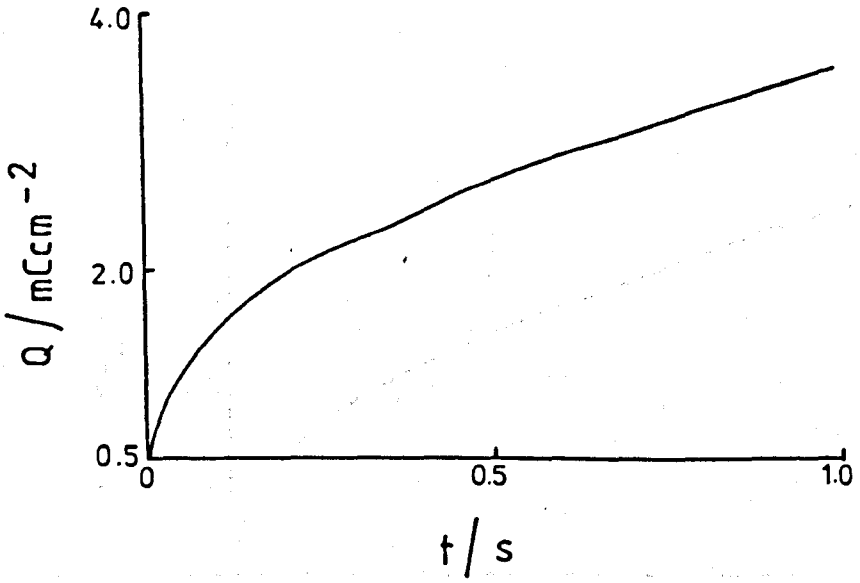

b)

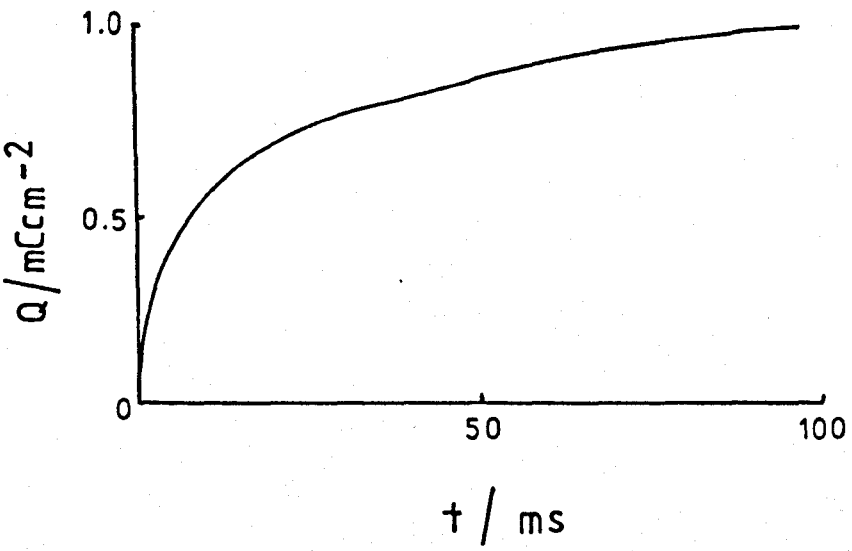

c)

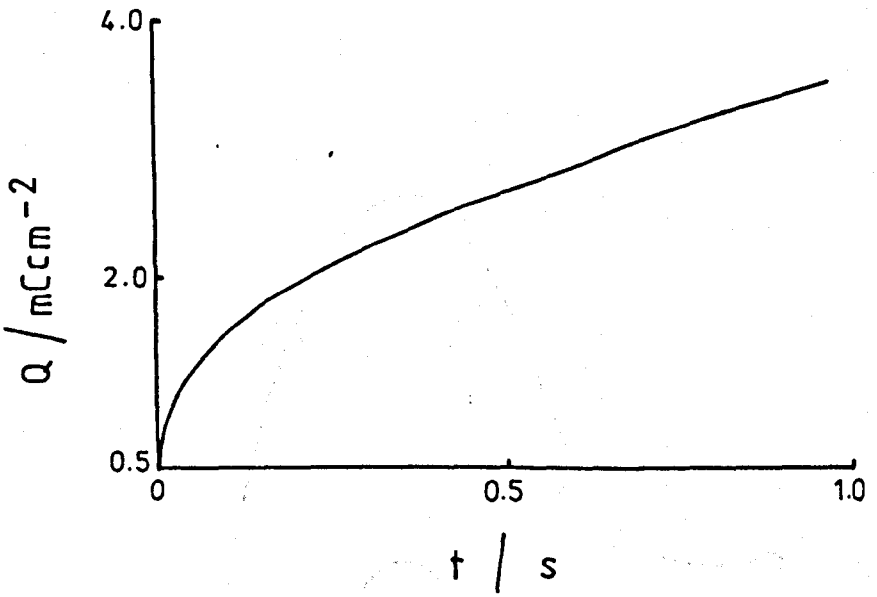

Figure 4.43

Charge vs. potential plots obtained from potential pulse measurements in KF.2HF.

(●) Pyrolytic graphite with edge orientation.

(■) Pyrolytic graphite with face orientation.

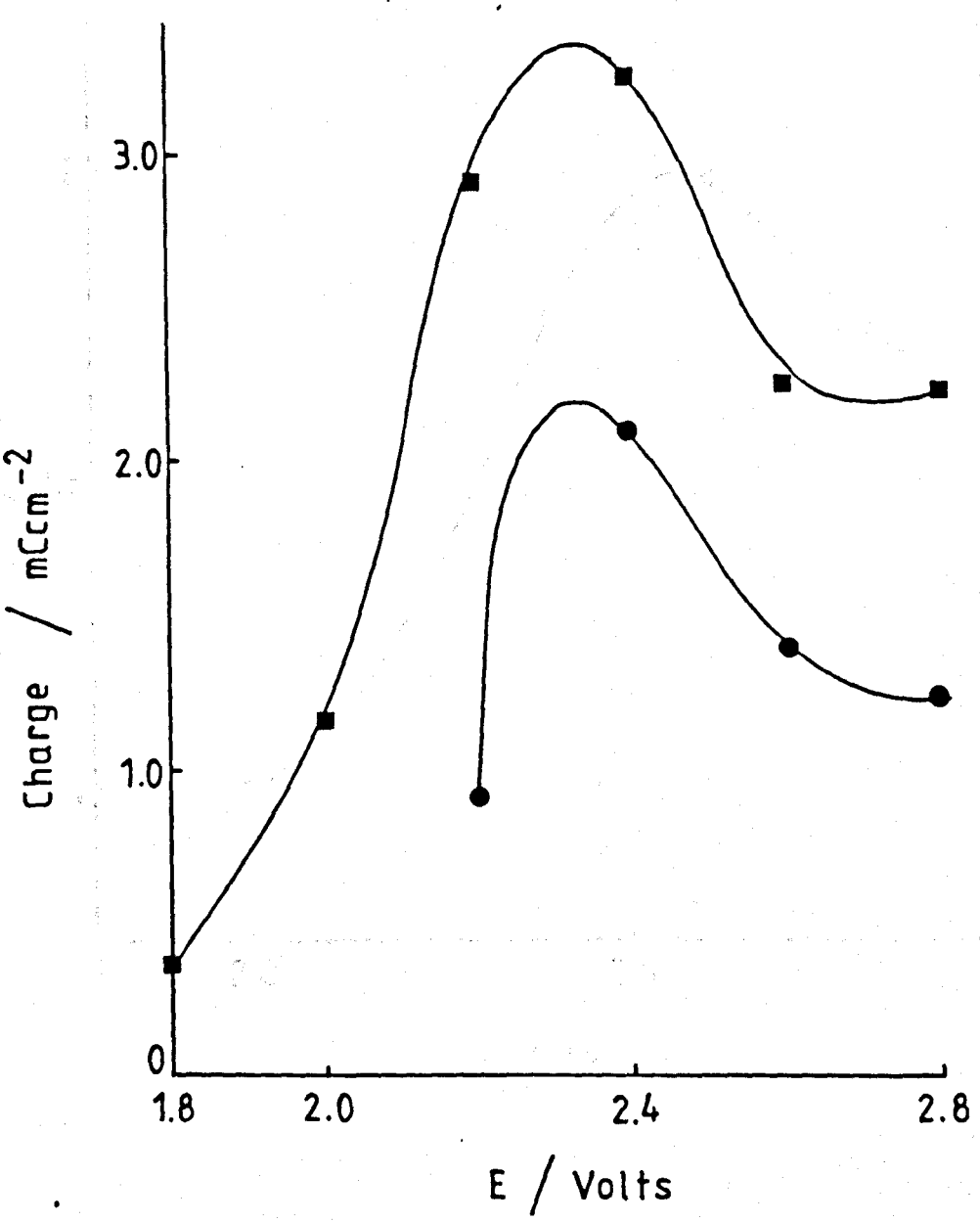

Figure 4.44

Charge vs. potential plot obtained from potential pulse measurements in KF.2HF at vitreous carbon.

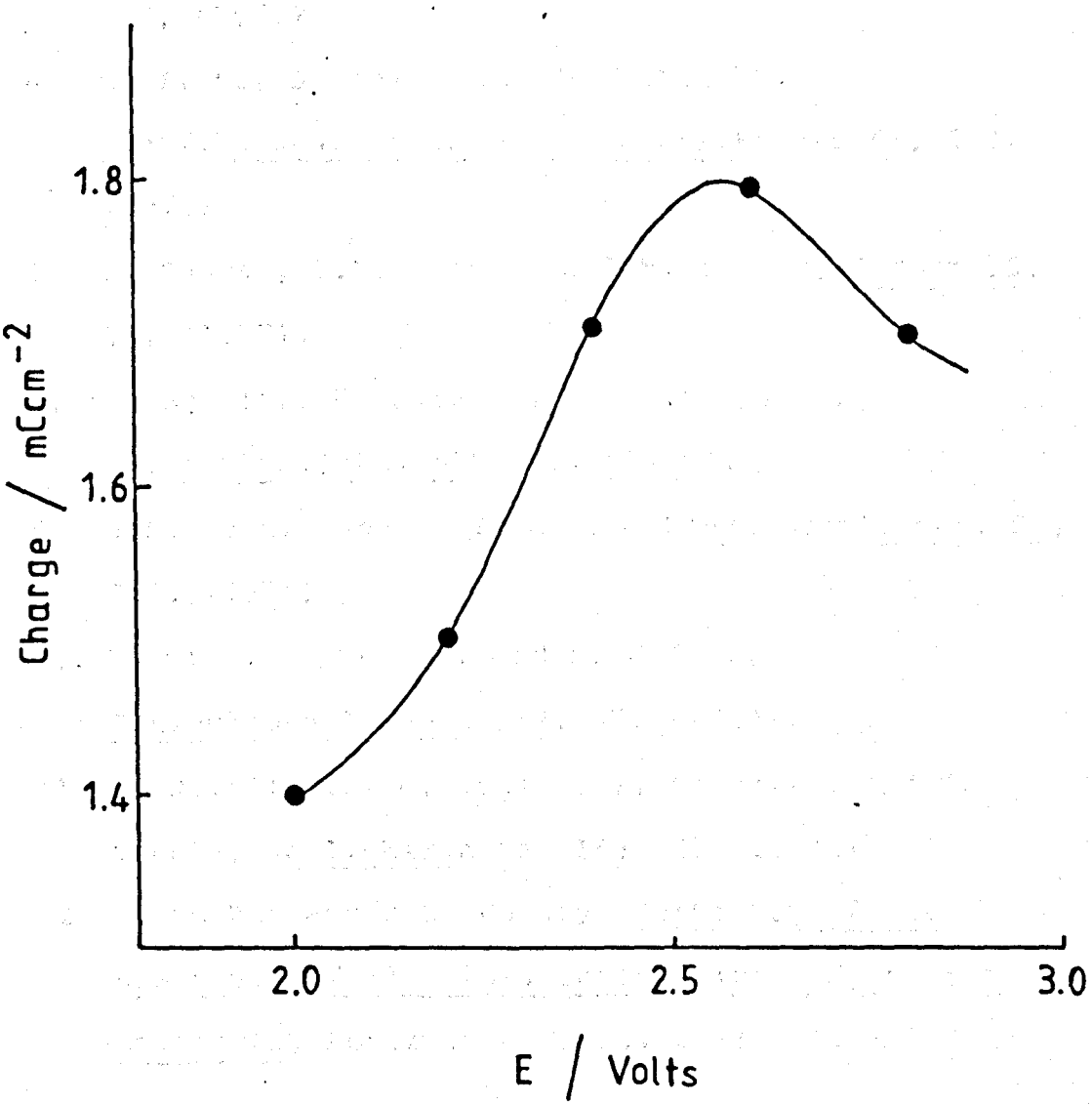

4.6 REFERENCES

1. O.R. Brown, Electrochimica.Acta. 25, 367, (1980).
2. D. Devilliers, F. Lantelme and M. Chemla, J. de Chim.Phys.Phys.Chim.Bio. 76, 428, (1979).
3. H. Imoto and N. Watanabe, Bull.Chem.Soc.Jpn. 49, 1736, (1976).
4. D. Devilliers, Thesis. Paris, (1986).
5. M. Armand and P. Touzain, Mat.Sci. and Eng. 31, 319, (1977).
6. H. Imoto, S. Koyama and N. Watanabe, Denki.Kagaku.Ogobi.Kogyo.Butsuri.Kagaku 46, 680, (1978).
7. P. Cadman, J.D. Scott and J.M. Thomas, Carbon 15, 75, (1977).
8. L. Bjelica, R. Parsons, and R.M. Reeves, Croat.Chem.Acta. 53, 211, (1980).
9. J.P. Randin and E. Yeager, J.Electroanal.Chem. 58, 313, (1975).
10. Y. Oren, M. Tobias, and S. Soffer, J.Electroanal.Chem. 162, 87, (1984).
11. D. Devilliers, M. Vogler, F. Lantelme, and M. Chemla, Anal.Chim.Acta. 153, 69, (1983).
12. Lijun Bai and B.E. Conway, Centenary of the Discovery of Fluorine, International Symposium Abstracts, Abstract E6 P213, Paris, (1986).

CHAPTER 5

SPECTROSCOPIC STUDIES OF ELECTRODES EXPOSED TO FLUORINE

5.1 INTRODUCTION

In this chapter the results of an XPS and SIMS study of carbon anodes used for fluorine evolution are presented. Attempts were made to examine electrodes which had been exposed to fluorine at various anode potentials by means of infrared diffuse reflectance spectroscopy using a FTIR spectrometer. Comparison was made between fluorinated electrodes and standard carbon fluorides (Fluorocarbon Ltd.).

5.2 XPS/SIMS STUDIES OF CARBON ANODES USED FOR FLUORINE GENERATION

XPS studies of carbon fluorides and of vitreous carbon electrodes used for fluorine evolution have been reported previously.[1,2] The present work attempts to differentiate between samples exposed to fluorine at two different potentials. Comparison was made between fluorinated samples and freshly-polished electrodes, and peak positions were compared with values given in the literature for "standard" carbon fluoride samples;[3,4,5] financial restrictions precluded a study of standard samples in this work. The results obtained were not very reproducible. This is not surprising as the properties of carbons depend on many factors including pore size, surface area and impurities. Small changes in the carbon surface can lead to significant changes in reactivity.

5.3 XPS EXAMINATION (Al Kα RADIATION $h\nu$ = 1486eV)

5.3.1 Fresh Vitreous Carbon Electrodes

Only carbon and oxygen were detected by the XPS

method on freshly polished electrodes. Figure 5.1 shows the wide scan spectrum and Figure 5.2 the narrow spectrum of a freshly polished carbon sample. The carbon 1s photoelectron peak was located at 1197-1198eV whilst the O1s peak was at 949-950eV. The corresponding binding energies are shown in Table 5.1. After short periods of etching by argon ions, the amount of oxygen decreased, but there were no significant changes in the location or shape of the photoelectron peaks. Composition and etching data are shown in Table 5.2.

5.3.2 Electrodes used for Fluorine Generation at 5V for 24hrs

Electrodes polarised at 5V in KF.2HF did not give reproducible XPS spectra. The elements detected were carbon, oxygen and fluorine (Figure 5.3). Prior to ion etching the C1s peak comprised several components the largest being at 1192-1193eV and at 1197eV with minor components at 1188eV. A small component at 1186eV was thought to be due to the presence of potassium. Potassium was also detected in the SIMS analysis but the XPS peak could not be resolved with sufficient accuracy to permit quantification (Figure 5.4). The assignments for the various C1s peaks are shown in Table 1. The 1197eV peak corresponds to carbon as C-C or C-H. The peak at 1192eV corresponds to carbon as C-F[3] and the peak at 1188eV can be assigned to carbon in CF_3 groups. A slight shoulder was observed at 1191eV suggesting that a small proportion of CF_2 was also present. Estimates are shown in Table 5.2 of the amounts of carbon attached

to fluorine and carbon as unchanged carbon but are to be regarded as approximate.

The Fls peak was located at 794eV and the Ols at 949eV. After argon ion etching the amounts of fluorine and carbon combined with fluorine both decreased (Figure 5.5) and other carbon (C-C, C-H) components increased. This was matched by a change in shape of the Cls peak where the component at 1192eV shrank into a shoulder on the side of the main peak at 1197eV. After argon ion etching the fluorine 1s peak developed a second component at 797eV, which was attributed to a C_4F^5 species, (Figure 5.6). After prolonged ion etching the peak at 797eV became the major component of the Fls peak, but there was little change in the shape of the Cls peak, (Figure 5.7).

5.3.3 Electrodes used for Fluorine Generation at 9V for 24hrs

The amount of fluorine detected by XPS was similar to that found on electrodes used for fluorine evolution at 5V. The Cls component consisted of two major components at 1197eV (C-C) and 1192eV (C-F). A small amount of CF_3 was shown to be present with a peak at 1188eV. The Fls peak was found at 792eV. Ion etching caused a decrease in the proportion of C-F groups. These results are shown in Figures 5.8 and 5.9.

5.4 SIMS STUDIES

5.4.1 Fresh Electrodes

Fresh unused electrodes produce simple SIMS spectra.

Both positive and negative ion spectra were recorded (Figures 10,11). The positive ion spectrum indicated the presence of C, Na, K, Al, Mg, Ca, Co, Fe, Cr and Si. The negative ion spectrum indicated C, F, Cl, O and H as C-H and OH^-. There was also evidence for nitrogen (as CN^-) at mass 26 (this could also be attributed to C_2H_2). The most intense signals in the negative ion spectra were due to C_2^- and C_4^- species, whilst multiple carbon ion species were found in the range $C_2 \longrightarrow C_{10}$. Ions of the form C_nH^- and $C_nH_2^-$ were also detected.

5.4.2 Fluorine Anodes

The SIMS spectra of electrodes used for fluorine generation were much more complicated than those obtained from untreated electrodes. These spectra contained features from ions containing (C-F) and (K-F) species in both the +ve and -ve ion SIMS spectra. An attempt was made to compare these spectra with a PTFE standard. However this proved unsuccessful. A sample of PTFE tape was visibly degraded by the ion beam, and a PTFE spray contained an unknown binder which resulted in highly complex spectra interfering with some of the peaks due to C-F species.

5.4.2.1 Electrodes treated at 5V

The positive ion SIMS spectra for electrodes exposed to fluorine at 5V showed peaks due to $K(KF)_n^+$ species ($n = 0,1,2$) and to C^+, F^+, CF^+, CF_2^+, CF_3^+, C_3F^+, $C_3F_2^+$, $C_3F_3^+$ and (Figure 5.12) $C_3F_5^+$. It is noteworthy that positive ion SIMS spectra do not usually record F^+, due

to its low sensitivity; the detection of F^+ therefore implies that there is extensive coverage of the surface by fluorine (probably as C-F species). The negative ion spectra showed peaks due to C_n^- and C_nF^- and also $F(KF)_n^-$ (n = 0,1) (Figure 5.13).

Argon ion etching was used to determine depth profiles of the electrode surfaces. The etch rate was in the range 0.1-0.2nm per minute. Etching shows a rapid decrease in the signal due to CF^+, CF_3^+ and $C_3F_3^+$ ions relative to the C^+ and C_3^+ ions, and indicates film thicknesses in the range 3 to 6nm (Figure 5.14).

5.4.2.2 Electrodes treated at 9V

Such electrodes gave SIMS peaks similar to those observed with electrodes treated at 5V. However, it was noted that the negative ion SIMS spectra showed an increase in the C-F species compared with electrodes treated at 5V (Figure 5.15). The positive ion spectra showed an increase in the signal due to CF^+ compared with electrodes fluorinated at 5V. However, interestingly, in the negative SIMS spectra there was a fall in intensity of peaks due to lower fluorides such as C_4F^-, C_3F^- and C_2F^- (Figure 5.15 and 5.16).

Argon ion etching again showed a rapid fall off in C-F species as ion etching proceeded. The film thicknesses obtained were in the range 3.5nm to 7nm. (Figure 5.17).

5.5 DISCUSSION OF ESCA AND SIMS RESULTS

ESCA examination revealed very little difference between electrodes fluorinated at 5V and at 9V in KF.2HF. However, following argon ion etching the XPS spectra of electrodes fluorinated at the lower potential revealed the existence of a C_4F species on the electrode surface.

SIMS examination of the electrodes revealed a decrease in the amount of "lower" fluorides at electrodes subjected to higher fluorination potentials.

These results indicate that at higher potentials the degree of fluorination of a carbon anode is greater. Lower fluorides such as C_4F are shown to exist at the lower fluorination potentials. These lower fluorides are known to be more conducting than $(C\text{-}F)_n$ species and are likely to inhibit the fluorine evolution reaction less than electrodes exposed to higher fluorination potentials.[7]

These findings are consistent with results obtained by examination of model redox systems using fluorinated electrodes (Chapter 6).

Depth profiles for electrodes treated at 5V and 9V reveal similar film thicknesses (3-7nm). Film thicknesses obtained from capacitance data were slightly less, in the region of 1nm (maximum) (Chapter 4).

These results lead to the idea of a graded fluoride film on the carbon anode in fluorine cells. The film is coherent, varying from an outer fluorine-rich (and thus insulating) region, through a carbon-rich

(semiconducting) region to the carbon anode itself. (Figure 5.18).

Figure 5.18

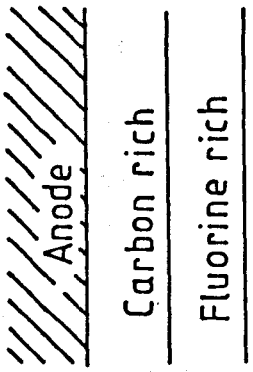

It is unlikely that abrupt boundaries between these layers (as drawn) actually exist.

5.6 INFRARED STUDIES

Examination was first made of carbon fluoride samples of known stoichiometry. Infrared diffuse reflectance spectra for CF_x compounds (x = 0.25, 0.6, 1.0) are shown in Figure 5.19. In each case the dominant peak is at 1218cm^{-1}. This is attributed to a C-F stretch. The intensity increases with increasing value of x. The spectrum of a pyrolytic graphite (face) electrode subjected to 24hrs fluorine evolution at 6V is shown in Figure 5.20, along with its spectrum before fluorine evolution. There is clear evidence for the emergence of a peak at 1217cm^{-1}, due to C-F stretching in the fluorinated sample.

A vitreous carbon electrode was examined by diffuse reflectance spectroscopy before and after anode effect (Figure 5.21). After anode effect the spectrum is

extremely complicated, being dominated by a strong peak at 1070cm^{-1} characteristic of a CF_2 symmetric stretch.[5] The absence of the C-F stretch at 1218cm^{-1} is difficult to explain, but may be due to a higher level of fluorination of the elctrode surface. A sample of PTFE gave the spectrum shown in Figure 5.22 where there is a shift in the peak position of the C-F stretch, although only slight.

The measurement of infrared spectra of electrode surfaces has proved very insensitive and was thus not pursued any further. It was thought that CF_x on the electrode surface was affected on transferring to acetonitrile solvent. A standard sample of CF_x x = 1.0 was extracted three times with acetonitrile. Between each extraction the solution was filtered. After the final extraction the sample was filtered and the resultant liquid examined by capillary film infrared spectroscopy. Comparison was made betweeen this liquid and a sample of the acetonitrile used. Figure 5.23a shows the infrared spectrum of acetonitrile whereas 5.23b is the spectrum of acetonitrile used to extract the CF_x compound. All peaks seen in 5.23b are due to acetonitrile; no C-F peaks have developed. Thus infrared spectroscopy has provided no evidence that C-F compounds are soluble in acetonitrile.

TABLE 5.1

Binding Energies determined from XPS measurements

Electrode Condition	Core Level	Binding Energy/eV (This Work)	Binding Energy/eV (Previous Work)[3,6]	Assignment
Fresh	C1s	288-9	287	C-C or C-H
	O1s	536-7	536	C-O
5V Before Etching	C1s	288	287	C-C,C-H
		294	292	C-F
		298	296	$-CF_3$
		300	-	K^+
	O1s	537	536	C-O
	F1s	692	692	C-F
5V After Etching	C1s	288	287	C-C, C-H
		294	292	C-F
	O1s	536	536	C-O
	F1s	691	692	C-F
		689	-	C_4F
9V	C1s	289	287	C-C, C-H
		291	292	C-F
		298	296	$-CF_3$
	O1s	537	536	C-O
	F1s	694	692	C-F

TABLE 5.2

Summary of XPS Results

SAMPLE	Etch Time /Mins	Approx Depth/nm	Atom % F*	O*	C(C-F)	C(C-H) (C-C)
Fresh	0	0	-	12	-	88
Electrode	1	0.7	-	4	-	96
	2	1.5	-	4	-	96
5V	0	0	46	5	27	22
Electrolysis	1	0.4	19	6	12	63
In KF.2HF	2	0.8	15	6	15	64
	4	1.6	11	5	15	69
	9	3.6	7	5	17	71
	19	7	6	5	15	74
	39	14	4	2	15	78
9V	0	0	44	9	23	24
Electrolysis	1	0.3	23	8	9	60
in KF.2HF	2	0.6	16	7	9	68

* The columns designated 'F' and 'O' refer to total fluorine and total oxygen respectively. It is probable that all the fluorine, and most of the oxygen, are chemically bonded to the carbon.

Figure 5.1

Wide scan XPS spectrum of a polished vitreous carbon.

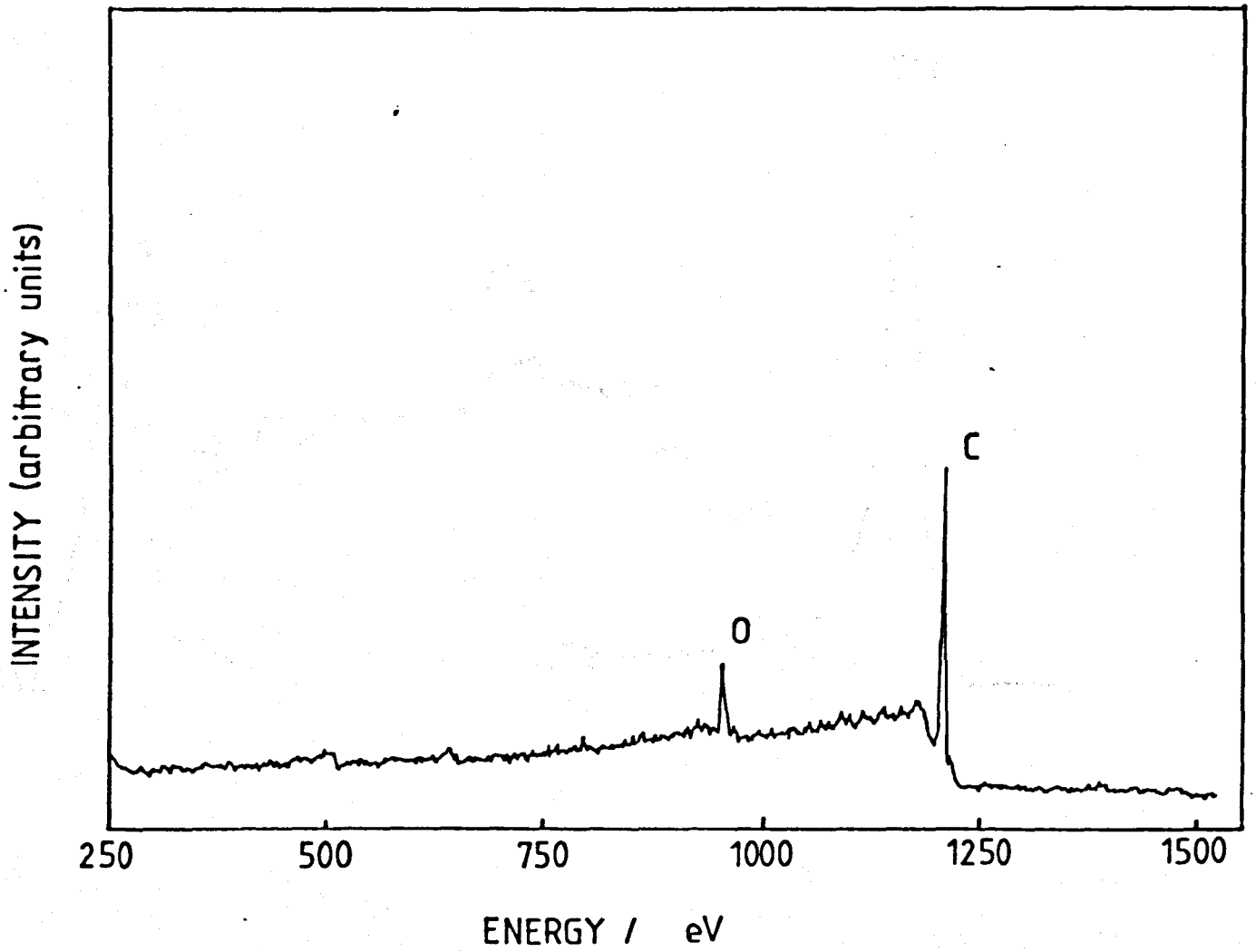

Figure 5.2

Narrow scan XPS spectrum of a polished vitreous carbon.

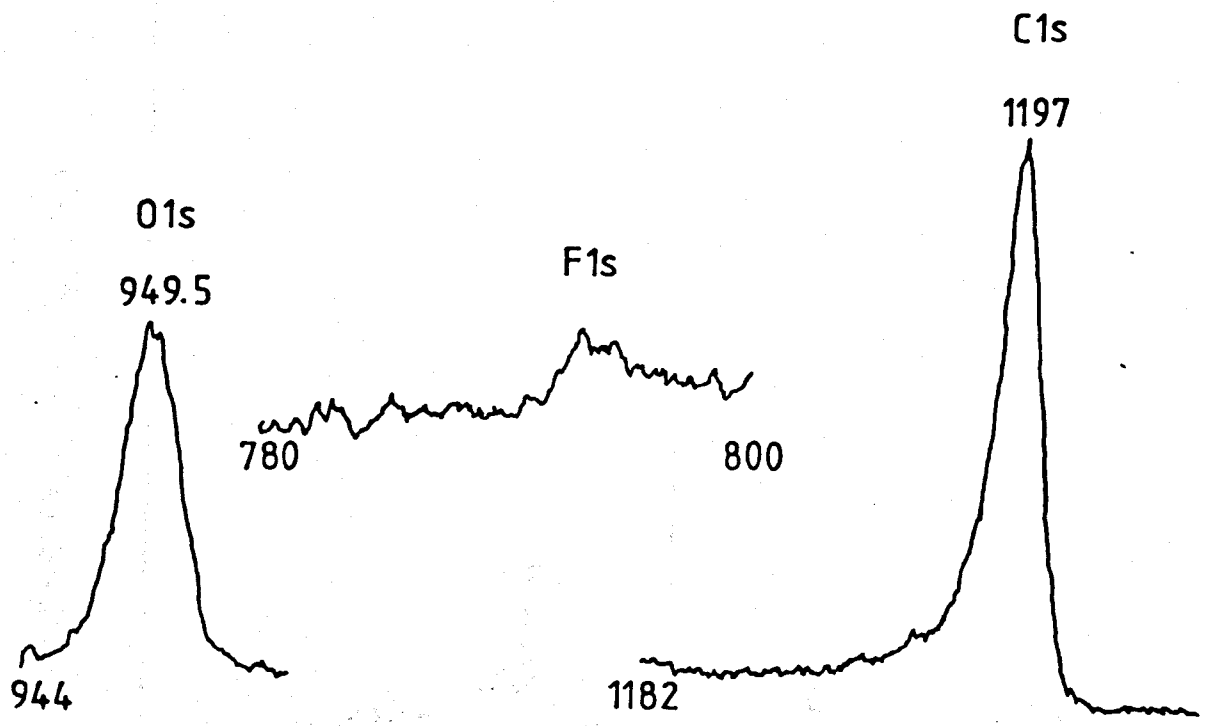

Figure 5.3

Wide scan XPS spectrum of a vitreous carbon exposed to Fluorine at 5V for 24hrs in KF.2HF.

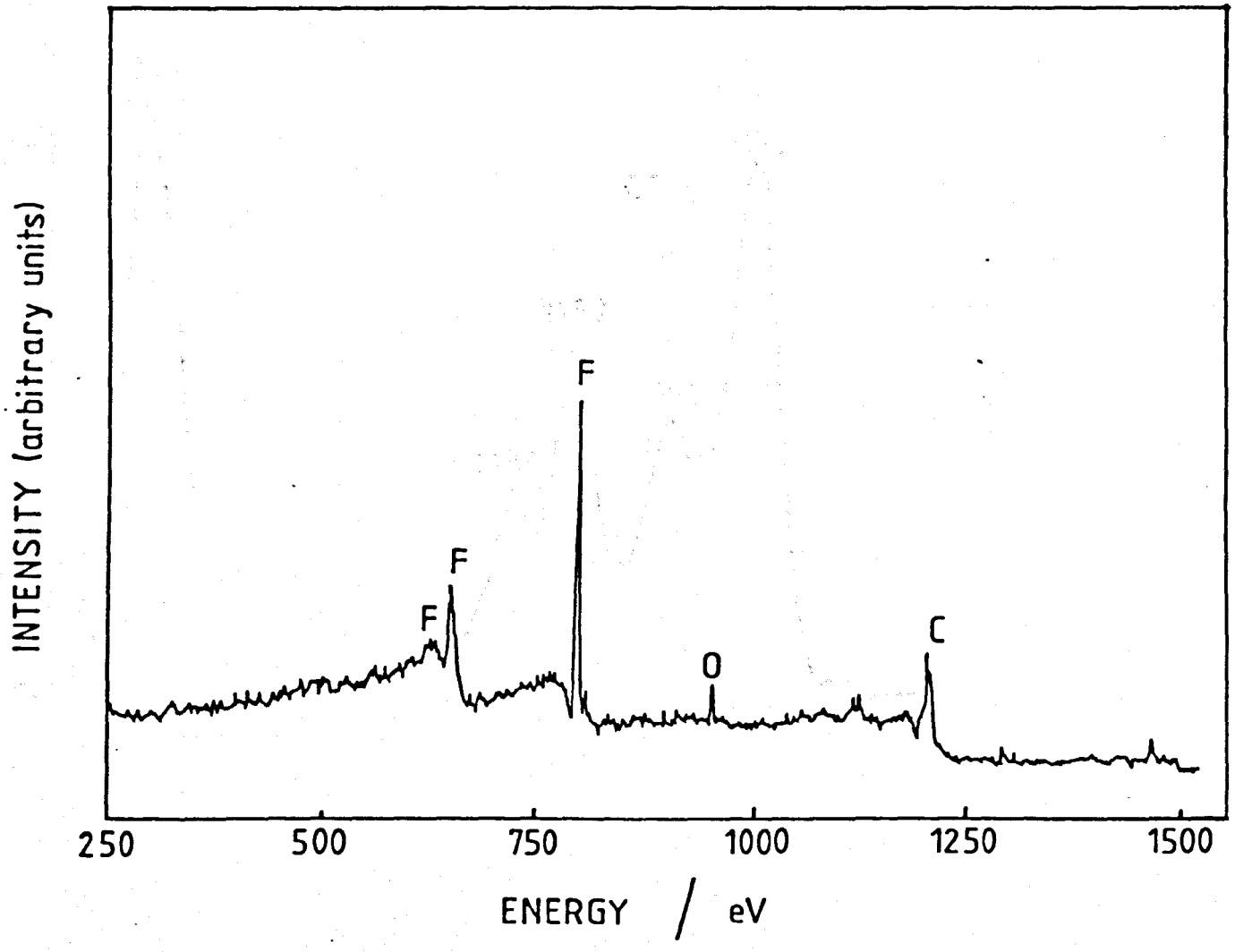

Figure 5.4

Narrow scan XPS spectrum of a vitreous carbon exposed to Fluorine at 5V for 24hrs.

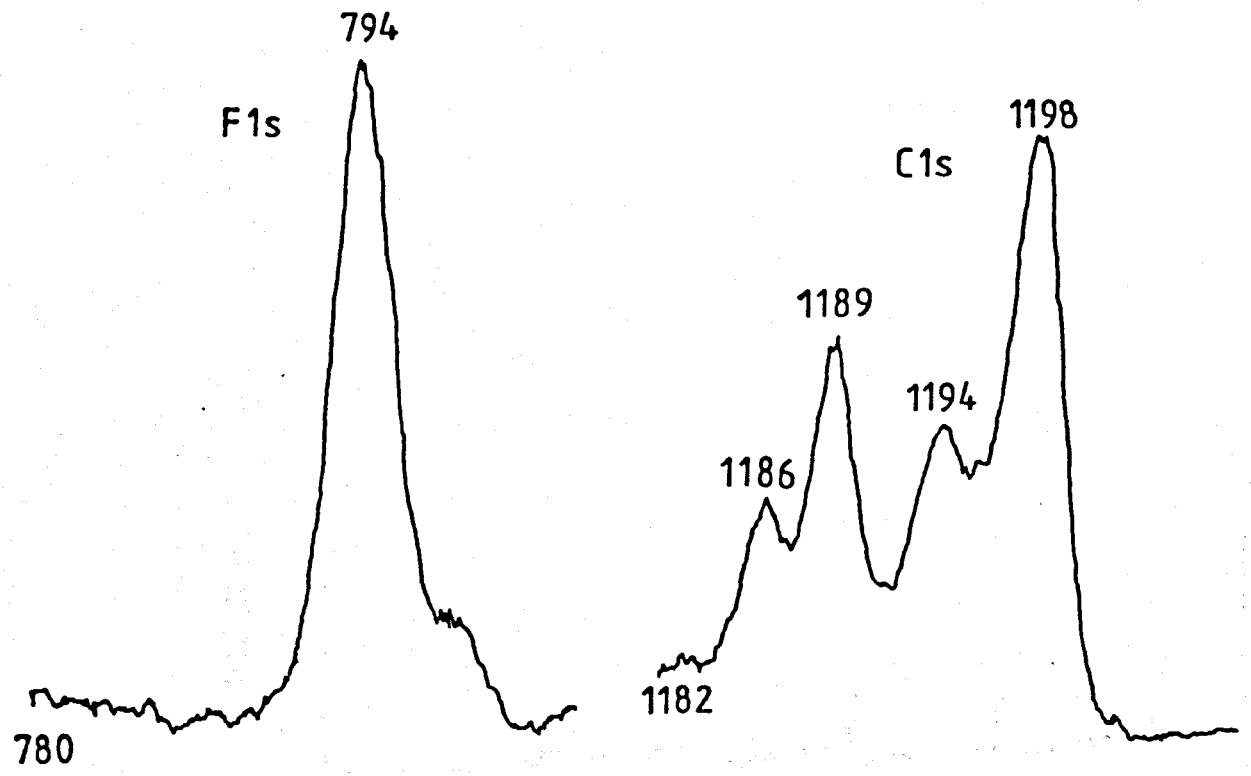

Figure 5.5

Wide scan XPS spectrum of a vitreous carbon exposed to Fluorine at 5V (24hrs). Spectrum recorded after 39 minutes argon ion etching.

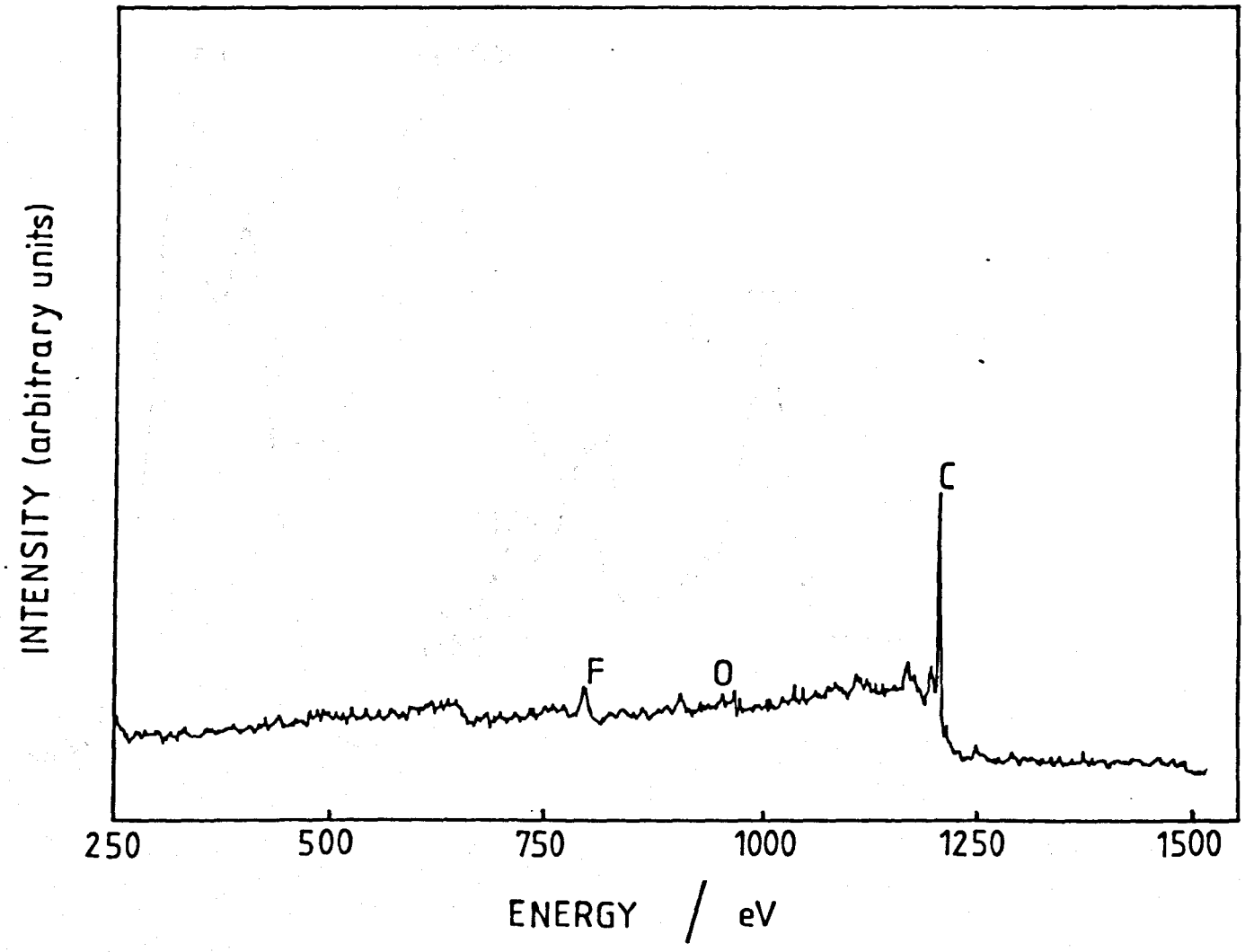

Figure 5.6

Narrow scan spectrum recorded after 1 minute argon ion etching for a vitreous carbon anode exposed to fluorine at 5V for 24hrs.

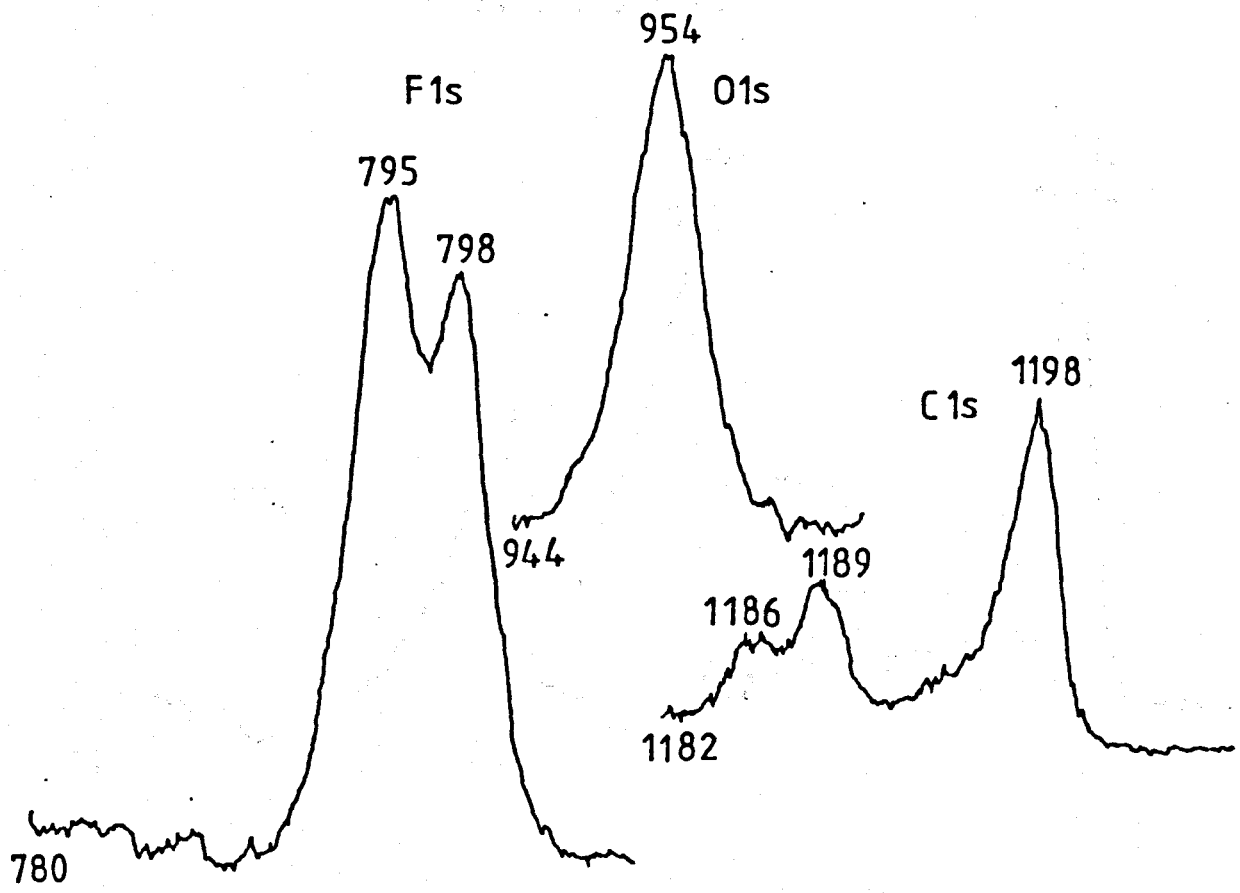

Figure 5.7

Narrow scan spectrum recorded after 39 minutes argon ion etching for a vitreous carbon anode exposed to fluorine at 5V for 24hrs.

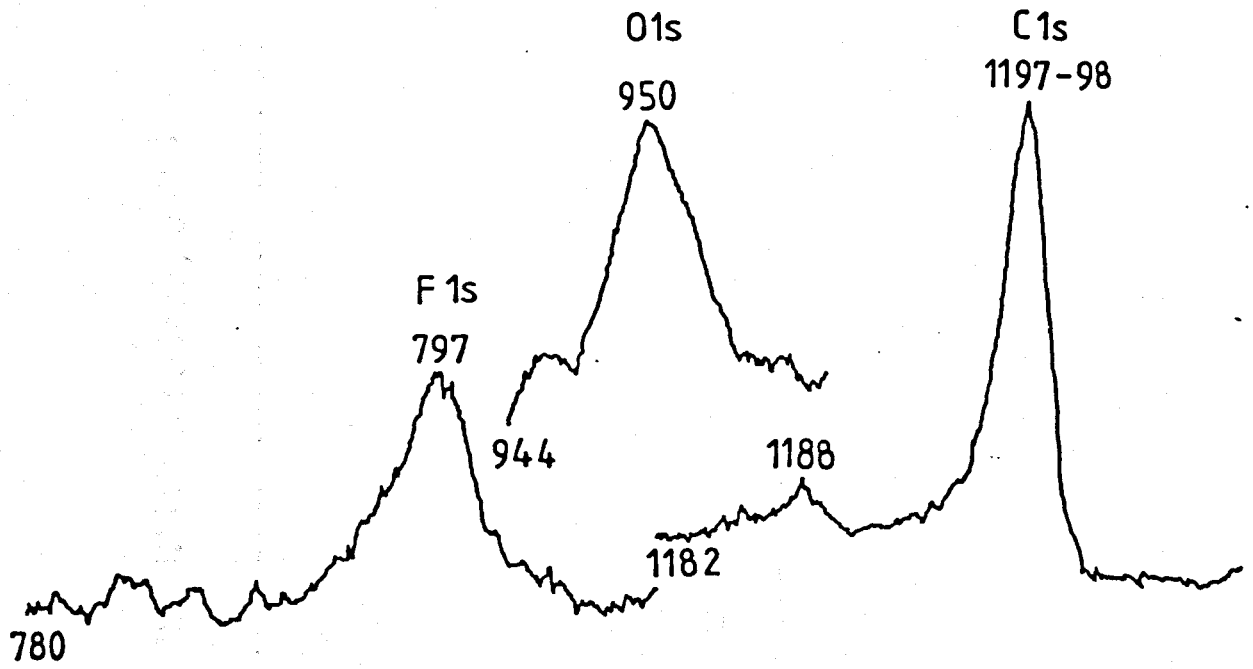

Figure 5.8

Wide scan XPS spectrum of a vitreous carbon exposed to Fluorine at 9V for 24hrs.

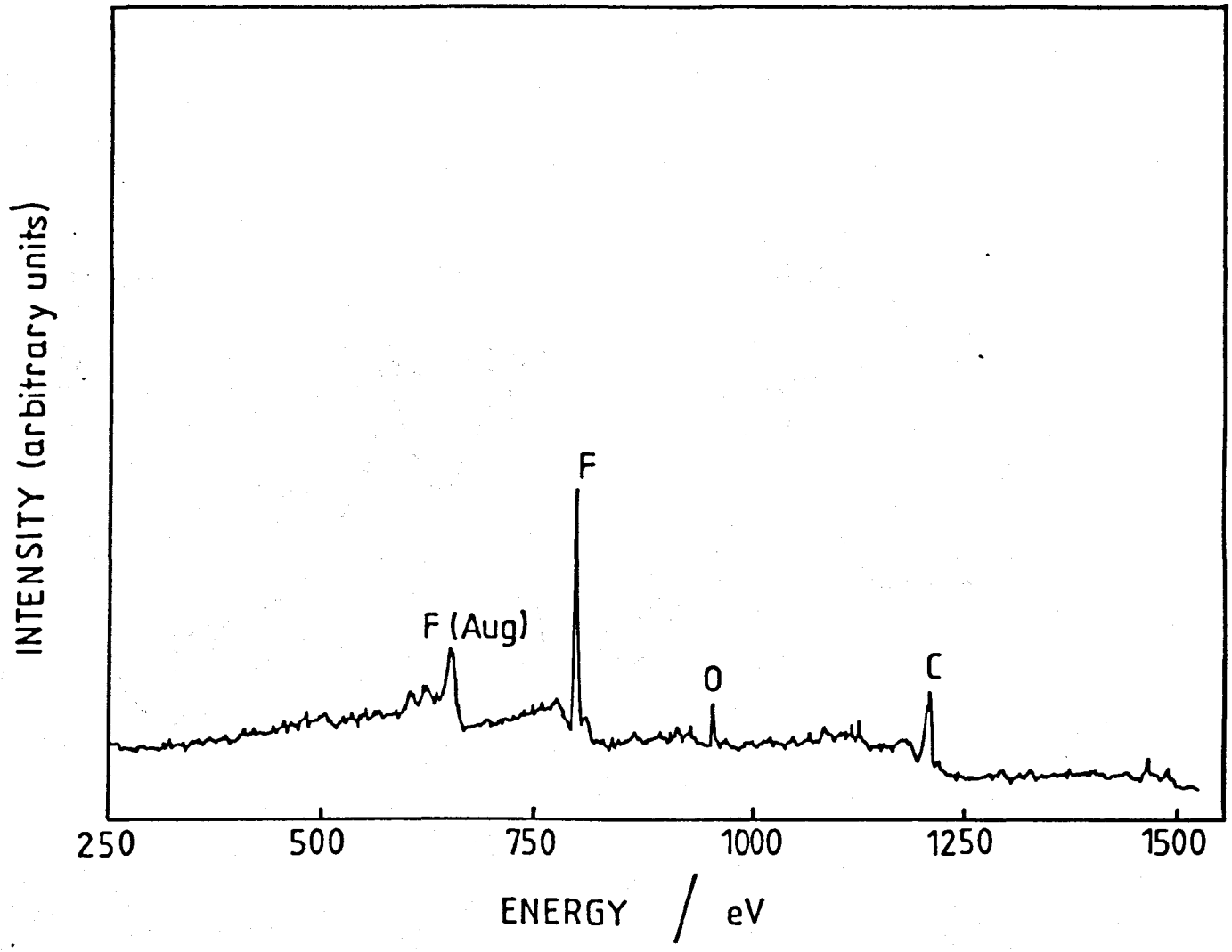

Figure 5.9

Narrow scan XPS spectrum for a vitreous carbon exposed to fluorine at 9V for 24hrs.

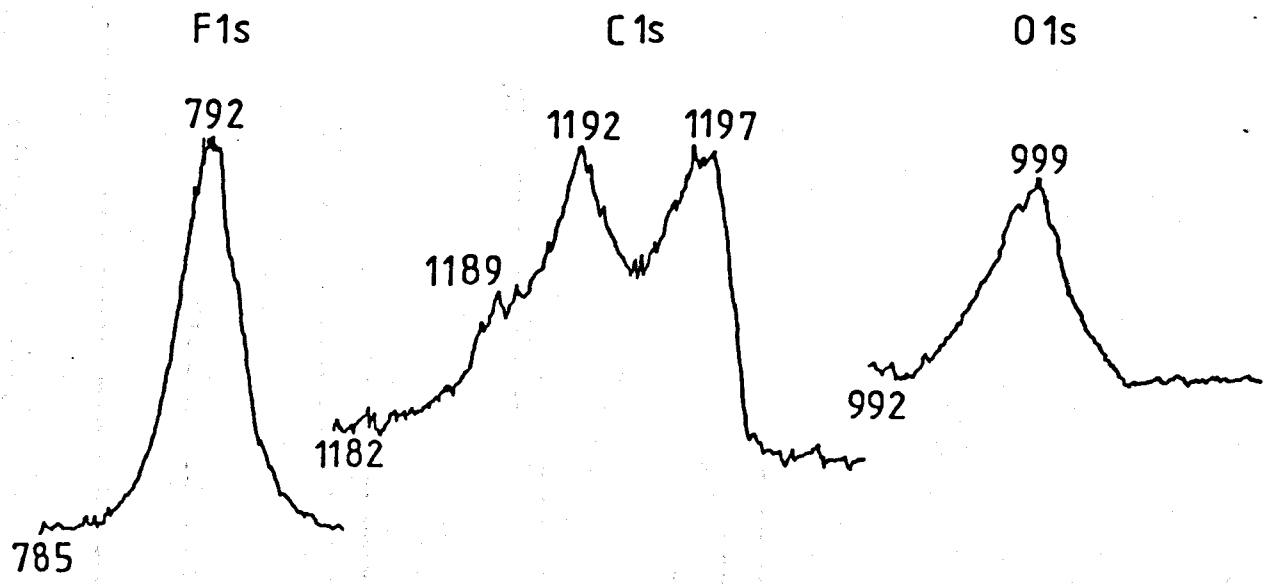

Figure 5.10

+ve ion SIMS spectrum (mass range 5-130 units) of unused vitreous carbon.

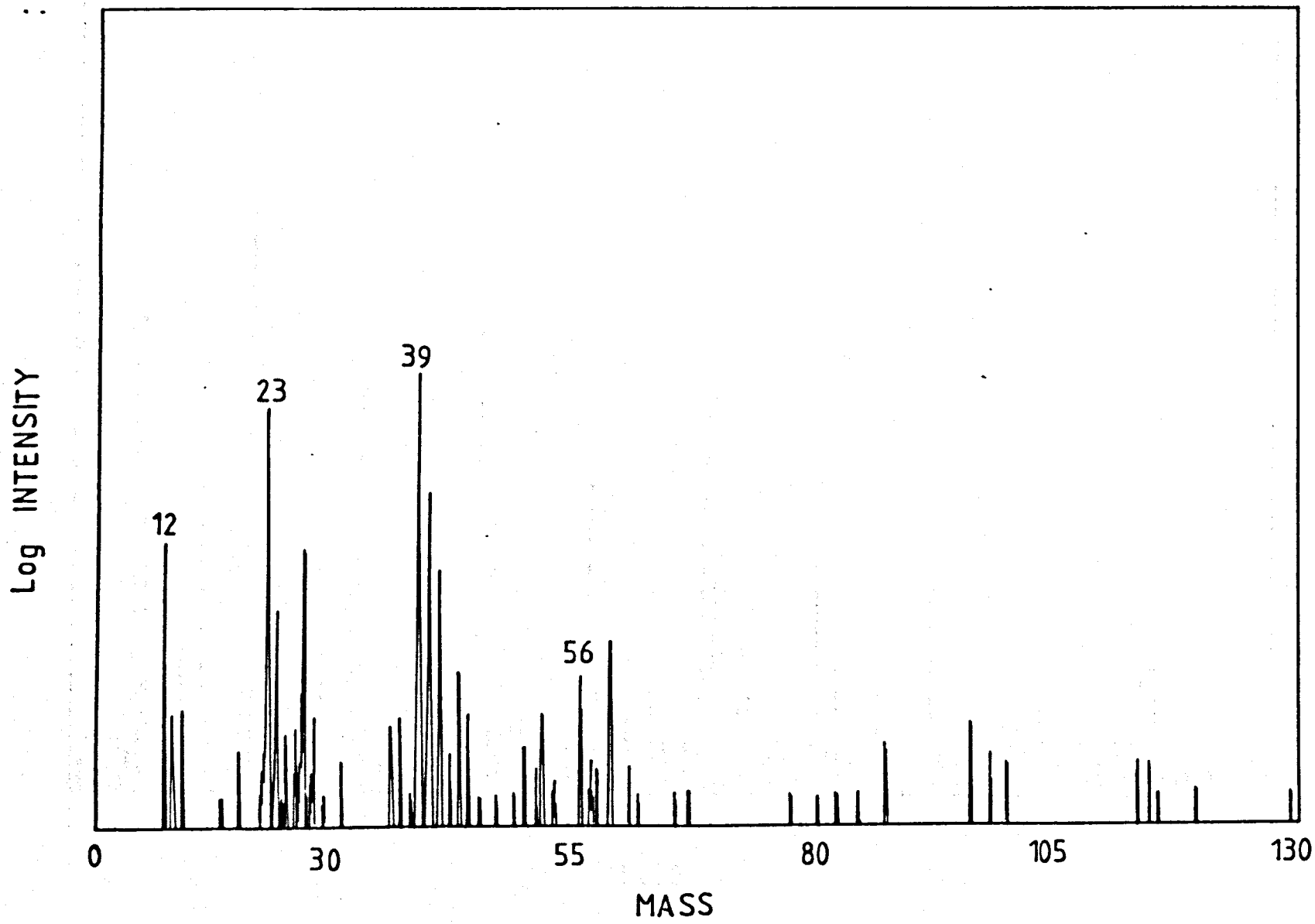

Figure 5.11

-ve ion SIMS spectrum (mass range 5-130 units) of unused Vitreous Carbon.

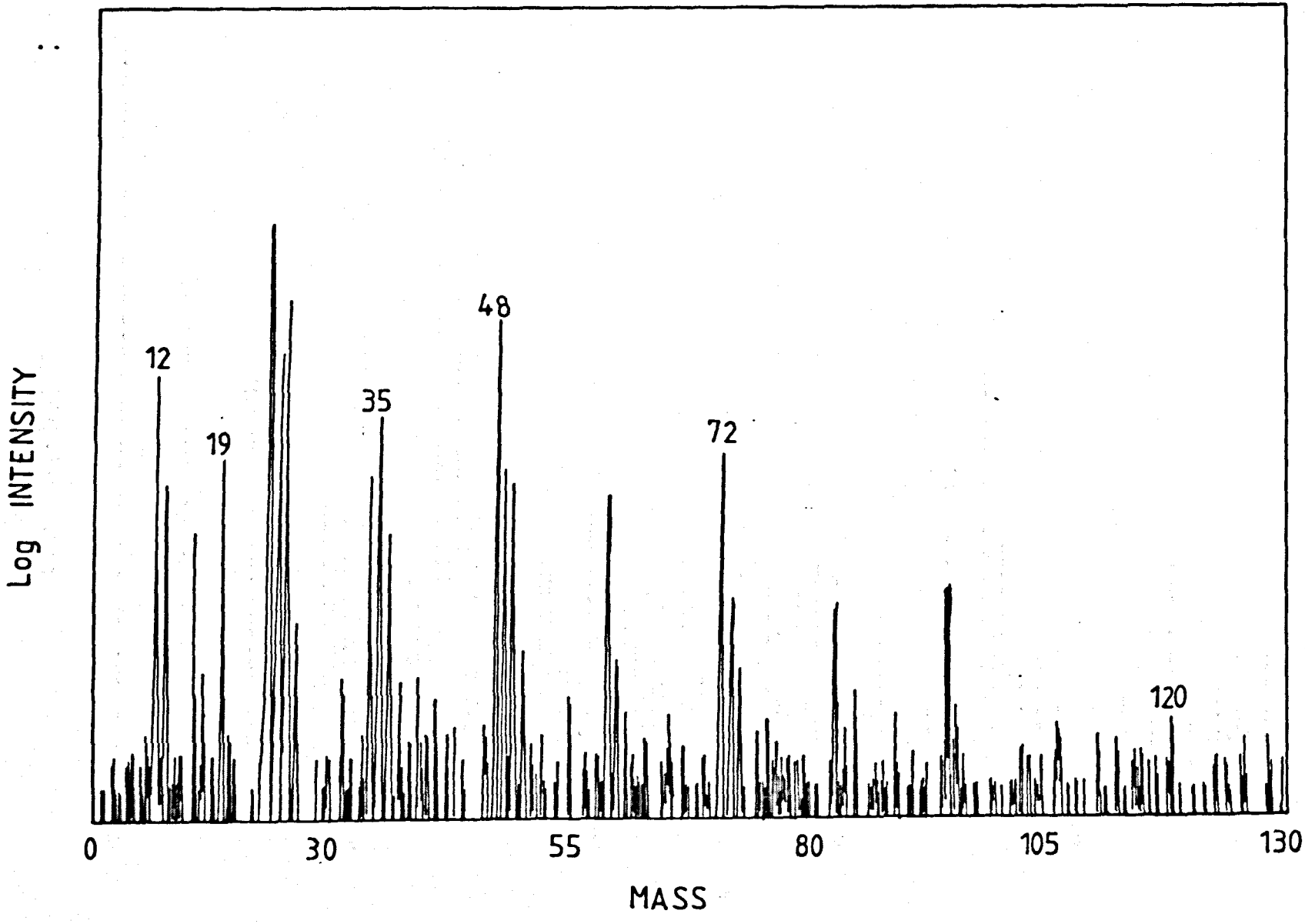

Figure 5.12

+ve ion SIMS spectrum (mass range 5-130 units). Vitreous carbon electrode exposed to fluorine at 5V for 24hrs.

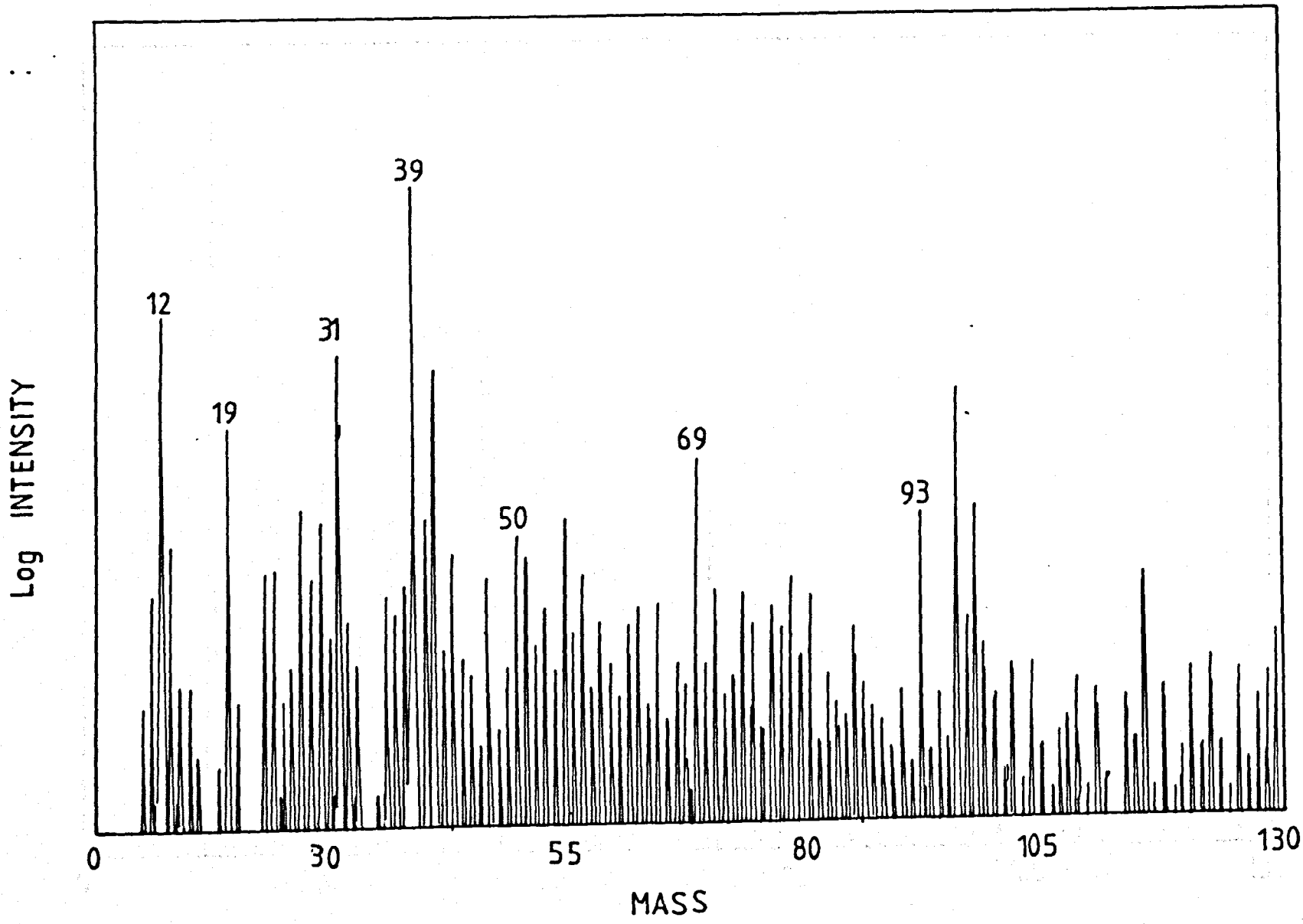

Figure 5.13

-ve ion SIMS (mass range 5-130 units). Vitreous carbon electrode exposed to fluorine at 5V for 24hrs.

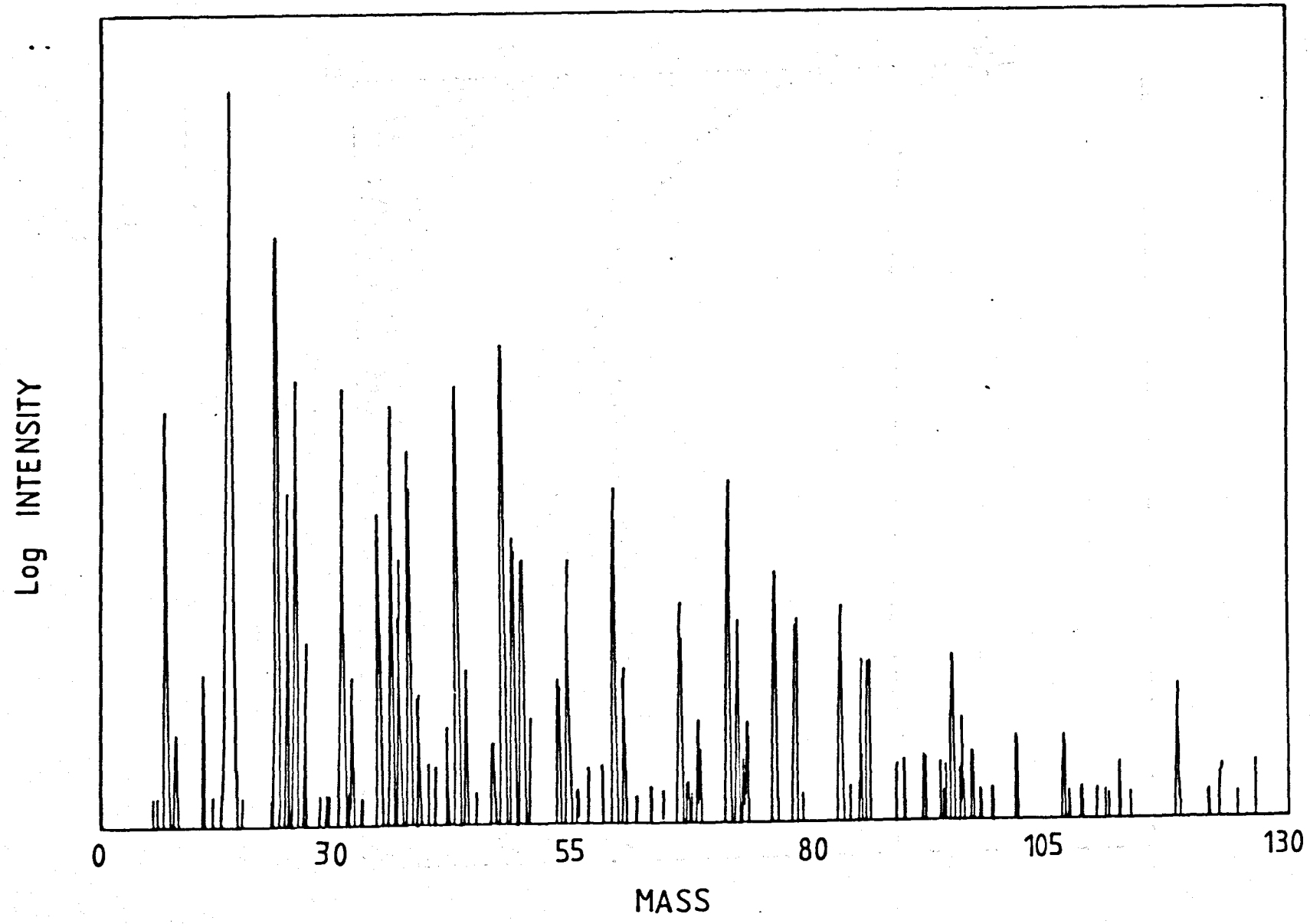

Figure 5.14

Depth profile on argon ion etching of an electrode exposed to fluorine at 5V for 24hrs.

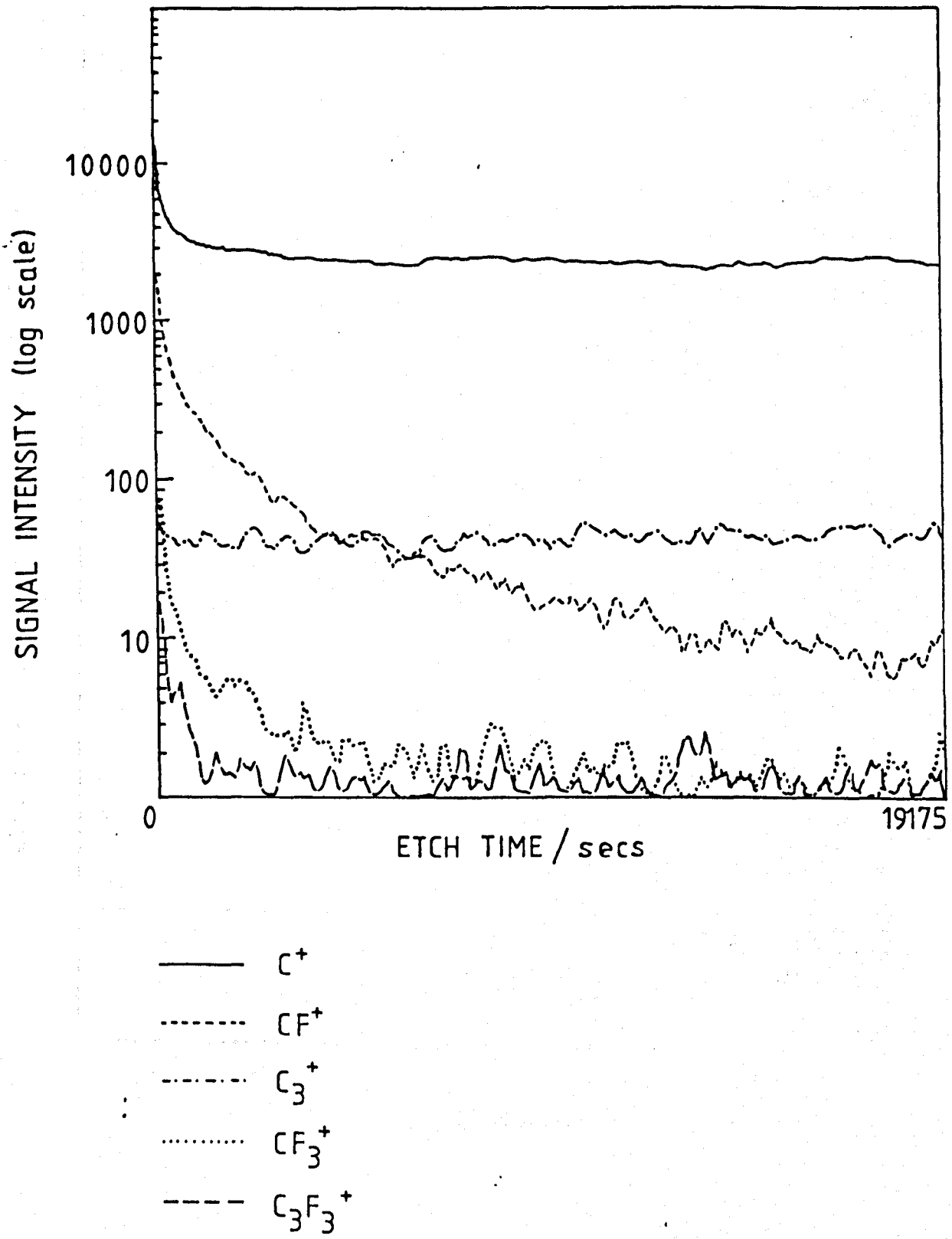

Figure 5.15

-ve ion SIMS (mass range 5-130 units). Vitreous carbon electrode exposed to fluorine at 9V (24hrs).

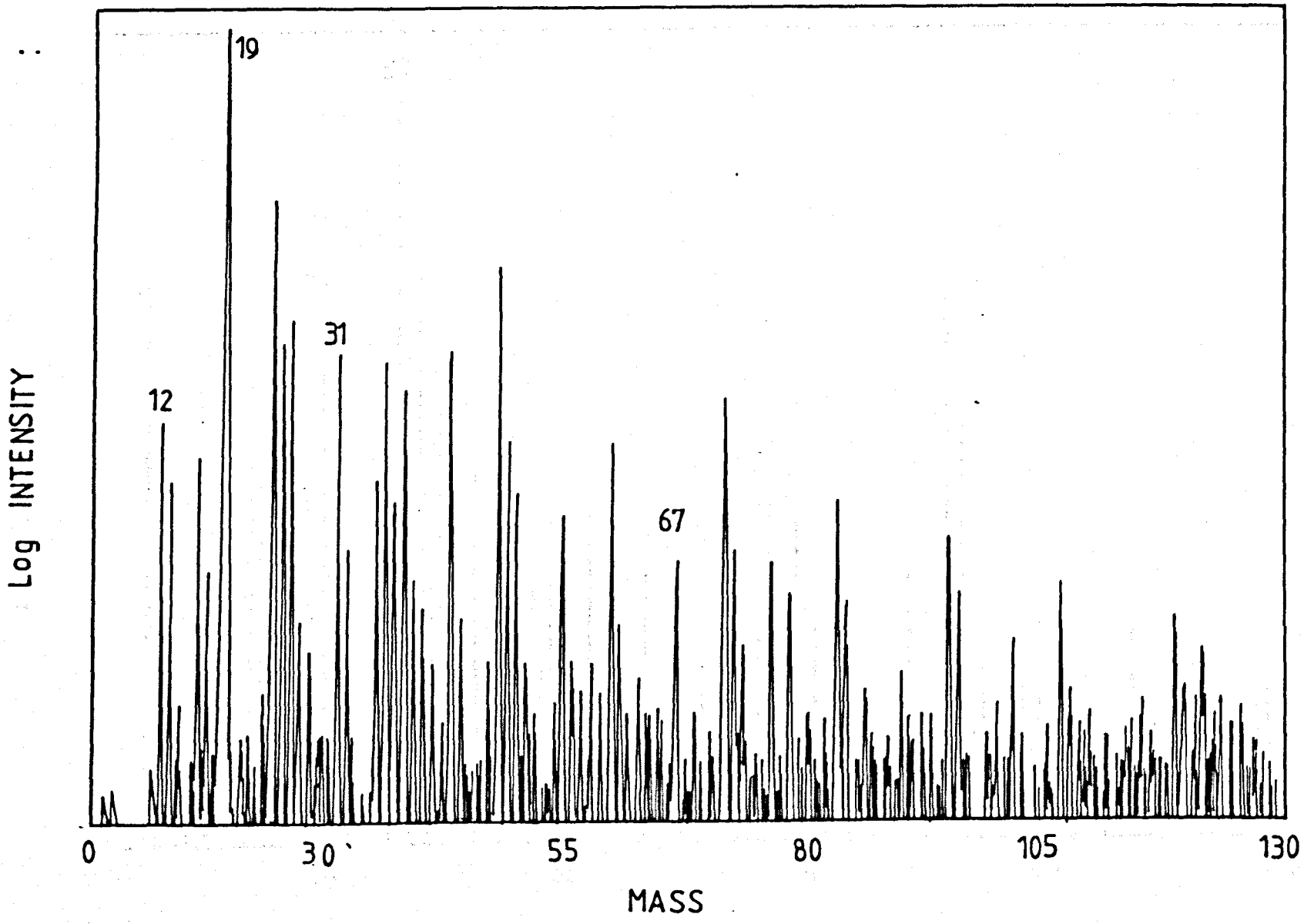

Figure 5.16

+ve ion SIMS (mass range 5-130 units). Vitreous carbon electrode exposed to fluorine at 9V (24hrs).

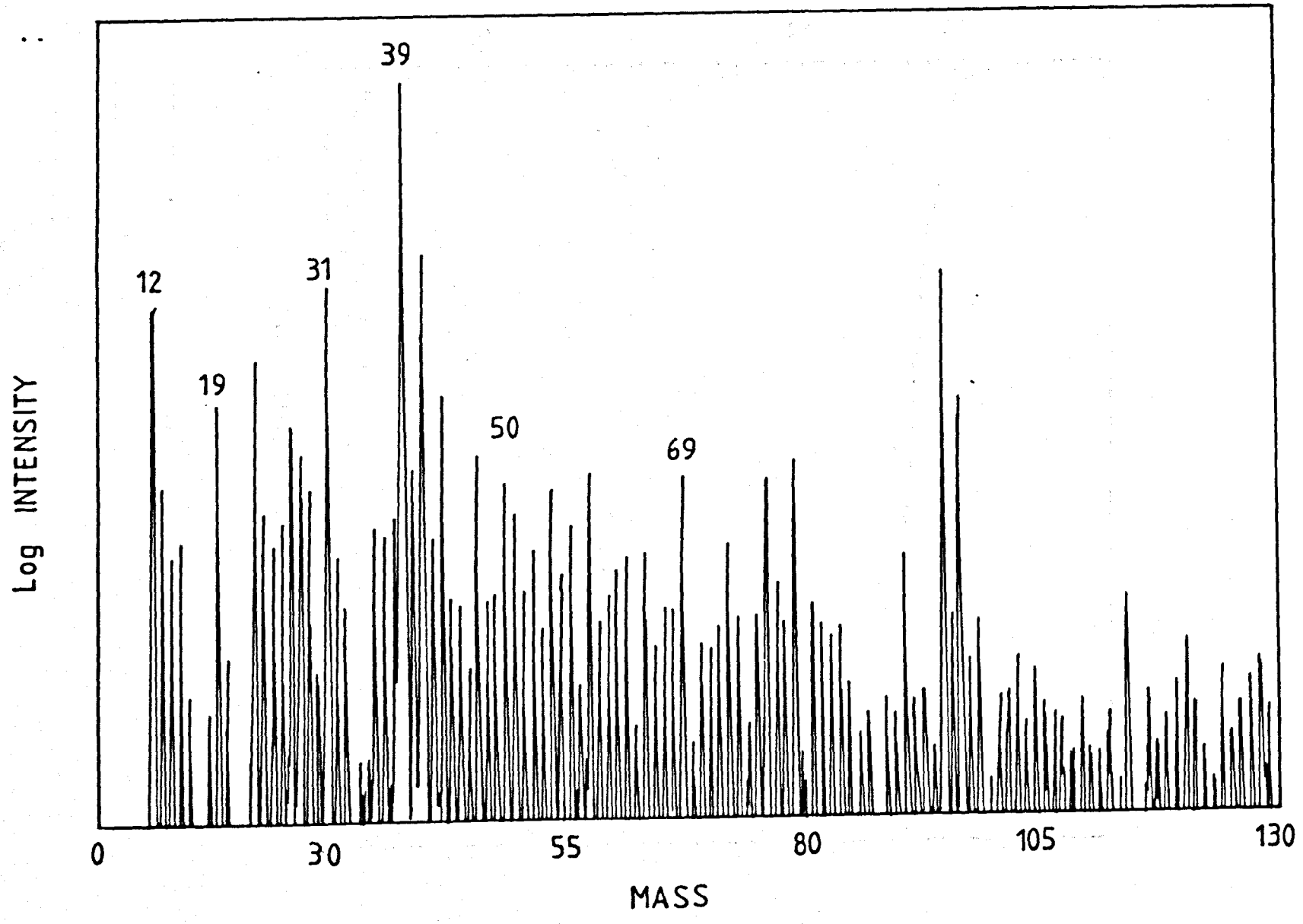

Figure 5.17

Depth profile on argon ion etching of an electrode exposed to fluorine at 9V for 24hrs.

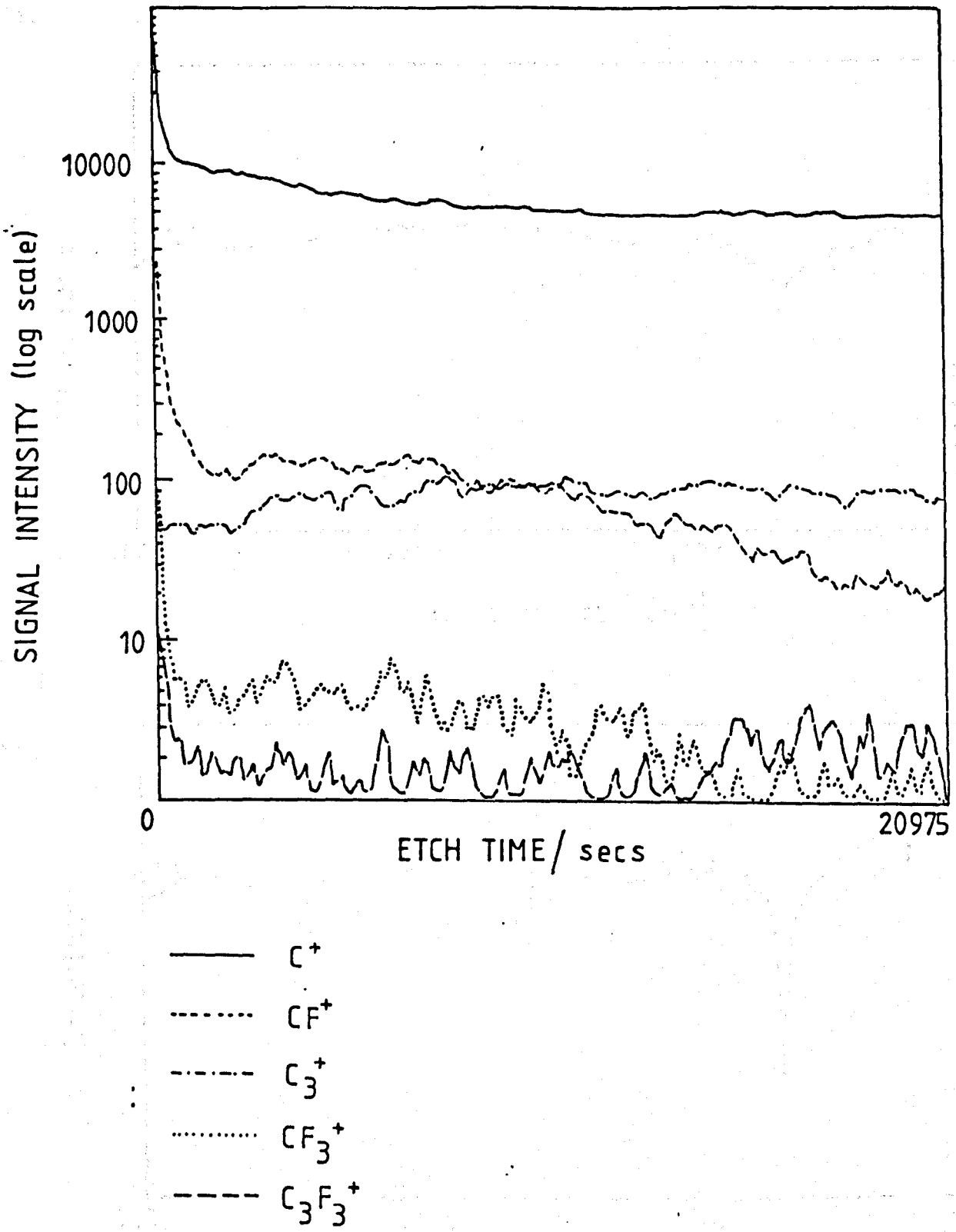

Figure 5.19

Infra-red diffuse reflectance spectra of standard $(CF_x)_n$ compounds

a) CF_x x = 0.25

b) CF_x x = 0.6

c) CF_x x = 1.0

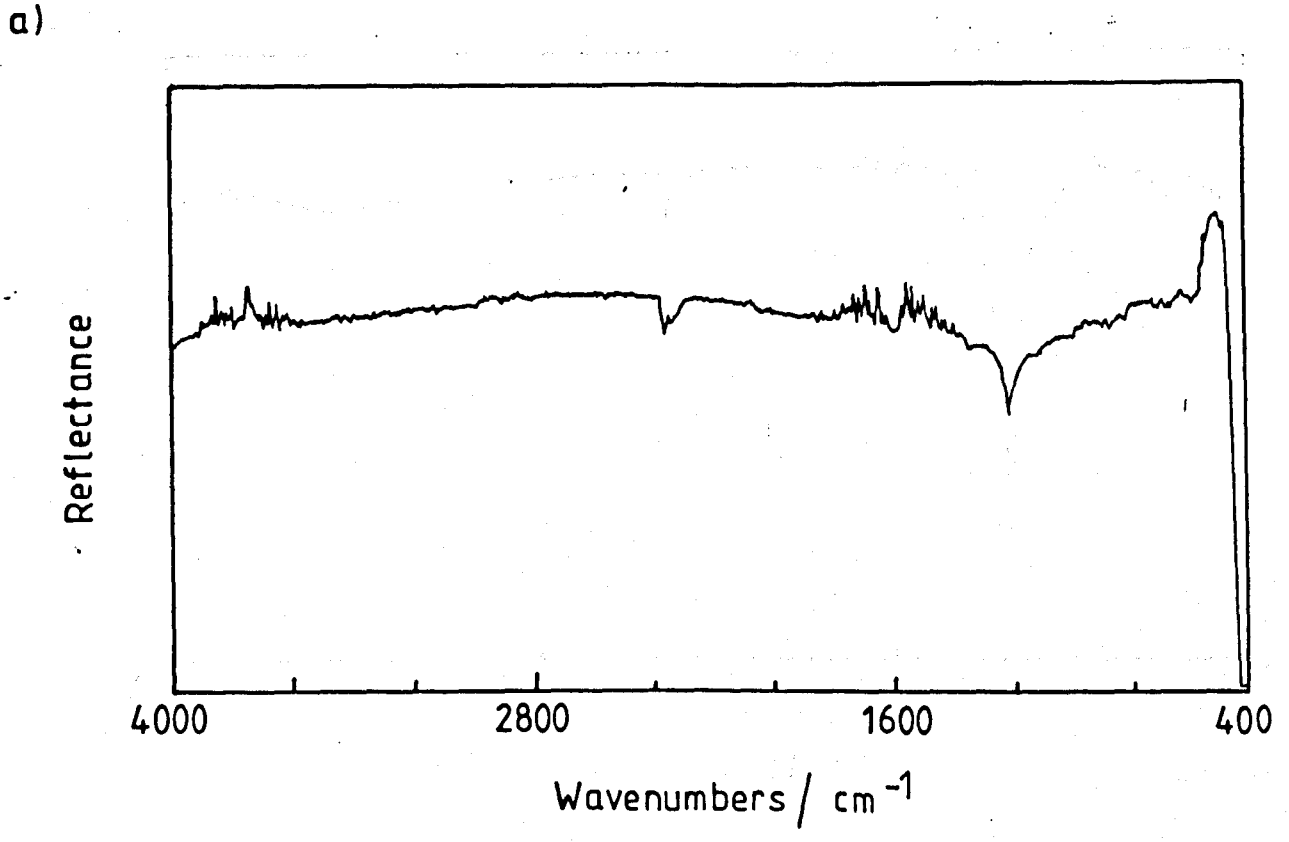

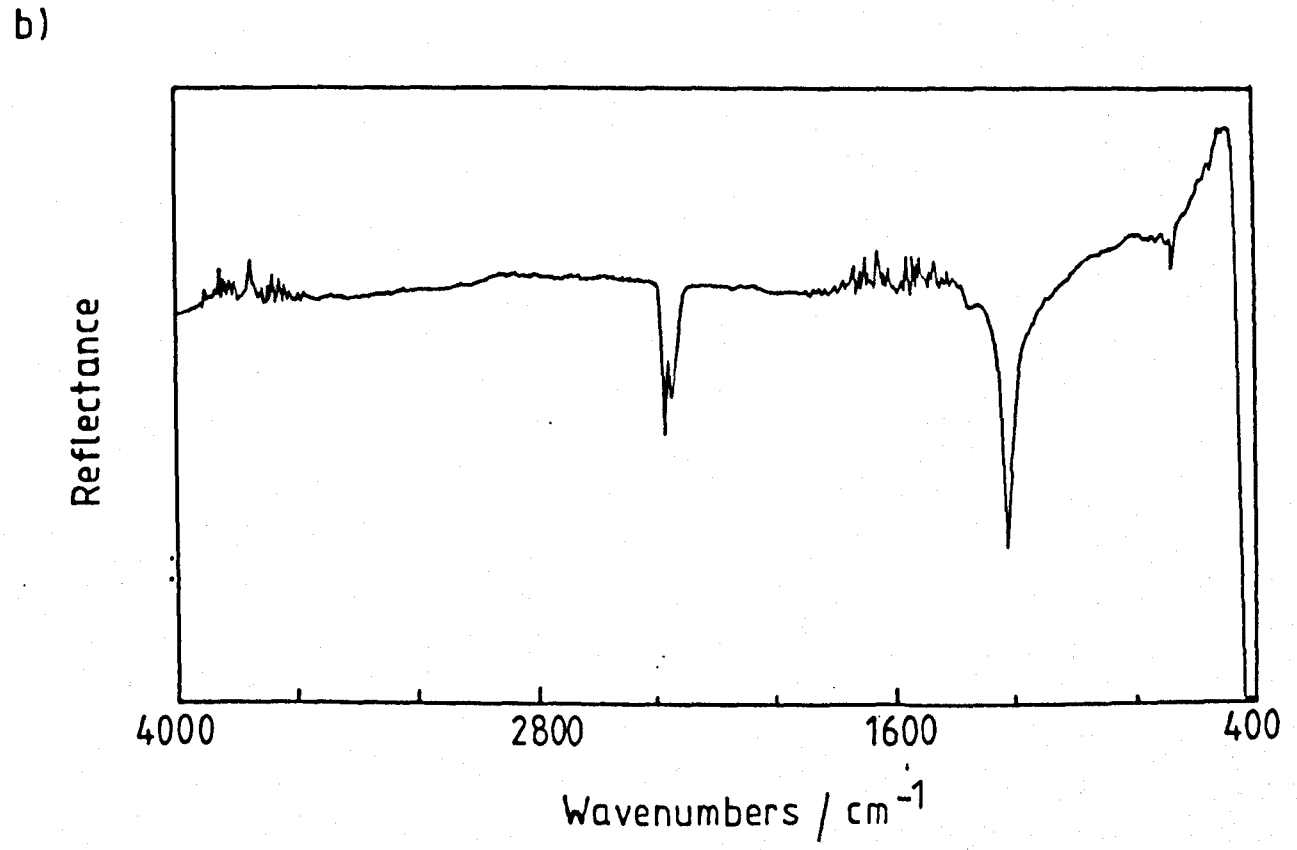

c)

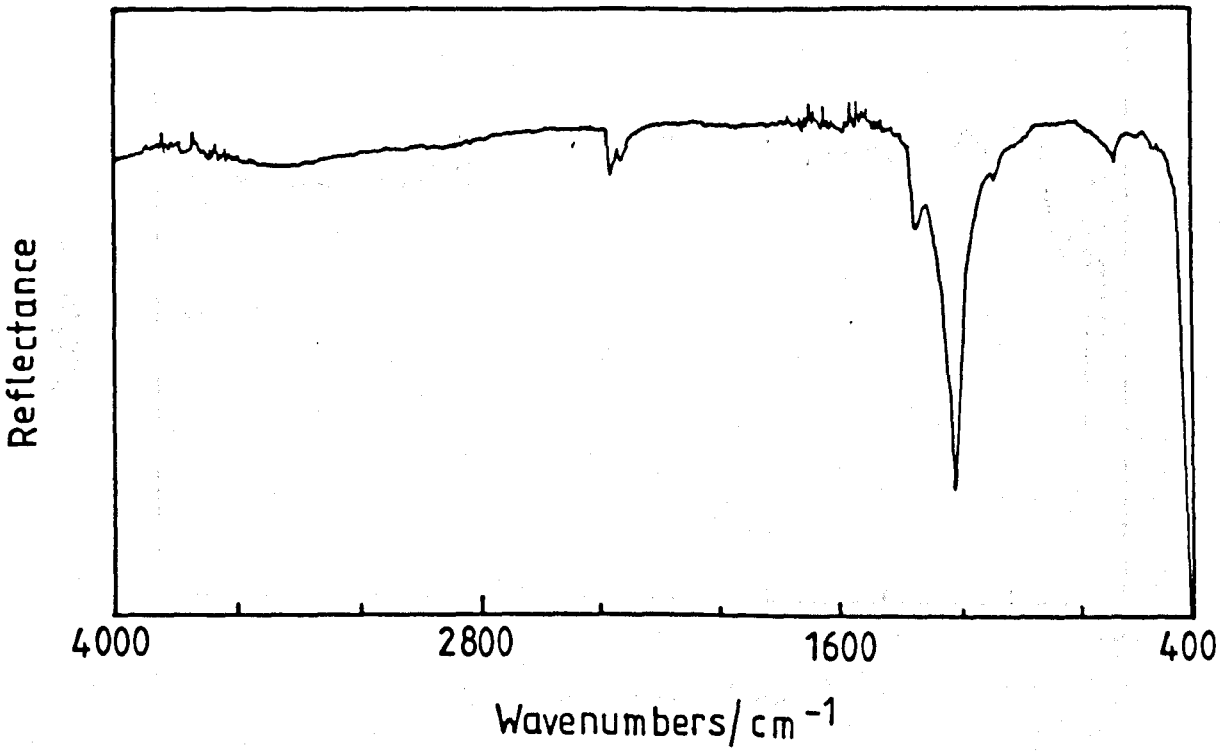

Figure 5.20

Infra-red diffuse reflectance spectra of pyrolytic graphite electrode surfaces

a) Before exposure to fluorine

b) After exposure to fluorine at 6V (30mins).

a)

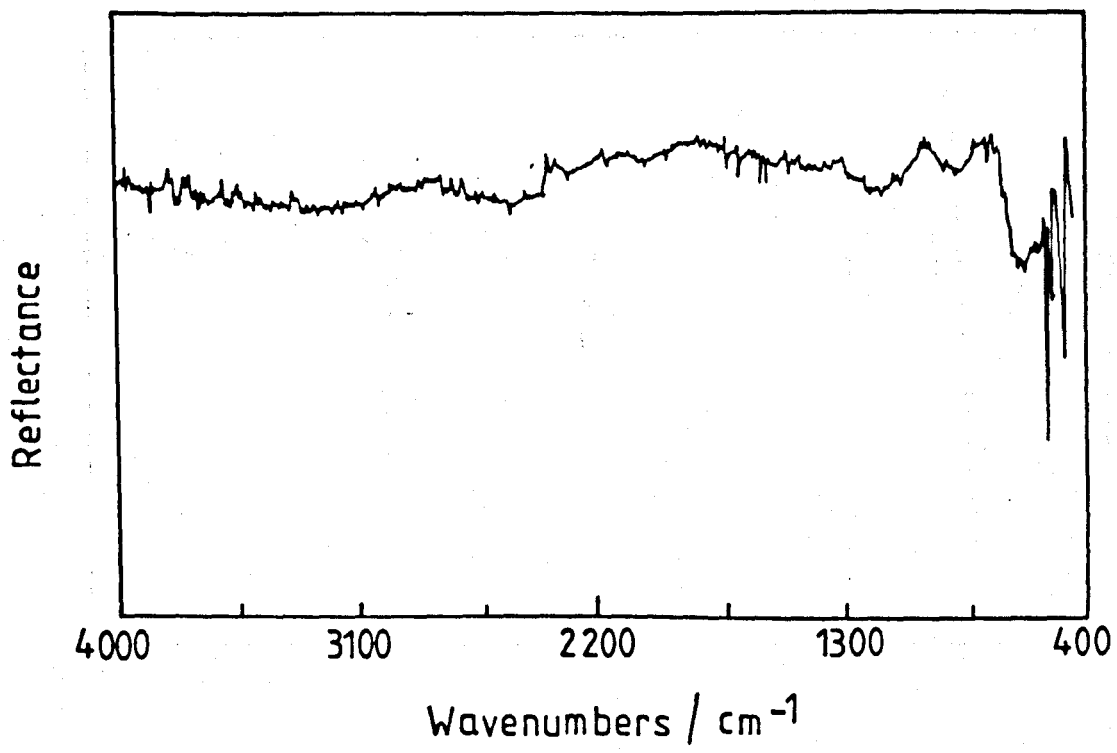

b)

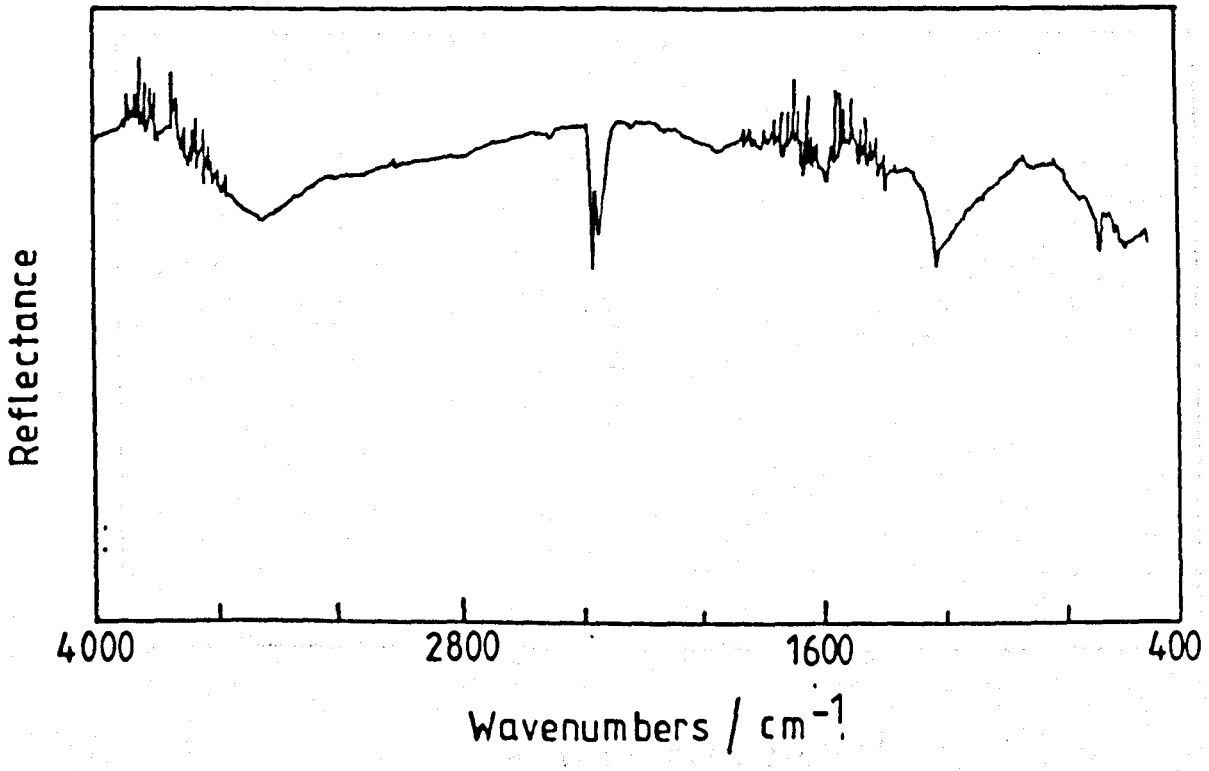

Figure 5.21

Infra-red diffuse reflectance spectra of vitreous carbon electrode surfaces

a) Before anode effect

b) After anode effect ($50mAcm^{-2}$ 24hrs).

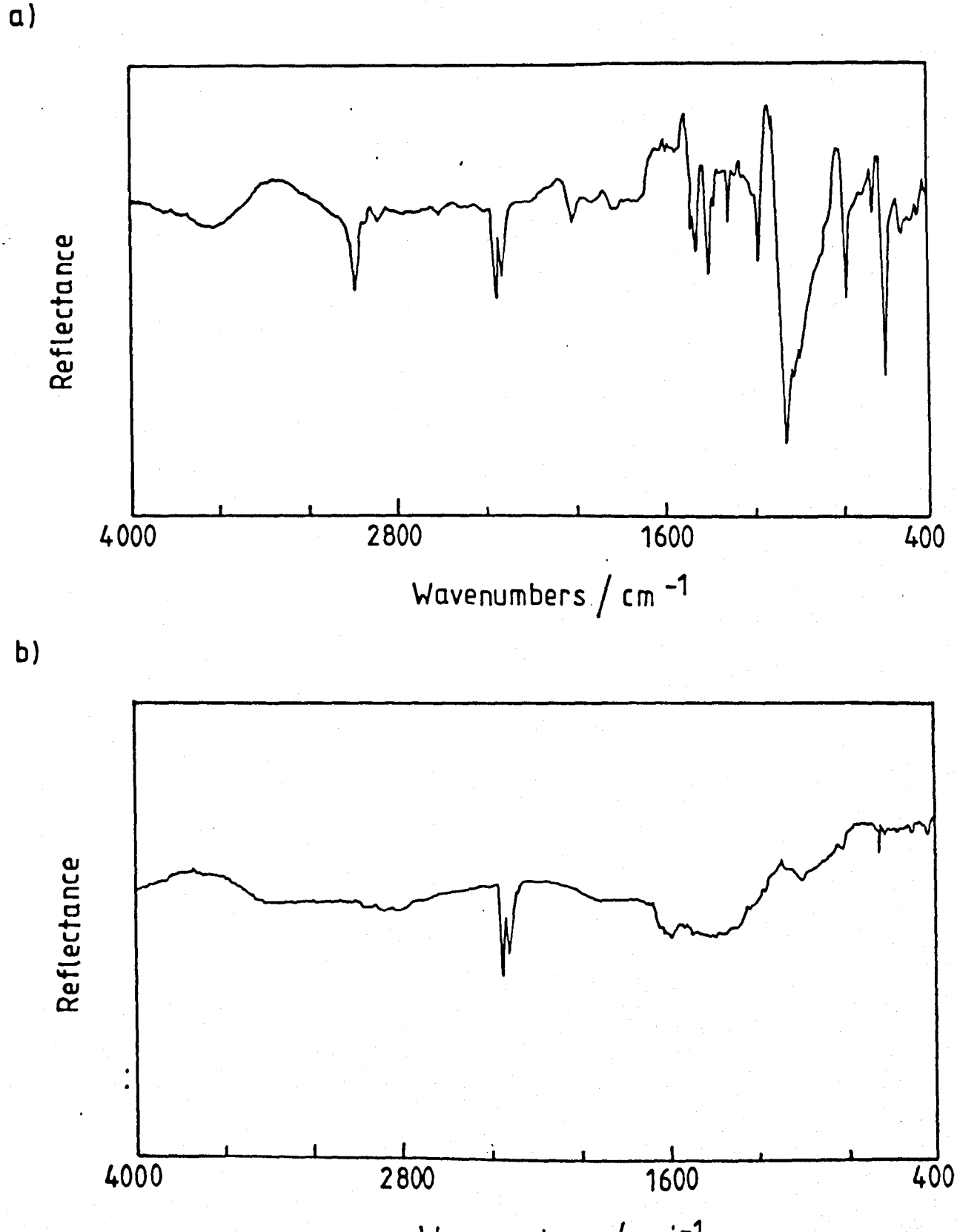

Figure 5.22

Infra-red diffuse reflectance spectrum of PTFE.

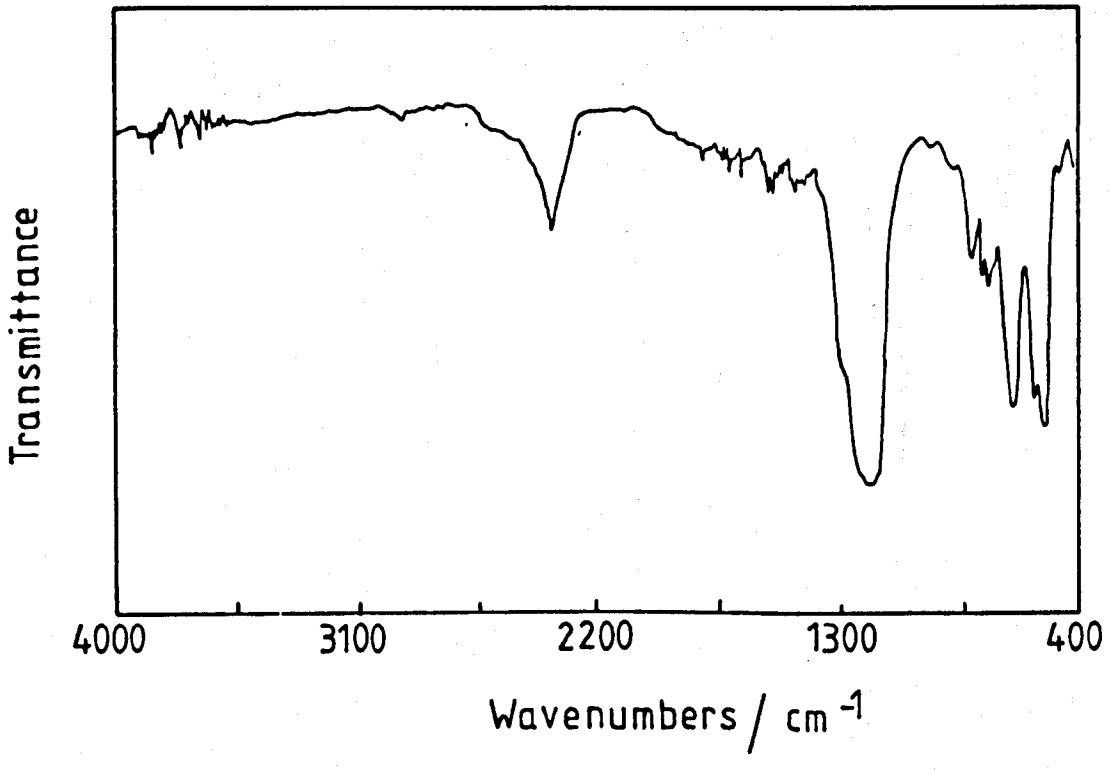

Figure 5.23

a) Infra-red capillary film spectrum of acetonitrile

b) Spectrum of acetonitrile used to extract CF_x x = 1.0. Spectrum is that obtained after subtraction of 23a). All remaining peaks can be attributed to acetonitrile residues.

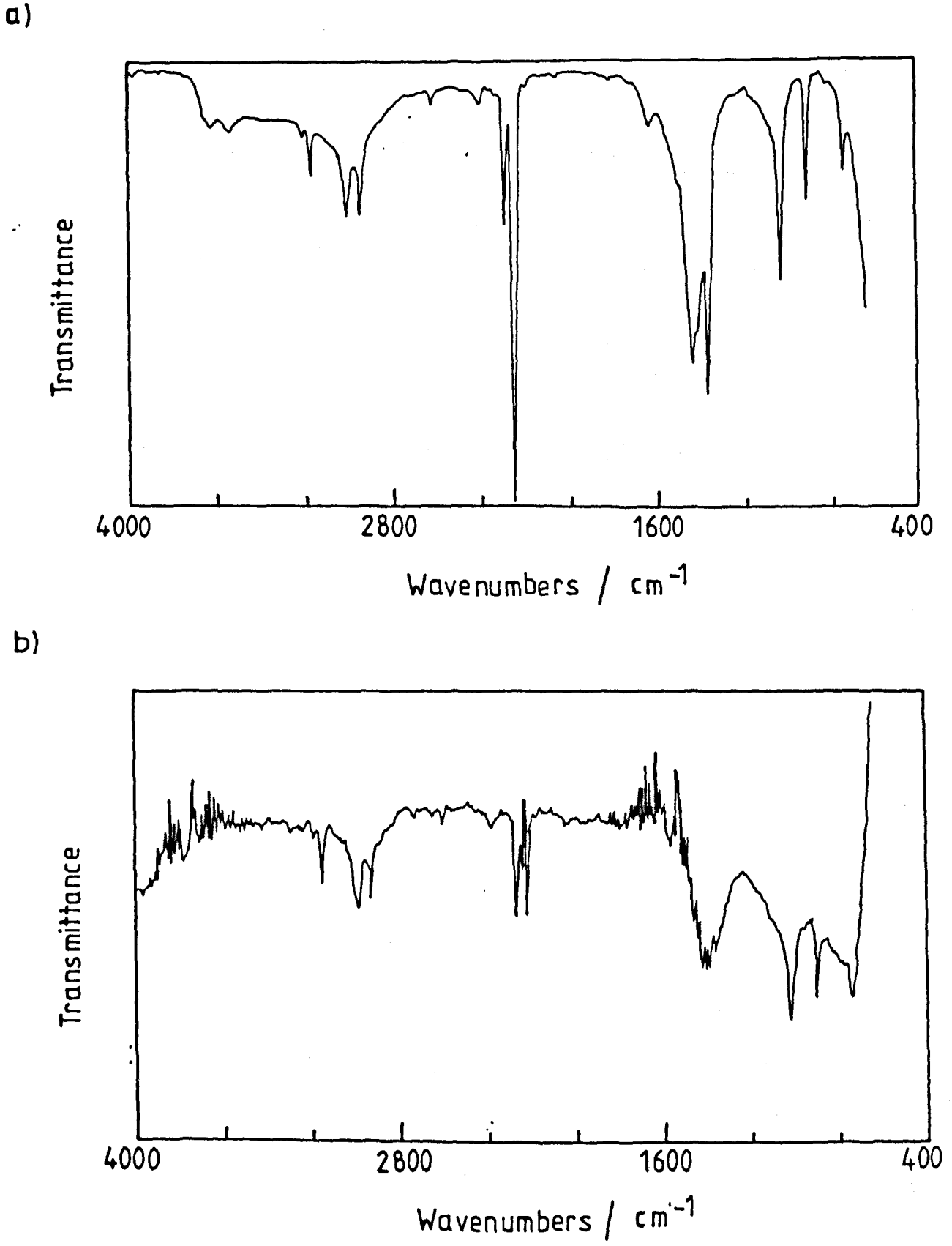

5.7 REFERENCES

1. H. Imoto, S. Koyama, and N. Watanabe, Denki Kagaku Oyobi Kogyo Butsuri Kagaku (Electrochemistry and Industrial Physical Chemistry) 46, 680-683, (1978).
2. H. Imoto, T. Nakajima, and N. Watanabe, Bull.Chem.Soc.Jpn. 48, 1633-4, (1975).
3. P. Cadman, J.D. Scott, and J.M. Thomas, Carbon 15, 75-86, (1977).
4. P. Cadman and G.M. Gossedge, J.Materials Science 14, 1465-72, (1979).
5. Y. Kita, N. Watanabe and Y. Fujii, J.Am.Chem.Soc. 101, 3832-3841, (1979).
6. A. Proctor and P.M.A. Sherwood, Carbon 21, 53-59, (1983).
7. T. Mallouk and N. Bartlett, J.Chem.Soc.Chem.Comm. 103-105, (1983).

CHAPTER 6

ELECTRON TRANSFER REACTIONS AT ELECTRODES SUBJECTED TO FLUORINE EVOLUTION

6.1 INTRODUCTION

Several authors have concluded that the large anode overvoltage associated with fluorine evolution is a consequence of the presence of a layer of polycarbonfluoride, $(CF_x)_n$, on the carbon surface.[1,2] Two mechanisms can be proposed by which the electron transfer from fluoride-containing ions (HF_2^-, $H_2F_3^-$) to the anode is inhibited by this film. These are :
i) direct blocking by the insulating film itself, and
ii) indirect blocking in which the effective insulator is the fluorine gas film.

This latter bubble overvoltage is believed to be especially severe at fluorinated carbon surfaces as a result of the non-wetting properties of polycarbonfluoride; instead of forming spherical bubbles the gas tends to spread over the surface as a thin lenticular film.[3,4]

Throughout this work we have tried to differentiate between these two roles of polycarbonfluoride. One way to do this is to remove the carbon anodes from the molten salt after fluorination and investigate model redox systems at the fluorinated electrodes. A comparison was made between the redox kinetics at freshly cleaned electrodes, and those fluorinated by anodic treatment in KF.2HF. The effects of potential and time of fluorination were examined.

The model redox systems investigated are shown in Table 6.1.

Each couple was first examined by cyclic voltammetry in order to determine the reversible potential for the

couple. Rate constants were obtained using interfacial impedance methods.

6.2 THE FERROCENE/FERROCINIUM REDOX COUPLE

Cyclic voltammetric examination of the ferrocene/ferrocinium redox couple on a freshly polished vitreous carbon at $0.01Vs^{-1}$ permitted evaluation of the reversible half-wave potential E_r as 0.300V (vs. Na SCE) with ΔE_p, the separation between the anodic and cathodic peaks, 0.060V (Figure 6.1).

The complex plane impedance plot for this couple at a freshly polished vitreous carbon electrode is shown in Figure 6.2. The reaction is totally controlled by diffusion; no charge transfer semicircle is obtained. Evaluation of the charge transfer semicircle is not directly possible although a lower limit to the rate constant can be determined using the method suggested by Macdonald and McKubre[5] in which the separate real and imaginary parts of the impedance are plotted against the reciprocal square root of the angular frequency, ω. The method allows evaluation of θ, the charge transfer resistance which can be used to evaluate the apparent standard rate constant k_o using the equation :

$$k_o = 2RT/n^2F^2\theta C_b \qquad 6.1$$

The method is discussed in Chapter 2. Such a plot for the ferrocene/ferrocinium couple is shown in Figure 6.3 and the evaluated kinetic parameters are shown in Table 6.2. The mean diffusion coefficient, D, for $FeCp_2$

and $FeCp_2^+$, was evaluated using the equation :

$$\sigma = 4RT/2^{\frac{1}{2}}n^2F^2C_bD^{\frac{1}{2}} \qquad 6.2$$

The potential dependence of the ferrocene couple was not examined because charge transfer data could not be determined at clean electrodes (and so Tafel-type plots of log θ against potential would be very inaccurate).

Vitreous carbon electrodes were polarised positively in the KF.2HF melt for 30 minutes at potentials in the range 2V to 9V (vs. Pd/H_2). After polarisation the electrodes were removed from the melt, washed with thrice distilled water, dried, and stored in a desiccator until required for the kinetic studies.

A complex plane impedance plot for the ferrocene system at an electrode fluorinated at 6V in KF.2HF is shown in Figure 6.4. The development of a charge transfer semicircle indicates that the electron transfer process is retarded by an insulating film on the electrode surface. Table 6.2 shows the effect of increasing potential of fluorination on the charge transfer kinetics of the ferrocene redox couple.

Double layer capacitance values were obtained from high frequency impedance data, and it can be seen that the capacitance decreases with increasing fluorination potential. This decrease is presumably due to an increasingly thick dielectric layer corresponding to the polycarbonfluoride film. The film thickness was calculated using a simple model for the fluorinated

electrode treating it as a parallel plate capacitor, for which $d = \varepsilon\varepsilon_o/C_d$ where ε is the dielectric constant of the film and d the film thickness. A value for ε was not known and in this work a value for that of PTFE of 2.1 was assumed to be near to the value for polycarbonfluoride. This model also assumes that the film is coherent and uniform. Values for film thickness are small and at 6V the value obtained was 0.54nm. This value is similar to that obtained from the ESCA/SIMS measurements.

The rate of the charge transfer was seen to decrease as the potential of fluorination increased, and at 6V the rate was seen to have fallen by a factor 10^2 compared with the rate on a fresh electrode.

Polarisation at 9V (Table 6.2) is seen to cause an increase in the series resistance of the impedance as well as a further fall in the double layer capacitance. This behaviour has also been observed during impedance studies in KF.2HF (see Chapter 4).

6.3 THE HEXACYANOFERRATE II/III REDOX COUPLE

Owing to the reversibility of the ferrocene/ ferrocinium redox system at fresh carbon electrodes it was not possible to evaluate the factor by which the fluoride film inhibited the redox kinetics.

The hexacyanoferrate II/III couple was chosen as a quasi-reversible system with which it would be possible to determine the effect of the fluoride film on redox kinetics.

Cyclic voltammetric studies of the hexacyanoferrate II/III couple at a freshly polished vitreous carbon enabled a value of +230mV (vs. SCE) to be determined for the reversible potential E_o Figure 6.5. The complex plane impedance plot for the redox couple at +230mV is shown in Figure 6.6. The potential dependence of the charge transfer resistance was studied and the results are shown in Figure 6.7. This plot is a Tafel-type plot enabling the transfer coefficients α_a and α_c to be evaluated.

Electrodes were fluorinated by constant potential electrolysis for 30 minutes in KF.2HF. The effect of fluorination potential was examined. The results are shown in Table 6.3. As with the ferrocene redox couple the charge transfer resistance is seen to increase as the potential of fluorination is made more positive; similarly the series resistance also increases.

6.4 DISCUSSION OF THE FERROCENE/FERROCINIUM AND HEXACYANOFERRATE II/III REDOX COUPLES

The lower limit for the ferrocene redox kinetics at a freshly polished carbon electrode is $1 cms^{-1}$. It is seen that fluorination of an electrode at 6V in KF.2HF results in the measured rate constant for the redox couple falling to $1.5 \times 10^{-2} cms^{-1}$. The apparent standard rate constant for this redox couple is lower by at least two orders of magnitude.

It is possible to measure the rate constant of the hexacyanoferrate II/III redox couple at a freshly cleaned vitreous carbon electrode. It was found to be

$1.46 \times 10^{-2} cms^{-1}$. After fluorination of an electrode at 6V the rate constant for the hexacyanoferrate II/III couple has fallen to $8.23 \times 10^{-4} cms^{-1}$ a decrease by a factor of 17. Similar inhibitions of charge transfer reactions, at oxide electrodes, have been reported previously.[6-13] There are two explanations for the observed behaviour.

1. The $(CF)_n$ film is coherent and causes a decrease in electron transfer probability by a factor $> 10^2$.
2. The $(CF)_n$ film is an insulator which covers the entire surface except for a small fraction $< 10^{-2}$.

The second alternative is unlikely. Under the extreme oxidising conditions which prevail during fluorine evolution at considerable overvoltages, it is unlikely that any part of the surface remains unattacked. If breaks do exist in the fluroide film they should be exposed in the Randles plots as a result of transitions from planar diffusion at high frequencies to hemispherical diffusions at intermediate frequencies and to planar diffusion again at low frequencies. Such transitions would result in non-linearity of the Randles plots at intermediate and low frequencies. This has been discussed elsewhere.[14,15] Such deviations were not observed over the frequency range examined and so it is unlikely that active centres exist.

The ratio of electron transfer rates :

$$k_{covered}/k_{uncovered}$$

might be expected to be similar both for the fluorine evolution reaction and for the model redox systems studied.

Heusler[6] has discussed electron transfer at

film-covered electrodes. For thin coherent films it was found that the exchange current density falls with increasing film thickness as the probability of electron tunnelling falls. The probability P of electron tunnelling through a barrier of thickness d and mean height ΔE_t is given by

$$P/P_o = \exp -4\pi d(2m^*\Delta E_t)^{\frac{1}{2}}/h$$

where P_o = tunnelling probability at a bare electrode, m^* is the effective tunnelling mass of the electron and h is Planck's constant. A value for m^* at the C-F polymer is unknown but approximating this to the rest mass of the electron, the observed inhibition factor of 10^2 by a film of 0.54nm thickness can be explained in terms of a band gap of 0.7eV. The band gap for a typical oxide is in the range 1 to 4eV. It is likely that the band gap for the carbon polyfluoride film is larger than 4eV.

In the case of the hexacyanoferrate II/III couple the inhibition factor was even less, being only 17. This results in a band gap of 0.3eV.

Such apparently low values of band gap may be due to the unstability of the $(CF_x)_n$ film in aqueous and non-aqueous solvents resulting in partial disolution of the films following removal from the fluorinating conditions.

At high fluorination potentials an increase in the series ohmic resistance was consistently found in

aqueous, non-aqueous and KF.2HF solvents. The resistance of polycarbonfluorides, $(CF_x)_n$, increases with increasing fluorine content in the region x = 0.5.[16] This observation can be explained in terms of a carbon fluoride film of non-uniform chemical composition. The outermost region of the film will be fluorine-rich and hence insulating. The inner region will be carbon rich and hence highly conducting, a narrow intermediate region will be semiconducting. Thus the film can be approximately represented by two distinct layers : an insulating dielectric outside a semiconducting layer. At high fluorination potentials it can be supposed that both layers are thicker than under milder conditions, so that both give rise to increasing impedances with electrode potential. The observed increase in series resistance of $10\Omega cm^2$ would lead, at an operating current density of $0.2Acm^{-2}$ to a contribution of 2.0V to the operating anode overvoltage.

This variation in composition with depth in the film is also observed during ion beam etching of fluorinated carbon electrodes (see Chapter 5).

6.5 OTHER ELECTRON TRANSFER REACTIONS

It is shown in Table 6.1 that two other electron transfer processes were characterized for use as model systems in the study of fluorinated electrodes, namely $Cu(NH_3)_4^{2+}/Cu(NH_3)_2^{+}$ and $IrCl_6^{2-}/IrCl_6^{3-}$.

6.5.1 The Hexachloroiridate III/IV Couple

Later in this chapter it will be shown that the choice of model redox systems for the study of fluorinated electrodes is limited to those systems with a positive reversible potential. With this in mind the hexachloroiridate III/IV system was chosen. At a freshly polished vitreous carbon electrode the reversible potential for this system was found to be +685mV (vs. SCE) Figure 6.8. The complex plane impedance plot for this system is shown in Figure 6.9. It is fully reversible and obviously a value for the apparent standard rate constant can only be estimated from a Randles plot. The lower limit is thus $1 cms^{-1}$.

Electrodes fluorinated at 6V in the KF.2HF melt were examined using the hexachloroiridate III/IV redox couple and gave the impedance spectrum shown in Figure 6.10. The impedance has increased but no charge transfer impedance was observed. No further measurements were performed with this redox couple.

6.5.2 The $Cu(NH_3)_4^{2+}/Cu(NH_3)_2^{+}$ Redox Couple

Copper(I) and Copper(II) are known to exist as their ammine complexes in aqueous solutions containing ammonia. In aqueous media[17] and liquid ammonia[18] the cathodic reduction of copper(II) ammines proceeds stepwise to Cu(0) through Cu(I) ammines; two distinct polarographic waves are obtained. In liquid ammonia, Cu(II) exists as the hexammine, but in aqueous solutions containing ammonia replacement of the water ligands by ammonia is incomplete.[19] In molar solutions of ammonia

at 25°C the predominant Cu(II) species is the square planar tetraammine.[20] There have been many determinations of the stability constants for copper ammine formation in aqueous media.[21-24]

In its linear ammine complex, Cu(I) has an untypically low coordination number of 2.[25] This species predominates in aqueous solutions of ammonia[21-24] and is isolated as Cu(I) salts formed in liquid ammonia.[26] Even in the gas phase, evidence suggests that Cu(I) can co-ordinate no more than two molecules of ammonia.[27] The difference in the number of ammonia ligands co-ordinated to Cu(I) and Cu(II) ions suggests that the overall redox reaction 6.3 must consist of several steps :

$$Cu(NH_3)_4^{2+} + e^- \rightleftharpoons 2NH_3 + Cu(NH_3)_2^{+} \qquad 6.3$$

Several electrochemical studies have been made of the charge transfer kinetics of this reaction in aqueous solution but without investigating the effect on the rate of changing the ammonia concentration[13,28,29] . The kinetics of reduction of various copper(II) ammines $Cu(NH_3)_n^{2+}$ for n = 3 to 6 has been examined by Ksenzhek et al.[30] These authors claim that by adjusting the pH of the solution the value of n could be altered. However, the generation of solutions containing hexammines and pentammines as the predominant species conflicts with stability constant data.[21-24] Ksenzhek et al. did not draw conclusions from their results about the mechanism of reaction 6.3

Shumilov et al.[31] investigated the mechanism of reaction 6.3 at platinum cathodes in concentrated solutions of copper chlorides and concluded that the rate-determining charge transfer reaction involves the Cu(II) triammine.

During our study we were unaware of the work of Shumilov et al, in the original Soviet literature and evaluated the mechanism of reaction 6.3 at vitreous carbon electrodes and pyrolytic graphite electrodes.

6.5.3 Results

Preliminary cyclic voltammetric experiments were carried out using a hanging mercury drop electrode. Two processes could be separated at this electrode corresponding to the processes

$$Cu^{2+} + e^- \rightleftharpoons Cu^+ \qquad 6.4$$

$$Hg + Cu^+ + e^- \rightleftharpoons Cu^o/Hg \qquad 6.5$$

and the results are displayed in Figure 6.11. Kinetic measurements were not made at the HMDE.

At vitreous carbon and pyrolytic graphite electrodes the negative limit of potential scan was limited to -0.88V (vs $Hg/HgSO_4$ /0.5M $(NH_4)_2SO_4$) in order to avoid electrodeposition of copper according to 6.6

$$Cu(NH_3)_2^+ + e^- \rightleftharpoons Cu^o + 2NH_3 \qquad 6.6$$

A set of voltammograms at varying NH_3 concentrations are shown in Figure 6.12. As the NH_3 concentration is increased the peaks in the voltammograms are seen to shift in a negative direction. This is expected from the Nernst equation :

$$Cu^{+} + 2NH_3 \rightleftharpoons Cu^{2+} \qquad 6.7$$

$$E_r = E^{o} + \frac{RT}{F} \cdot \ln \left[\frac{a_{Cu^{2+}}}{a_{Cu^{+}} . a_{(NH_3)^2}} \right] \qquad 6.8$$

Thus for a 10-fold increase in $[NH_3]$, E_r will move negative by 120mV. This is shown in Figure 6.13.

The quasi-reversible nature of the redox reaction was indicated by a peak separation of 0.08V to 0.13V, the higher separation occurring with high copper concentrations and fast scan rates.

Complex plane impedance plots were obtained within 100mV of the reversible potential. These consisted of good quality semicircles as shown in Figure 6.14. Charge transfer resistances were obtained from the diameter of the semicircles and were plotted against the electrode potential E in the form $\log(\theta/[1 + \exp -f(E-E_r)])$ vs. E. This is essentially a Butler-Volmer plot enabling the transfer coefficient α to be obtained from the slope. The species involved in the charge transfer step can be identified from the dependence of the data on the ammonia concentration. Similar results were obtained for vitreous carbon and pyrolytic graphite electrodes, Figures 6.15 and 6.16. The slopes of the lines were

120mVdec^{-1} and it can be seen that the lines are separated showing a dependence on the ammonia concentration and also showing that the tetrammine is not the electroactive species. If it were, the electron transfer process would be :

$$Cu(NH_3)_4^{2+} + e^- \rightleftharpoons Cu(NH_3)_4^{+} \qquad 6.9$$

which shows no dependence on the concentration of ammonia, so the Butler-Volmer plots for each ammonia concentration would be superimposed. Figure 6.17 shows the effect of copper concentration (at fixed ammonia concentration) on the kinetics of this redox reaction. A ten-fold increase in $[Cu^{2+}]$ results in a ten-fold decrease in the charge transfer resistance as expected (Figure 6.18).

Electron transfer processes at electrodes are adiabatic[32,33] and therefore it can be supposed that the coordination numbers of the oxidised and reduced forms of the species involved in the charge transfer step must be identical. The mechanism for the reaction being considered can be written in the form :

$$Cu(NH_3)_4^{2+} \rightleftharpoons Cu(NH_3)_m^{2+} + (4-m)NH_3 \qquad 6.10$$

$$Cu(NH_3)_m^{2+} + e^- \rightleftharpoons Cu(NH_3)_m^{+} \qquad 6.11$$

$$Cu(NH_3)_m^{+} \rightleftharpoons Cu(NH_3)_2^{+} + (m-2)NH_3 \qquad 6.12$$

The charge transfer step is represented by equation

6.11. This may be preceeded by one or more chemical steps represented by equation 6.10 and followed by further chemical steps represented by 6.12. One mechanism will predominate. The rate-determining step can be distinguished by the nature of the dependence of the reaction rate upon electrode potential. The observed Tafel slopes of $0.12 V dec^{-1}$ indicate that the electron transfer step is rate determining.

Using an abbreviated notation for the oxidised and reduced forms involved in the charge transfer step we can rewrite equation 6.11 as 6.11a

$$O + e^- \rightleftharpoons R \qquad 6.11a$$

The majority copper species $Cu(NH_3)_2^+$ and $Cu(NH_3)_4^{2+}$ can be represented as Cu^I and Cu^{II}. The equilibrium constants of reactions 6.10 and 6.12 can be expressed as :

$$K_{10} = \frac{[O][NH_3]^{4-m}}{[Cu^{II}]} \qquad 6.13$$

$$K_{12} = \frac{[Cu^I][NH_3]^{m-2}}{[R]} \qquad 6.14$$

Denoting the standard electrode potentials for reactions 6.3 and 6.11 respectively as E^0 and $E^{0'}$, we can write :

$$\exp f(E-E^0) = \frac{[Cu^{II}]}{[Cu^{I}][NH_3]^2} = \frac{[O]}{K_{10}K_{12}[R]} = \frac{1}{K_{10}K_{12}} \exp f(E-E^{0'}) \quad 6.15$$

In the case of a.c. impedance measurements at a fixed d.c. potential E, a Nernst equation 6.16 relates the potential to the concentrations of the copper species adjacent to the electrode surface, denoted by superscript s.

$$E = E^0 + \frac{RT}{F} \ln \left[\frac{[Cu^{II}]_s}{[NH_3]^2([Cu^T]-[Cu(II)_s]} \right] \quad 6.16$$

$[Cu^T]$ represents the total concentration of dissolved copper $[Cu^{II}]$ plus $[Cu^I]$. Equation 6.16 implies that the diffusion coeffients of Cu^I and Cu^{II} are similar so that Cu^T can be supposed uniform. Rearrangement of 6.16 yields 6.17 :

$$[Cu^{II}]_s = \frac{[Cu^T]}{1+[NH_3]^{-2}\exp -f[E-E^0]} \quad 6.17$$

The charge transfer current density i is expressed by the Butler-Volmer equation 6.18

$$i = Fk_o'\left[[R]_s \exp(1-\alpha)f(E-E^{o'}) - [O]_s \exp -\alpha f(E-E^{o'})\right] \quad 6.18$$

where k_o' represents the charge transfer rate constant of step (11) and α is the cathodic transfer coefficient. Differentiation of 6.18 leads to an expression for the

charge transfer resistance

$$\theta^{-1}=\frac{di}{dE}=Fk_o'f\left[(1-\alpha)[R]_s\exp^{(1-\alpha)F}(E-E^{o'})+\alpha[O]_s\exp-\alpha f(E-E^{o'})\right] \quad 6.19$$

Assuming equilibrium in the chemical steps 6.10 and 6.12, equations 6.13 and 6.14 can be substituted into 6.19 for $[O]_s$ and $[R]_s$. Equation 6.15 enables $[Cu^I]_s$ to be expressed in terms of E^o. By means of these substitutions 19 can be replaced by 6.20

$$\frac{1}{Ffk_o'\theta} = \frac{[Cu^T][NH_3]^{m-4}K_{10}{}^{1-\alpha}\exp-\alpha f(E-E^{o'})}{K_{12}{}^{\alpha}\left[1+[NH_3]^{-2}\exp-f(E-E^{o'})\right]} \quad 6.20$$

The half wave potential, E_r, can be expressed by 6.21

$$\exp f(E_r - E^o) = [NH_3]^{-2} \quad 6.21$$

Thus equation 6.20 can be rearranged to yield 6.22

$$\log\left[\frac{\theta}{1+\exp(E-E_r)}\right]+\log\left[\frac{fFk_o'[NH_3]^{m-4}[Cu^T]}{k_{12}{}^{\alpha}k_{10}{}^{\alpha-1}}\right]=\frac{\alpha f(E-E^o)}{2.303} \quad 6.22$$

As stated earlier the charge transfer resistance was plotted against E in the form of $\log\theta/1+\exp(E-E_r)$ vs E. A linear relationship is expected with gradient $\alpha f/2.303$. This was found to be the case experimentally (Figures 6.15,6.16,and 6.17). The gradients of these plots gave a value for the transfer coefficient α of

0.5.

Equation 6.22 suggests that $\log \theta/1+\exp(E-E_r) + \log[Cu^T]$ should be constant at constant electrode potential and this was found to be the case experimentally, Figure 6.17. From Figures 6.15 and 6.16 it is evident that $\delta\log[\theta/1+\exp(E-E_r)]/\delta\log[NH_3] = 1.0$ indicating that 4-m = 1 and showing that the species O and R participating in the charge transfer step 6.11 are the triammines. Similar behaviour was observed for both vitreous carbon and pyrolytic graphite electrodes suggesting that there is minimal interaction between the transition state and the electrode material.

The rate constant k_o' for the charge transfer step can only be estimated because a value for the equilibrium constant K_{12} is not accurately known. However, the rate constant for the overall reaction 6.3 k_o can be evaluated using the experimental values of the charge transfer resistance θ and transfer coefficent α. By analogy with equation 6.19 we can write :

$$\theta^{-1} = Fk_o f\left[(1-\alpha)[Cu^I]_s[NH_3]\exp(1-\alpha)f(e-E^o) + \alpha[Cu^{II}]_s[NH_3]^{-1}\exp-\alpha f(E-E^o)\right] \qquad 6.23$$

Values for k_o at the half-wave potential E_r were evaluated using this equation and are shown in Table 6.4.

Values for k_o' are also tabulated and were evaluated using equation 6.22. These values are only a lower limit. Braish et al.[33] have found u.v. spectroscopic evidence for the existence of $Cu(NH_3)^+$ in Cu(I)

solutions containing high ammonia concentrations. They determined a lower limit for the equilibrium constant K_{12} as $5x10^{2}moldm^{-3}$ at unit ionic strength and 25°C. This value was used in equation 22 to evaluate a lower limit for k_o'. The value taken for K_{10} is that reported by Etimova et al.[35] of $9.1x10^{-3}moldm^{-3}$ at 25°C and unit ionic strength.

These measurements have shown that the rate-determining step for the reaction :

$$Cu(NH_3)_4^{+} + e^{-} \rightleftharpoons 2NH_3 + Cu(NH_3)_2^{+}$$

at carbon electrodes in $0.1moldm^{-3}$ aqueous ammonium sulphate solution is

$$Cu(NH_3)_3^{2+} + e^{-} \rightleftharpoons Cu(NH_3)_3^{+}$$

The rate constants k_o for the overall reaction at 25°C are $3.7\pm1.3x10^{-3}cms^{-1}$ on vitreous carbon and $2.7\pm0.7x10^{-3}cms^{-1}$ on pyrolytic graphite (basal plane orientation). Cathodic transfer coefficients were found to be 0.53±0.02 and 0.56±0.01 respectively. The rate constant for the actual electron-transfer step exceeds $0.5cms^{-1}$.

6.5.4 CuII/CuI Redox Reaction at Other Electrode Materials.

Two other carbon materials were used to examine the redox kinetics of the $Cu(NH_3)_4^{2+}/Cu(NH_3)_2^{+}$ reaction. These were pyrolytic graphite with edge orientation and

Union Carbide YBD hard carbon. As shown in Figures 6.19 and 6.20 it was not possible to obtain charge transfer semicircles with such electrode materials. This is most likely due to the increased surface area of such electrodes. As this surface area was unknown, further measurements were not performed with these materials. Impedance measurements for pyrolytic graphite with edge orientation and YBD hard carbons yield large values of double layer capacitance per electrode geometric area indicating that the true area of such electrodes is large (see Chapter 4).

6.5.5 CuII/CuI at Electrodes Subjected to Fluorine Evolution

Electrodes that had been subjected to fluorine evolution at 6V in KF.2HF were removed from the melt, washed with thrice distilled water and dried. The effect of this treatment on the redox kinetics of the Cu^{2+}/Cu^{+} redox couple was examined using a solution of composition :

$[Cu^{2+}] = 10^{-2}M$

$[NH_3] = 2.0M$

$[(NH_4)_2SO_4] = 0.1M$

The reference electrode was again mercury/mercurous sulphate 0.5M $(NH_4)_2SO_4$.

The charge transfer resistance was obtained for this redox couple at a vitreous carbon electrode subjected to seven hours electrolysis at 6V in KF.2HF at the reversible half-wave potential of -680mV

(merury/mercurous sulphate), and θ was found to be $26.04\Omega cm^2$. This corresponds to a four-fold decrease in the rate of the reaction. Thus initial results lead to the belief that the redox couple might be suitable for investigating the effects of fluorination of the electrodes. However, two more impedance plots were subsequently obtained at -680mV at ten minute intervals. The second plot resulted in a value of $12.6\Omega cm^2$ for the charge transfer resistance whilst the third gave a value of $9.8\Omega cm^2$. These results are depicted in Figure 6.21. The final value of $9.8\Omega cm^2$ is similar to that obtained on a freshly polished carbon surface. Such results were obtained consistently irrespective of the time of electrolysis. (The effect of increased potential was not examined). Obviously the $Cu(NH_3)_4^{2+}/Cu(NH_3)_2^{+}$ redox system is not suitable as a model for the study of fluorinated electrodes.

To investigate further the reason why this system is not suitable for the study of fluorinated electrodes it was necessary to distinguish between chemical dissolution of the fluoride film in the aqueous ammonia system and electrochemical dissolution due to polarisation at -680mV (Hg/Hg_2SO_4).

This was achieved by examining the redox kinetics of the ferrocene/ferrocinium couple at fluorinated electrodes and investigating the effect of aqueous ammonia solutions and potential on these kinetics.

The impedance plot for the ferrocene/ferrocinium couple at an electrode polarised at 6V in the KF.2HF melt is shown in Figure 6.4. The electrode was then

removed from the acetonitrile system, washed, and immersed in a solution which was 2.0M in NH_3, 10^{-2}M in Cu^{2+} and 0.1M in $(NH_4)_2SO_4$ for ten minutes. The electrode was then washed and dried and returned to the acetonitrile system. The charge transfer resistance for the ferrocene couple was found to have been unaffected by immersion in aqueous ammonia solutions. The electrode was then polarised at -300mV (vs. saturated NaCl calomel) in the acetonitrile system for ten minutes (equivalent to -680mV (Hg_2SO_4/Hg). The impedance plot for the ferrocene couple was then re-measured at the equilibrium potential for this couple (0.300V) and was found to be the same as at a freshly polished electrode as shown in Figure 6.2.

This, again, was very reproducible and seems to indicate that it is polarisation at the negative potential that removes the film and not simple dissolution.

An electrode which had been fluorinated at 6V in KF.2HF gave an impedance plot for the ferrocene couple as shown in Figure 6.4. This was then polarised at -300mV (vs. saturated NaCl calomel) for ten minutes. (This electrode had not been subjected to any treatment with ammonia solutions). The impedance plot then obtained for the ferrocene couple was identical to that found for a fresh carbon electrode.

Due to the reduction of the fluoride film at negative potentials in both aqueous and non-aqueous media the choice of redox couples that could be used as model systems for the study of fluorinated electrodes

was limited to redox couples with positive reversible potentials.

On the time scale of the impedance measurement (10 minutes 10kHz to 1Hz) there appears to be no effect due to simple dissolution of the fluoride films formed at carbon anodes in KF.2HF. However, capacitance measurements, (chapter 4), did indicate that various solvents, both aqueous and non-aqueous, can have an effect on the fluoride films. For this reason electrodes that had been fluorinated were exposed to solvents for the minimum amount of time so that dissolution effects were minimised.

6.6 GENERAL DISCUSSION

Fluoride films formed on carbon electrodes in KF.2HF can be studied by removal of the electrodes from the molten salt and their subsequent examination in aqueous or non-aqueous solvents containing model redox systems.

It has been shown that a film as thin as 7Å can have a profound effect on the rate of electron transfer of such model systems. A decrease in the rate constant for the reaction

$$FeCp_2 \rightleftharpoons FeCp_2^+ + e^-$$

by a factor 10^2 was obtained.

A similar inhibition of fluorine evolution is expected in the KF.2HF melt; the factor 10^2 is probably a minimum value for the inhibition factor.

It has been shown that model redox systems are

retarded more by electrodes that are fluorinated at higher potentials in KF.2HF. It was also shown that at higher fluorination potentials a contribution to the impedance was due to increased ohmic resistance of the fluoride film. This contribution was of the value $10\Omega cm^2$. At an operating cell current of $200mAcm^{-2}$ this ohmic resistance would result in an overvoltage of 2.0V. The significance of this contribution is discussed later in this thesis, but it clearly shows that carbonpolyfluoride films do make a significant contribution to the anode overvoltage observed in fluorine cells.

TABLE 6.1

Redox Couples studied in this work

REDOX COUPLE	SOLVENT	SUPPORT ELECTROLYTE
$FeCp_2/FeCp_2^+$	Acetonitrile	$NaClO_4$
$Fe(CN)_6^{3-}/Fe(CN)_6^{4-}$	Water	KCl
$IrCl_6^{2-}/IrCl_6^{3-}$	Water	KCl
$Cu(NH_3)_4^{2+}/Cu(NH_3)_2^+$	Aqueous NH_3	$(NH_4)_2SO_4$

TABLE 6.2

Kinetic parameters for Ferrocene/

Ferrocinium redox couple

V*	R_Ω Ωcm^2	θ Ωcm^2	σ $	k_o cms^{-1}	$10^5 D$ $cm^2 s^{-1}$	C_d μFcm^{-2}
None	13.2	<1	130	>1	2.3	24.5
+2	11.0	<1	123	>1	2.6	23.7
+4	11.5	1.38	121	0.32	2.7	20.7
+6	12.5	29.6	123	0.015	2.6	3.4
+9	20.1	18.21	131	0.0244	2.3	2.1

* V = Fluorination Potential/V

$ Units $cm^2 rad^{\frac{1}{2}} s^{-\frac{1}{2}}$

TABLE 6.3

Kinetic parameters for the Hexacyanoferrate II/III redox couple

Fluorination Potential/V	R_Ω Ωcm^2	θ Ωcm^2	$10^4 k_o$ cms^{-1}
None	5.0	7.4	146
4	5.7	21.7	50
6	7.1	132	8.23
8	23.1	335	3.24

TABLE 6.4

Kinetic parameters for the Cu(II)/Cu(I) redox system in aqueous ammonia

VITREOUS CARBON

$[NH_3]$ $moldm^{-3}$	θ $ohmcm^2$	α	$-E_r$ V	$10^3 k_o$ cms^{-1}	k_o' cms^{-1}
0.22	23.1	0.51	0.56	2.38	> 0.56
0.68	13.9	0.53	0.62	3.93	> 0.96
2.0	9.9	0.55	0.68	4.93	> 1.26

PYROLYTIC GRAPHITE

0.23	31	0.56	0.56	2.08	> 0.52
0.7	21.5	0.56	0.61	2.66	> 0.66
2.1	15	0.56	0.68	3.22	> 0.83

Figure 6.1

Cyclic voltammogram for the ferrocene/ferrocinium redox couple (1 x 10^{-2}M ferrocene) in acetonitrile/$NaClO_4$ (0.5M) at a freshly polished vitreous carbon electrode (A=0.5cm^2) at 0.01Vs^{-1}.

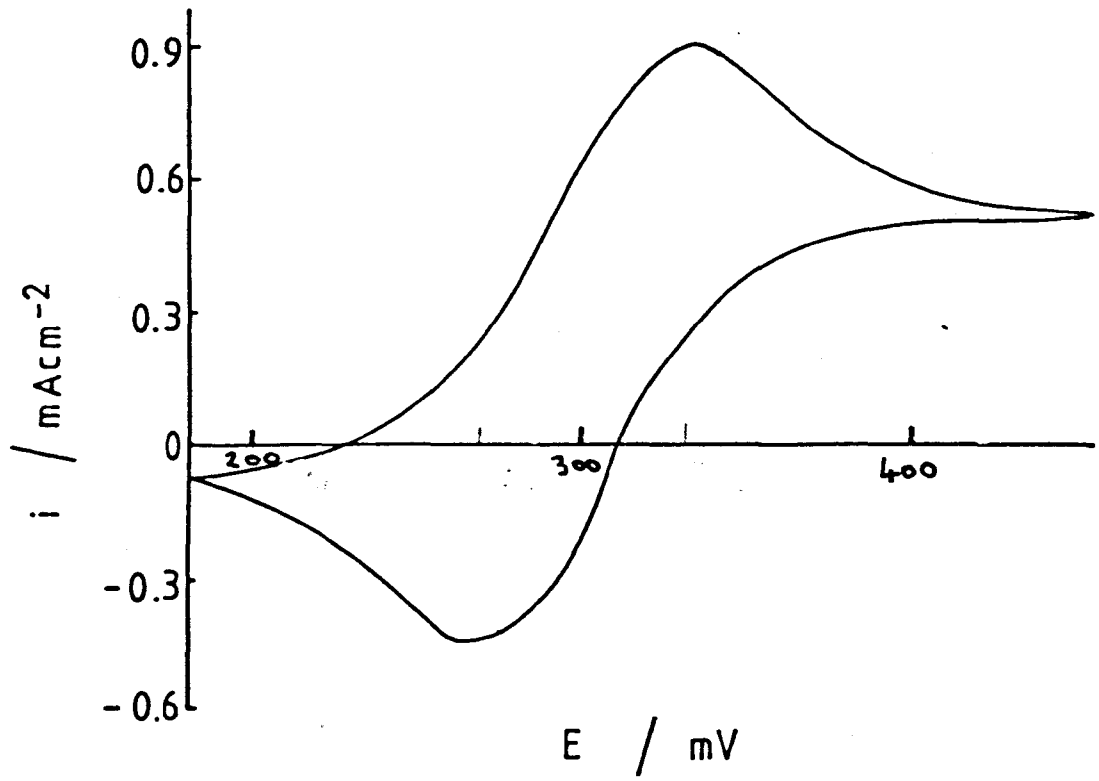
0.9
0.6
0.3
0
-0.3
-0.6
i / mAcm^{-2}
200
300
400
E / mV

Figure 6.2

Impedance spectrum for the $FeCp_2/FeCp_2^+$ redox couple at the E^0 potential (0.300V vs. SCE) in acetonitrile/$NaClO_4$ at a polished vitreous carbon electrode. Numbers refer to frequencies in Hz. Electrode area = $0.5cm^2$

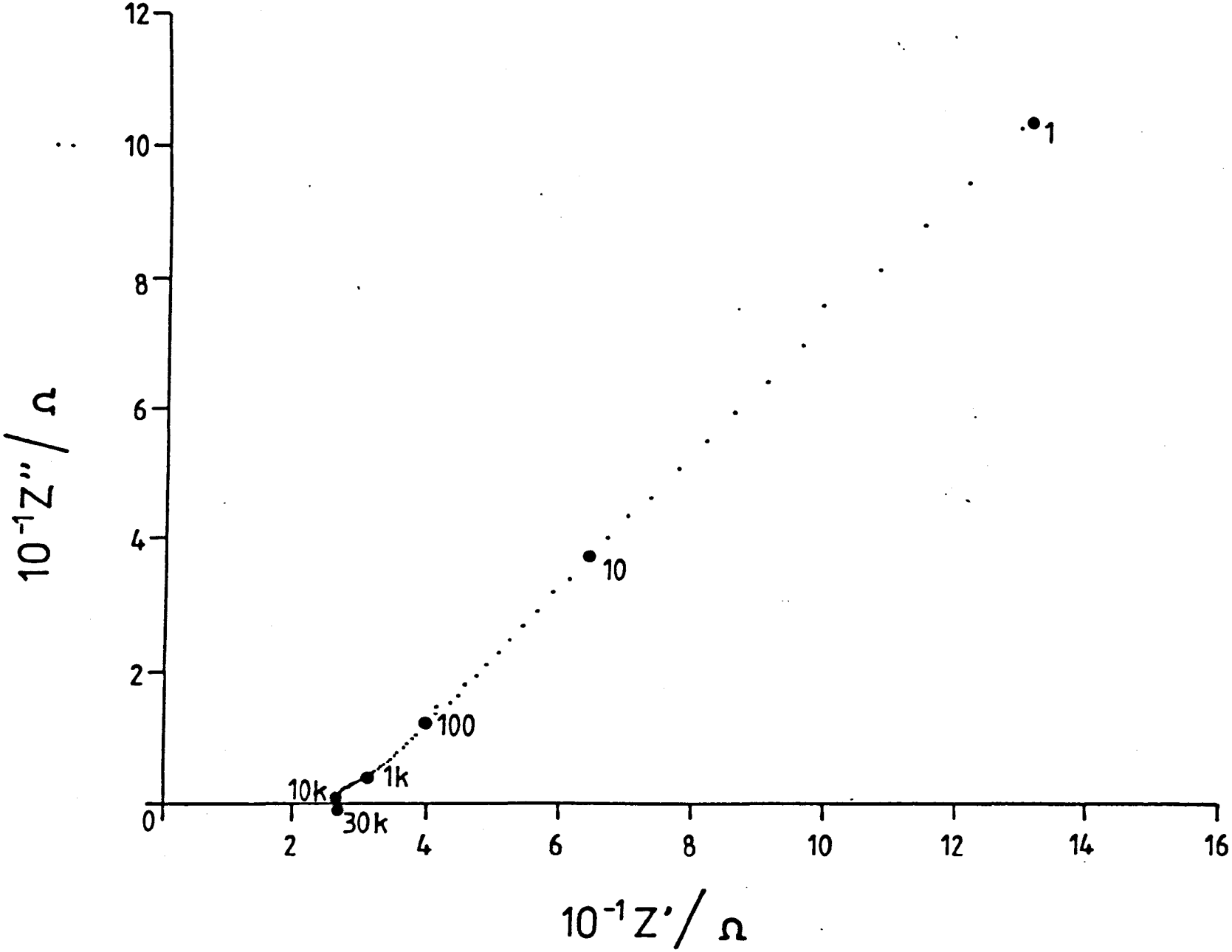
12
10
8
6
4
2
0
2
4
6
8
10
12
14
16
1
10
100
1k
10k
30k
$10^{-1}Z''/\Omega$
$10^{-1}Z'/\Omega$

Figure 6.3

Low frequency data from figure 6.2 reploted as Z' (■) and Z'' (▼) vs. $\omega^{\frac{1}{2}}$. Electrode area = $0.5cm^2$

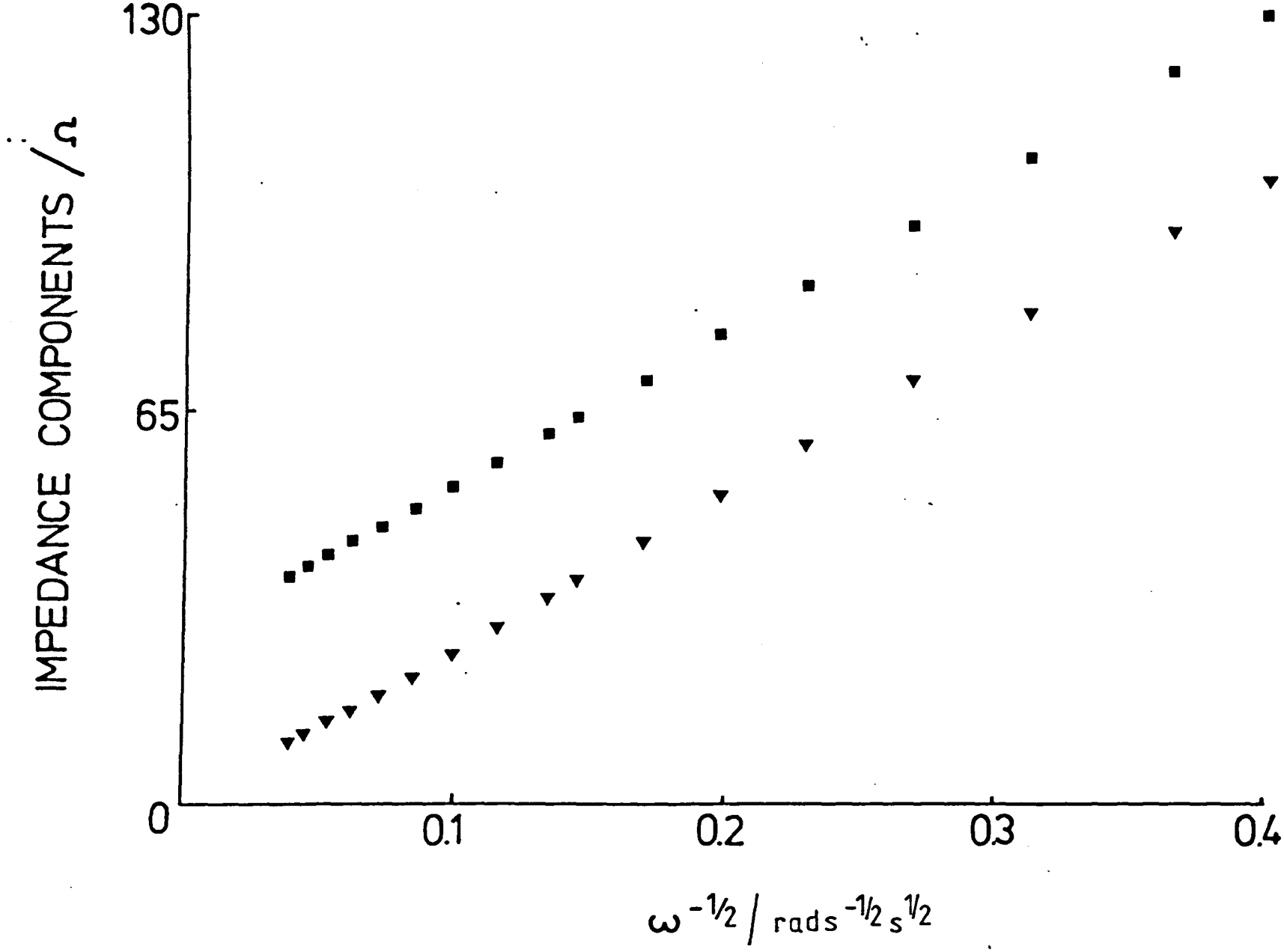
130
65
0
IMPEDANCE COMPONENTS / Ω
0.1
0.2
0.3
0.4
ω^-1/2 / rads^-1/2 s^1/2

Figure 6.4

Impedance spectrum for the $FeCp_2/FeCp_2^+$ redox couple at the E^0 potential (0.300V vs. SCE) in acetonitrile/$NaClO_4$ at a vitreous carbon electrode previously subjected to fluorine evolution for 30 minutes at 6V in KF.2HF. Electrode area = $0.5cm^2$

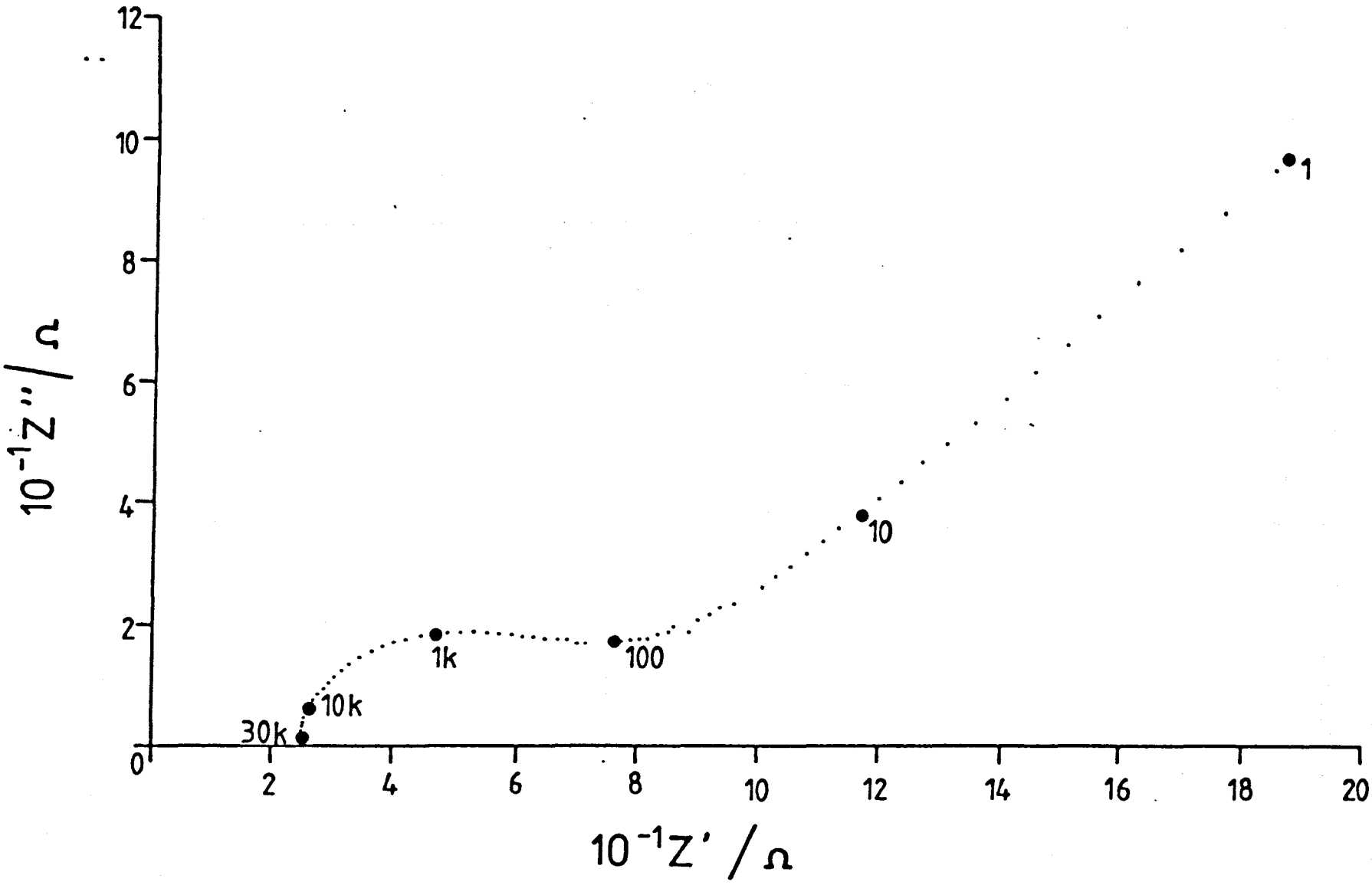
12
10
8
6
4
2
0
2
4
6
8
10
12
14
16
18
20
1
10
100
1k
10k
30k
$10^{-1}Z''/\Omega$
$10^{-1}Z'/\Omega$

Figure 6.5

Cyclic voltammogram for the hexacyanoferrate (II/III) redox couple ($5x10^{-3}$M Hexacyanoferrate II) in aqueous KCl (0.5M) at a freshly polished vitreous carbon electrode (A=0.5cm^2) at 0.030Vs^{-1}).

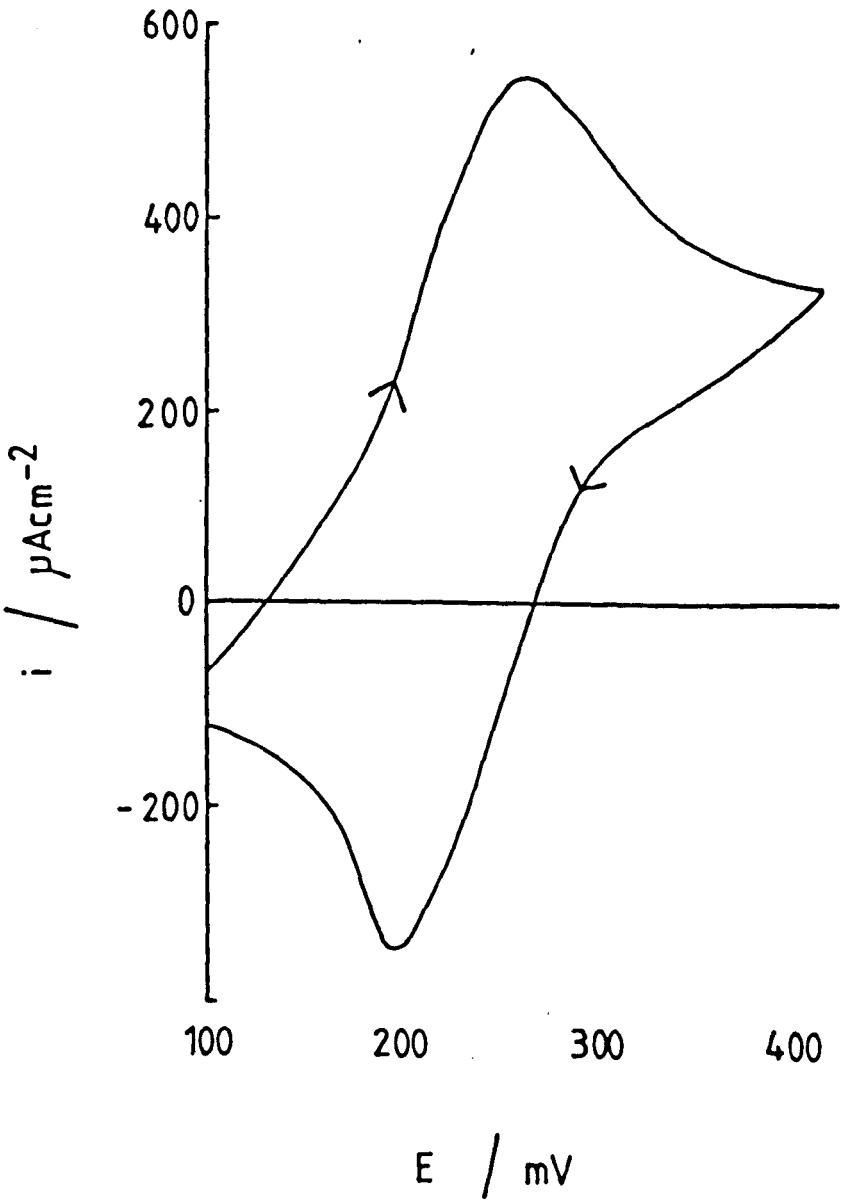

Figure 6.6

Impedance spectrum for the hexacyanoferrate (II/III) redox couple at the E^0 potential (+0.230V vs. SCE) in aqueous KCl at a polished vitreous carbon electrode. Numbers refer to frequencies in Hz. Electrode area = $0.5cm^2$

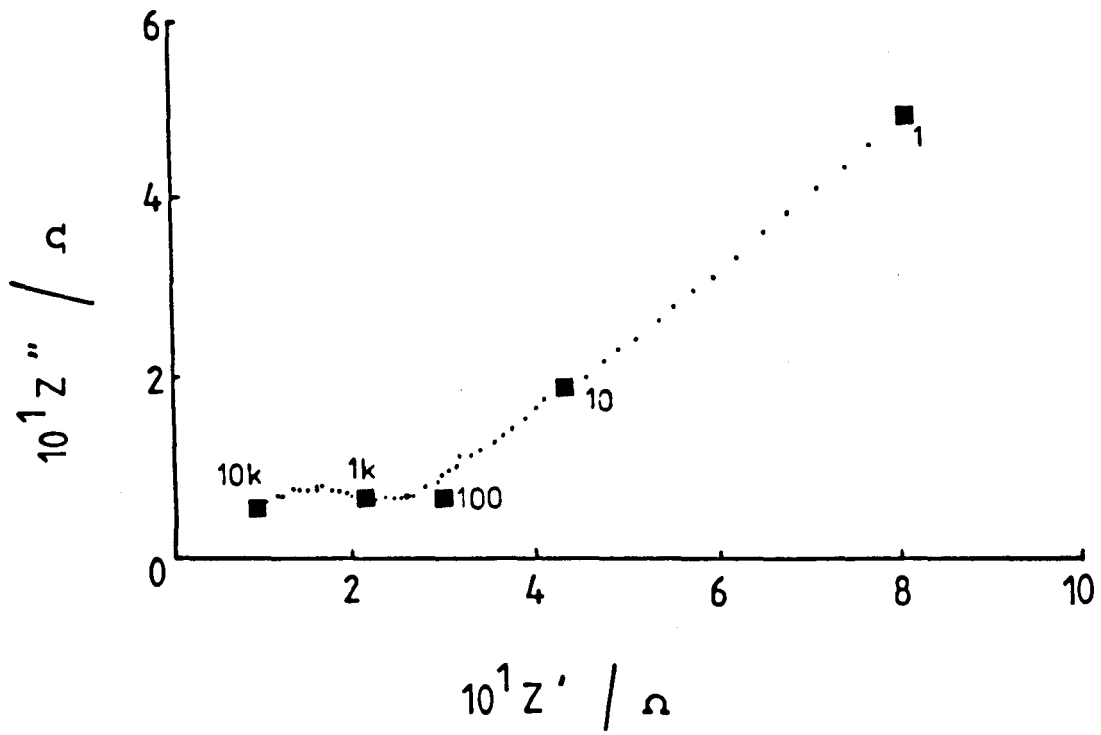

Figure 6.7

Tafel-type plot of charge-transfer resistance obtained from impedance data against potential (vs. SCE) for the hexacyanoferrate (II/III) redox couple.

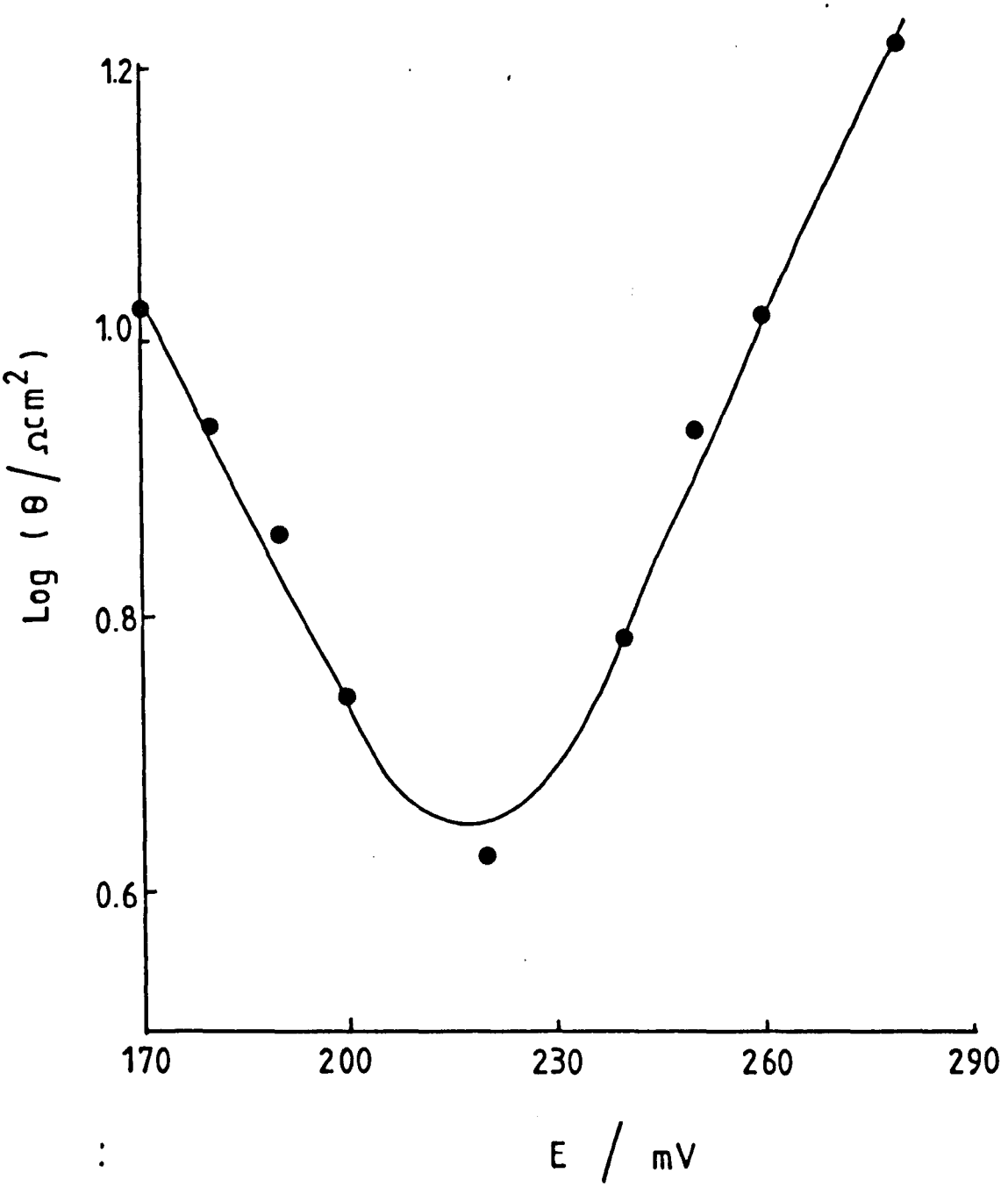

Figure 6.8

Cyclic voltammogram for the hexachloroiridate III/IV redox couple (9.5×10^{-4}M K_2IrCl_6) in 0.5M HCl at a polished vitreous carbon electrode (A=0.5cm^2) at 0.1Vs^{-1}.

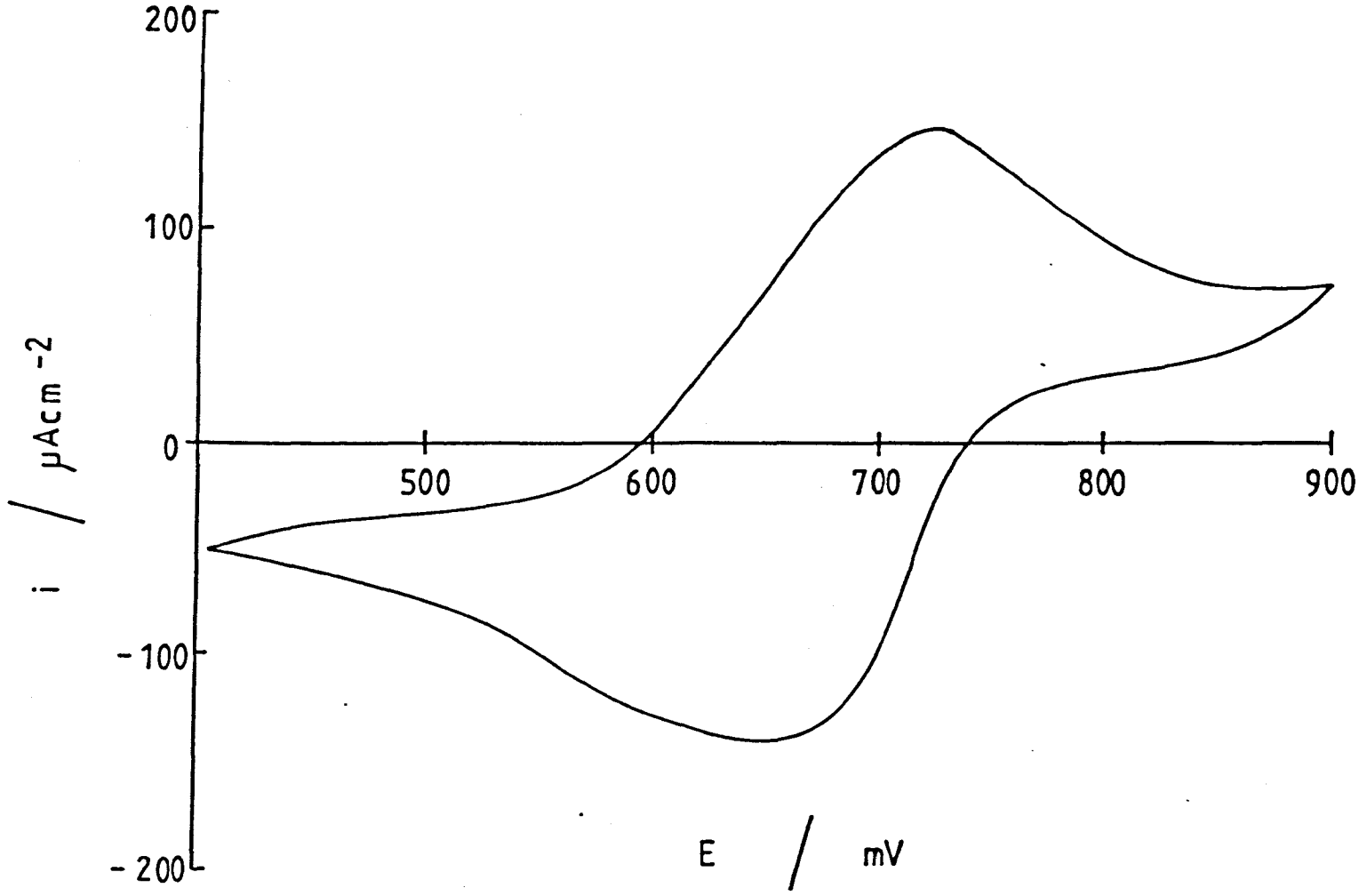
200
100
0
-100
-200
500
600
700
800
900
i / μAcm -2
E / mV

Figure 6.9

Impedance spectrum for the hexachloroiridate III/IV redox couple (9.5×10^{-4}M K_2IrCl_6) in 0.5M HCl at a polished vitreous carbon electrode (A=0.5cm^2) E=+0.685V (vs. SCE).

Figure 6.10

Impedance spectrum for the hexachloroiridate III/IV redox couple (9.5×10^{-4}M K_2IrCl_6) in 0.5M HCl at an electrode subjected to fluorine evolution in KF.2HF at 6V for 30 minutes. E=+0.685V (vs. SCE). (A=0.5cm^2)

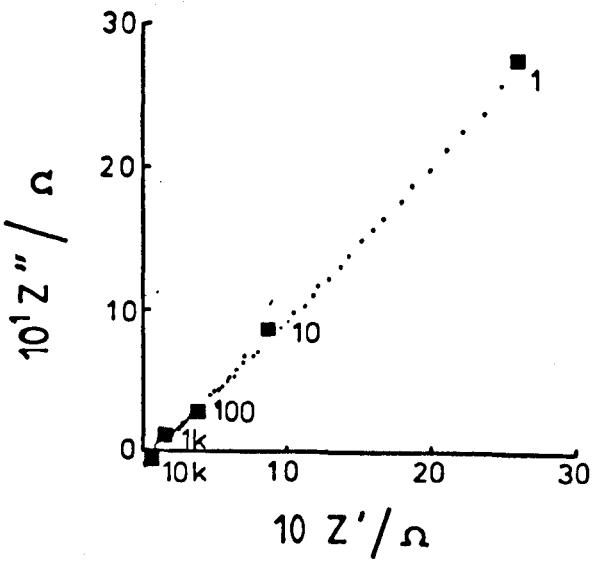
30
20
10
0
$10^1 Z'' / \Omega$
1
10
100
1k
10k
10
20
30
$10 Z' / \Omega$

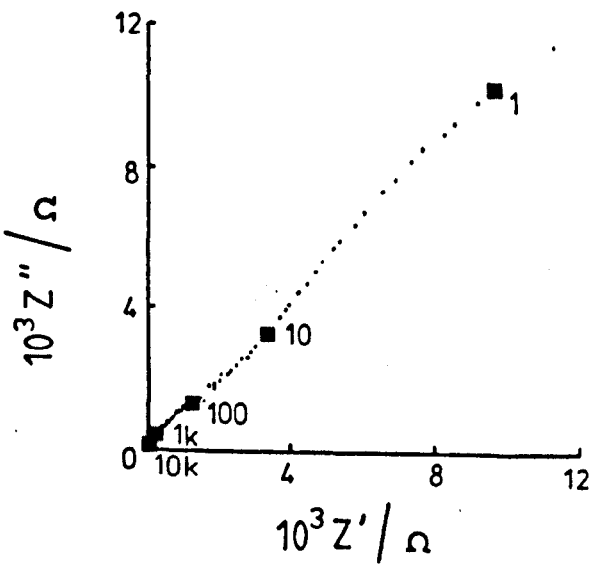
12
8
4
0
$10^3 Z'' / \Omega$
1
10
100
1k
10k
4
8
12
$10^3 Z' / \Omega$

Figure 6.11

Cyclic voltammogram obtained at a hanging mercury drop electrode for the $Cu(NH_3)_4^{2+}/Cu(NH_3)_2^{+}$ redox couple in aqueous ammonia solution 0.3M NH_3, $1x10^{-2}$M Cu^{2+}, 0.5M $(NH_4)_2SO_4$, at a sweep rate of $0.1Vs^{-1}$. Electrode area = $2.09x10^{-2}cm^2$

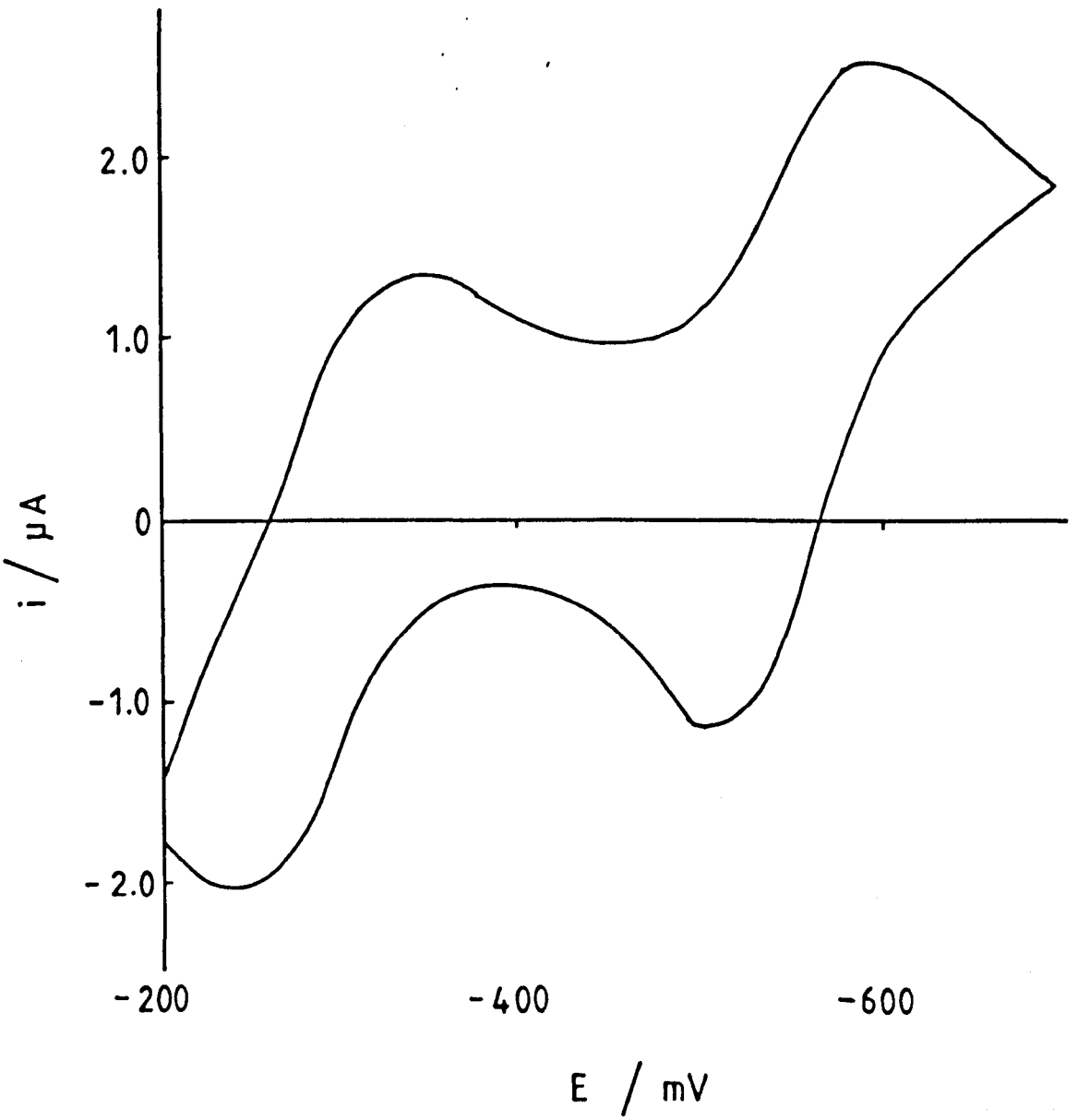

Figure 6.12

Cyclic voltammogram obtained for the $Cu(NH_3)_4^{2+}/Cu(NH_3)_2^{+}$ redox couple at a polished vitreous carbon electrode at a sweep rate of $0.010 Vs^{-1}$. $[Cu^{2+}] = 1 \times 10^{-2} M$; $[(NH_4)_2SO_4] = 0.5M$.

———— $[NH_3]=2.0M$

- - - - - $[NH_3]=0.68M$

..... $[NH_3]=0.22M$.

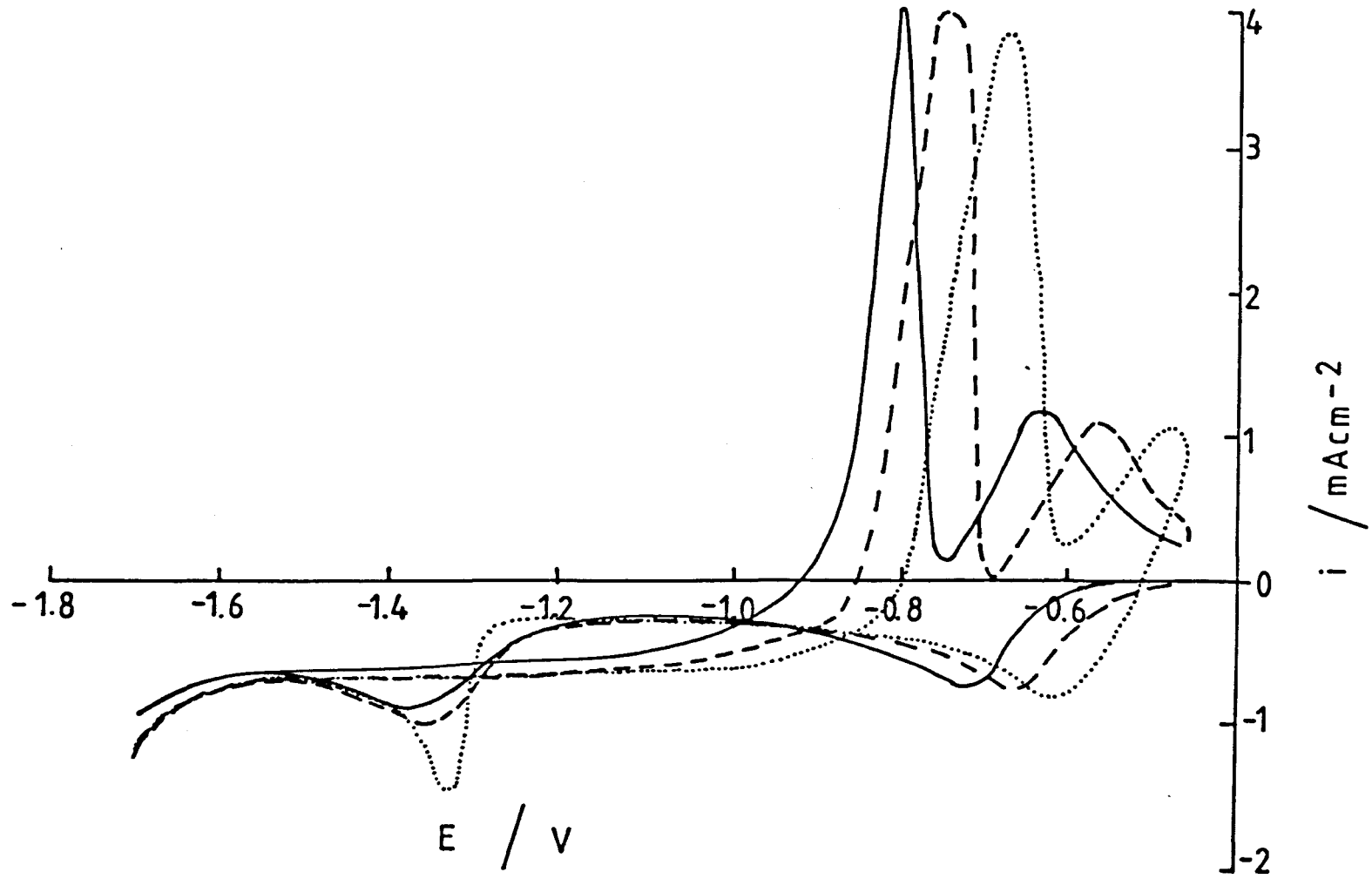
-1.8
-1.6
-1.4
-1.2
-1.0
-0.8
-0.6
4
3
2
1
0
-1
-2
i / mAcm-2
E / V

Figure 6.13

Dependence of the half-wave potential E_r upon ammonia concentration. (▲) vitreous carbon, (■) pyrolytic graphite with face orientation. All solutions were $1x10^{-2}$M $CuSO_4$, and 0.10M $(NH_4)_2SO_4$ aq.

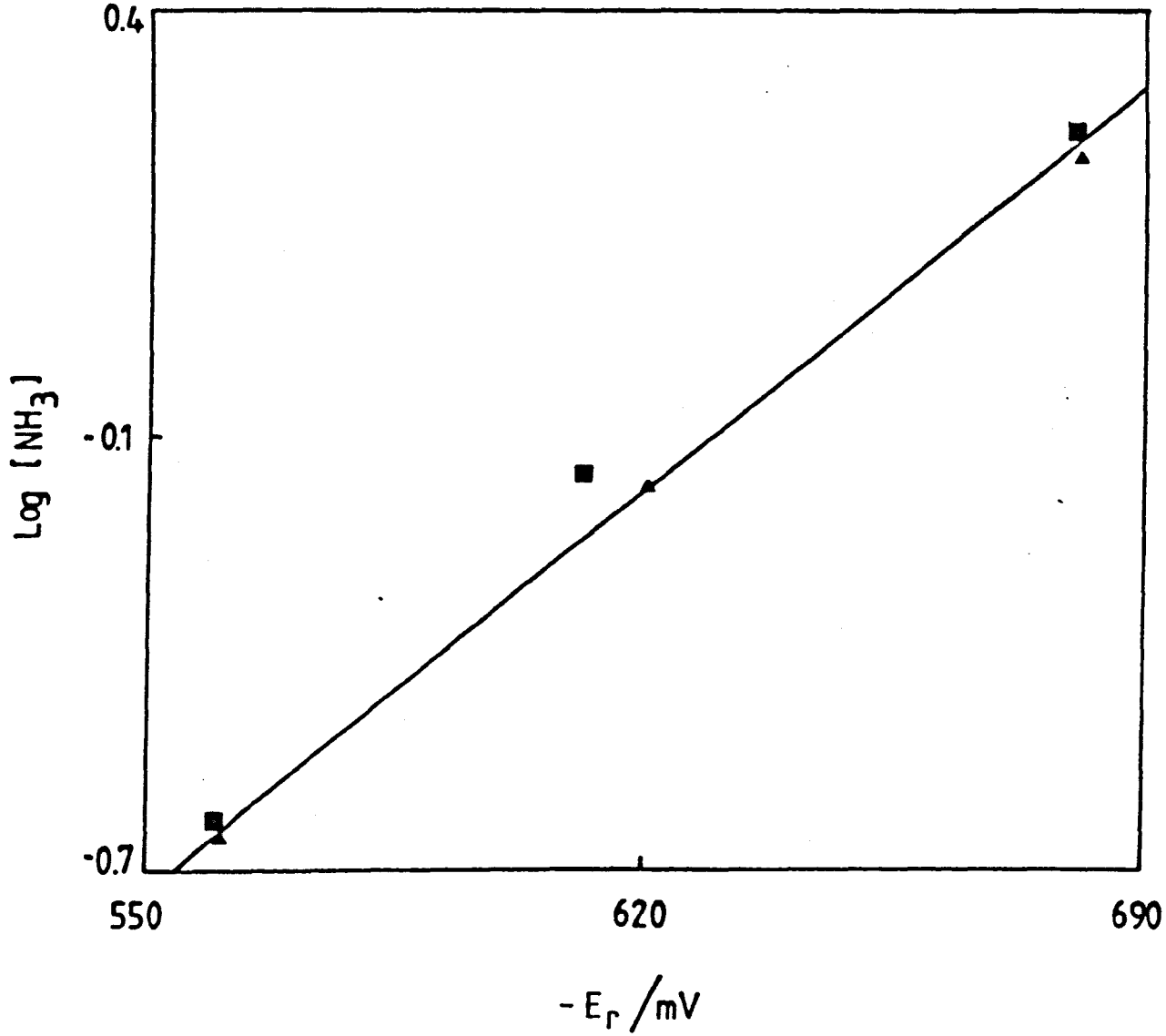
0.4
-0.1
-0.7
Log [NH3]
550
620
690
- Er /mV

Figure 6.14

Impedance spectrum over the frequency range 1.0Hz to 10kHz. Electrode potential -0.560V. At vitreous carbon ($A=0.5cm^2$) solution composition $1.0x10^{-2}M$ $CuSO_4$, 0.22M NH_3, 0.10M $(NH_4)_2SO_4$ aq.

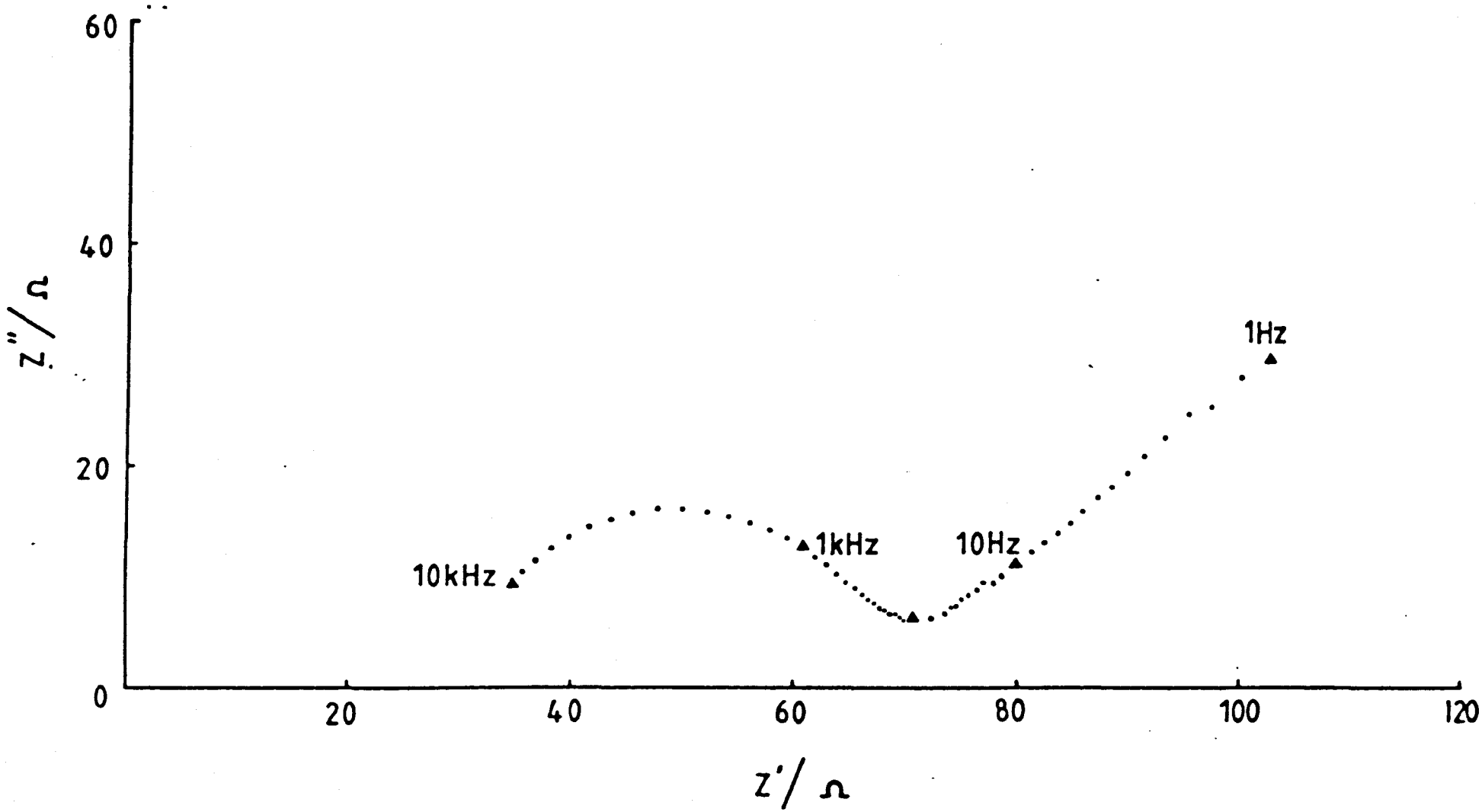
60
40
20
0
Z''/ Ω
20
40
60
80
100
120
Z'/ Ω
10kHz
1kHz
10Hz
1Hz

Figure 6.15

Butler-Volmer type plot using vitreous carbon for the $Cu(NH_3)_4^{2+}/Cu(NH_3)_2^{+}$ redox couple. All solutions were $1x10^{-2}M$ $CuSO_4$, and 0.10M $(NH_4)_2SO_4$ aq. Ammonia concentrations: (■) 0.22M, (▲) 0.68M, (●) 2.0M.

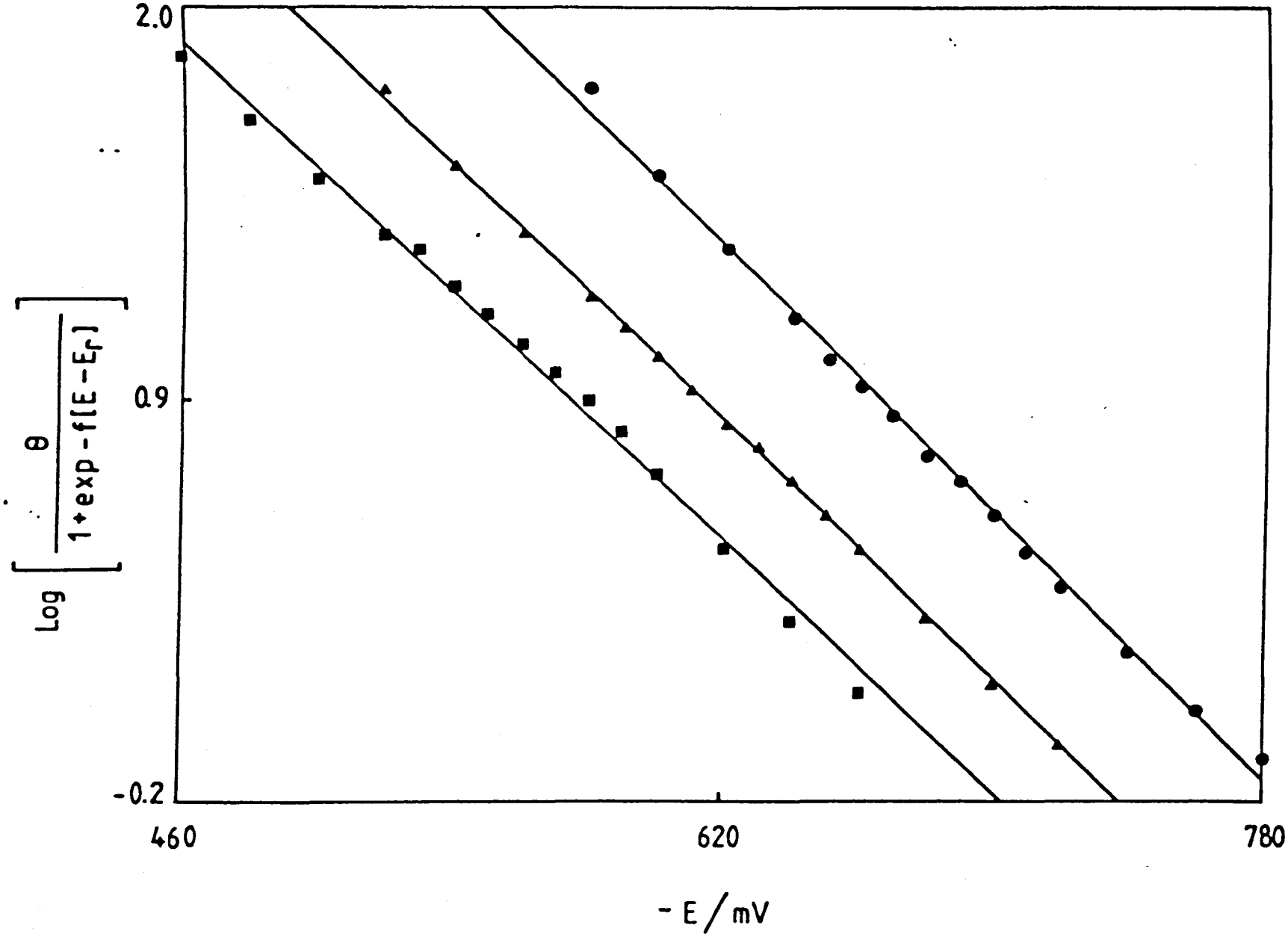
2.0
0.9
-0.2
460
620
780
- E / mV
Log [θ / 1+exp-f(E-Er)]

Figure 6.16

Butler-Volmer type plot using pyrolytic graphite electrodes with face orientation for the $Cu(NH_3)_4^{2+}/Cu(NH_3)_2^{+}$ redox couple. All solutions were $1x10^{-2}M$ $CuSO_4$, and 0.10M $(NH_4)_2SO_4$ aq. Ammonia concentrations: (■) 0.23M, (▲) 0.70M, (●) 2.1M.

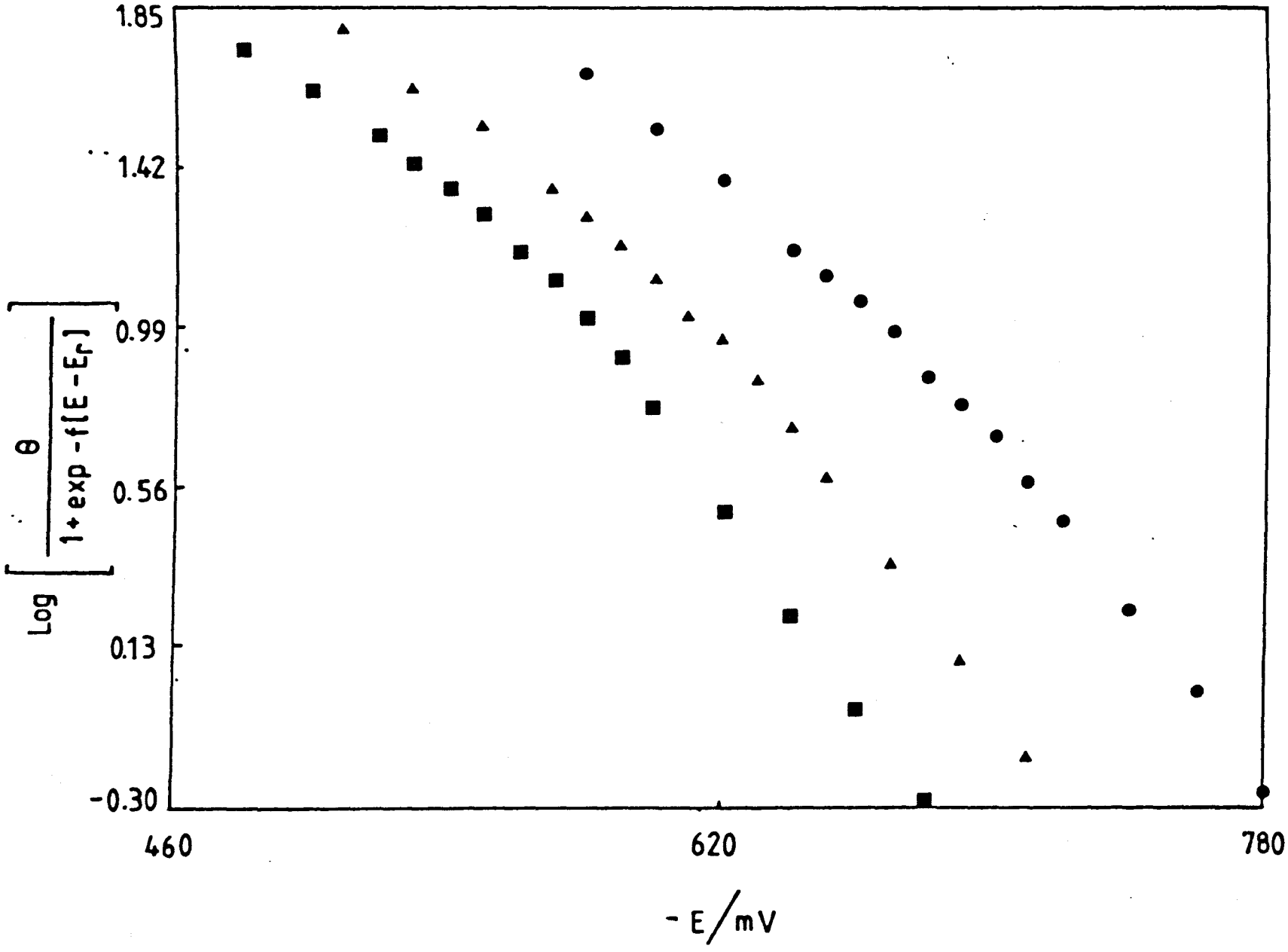
1.85
1.42
0.99
0.56
0.13
-0.30
Log [θ / (1+exp -f[E-Er])]
460
620
780
- E/mV

Figure 6.17

Butler-Volmer type plot using vitreous carbon for the $Cu(NH_3)_4^{2+}/Cu(NH_3)_2^{+}$ redox couple. Both solutions 1.02M in NH_3 and 0.10M in $(NH_4)_2SO_4$. $CuSO_4$ concentrations (●) 5.0×10^{-2}M, (▲) 5.0×10^{-3}M.

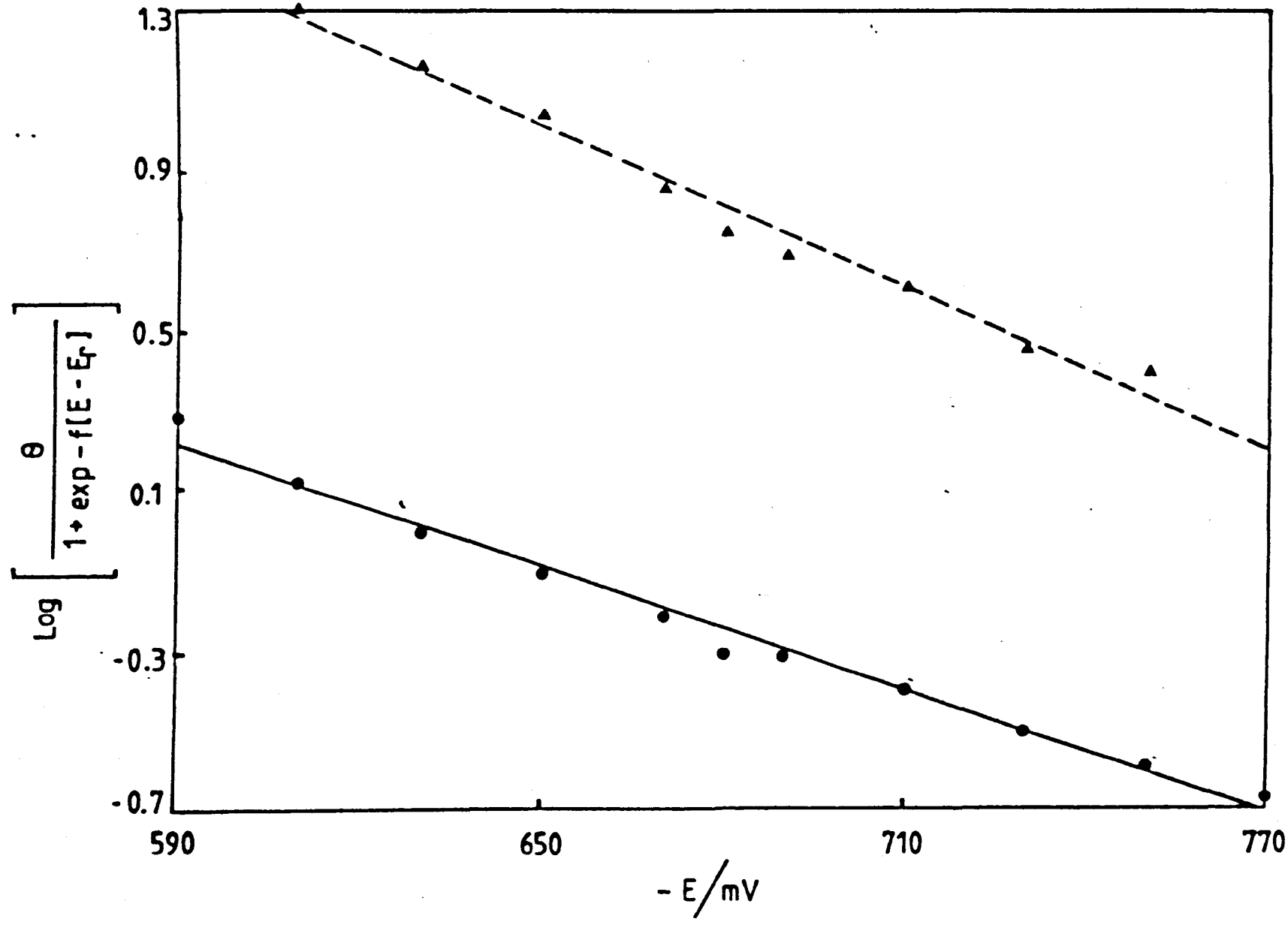
1.3
0.9
0.5
0.1
-0.3
-0.7
590
650
710
770
- E/mV
Log [θ / (1 + exp - f(E - E_F))]

Figure 6.18

Impedance spectra obtained at vitreous carbon ($A=0.5cm^2$) for the $Cu(NH_3)_4^{2+}/Cu(NH_3)_2^{+}$ redox couple. Solutions 1.02M in NH_3 and 0.10M in $(NH_4)_2SO_4$.

a) $CuSO_4=5.0x10^{-2}M$

b) $CuSO_4=5.0x10^{-3}M$

E=-0.68V (vs. Hg/Hg_2SO_4).

a

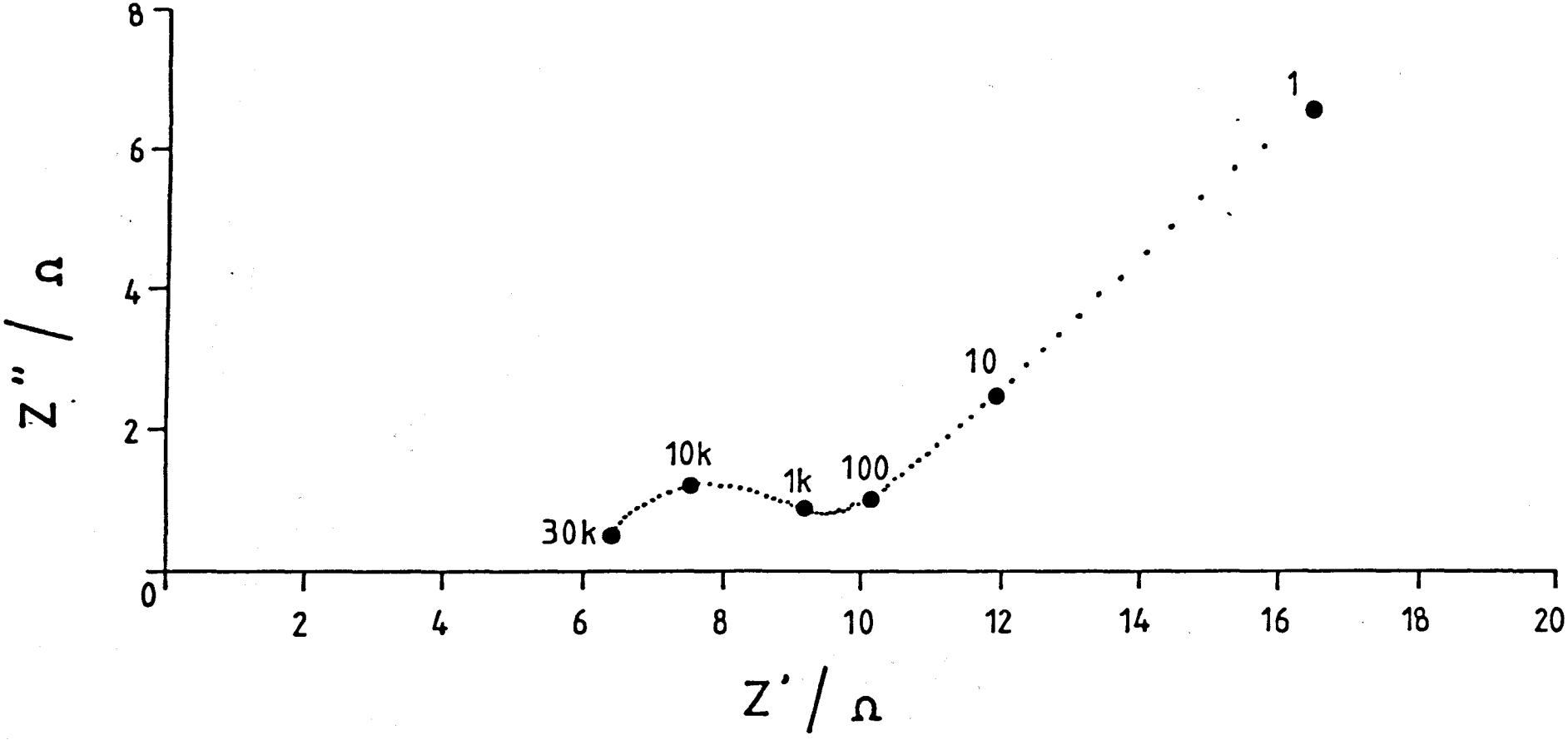

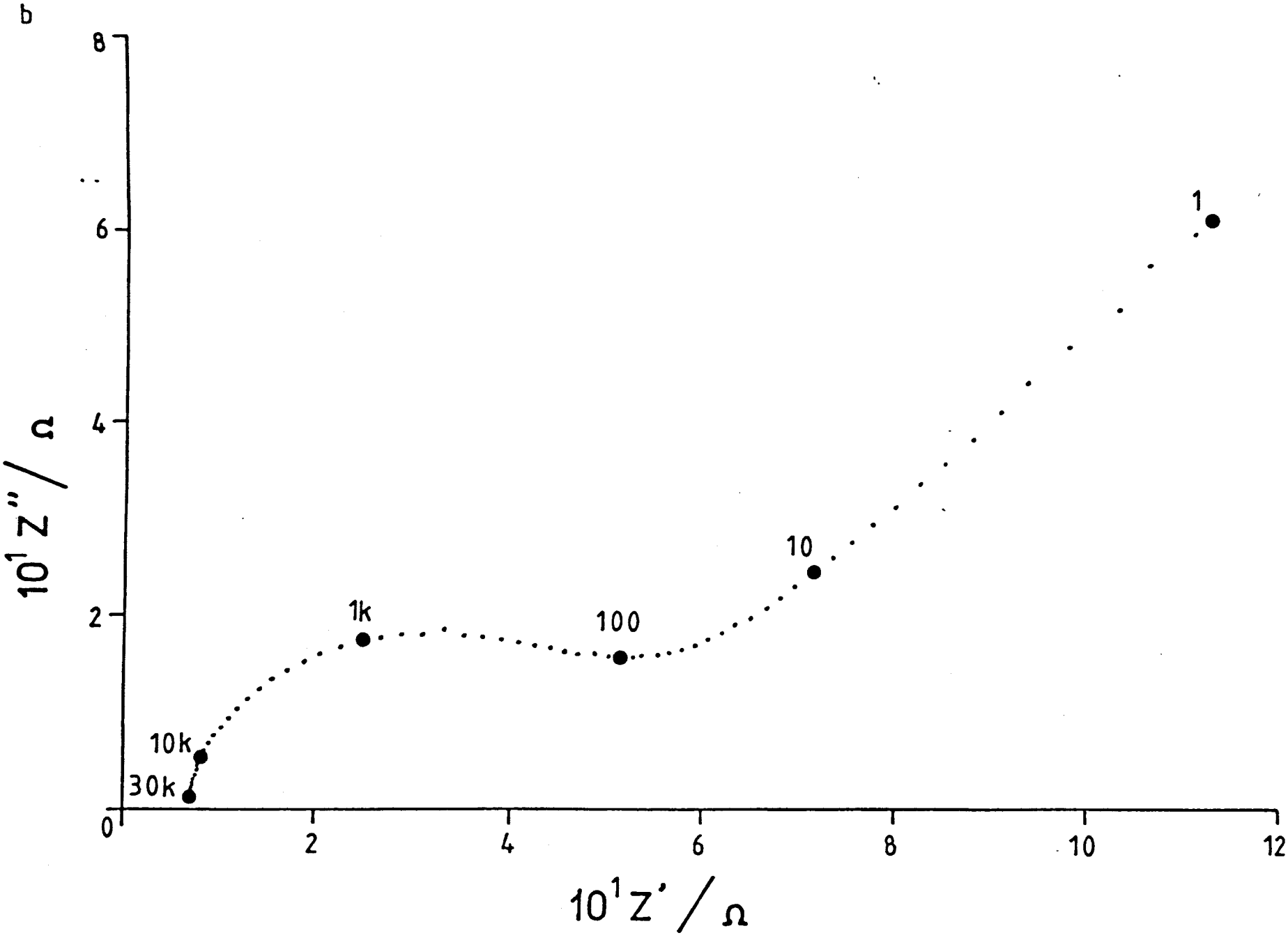
b
8
6
4
2
0
2
4
6
8
10
12
$10^1 Z'' / \Omega$
$10^1 Z' / \Omega$
1
10
100
1k
10k
30k

Figure 6.19

Impedance spectra obtained at pyrolytic graphite with edge orientation for the $Cu(NH_3)_4^{2+}/Cu(NH_3)_2^{+}$ redox couple. Solution composition 0.10M $(NH_4)_2SO_4$, 1.0×10^{-2}M $CuSO_4$, 1.8M NH_3. E=-0.68V (vs. Hg/Hg_2SO_4). Geometric area = $0.5cm^2$

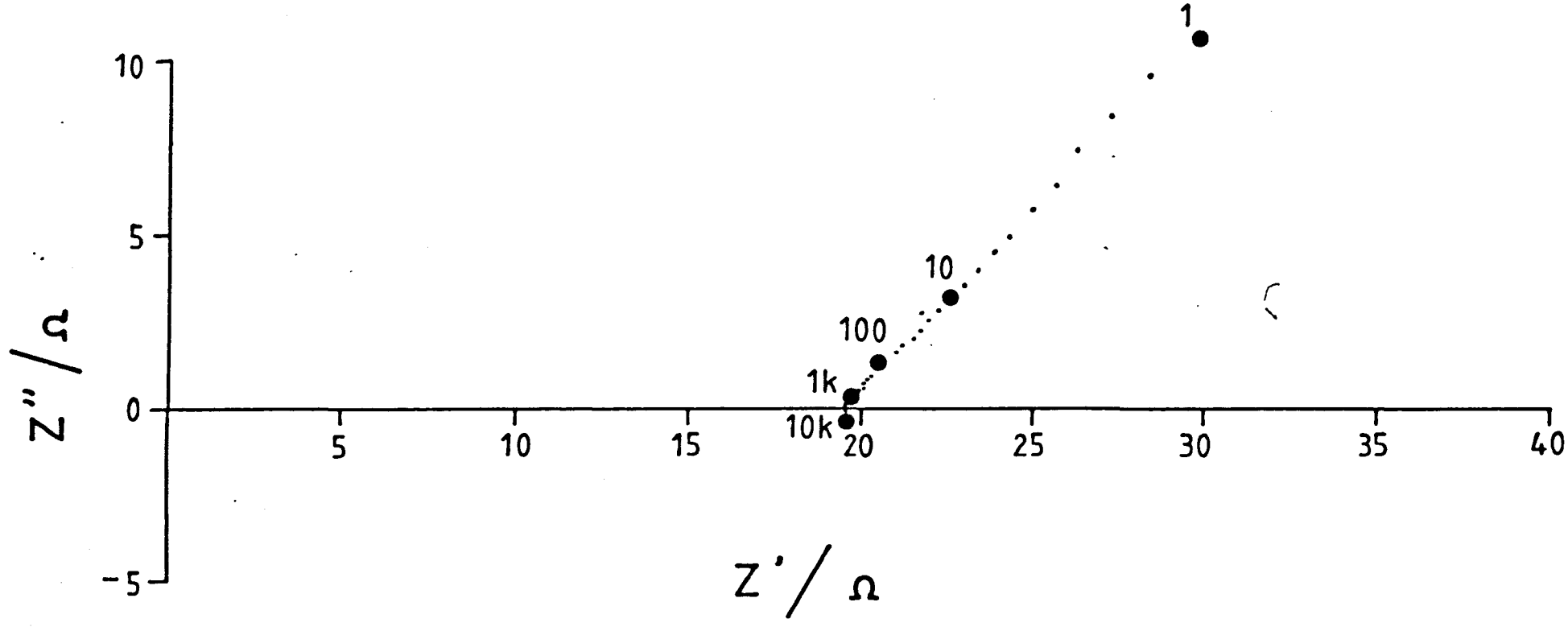
10
5
0
−5
Z'' / Ω
5
10
15
20
25
30
35
40
Z' / Ω
1
10
100
1k
10k

Figure 6.20

Impedance spectra obtained at YBD porous carbon for the $Cu(NH_3)_4^{2+}/Cu(NH_3)_2^{+}$ redox couple. Solution composition 0.10M $(NH_4)_2SO_4$, 1.0 x 10^{-2}M $CuSO_4$, 1.8M NH_3. E=-0.68V (vs. Hg/Hg_2SO_4). Geometric area = $0.5cm^2$

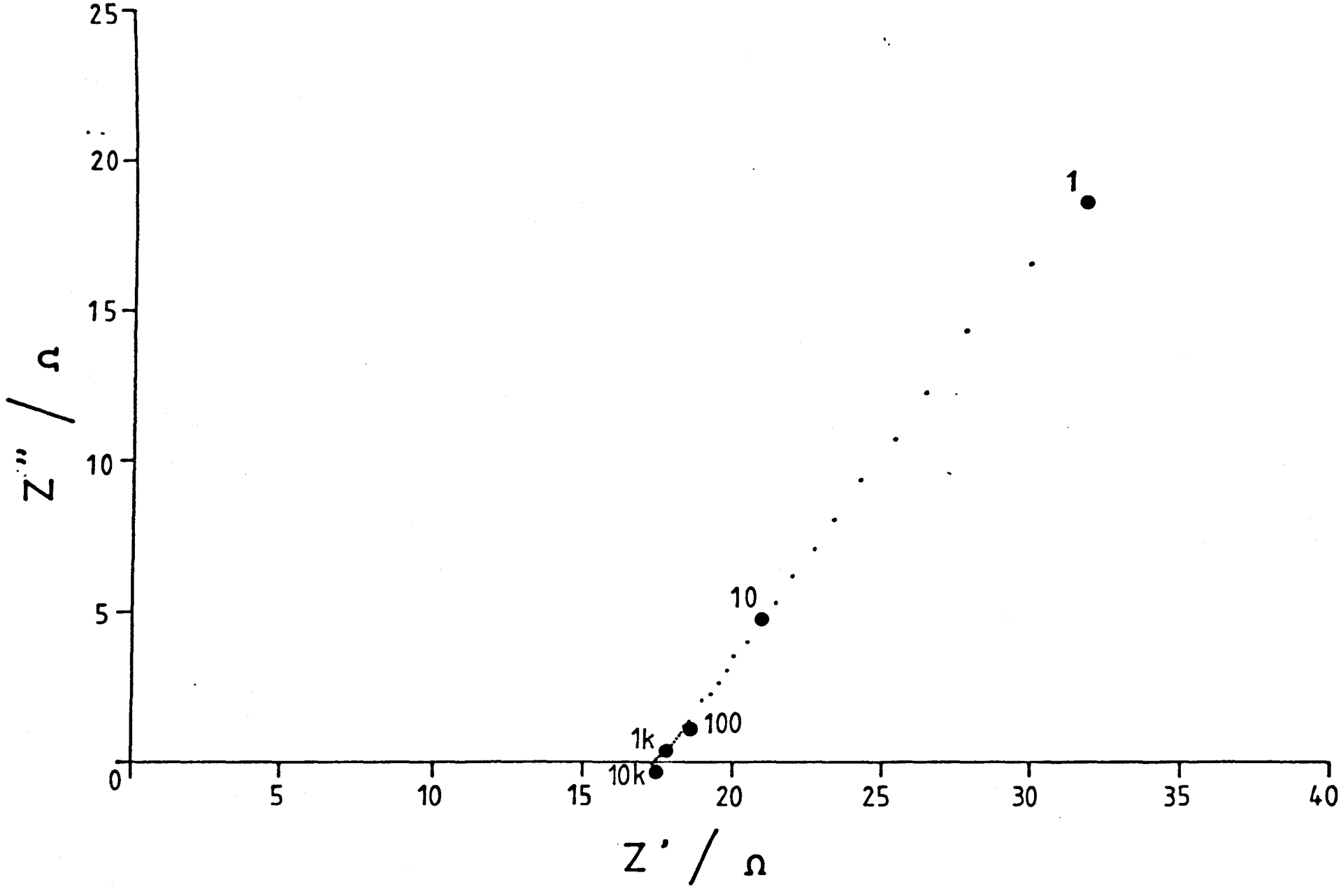
25
20
15
10
5
0
Z'' / Ω
1
10
100
1k
10k
5
10
15
20
25
30
35
40
Z' / Ω

Figure 6.21

Impedance spectra obtained at vitreous carbon subjected to fluorine evolution at 6V in KF.2HF for seven hours for the $Cu(NH_3)_4^{2+}/Cu(NH_3)_2^{+}$ redox couple. Solution composition 0.10M $(NH_4)_2SO_4$, 1.0 x 10^{-2}M $CuSO_4$, 2.0M NH_3. E=-0.68V (Vs. Hg/Hg_2SO_4).

(●) immediately after fluorine evolution.

(▲) held at -0.68V (vs. Hg/Hg_2SO_4) for 5 minutes.

Electrode area = $0.5cm^2$

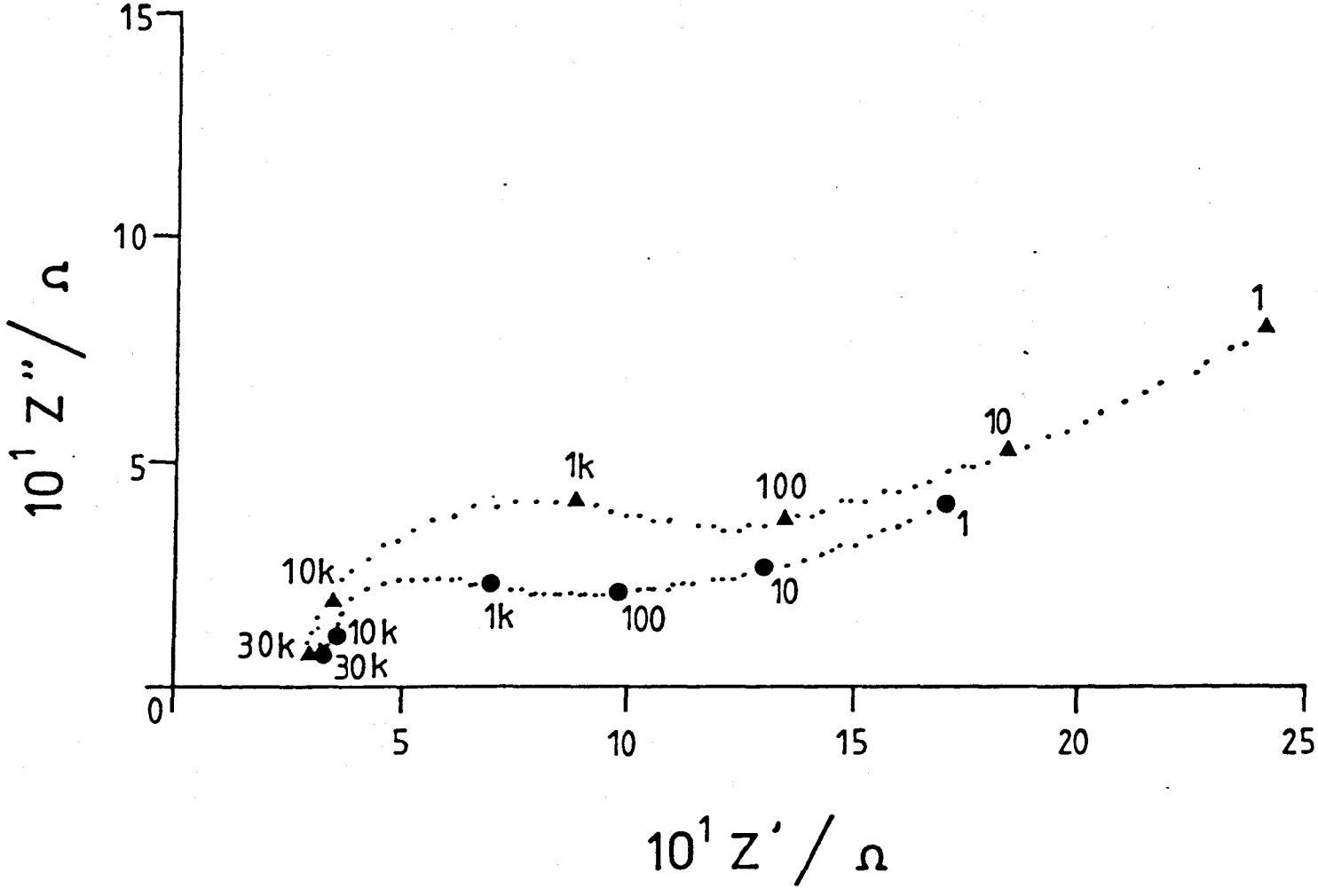
15
10
5
0
5
10
15
20
25
10^1 Z'' / Ω
10^1 Z' / Ω
1
10
100
1k
10k
30k
1
10
100
1k
10k
30k

6.7 REFERENCES

1. N. Watanabe, M. Inoue and S.Yoshizawa, J.Electrochem.Soc.Jpn. 31, 168, (1963).
2. D. Devilliers, M. Vogler, F. Lantelme and M. Chemla, Anal.Chem.Acta. 153, 69, (1983).
3. A.J. Rudge in "Industrial Electrochemical Processes". ed A.T. Kuhn, Elsevier, London, pl. (1971).
4. Lijun Bai and B.E. Conway, Centenary of the Discovery of Fluorine Symposium Abstracts E6 Paris (1986).
5. D.D. MacDonald and M.C.H. McKubre, in "Modern Aspects of Electrochemistry" No.14, eds. J. O'M. Bockris, D.E. Conway, and R.E. White. Plenum, New York, p61, (1982).
6. K.E. Heusler and Kyung Suk Yun, Electrochim.Acta. 22, 977, (1977).
7. R. Greef and M. Aulich, J.Electroanal.Chem. 18, 295, (1968).
8. R.D. Armstrong, M. Fleischmann and J.W. Oldfield, Trans.Faraday Soc. 65, 3053, (1969).
9. W. Shmickler, "Passivity of Metals and Semiconductors" ed. M. Froment, Elsevier, Amsterdam p.23. (1983).
10. R.R. Dogonadze, A.M. Kuznetsov and J. Ulstrup, Electrochim.Acta. 22, 967, (1977).
11. A. Makrides, J.Electrochem.Soc. 111, 392, (1964).
12. K.E. Heusler and M. Schultze, Electrochim.Acta. 20, 237, (1975).

13. K. Doblhofer, D. Nolte and J. Ulstrup, Ber.Bunsenges.Phys.Chem. 82, 403, (1978).

14. H. Gerischer, Z.Physik.Chem. 286, (1951).

15. M.J. Wilmott, M.Sc. Thesis, University of Newcastle upon Tyne, (1983).

16. T. Mallouk and N. Bartlett, J.Chem.Soc.Chem.Comm. 103-105 (1983).

17. M. Von Stackleberg and H. Von Freyhold, Z.Electrochem. 46, 120, (1940).

18. O.R. Brown, S.A. Thornton, J.Chem.Soc. Faraday Trans. 1 70, 1269, (1974).

19. F.A. Cotton and G. Wilkinson, "Advanced Inorganic Chemistry" Second Edition p.905 Interscience, New York, (1966).

20. K. F. Purcell and J.C. Kotz, "Inorganic Chemistry" p.526, Holt Saunders, Philadelphia (1977).

21. J. Bjerrum, K.Dan.Vidensk.Selsk.Math.-FYS.Medd. 12, No.15, (1934).

22. J.F. Fisher and J.L. Hall, Analyt.Chem. 34, 1094, (1962).

23. K. Srinivasan, and R.S. Subrahmanya, J.Electroanal.Chem. 31, 233, (1971).

24. J. Bjerrum, B.V. Argawala, Acta.Chem.Scand. A34, 475, (1980).

25. F.M. Jardine, Advances in Inorganic Chemistry and Radiochemistry 17, 116, (1975).

26. R. Nast and C. Schultze, Z.Anorg.Allgem.Chem. 307, 15, (1960).

27. R.C. Burnier, T.J. Carlin, W.D. Reents, R.B. Cody, R.K. Lengel, and B.S. Freiser, J.Am.Chem.Soc. 101, 7127, (1979).

28. A.W.M. Verkroost, M. Sluyters-Rehbach and J.M. Sluyters, J.Electroanal.Chem. 39, 147, (1972), and 47, 323 and 329, (1973).

29. H.A. Laitinen, and W.J. Subcasky, J.Am.Chem.Soc. 80, 2623, (1958).

30. O.S. Ksenzhek, G.G. Motyagina, L.S. Burachenko and I.O. Volodina, Soviet.Electrochem. 11, 285, (1975).

31. V.I. Shumilov, V.I. Kucherenko, and V.N. Flerov, Soviet.Electrochem. 19, 1477, (1983).

32. R.A. Marcus, Ann.Rev.Phys.Chem. 15, 155, (1964).

33. A.A. Vlcek, Progress in Polarography 1, 269, (1962).

34. T.F. Braish, R.E. Duncan, J.J. Harber, R.L. Steffen, and K.L. Stevenson, Inorg.Chem. 23, 4072, (1984).

35. B. Etimova, J.P. Scharf, M.R. Paris, Bull.Soc.Chim.France. 81, (1969).

CHAPTER 7

GENERAL DISCUSSION OF THE FLUORINE EVOLUTION REACTION AT COMMERCIAL ELECTRODES

7.1 NATURE OF THE SURFACE FILM

The existence of a fluorine-containing film on anodes used for fluorine evolution has been demonstrated by XPS and SIMS analysis. The degree of fluorination of such anodes has been shown to increase with increasing electrode potential, but it was also shown by XPS and SIMS that the film thickness does not vary considerably with electrode potential. Detection of F^+ in the positive ion SIMS spectra also indicates extensive coverage of the electrode surface by fluorine probably as C-F species.

Breaks in the film should be shown up by impedance analysis i.e. by deviation from simple behaviour in impedance plots and Randles plots obtained for simple redox reactions. Such deviations were not observed, so indicating that the film is either coherent or breaks are very closely spaced.

Film thickness determined with depth profiling by ion beam etching, from interfacial capacitance data and from cyclic voltammetry were in broad agreement ranging from 1.0nm at 3.5V to 10nm at 9V polarisations. These values agree with published data.[1]

It is unlikely that the film behaves as a semiconductor. The Mott-Schottky relation :[2]

$$C_s = e(\varepsilon\varepsilon_o N_D/2kT)^{\frac{1}{2}} (-y-s + \ln s)^{-\frac{1}{2}} \qquad 7.1$$

predicts a linear variation of $1/C^2$ with electrode potential for a semiconductor. Electrodes fluorinated at high potentials are unlikely to possess a semiconducting

film and indeed the film has been shown by impedance measurements to be resistive. The only possibility of producing a semiconducting film is in the potential range negative to fluorine evolution. A Mott-Schottky plot over the range 0 - 2.6V at pyrolytic graphite (face orientation) anodes shows a linear section between 2.0 and 2.6V (Figure 7.1). This may point to the existence of a lower semiconducting fluoride being produced in the pre-fluorine evolution range.

The structure of the fluoride film is not simple. Mallouk and Bartlett[3] have shown that there is a marked increase in resistivity of carbon fluorides in the composition region C_2F, and the results presented here show that above 5.0V there is indeed an increase in the ohmic contribution to the impedance of the fluoride film. The film can be represented schematically as in Figure 7.2.

XPS results also point to a film which has a graded composition. Films formed at low potentials contain species such as C_4F when examined by XPS analysis whilst electrodes fluorinated at higher potentials show a higher degree of fluorination.

7.2 REDOX KINETICS

At a filmed electrode the apparent rate constant for the ferrocene/ferrocinium couple was found to decrease by a factor of at least 10^2. Similar reductions in the rate of charge-transfer reactions have been reported previously.[2,4,6] There are two interpretations of

this result. Either :

i) The $(CF)_n$ film is uniform and causes a decrease in the electron transfer probability by a factor $> 10^2$

or

ii) The $(CF)_n$ film is a highly effective insulator and covers the entire surface except for a small area fraction $< 10^{-2}$

The ratio of redox rates $k_{covered}/k_{uncovered}$ are expected to be similar for the fluorine evolution reaction as for the ferrocene system.

A typical experimental impedance plot for the ferrocene/ferrocinium redox couple at a filmed electrode is shown in Figure 6.4. The Warburg impedance is seen to occur from 75Hz to 1Hz.

At a filmed electrode which has small breaks in the film, planar diffusion is expected at very high frequencies, hemispherical diffusion at moderate frequencies and planar diffusion at low frequencies.

The frequency at which the high frequency transition occurs will depend on the diameters of the active regions, whereas the frequency at which the low frequency transition occurs will depend on the distances between such centres.

Such transitions were not evident so active centres, if they exist, must be so small and closely spaced that their effects on impedance behaviour occur above the accessible range.

For a thin film it has been shown[6] that the exchange current density falls with increasing film thickness as the probability of electron tunnelling falls.

Various mechanisms of electron tunnelling have been proposed.[7] If we take the ideal case of a rectangular barrier of mean height ΔE_t (Figure 7.4) then the tunnelling probability is given by equation 7.2:

$$p/p_o = \exp -4\pi d(2m^* \Delta E_t)^{\frac{1}{2}}/h \qquad 7.2$$

where p_o is the tunnelling probability at the bare electrode, m^* is the effective tunnelling mass of the electron, h is Planck's constant and d the film thickness (chapter 6). Taking m^* as the rest mass of the electron, 0.54nm as the film thickness (as determined in acetonitrile), then the minimum inhibition factor of 10^2 observed for the ferrocene system corresponds to a minimum band gap of 0.7eV for the fluoride film. As the band gap of an insulator is more typically 6eV, it is likely that the inhibition factor caused by the film is 2×10^3.

Inhibition presented by such a film will contribute significantly to the anode overvoltage in fluorine cells. In view of the large Tafel slope associated with the fluorine evolution reaction an inhibition factor in the range 10^2 to 2×10^3 corresponds to an overpotential of the order of volts.

7.3 THE CELL VOLTAGE

Industrial fluorine cells operate in the region 10-14 volts depending on the nature of the anodes used. (Lower values will be obtained at porous electrodes).

It is possible to separate the various contributions to this cell voltage as a result of our measurements.

Hydrogen evolution at the cathode occurs at -200mV (vs Pd/H_2) whilst the cathode voltage in an operating fluorine cell is -1.0V[8]. The decomposition voltage of HF in KF.2HF is 2.9V.[9,10] The conductivity of the KF.2HF system varies from $0.11\Omega^{-1}cm^{-1}$ at 90°C and 37wt% HF to $0.28\Omega^{-1}cm^{-1}$ at 100°C and 45wt% HF. For an anode-cathode distance of 3cm at an operating current of $0.2Acm^{-2}$ the corresponding voltage drop due to the electrolyte resistance is 2.1 to 5.4V. The activation energy for the fluorine evolution reaction is $80kJmol^{-1}$ and this contributes approximately 0.8V to the cell voltage. The resistance of the fluoride film produced during fluorine evolution is some $10\Omega cm^2$ which will contribute 2.0V to the cell voltage at $0.2Acm^{-2}$.

Bubble overvoltage will be significant because some 95% of the electrode surface (at a non porous anode) is blocked by fluorine gas bubbles. Bubble overvoltage will be more significant in cells which use dense carbon anodes (American cells). Bubble overvoltage probably contributes 1V to the cell voltage, but it will be lower on anodes which are porous (UK cells).

Bubbles produced on fluorine anodes are said to be lenticular[11] and this is a result of partial non-wetting of the anode by the electrolyte :

$$\gamma \text{ electrode/electrolyte} > \gamma \text{ electrode/gas}$$

This results in the electrode/electrolyte contact angle

becoming greater than 90°. Bubbles are not released from the surface and so the active surface area is diminished. Efficient removal of the gas bubbles would therefore result in a decrease in the cell operating voltage.

Modification of the fluoride film on fluorine evolving anodes either to increase the electron transfer probability or to improve the wetting of the anode by the electrolyte would result in a lower operating cell voltage. Attempts at modification of the film are discussed in Chapter 8.

7.4 MECHANISM OF FLUORINE EVOLUTION

Early studies of the fluorine evolution reaction proposed mechanisms involving intermediates adsorbed on the anode surface.[12,13] Consideration of the bond energies[14] of the C-F ($441 kJmol^{-1}$) and F-F ($153 kJmol^{-1}$) bonds shows such mechanisms to be improbable as they must involve steps of the type :

$$2F_{ad} \longrightarrow F_2 \qquad 7.3$$

or

$$F_{ad} + HF_2^- \longrightarrow e^- + F_2 + HF \qquad 7.4$$

The former involves breaking two strong C-F bonds in the course of forming a weak single F-F bond; a highly endothermic and unfavourable process. The reversible potential for the latter can be estimated and is positive to the reversible fluorine electrode potential by some 3.5V. A more probable mechanism is one in which

charge transfer from HF_2^- through the carbon fluoride film produces free fluorine atoms according to :

$$HF_2^- \xrightarrow{\text{R.D.S}} e^- + HF + F^\cdot \qquad 7.5$$

$$2F^\cdot \xrightarrow{\text{fast}} F_2 \qquad 7.6$$

However, the high overvoltage values and high Tafel slopes observed for the fluorine reaction indicate that the electrode kinetic behaviour is not that expected for a simple mechanism involving the initial electron transfer as the rate-determining step.

Using absolute reaction rate theory, Ikeda[15] estimated the minimum possible value of exchange current density, i_o, for the fluorine evolution reaction

$$HF_2^- \longrightarrow e^- + HF + \tfrac{1}{2}F_2 \qquad 7.7$$

occurring by steps 7.5 and 7.6 assuming that the probability of electron transfer from the transition state to the electrode is unity.

Ikeda calculated, at the standard equilibrium potential, the activiation energy for whichever of the likely mechanisms is energetically least favourable. Several approximations such as the neglect of entropy terms, are involved. The activation process can be supposed to be :

$$(F\text{-}H\text{-}F)^- \longrightarrow F\text{-}H \text{ ——— } F^- \qquad 7.8$$

or

$$(HF_2\text{-}H\text{-}F)^- \longrightarrow HF_2\text{-}H \text{ ——— } F^- \qquad 7.9$$

i.e. the proton in the hydrogen bond moves away from F^- and towards the residual reactant molecule until the system is isoenergetic with one in which the positions of the nuclei are unchanged but the electron has transferred to the anode and a fluorine atom has been eliminated. Under these circumstances adiabatic electron transfer would normally be expected to take place. We assume that the reorganisation process consists of movement of only the proton. The electron can transfer only when the energy of the reactant species $F\text{-}H\text{-}F^-$ is the same as that of the products (e^- anode, F^- and F-H), where the F-H bond length is identical in both reactant and product species. The reaction pathway can be represented as in Figure 7.3.

If we regard the F-H and F-H-F systems as harmonic oscillators we can use literature data for the force constants and for the equilibrium bond lengths to calculate the activation energy. The F-H-F distance in solid KH_2F_3 is 0.233nm[16] so the mean F-H distance is 0.1165nm. The H-F distance in monomeric HF gas is 0.0917nm.[17] The infrared F-H stretching wavenumber in HF(g) monomer is 3961.6cm^{-1}.[16] For the HF_2^- ion the wavenumber for the asymmetric vibration is 1450cm^{-1}[18] although values of 1800cm^{-1} and 2500cm^{-1} have also been suggested.[19,20]

The equation for the potential energy parabola for

the reactant HF_2^- species is given by:

$$E_1 = \tfrac{1}{2}K_1(x-0.1165)^2 \qquad 7.10$$

where K_1 is the force constant for the combined F-H- and -H-F^- bonds and x is the length/nm of the -H-F^- bond to be broken on oxidation. the equation for the potential energy parabola of the H-F product species is given by

$$E_2 = \tfrac{1}{2}K_2(x-0.0917)^2 + 79500/6.023\text{x}10^{23} \qquad 7.11$$

K_1 is calculated using :

$$K_1 = \mu_1(2\pi\nu_{01})^2 = \mu_1(2\pi c\bar{\nu}_1)^2 \qquad 7.12$$

where ν_{01} is the bond vibration frequency, $\bar{\nu}_1$ is the corresponding wavenumber and c is the velocity of light. The reduced mass μ_1 is :

$$\mu_1 = \frac{m_H.m_{F_2}}{m_H + m_{F_2}} = \frac{1.008\text{x}38}{39.008\text{x}6.023\text{x}10^{26}} = 1.630\text{x}10^{-27}\ \text{kg} \qquad 7.13$$

Thus :

$$K_1 = 658.5\text{Nm}^{-1}$$

K_2 is calculated in the same manner and is found to be 884.4Nm^{-1}.

In the transition state $E_1 = E_2$ and $x = x_T$. Combining equations 7.10 and 7.11 and solving the

resulting quadratic equation leads to :

$$x_T = 0.10nm \text{ and } E_1 = E_2 = 85kJmol^{-1}$$

The activation energy is only slightly higher than half the dissociation energy of the fluorine molecule ($79.5kJmol^{-1}$).

Using equation 7.14 we can calculate the apparent standard rate constant k_o[21]

$$k_o = (kT/h).\delta.\exp -\Delta G^{o*}/RT \qquad 7.14$$

The reaction layer thickness, δ , is taken as 0.10nm and ΔG^{o*} is taken as E_1. Thus $k_o = 3x10^{-10}ms^{-1}$.

The exchange current density i_o can be found using

$$i_o = Fk_oC_{HF_2^-} \qquad 7.15$$

Taking the electrolyte concentration as $20moldm^{-3}$, $i_o = 6x10^{-5}Acm^{-2}$.

If the fluorine evolution reaction followed a simple atom recombination mechanism with a symmetry factor of 0.5 for the charge transfer step (assumed uninhibited) then at 90°C a Tafel slope of $0.144Vdec^{-1}$ would be expected, corresponding to some $500Acm^{-2}$ at an overvoltage of 1.0V. Experimentally it is found that at 1.0V overvoltage the actual current density is $5mAcm^{-2}$ and the observed Tafel slope is much higher than $0.144Vdec^{-1}$. It must be concluded that the probability of electron transfer is much lower than unity.

Novak and Hough[22] also observed high Tafel slopes for fluorine evolution on highly porous non-graphitised carbon anodes, which are used for the industrial process and are relatively free from bubble overvoltage. They too ascribed the high overvoltages and high Tafel slopes to inhibition of charge transfer by a polycarbonfluoride film.

Two groups of authors have recently attempted to explain the observed potential dependence of the fluorine evolution reaction. Watanabe[23] supposed that discharge of fluoride ion to form fluorine is restricted to the fraction $(1-\theta)$ of the anode surface uncovered by the polycarbonfluoride film. In the steady state θ is supposed to be determined by a balance in the rates of formation (reaction 7.16) and thermal decomposition (reaction 7.17) of the film.

$$C + HF_2^- \longrightarrow HF + (CF) + e^- \qquad 7.16$$

$$(CF) \longrightarrow C + CF_4 \quad \text{etc.,} \qquad 7.17$$

Supposing behaviour analogous to the Langmuir isotherm, the rate of 7.16 is proportional to $(1-\theta)$ and the rate of reaction 7.17 increases with θ. The electrochemical nature of 7.16 ensures that $(1-\theta)$ falls with potential. Whilst this model qualitatively explains the occurrence of an unusually high Tafel slope, it seems to ignore the fact that the polycarbonfluoride film is much thicker than a monolayer; $(1-\theta)$ is expected to be zero.

Devilliers et al.[24] also explain the high Tafel slope for the fluorine reaction in terms of reactions 7.16 and 7.17 but they suppose that it is a mean thickness of the film and not the two dimensional coverage θ, which determines the rate of fluorine formation. The probability of electron transfer through an insulating barrier depends upon the width as well as the height of the barrier.

If the film became excessively thick then fluorine generation would cease. Fluorine generation requires the continued thermal decomposition of the film (7.19). The continuous production of traces of volatile carbon fluorides in the off-gas from fluorine cells[25] is consistent with these interpretations. The thermal decompositon of polycarbonfluoride depends upon the local heating caused by the flow of current at the anode surface. If, for whatever reason, the film does become unduly thick then the anode will become inactive and will require excessive overvoltages to drive current through the film. This condition, known as "anode effect" can occur in fluorine cells.

It is proposed here that the high Tafel slope observed for fluorine evolution arises from three effects, all associated with the presence of the insulating polycarbonfluoride film. The usual acceleratiing effect of electrode potential on electrode reactions, whereby the transition state is achieved more readily at higher overvoltages, is offset by all these three effects. The first is expected to arise whenever an electrode carries a film sufficiently insulating to

affect the probability of electron transfer from the transition state. The exact shape of the potential barrier presented by the film is not known but a simple model would treat it as a rectangular barrier superimposed upon a linear field of the interface (Figure 7.4). The effect of increasing $\Delta\phi$ is to increase the mean height of the energy barrier through which the electron must tunnel. This effect, which will decrease the potential dependence of the reaction rate, will exist even if the chemical nature and thickness of the film are invariant with electrode potential. However, in the case of fluorinated anodes two further effects also diminish the potential sensitivity of the fluoride discharge rate. With increasing electrode potential there is an increase in both the width (increasing film thickness) and band gap (increasing degree of fluorination) of the rectangular barrier. Taken together these three effects cause the Tafel slope for the fluorine evolution reaction to be very high.

Figure 7.1

Mott-Schottky plot of Capacitance data obtained at a vitreous carbon electrode in KF.2HF over the range 2.0 to 2.6V

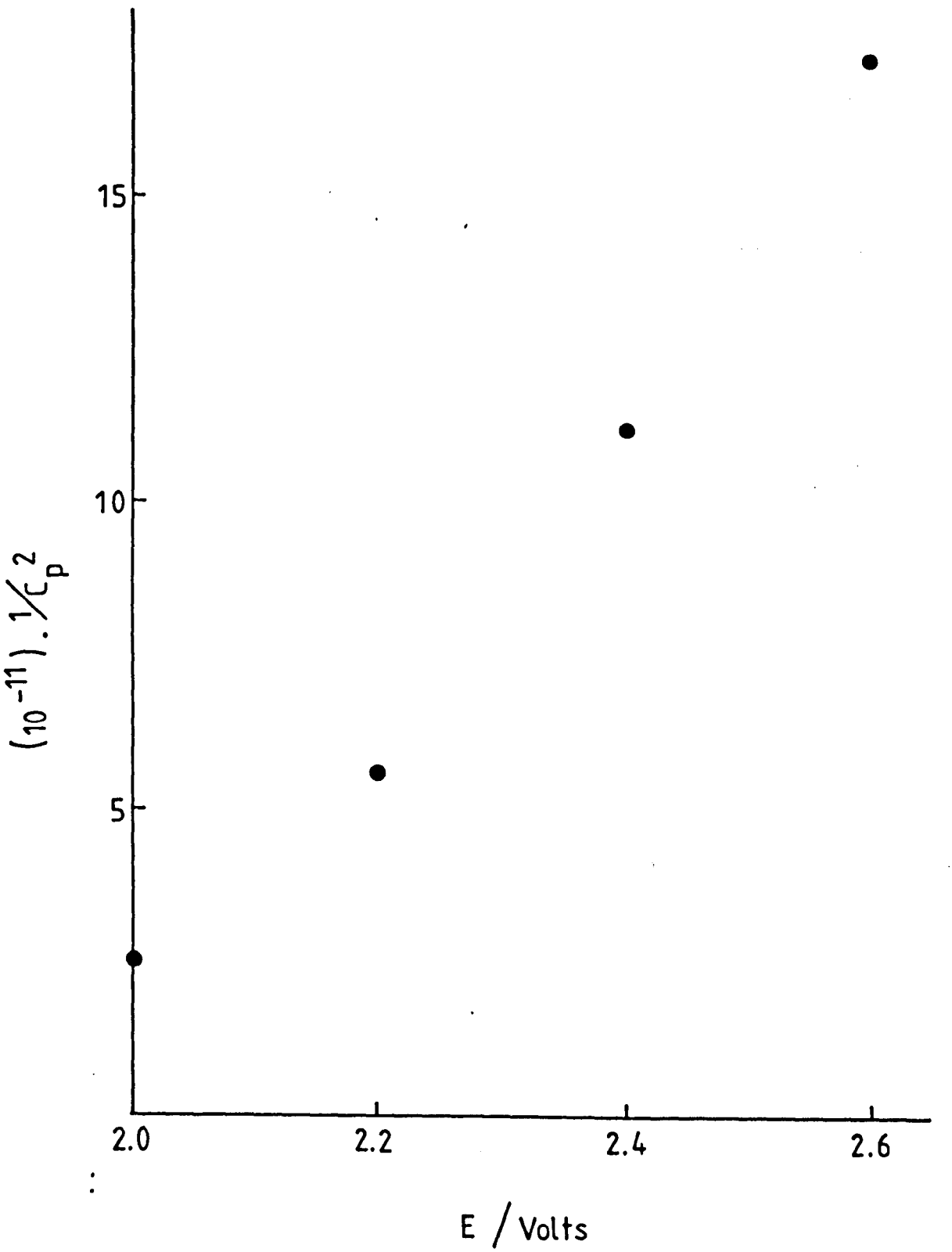

Figure 7.2

Schematic Representation of an anode evolving fluorine.

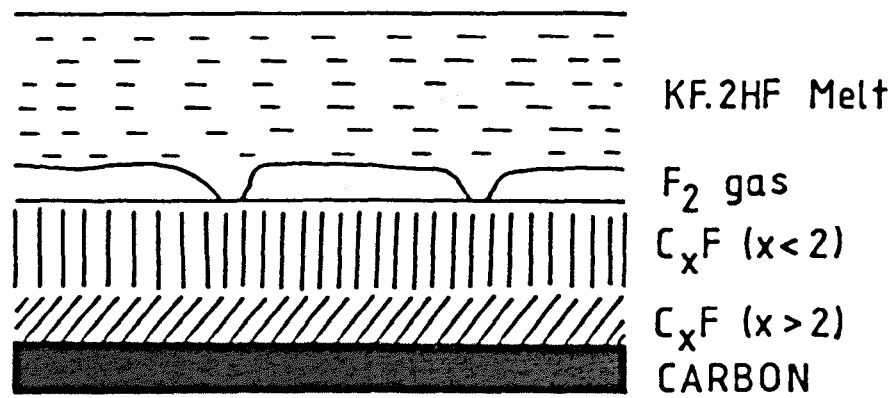

Figure 7.3

Model used to calculate a maximum value for the activation energy of the fluorine evolution reaction at the standard potential

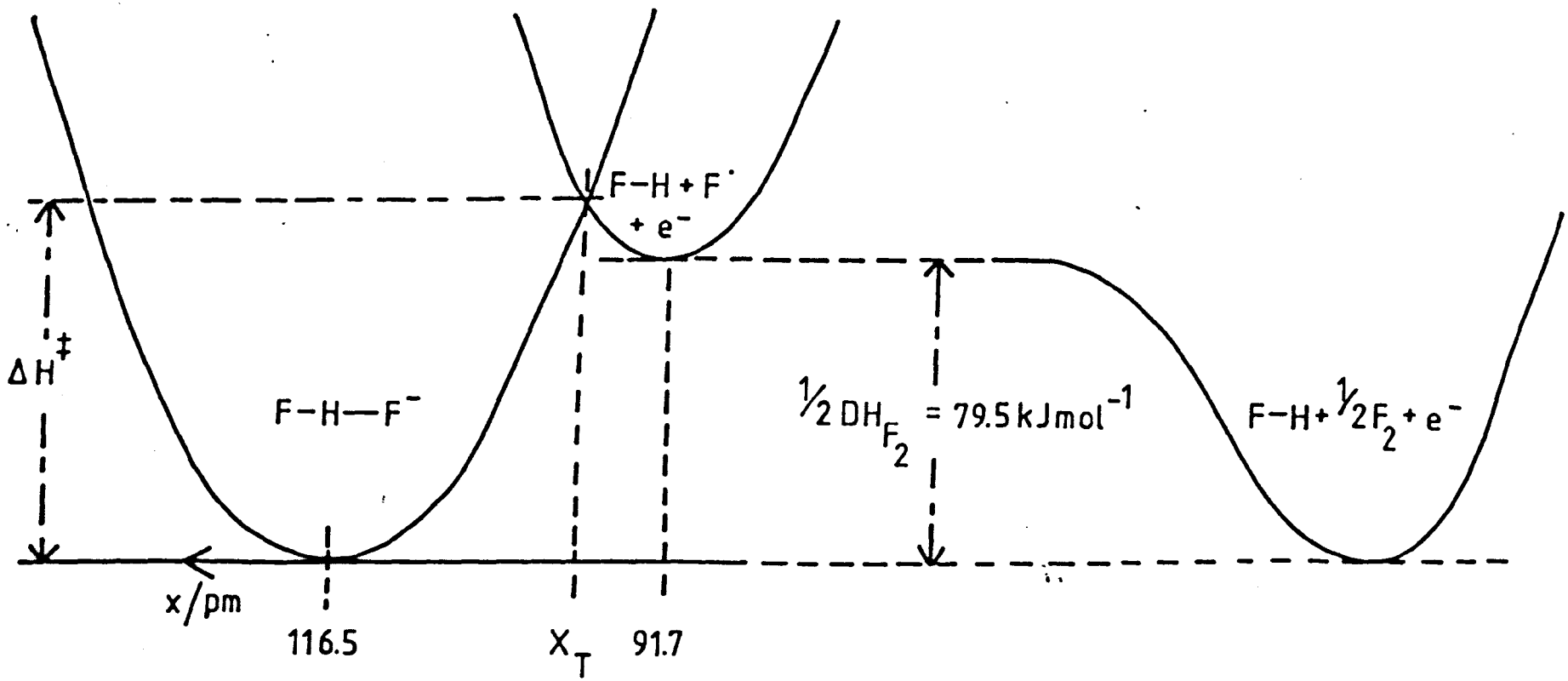

Figure 7.4

Model used to explain the effect of overvoltage on the mean height of the tunnelling barrier for electron transfer during fluoride discharge

a) Low Overvoltages

b) High Overvoltages

a.

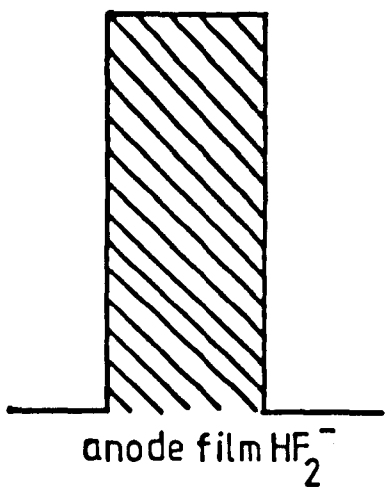

ENERGY BARRIER FOR TUNNELING

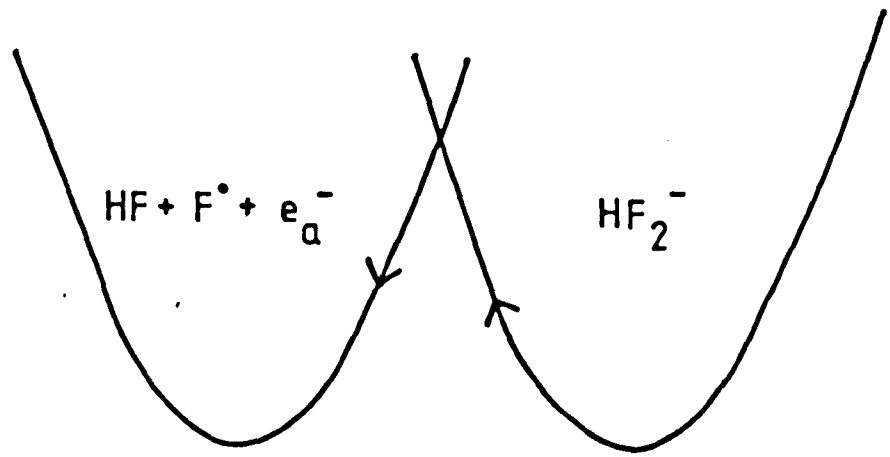

ENERGY PROFILE OF THE REACTION

b.

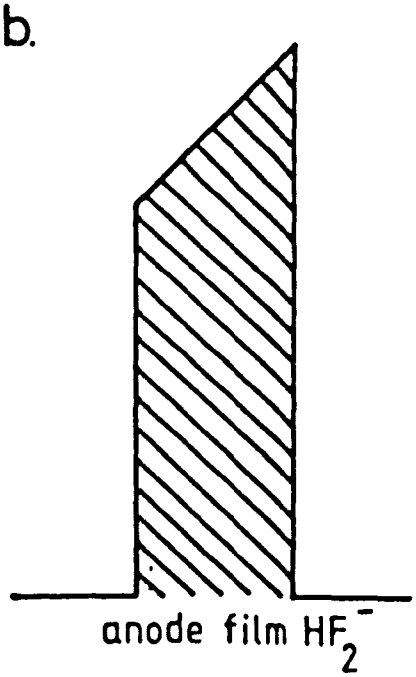

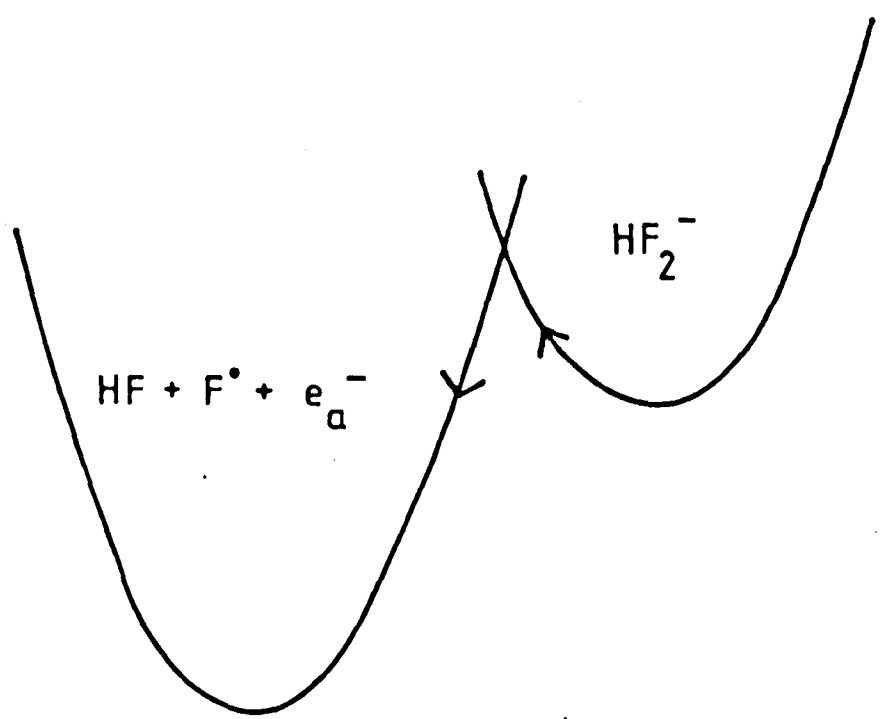

7.5 REFERENCES

1. H. Imoto, S. Koyama and N. Watanabe, Denki Kagaku Ogobi Kogyo Butsuri Kagaku 46, 680, (1978).
2. K.E. Heusler and Kyung Suk Yun, Electrochim.Acta. 22, 977, (1977).
3. T.E. Mallouk and N. Bartlett, J.Chem.Soc.Chem.Comm. 103, (1983).
4. R. Greef and H. Aulich, J.Electroanal.Chem. 18, 295, (1968).
5. R.D. Armstrong, M. Fleischmann and J.W. Oldfield, Trans.Faraday.Soc. 65, 3053, (1969).
6. W. Schmickler in "Passivity of Metals and Semiconductors" ed. M. Forment Elsevier Amsterdam p23, (1983).
7. R.P. Bell "The Tunnel Effect in Chemistry", Chapman and Hall Limited, London, (1980).
8. G.F. May, Private Communication.
9. O.R. Brown, Electrochim.Acta. 25, 367, (1980).
10. D. Devilliers, F. Lantelme and M. Chemla, J.Chim.Phys.Phys.Chem.Biol. 76, 428, (1979).
11. A.J. Rudge, in "Industrial Electrochemical Processes", ed. A.T. Kuhn, Elsevier Amsterdam p1, (1971).
12. A.J. Arvia and J. Bebczuk de Cusminsky, Trans.Faaraday.Soc. 58, 1019, (1962).
13. N. Watanabe, M. Inoue, and S. Yoshizawa, J.Electrochem.Soc.Jpn., 31, 168, (1961).
14. L. Pauling, "Nature of the Chemical Bond". Cornell University Press 3rd Edn. (1960).

15. B. M. Ikeda, Ph.D. Thesis University of Newcastle upon Tyne, (1982).

16. M.F.A. Dove and A.F. Clifford in "Chemistry of Non Aqueous Ionising Solvents", 3, Part 1, eds G. Jander, H. Spandau, and C.C. Addison, Oxford p121, (1971).

17. P.W. Atkins, "Physical Chemistry", 2nd Edn OUP Oxford p589, (1982).

18. J.J. Rush, L.W. Schroeder and A.J. Melviger, J.Chem.Phys. 56, 2793, (1972).

19. R.H. Maybury, S. Gordon and J.J. Katz, J.Chem.Phys. 23, 1277, (1955).

20. R.M. Adams and J.J. Katz, J.Mol.Spectroscopy 1, 306, (1957).

21. P. Delahay, "Double Layer and Electrode Kinetics" Interscience New York (1968).

22. D.M. Novak and P.T. Hough, J.Electroanal.Chem. 144, 121, (1983).

23. N Watanabe, J.Fluorine.Chem. 22, 205, (1983).

24. M Chemla, D. Devilliers and F. Lantlelme, Ann.Chim.Fr. 633, (1984).

25. D. Devilliers, M. Volger, F. Lantelme and M. Chemla, Anal.Chim.Acta. 153, 69, (1983).

CHAPTER 8

NOVEL CARBON ELECTRODES FOR FLUORINE EVOLUTION

8.1 INTRODUCTION

It has already been shown that an insulating film of polycarbonfluoride is formed on the surface of carbon anodes during fluorine evolution from KF.2HF melts. The film has been shown to inhibit electron transfer processes and to contribute considerably to the anode overvoltage in a fluorine cell.

This chapter presents results obtained at carbon anodes modified by the addition of transition metals to the polymers which are used for carbon production.

The aim behind this modification procedure was to incorporate transition metals in the fluoride film on the anode surface and thereby to enhance its electron-transfer characteristics.

Transition metals were chosen for their variable oxidation states which might provide additional electron states or "redox stepping stones" for electron transfer.

The addition of metal ions to the KF.2HF melt has been investigated by various workers.[1-6] Recent patents have also indicated the use of transition metal fluoride additions to the precursor mix for carbon production.[7,8]

The aim in this work has been to obtain a finely dispersed transition metal dopant throughout the carbon matrix. This differs from previous work in that the transition metal compounds were dissolved in the monomer precursors of the polymers used for carbon production. Carbonisation then resulted in a fine distribution of the transition metal throughout the carbon structure.

8.2 PRODUCTION OF CARBON MATERIALS

The aim was to produce a non graphitic, low porosity carbon material with sufficient strength to be used to manufacture carbon anode assemblies by compression moulding into Kel-F as described in Chapter 3.

Several types of monomeric materials were investigated:

8.2.1 Vinyl Acetate

Vinyl acetate was polymerised, without the removal of inhibitor (14ppm hydroquinone), by addition of 0.4 wt % of benzoyl peroxide, followed by careful heating under reflux, at 70°C. After 40 minutes a gel was produced. The polymer gel was dissolved in ethyl acetate or THF and cast into PTFE molds. On evaporation of the solvent the resulting sheet of polymer was less than 1mm thick: too thin for use as a carbon anode. It was later discovered[9] that polyvinyl acetate forms a graphitic carbon and would therefore be unsuitable as a fluorine anode. No further work was attempted with vinyl acetate polymers.

8.2.2 Novolak

This commercially available phenolic resin was obtained from the Carbon Research Laboratories at the University of Newcastle upon Tyne.

The orange powder was packed firmly into a silica boat and placed in the centre of a tube furnace and carbonised at $0.3°Cmin^{-1}$ from 120°C up to 980°C for 45

minutes before cooling to room temperature. Temperature control was afforded by a Sirect Controller (C.N.S. Instruments Ltd.) fitted with a motorised gearbox (Rayleigh Instruments Ltd.). The temperature was measured by means of a platinum-platinum 13% rhodium thermocouple, the temperature being displayed on a Cambridge Instruments meter.

The material resulting from carbonisation of the Novolak Resin powder was highly porous and fragile. Discs (4mmx13mmØ) were prepared by compression of the resin in a KBr press. Again carbonisation gave a highly porous material, with little strength. This was also unsuitable as an anode material.

8.2.3 Furfuryl Alcohol

Polymerisation of furfuryl alcohol was achieved by the addition of 0.6% (by volume) of 1M nitric acid. The mixture was maintained at 70°C for 48 hours and then at 120°C for a further 24 hours. This resulted in the production of a very hard dark brown polymer. Carbonisation in a tube furnace under a nitrogen atmosphere at $0.3\,^{\circ}C\,min^{-1}$ was carried out to a maximum temperature of 1000°C. The sample was held at 1000°C for 1 hour before cooling. In this case sheets of carbon material, similar in appearance to vitreous carbon, were obtained. In themselves these sheets were of no use as a carbon anode. However, it was noted that during the polymerisation procedure at 70°C a soft brown polymer was obtained. Polymerisation was therefore interrupted after treatment at 70°C for 48 hours. The polymer could

then be cut using a cork borer to produce polymer discs. Batches of discs (15-20 at a time) were then hardened at 120°C in the tubular furnace for 24 hours before carbonisation at 0.3°Cmin^{-1} to a temperature of 1000°C. Again samples were held at 1000°C for 1 hour before cooling to room temperature. This procedure gave discs of carbon 6mmϕx2mm which could be embedded into Kel-F as described in Chapter 3. The carbons produced in this way were similar in appearance to commercial vitreous carbon, and were non-graphitic.

Doping of the carbon materials was achieved by dissolving a transition metal acetylacetonate in the monomer prior to polymerisation. In this way carbon samples were prepared containing one of the first row transition metals or Cu, Zn or Mo. Another batch of samples was prepared containing both Nickel and Vanadium in one carbon material. The level of doping was 0.1 atom %. Table 8.1 indicates the carbon yields obtained from various polymers.

The low yields in certain cases can be explained as burning of the polymer caused by leakage of oxygen into the carbonisation chamber.

8.3 NON-ELECTROCHEMICAL CHARACTERISATION OF CARBON SAMPLES

8.3.1 Graphite Analysis

Samples of carbonised polyfurfuryl alcohol were analysed for graphite content, and comparison was made with commercial vitreous carbon (Le Carbone). The method (caried out at BNFL Springfields) involved oxidation of

the carbons with silver permanganate and measurement of the rate of CO_2 evolution. The graphite content of samples produced in these laboratories was determined as 0.3% by weight, whilst that of commercially available Le Carbone vitreous carbon was too high to be measured. Samples of doped carbon materials were not examined and so the graphite contents of these materials are unknown.

Typical analysis of commercial carbons used in fluorine cells is shown in Table 8.2. It can be seen that the level of doping (0.1%) is well above the transition metal impurity limits of commercial carbons.

8.3.2 EDAX/SEM Studies

Samples of carbonised polyfurfuryl alcohol were examined by scanning electron micropcopy and by EDAX, both before electrochemical treatment and after fluorine had been evolved on them.

Measurements Prior to Fluorine Evolution

Samples of carbon materials were examined by scanning electron micropcopy with an EDAX attachment which, by analysis of the X-ray emission characteristic of atoms in the sample, can be used to determine the distribution of metal within the sample.

Undoped carbons were first examined using both external and fracture surfaces for examination. The X-ray spectrum of such materials is shown in Figure 8.1. Impurities found in the material were Al, Si, S, Cl, K, Ca, Fe and Cu, all at low levels.

Doped materials were examined by the EDAX method and

the material was found to have an even distribution of metal dopant throughout it. Agglomeration of material did not occur with any of the dopants used. The x-ray spectra of doped materials always showed the background impurities of the undoped material, with a large peak due to the dopant material superimposed on this background (Figure 8.2). In the case of the material containing both nickel and vanadium two large peaks were observed in the x-ray spectrum (Figure 8.3) corresponding to Ni and V.

Electron Microscopy after Fluorine Evolution

The doped materials were all examined by electron microscopy/EDAX after they had been subjected to fluorine evolution. The dopants were still all found in the respective samples, though the level of dopant was not determined. Interestingly, however, after fluorine evolution potassium was found on the surface of all doped materials, except the titanium-doped material. It is difficult to say whether this potassium was carried over from the KF.2HF electrolyte or was incorporated in the electrode surface because F^{19} is at the detection limit of the EDAX technique. It was noted however that in general there was an increase in the amount of potassium on the surface as the atomic number of the dopant increased. More work is required before conclusions about this observation can be drawn. Figure 8.4 shows the x-ray spectra of a Ni-doped electrode, a vanadium-doped electrode and an electrode containing Niand V, all after fluorine evolution.

8.4 ELECTROCHEMICAL CHARACTERISATION OF DOPED ELECTRODES

A complete electrochemical study of the doped electrodes was not undertaken. The techniques used to investigate commercial electrode materials as discussed in Chapter 4 were employed in the examination of doped materials. Comparison was always made between undoped and doped materials. Further work would be required before firm conclusions could be drawn about the kinetics and mechanism of fluorine evolution at doped electrode materials. Initially all electrodes were examined using cyclic voltammetry in KF.2HF over the potential range 0 to 5V at sweep rates between 1 and $50Vs^{-1}$. The double pulse technique described in Chapter 4 was used to obtain polarisation data at all materials. The bubble-transient technique also described earlier was used to investigate all anode materials, as was steady state fluorine electrolysis at 6V in KF.2HF. Selected electrode materials were investigated in KF.2HF using the a.c. impedance technique, and finally selected materials were examined by the technique described in Chapter 6 whereby the electrodes were removed from the KF.2HF melt and used to examine the redox kinetics of model redox systems in other electrolyte solutions.

8.4.1 Cyclic Voltammetry

All electrodes made in these laboratories were initially examined using cyclic voltammetry in KF.2HF. The potential range examined was 0V to 5.0V and a sweep rate of $50Vs^{-1}$ was employed. This fast scan rate was

used to minimise the effect of fluorine bubble formation. If several sweeps were to be performed the electrodes were held at 0V for 75 seconds between sweeps to allow any fluorine gas bubbles to be reduced. Comparison was made between doped and undoped electrodes and after a doped electrode had been examined the condition of the electrolyte was checked by using an undoped anode to ensure that results obtained were not due to dissolution of the transition metals in the fluoride melt. Certain electrodes were examined in addition at sweep rates of $10Vs^{-1}$ and $1.0Vs^{-1}$. Sweep rate dependences were not obtained at all materials. Indeed many of the results obtained were similar from one doped electrode to another. Certain materials, however, showed significant differences from the others.

8.4.1.1 Undoped Anodes

As with commercial vitreous carbon a large anodic peak at 2.0V was observed on the first positive sweep at a freshly polished undoped material (Figure 8.5). No peaks were observed on the negative sweep. On subsequent scans the peak disappeared (Figure 8.6). As with commercial carbons the peak is attributed to formation of a surface film of carbon fluoride. The potential had not been taken sufficiently negative to reduce the film and as a result peaks were not observed on subsequent scans. The anodic peak can be regenerated if the negative limit is extended to -1.0V as with commercial electrodes.

8.4.1.2 Doped Anodes

Certain electrodes containing transition metals warrant individual discussion whilst others can be discussed as a group. In all cases, however, the presence of the transition metal resulted in higher currents at a given sweep rate than were observed on undoped materials.

8.4.1.3 Electrodes Containing Only Nickel

Electrodes containing 0.1% Ni showed substantially higher currents than undoped materials when scanned over the range 0 to 5.0V at $50Vs^{-1}$. An anodic peak was observed on the first positive sweep at 2.6V. The peak current exceeded of $500mAcm^{-2}$ (Figure 8.7) despite using a negative limit of only zero volts. After six cycles the peak was still clearly visible but the current had fallen to around $250mAcm^{-2}$ (Figure 8.8). The fall in the peak current indicated that the active anode surface had decreased, most likely due to formation of a surface fluoride film. However, observation of the peak on successive scans indicates either that the film is unstable in the presence of nickel or that nickel catalyses the formation of gaseous fluorocarbons such as CF_4 and C_2F_6. Analysis of the anode off-gas would clarify this point.

8.4.1.4 Electrodes Containing Vanadium

Electrodes containing 0.1% vanadium did not shown a marked peak at 2.0V. Significantly positive currents were observed and indeed the currents were double those

observed on an undoped material (Figure 8.9). Currents were lower on subsequent scans (Figure 8.10), but they were always higher than those obtained at undoped anodes.

The fall in currents can again be attributed to formation of a surface fluoride film but the extent of fluorination appears to be less than with undoped materials.

8.4.1.5 Electrodes Containing Ni and V Together

When electrodes contained 0.1% Ni and 0.1% V the behaviour observed was very similar to electrodes containing only nickel. The effect of sweep rate was examined using these electrodes. It was found that at faster sweep rates the anodic peak moved to more positive potentials. The peak current was a linear function of neither sweep rate ν nor $\nu^{\frac{1}{2}}$ (Table 8.3)

The shift in E_{pa} to more positive potentials by 1.5V on increasing the scan rate from 1 to $50Vs^{-1}$ is a result of the increased ohmic potential drop between the tip of the Luggin capillary and the surface of the working electrode.

8.4.1.6 Electrodes Containing Zn, Mn, Cr, Cu and Co

Carbon Electrodes were prepared containing either Cu, Zn, Mn, Cr or Co, in each case at a level of 0.1 atom %. These electrodes behaved similarly. An anodic peak was observed on the positive sweep and with all these materials significant anodic currents were observed on the return negative sweep (Figure 8.11). The

peak position shifted to more positive potentials on increasing the sweep rate and again the peak current was not proportional to ν or $\nu^{\frac{1}{2}}$.

An interesting feature with these materials is that significant anodic currents were observed on the negative sweep even down to a potential of 1.0V. These currents increased with increasing sweep rate indicating that a faradaic process rather than chemical or thermal decomposition was occurring.

8.4.1.7 Electrodes Containing Fe, Ti or Mo

Carbon electrodes were prepared containing either 0.1% Fe, 0.1% Ti, or 0.1% Mo. The behaviour of these materials was similar to undoped carbon apart from the fact that currents were higher (Figure 8.12).

8.5 CONSTANT CURRENT ELECTROLYSIS AT DOPED ELECTRODES

Industrial electrodes operate approximately in the galvanostatic mode at 200mAcm^{-2}. For this reason the true test of a "home-made" doped electrode is its constant current electrolysis performance.

Under galvanostatic conditions the maximum electrode potential that could be measured by the available equipment was 20V. Above this value saturation of the buffer amplifier occurred.

The planar, non-porous nature of the home-made electrodes made them prone to bubble overvoltage. The consequence of this was that high anode current densities could not be measured.

Initial measurements compared an undoped electrode

with an electrode containing nickel, both passing 50mAcm^{-2}. The undoped material operated at 17$\pm$2V whilst the electrode containing nickel operated at 6V. However, both electrode materials soon became polarised (i.e. the voltage increased to unmeasurable values) and so for this reason comparison of all electrode materials was made at 25mAcm^{-2}. Obviously this is not a true representation of the operating conditions of an industrial plant, but it is argued that the electrodes are unlike plant anodes, which can operate at higher current densities by virtue of their inherent porosity. The constant current work does, however, show the effect of the presence of transition metals in the carbon on the operating electrode potential.

At 25mAcm^{-2} the anode voltage was recorded through a buffer amplifier on a Chessel flat bed recorder.

Continual fluctuation of the voltage was observed and is attributed to the continual formation and release of bubbles from the electrode surface. A typical voltage vs. time trace is shown in Figure 8.13 for an undoped material. The average electrode potential for each material is shown in Table 8.4.

The voltage vs time behaviours of electrodes containing nickel and vanadium either together or separately were somewhat different from those of other electrode materials as is shown in Figures 8.14-8.16. In the case of the electrode containing only vanadium the voltage varied between 4.9V and 7.8V in the early stages of electrolysis, but after 35 minutes the difference between the lower and upper voltages started to increase

as in Figures 8.15a and 8.15b. Eventually the electrode became polarised. Similar behaviour was observed with the electrode materials containing only nickel. Early in the electrolysis the voltage varied between 4.5V and 5.5V but again after 40 minutes, polarisation occurred (Figure 8.14). The electrode material containing both nickel and vanadium behaved similarly to that containing only nickel (Figure 8.16).

Constant current electrolysis allows a quick and easy appraisal of a new anode material. Further work is needed using this technique as the aim of this work was only to investigate if doping would be beneficial.

Four electrode materials behave considerably better than any of the others: namely those materials containing nickel, vanadium, cobalt or a combination of nickel and vanadium.

All anode materials suffer polarisation, defined as the increase in cell voltage as a result of covering of the anode by a fluorine gas layer. The occurrence of this phenomenon indicates that on all anode materials a carbon fluoride layer, a prerequisite of polarisation, is produced.

Under extreme conditions a phenomenon known as "anode effect" can occur. This is arcing at the electrode surface as a result of complete sheathing of the anode by a fluorine gas layer; bluish sparks are seen to emit from the anode surface. Anode effect is associated with voltages in excess of 30V. With the instrumentation available it was not possible to measure voltages above 20V. However, in the case of the undoped

electrode and those electrodes containing zinc, anode efect was observed as blue arcing.

Polarisation occurred on all anode materials as a result of the small surface area of the materials. Further work is required using larger, more porous anodes containing transition metal dopants.

8.6 IMPEDANCE STUDIES

Commercial electrodes were examined in KF.2HF over the range 0 to 2.6V using the impedance technique (see Chapter 4). Above 1.0V a charge transfer semicircle was obtained. Time-dependent studies were made at 2.4V and it was found that the resistance increased whilst the capacitance decreased as a function of time spent at 2.4V.

Time dependent studies of the impedance characteristics of selected doped electrodes at 2.4V in KF.2HF were made and compared with the same measurements at undoped material. The materials examined were electrodes containing nickel and vanadium.

Semicircles were obtained at 2.4V with all electrode materials. The capacitance and resistance values were measured as a function of time and are shown in Figures 8.17 to 8.18. In all cases the capacitance falls with time as a result of the formation of a surface film at the electrode. In the case of the electrodes containing vanadium, nickel plus vanadium, or no dopant the fall in capacitance is similar: 0.2 to 0.3μFcm^{-2}. In the case of the electrode containing nickel alone the fall is less pronounced and the lowest value obtained was 0.96μFcm^{-2}.

Interestingly a marked difference was observed in the values of the diameters of the semicircles with time. Undoped electrodes and those containing only vanadium showed a large increase in resistance with time, whilst those containing nickel alone or with vanadium showed a much smaller increase in resistance (Figures 8.17 and 8.19).

The fall in capacitance indicates that, at all the materials studied, a surface film is being produced. This film presents a large resistive barrier at undoped electrodes and those containing only vanadium whilst at electrodes containing nickel alone or with vanadium a much smaller resistive barrier is formed. This indicates that nickel enhances the process which occurs at 2.4V in KF.2HF. There is no doubt that part of the process occurring at 2.4V is formation of a lower fluoride surface film at the electrode which is responsible for the observed decrease in capacitance. However, if nickel catalysed this process then a larger fall in capacitance would be expected, and a large increase in resistance would also be observed. As this is not the case then nickel must catalyse some other process: either decomposition of the surface film or increasing the production of gaseous fluorocarbons such as CF_4 and C_2F_6. Analysis of the off-gas from the anode would help in understanding the processes occurring at doped electrodes.

8.7 POTENTIAL STEP MEASUREMENTS

In an attempt to obtain polarisation data for the

fluorine evolution reaction at doped electrode materials a double potential step method was used as described in Chapter 4. The pulse train took the form:

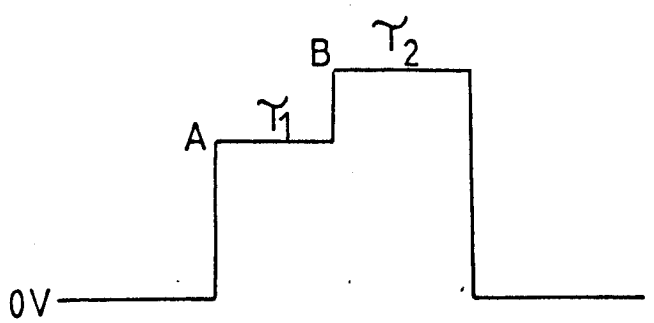

The A pulse was always to 3.0V for 5s (τ_1) whilst the B pulse was to potentials in the range 4.0 to 5.4V for 200ms (τ_2). After each B pulse the potential returned to 0V.

Comparison was made between undoped and doped electrodes. After examination of a doped electrode an undoped material was re-examined to ensure that leaching of the dopants had not occurred and erroneous results were therefore avoided.

Analysis of the electrolyte after using several doped electrodes did not show that dopants had been leached from the electrode materials into the electrolyte (Table 8.4).

In the treatment of results graphs were plotted of the currents measured 100ms after the start of the B pulse, against potential.

The currents were simple falling transients on all materials. At undoped electrodes they were always very low and potential-insensitive (Figure 8.21).

The addition of transition metals produced a marked

increase in the measured currents (Figures 8.20 to 8.29). Again polarisation data acquired by this method were fairly linear rather than following the exponential behaviour expected from Tafel's law.

The effect of fluorine evolution was investigated by repeating the pulse measurement at 5.0V after evolving fluorine at 6.0V for 30 minutes (and then removing any gas film). Electrodes fell into three catagories after fluorination:

i) Those seemingly unaffected by fluorine evolution (vanadium and copper)

ii) Those slightly affected by fluorine evolution (Ni, Co, Fe, Cr, Ni+V)

iii) Those severely affected by fluorine (Mo, Ti, Mn).

In the case of electrodes only slightly affected by fluorine evolution currents obtained were still higher than those obtained on a clean undoped material at the same potential whilst those electrodes severely affected by fluorine evolution gave very low currents. The behaviour of the various additive metals does not follow any obvious pattern based on position in the periodic table.

8.8 STEADY STATE ELECTROLYSIS AT 6V IN KF.2HF

All electrode materials were subjected to potentiostatic electrolysis at 6V in KF.2HF. The current vs. time characteristics were recorded on a Chessel flat-bed strip-chart recorder. Continual fluctuations in the currents were observed and are attributed to the

continual formation and removal of bubbles from the anode surface.

It was found that bubbles were released more frequently from electrodes containing nickel than from any other material. This was shown by the continual fluctuation in the current vs time trace (Figure 8.30). It was also noted that very large current densities were obtained with electrodes containing vanadium when bubbles were released from the electrode surface, but bubble release was less frequent than with the anode containing nickel (Figure 8.31). In the case of anodes containing both nickel and vanadium a regular pattern of bubble release was observed (Figure 8.32) but the rate of bubble release was not as high as at an electrode containing nickel alone. It was noted however, that the peak currents were higher than those obtained at an electrode containing nickel alone, but lower than those which contained vanadium alone.

The current vs time characteristics for an undoped material are shown in Figure 8.33.

The current vs time traces were analysed to obtain two current values, i_b is the base line current and i_p the peak in current observed just after bubble release from the anode surface. These results are shown in Table 8.5.

The peak current measured using a chart recorder will be somewhat lower than the actual peak current due to the response time of the chart recorder. For this reason the computer-based method of measuring current transients immediately after bubble release (Chapter 4)

was used to obtain the actual peak currents. It was initially hoped that this computer-based method would enable polarisation data to be acquired but, as explained in Chapter 4, bubble release does not clear gas from all of the electrode surface and the method is therefore unsuitable.

Peak currents obtained by the computer method are also shown in Table 8.6.

It is clear that some electrode materials, notably those containing vanadium or cobalt suffer more from bubble overvoltage than any of the other materials. Electrodes containing nickel alone or with vanadium are also very active towards fluorine evolution.

It is evident that a proper assessment of the performance of doped carbon electrodes as possible fluorine anodes requires that porous carbons, structurally similar to present-day commercial fluorine anodes, should be doped and examined. Measurements on smooth carbons may be dominated by the effects of bubble overvoltage which might mask the catalytic behaviour provided by certain additives.

8.9 MEASUREMENTS USING MODEL REDOX SYSTEMS

It was shown in Chapter 6, that the inhibiting effects of the fluoride film produced at carbon anodes subjected to fluorine evolution in KF.2HF could be investigated by measuring the kinetics of model redox systems at unfilmed and filmed electrodes.

Attempts were made to compare the kinetics of model redox systems at carbons undoped and doped with nickel,

in each case after fluorination in KF.2HF at 6V for 30 minutes.

First the ferrocyanide/ferricyanide sytem was investigated. The impedance plot at an undoped electrode for this redox couple in aqueous potassium chloride containing $5x10^{-3}M$ $K_3Fe(CN)_6$ is shown in Figure 8.34. Examination of the same redox couple using electrodes containing nickel resulted in the impedance plot shown in Figure 8.35. In the latter case no charge transfer resistance is measurable and at first sight it appears that the reaction is diffusion-controlled. The low frequency end of this plot however has a slope of 0.65: a value considerably lower than that expected for diffusion control (unity). When the impedance plot of the same electrode material was obtained at the same electrode potential in a KCl solution in the absence of the redox couple a very similar plot was observed, (Figure 8.36). It appears that redox chemistry of the metal species was being observed in the aqueous solvents. The possibility that the observed results could be due to the porosity of the electrodes was discounted, as examination of a highly porous YBD electrode in the same KCl solution at the same potentials produced the impedance plot shown in Figure 8.37. No further measurements were made using this system.

The non-aqueous system of ferrocene in acetonitrile was then examined using doped and undoped electrodes.

The effect of fluorination at 6V for 30 minutes can be clearly seen at undoped electrodes (Figures 8.38a and

b), but not at nickel-doped electrodes. Examination in acetonitrile/$NaClO_4$ in the absence of a redox couple gave the same result as in the presence of the redox couple (Figure 8.39a and b), and no effect due to fluorination was observed, (Figure 8.40c).

The presence of the transition metal dopant appears to complicate the electrochemical behaviour of the carbon electrodes in both aqueous and non-aqueous solvents, but the processes occurring were not established in this work.

8.10 DISCUSSION OF RESULTS OBTAINED AT DOPED MATERIALS

Measurements performed using doped electrodes are far from comprehensive. Determination of the mechanism by which dopants affect the kinetics of fluorine evolution requires much more work. The overiding point to emerge from this study, however, is that the addition of certain transition metal dopants to carbon anodes used for fluorine evolution is beneficial, resulting in lower operating voltages under constant current conditions. Four doped carbons were shown to behave considerably better than any of the other carbons. The four contained nickel, vanadium, cobalt or a combination of nickel and vanadium. Preparation of a more porous anode containing such dopants would reduce the polarisation problems encountered with planar electrodes and may lead to the development of an anode material for use in commercial cells which could operate at a lower voltage.

Constant voltage work at 6V indicated that the frequency of fluorine bubble release at anodes containing nickel was greater than with any other carbon. Nickel appears to play the role of a wetting agent in this instance. Impedance measurements also indicate that the film produced at 2.4V on electrodes containing nickel has a lower resitance than the film produced on undoped or vanadium electrodes. This indicates that the carbon fluoride film contains a lower ratio of fluorine : carbon at nickel-doped electrodes. Alternatively the film may be less thick or may have its semiconductor properties directly affected by the presence of nickel.

Evaluation of kinetic parameters using potential pulse techniques proved difficult. However, such pulse measurments emphasised the increased activity of the doped materials over the undoped materials, and showed that on the time scale of a pulse measurement vanadium electrodes and copper-containing electrodes were seemingly unaffected by fluorine evolution at 6V.

Attempts to examine model redox systems using nickel-doped electrodes were unsuccessful as decomposition of the films in aqueous or organic media seemed to be promoted by the presence of nickel.

Cyclic voltammetry showed a whole range of behaviours at doped electrodes and insufficient results were obtained to draw conclusions.

This work has shown that carbon materials doped with transition metals made in the laboratory can be successfully used as fluorine anodes. The benefit of the

method of carbon production described above is that the organic ligand, acetylacetonate, decomposes to leave only carbon residues containing finely-dispersed metal throughout the carbon matrix. The choice of transition metals as dopants was due to their variable oxidation states and a complete study of the remaining transition metals and perhaps the lanthanide and actinide elements may result in further developments.

Possible explanations for the role of the transition metal dopants are :

1. As originally conceived they improve electron transfer probably via a stepping stone mechanism, or
2. they assist in the decomposition of the film so that the film is thinner in the steady state, or
3. they affect the conductivity of the semiconducting layer of the surface either physically through semiconductor properties or chemically by changing the C:F ratio.

TABLE 8.1

Carbon yields (wt. of Carbon/wt. of Polymer)

SAMPLE	CARBON YIELD %
UNDOPED PFA	89
PFA 0.1% Fe	88
PFA 0.1% Ni	85
PFA 0.1% V	87
PFA 0.1% Cr	87
PFA 0.1% Cu	66
PFA 0.1% Co	62
PFA 0.1% Mn	48
PFA 0.1% Mo	51
PFA 0.1% Ti	50
PFA 0.1% Zn	50
PFA 0.1% Ni/V	46

TABLE 8.2

Typical levels of Metallic Impurities

in Commercial Anode carbons

Schumacher Carbo 30G

Pb 600	Cr 45	Ni < 10	Si 1200
Fe 420	Cu 21	K 290	S 5000
Al 250	Mg 60	V < 5	Na 410
	As< 200	Zn 1200	Mn 14

Stein LA2

Pb 80	Cr 10	Ni 180	Si 10,000-400
Fe 460	Cu 2	K 14	S 70,000-20,000
Al < 10	As ND	Zn ND	Mn ND
	Mg ND	V ND	Na ND

YBD

Pb < 200	Cr 8	Ni 35	Si 400
Fe 125	Cu 18	K 88	S 10,400
Al 100	Mg 9	V 70	Na 88
	As< 200	Zn 100	Mn 8

ND - No Data

All results quoted as ppm.

TABLE 8.3

Dependence of the anodic peak potential and peak current on sweep rate for an electrode containing nickel and vanadium.

sweep rate Vs^{-1}	i_{pa} $mAcm^{-2}$	E_{pa} V
50	400	3.25
10	274	2.6
1	75	1.75

TABLE 8.4

Electrolyte impurities before and after use of doped electrodes.

ELECTROLYTE	HF %wt	H_2O %wt	Fe	Ni	Cu ppm	Pb	Cr	Co	V
Pure Electrolyte Prepared from Addition of HF to KF.HF	43	0.1	12	10	5	20	ND	ND	ND
Pure Electrolyte After use of Doped Electrodes	ND	ND	11	10	5	ND	5	4	5

ND = Not Determined

TABLE 8.5

Constant current electrolysis results obtained at doped electrodes.

DOPANT	AVERAGE VOLTAGE/V AT 25mAcm^{-2}	COMMENTS
Undoped	18	Voltage exceeds 20V early; polarisation occurs.
0.1% Ni	5.8	Polarisation occurs after 40 mins.
0.1% V	6.0	Lowest voltage 5.2V Voltage increased with time but only slowly.
0.1% Co	5.0V	Suffered anode effect.
0.1% Ni + 0.1% V	5.6	Polarisation occurred but voltage returned to 5.6V.
0.1% Fe	16	
0.1% Cr	16	
0.1% Mo	16.5	Anodes become polarised.
0.1% Ti	15	
0.1% Cu	15.5	
0.1% Mn	16	
0.1% Zn	>20	Anode effect occurs.

TABLE 8.6

Currents obtained during steady-state electrolysis at 6V in KF.2HF using doped electrodes.

ADDITIVE(S)	$I_b/mAcm^{-2}$	$I_p/mAcm^{-2}$	$I_c/mAcm^{-2}$
None	0.38	0.79	8.7
Ni	8.0	27	78.3
V	0.38	170	415
Ni/V	4.8	68	98.2
Fe	2.86	7.6	11.0
Cu	8.2	47	59.7
Co	3.14	33	330
Cr	5.9	7.1	12.2
Zn	1.7	3.8	23.0
Mo	9.52	63.5	71.6
Mn	6.6	11	12.3
Ti	2.4	3.9	5.3

I_b = baseline current

I_p = peak current

I_c = peak current from computer method

All additives at 0.1% level.

Figure 8.1

X-Ray EDAX spectrum of carbonised polyfurfuryl alcohol, showing the impurities present in undoped carbon samples.

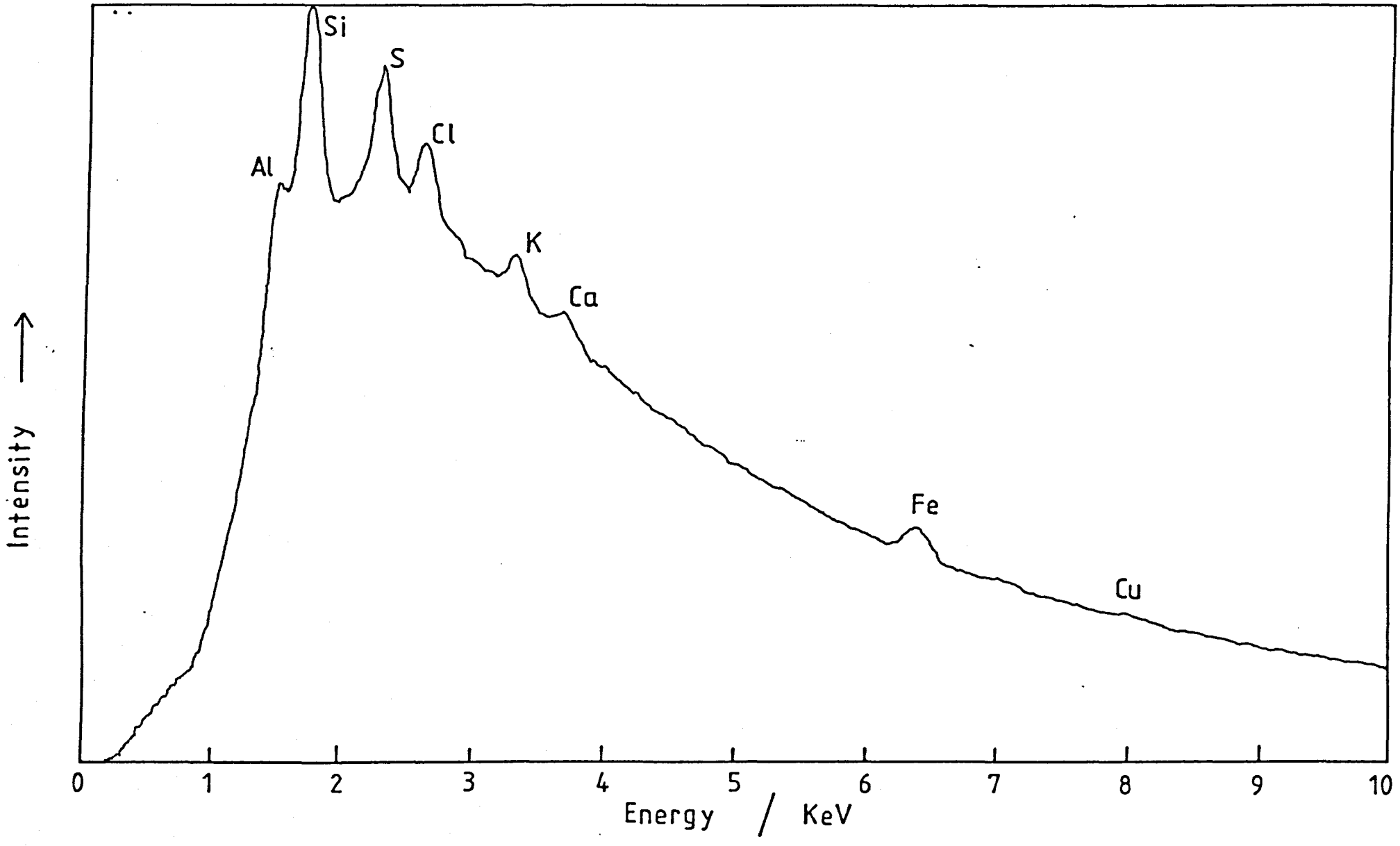
Si
S
Cl
Al
K
Ca
Fe
Cu
Intensity
0
1
2
3
4
5
6
7
8
9
10
Energy / KeV

Figure 8.2

a) X-Ray EDAX spectrum of carbonised polyfurfuryl alcohol containing nickel only.

b) X-Ray EADX spectrum of carbonised polyfurfuryl alcohol containing vanadium only.

a

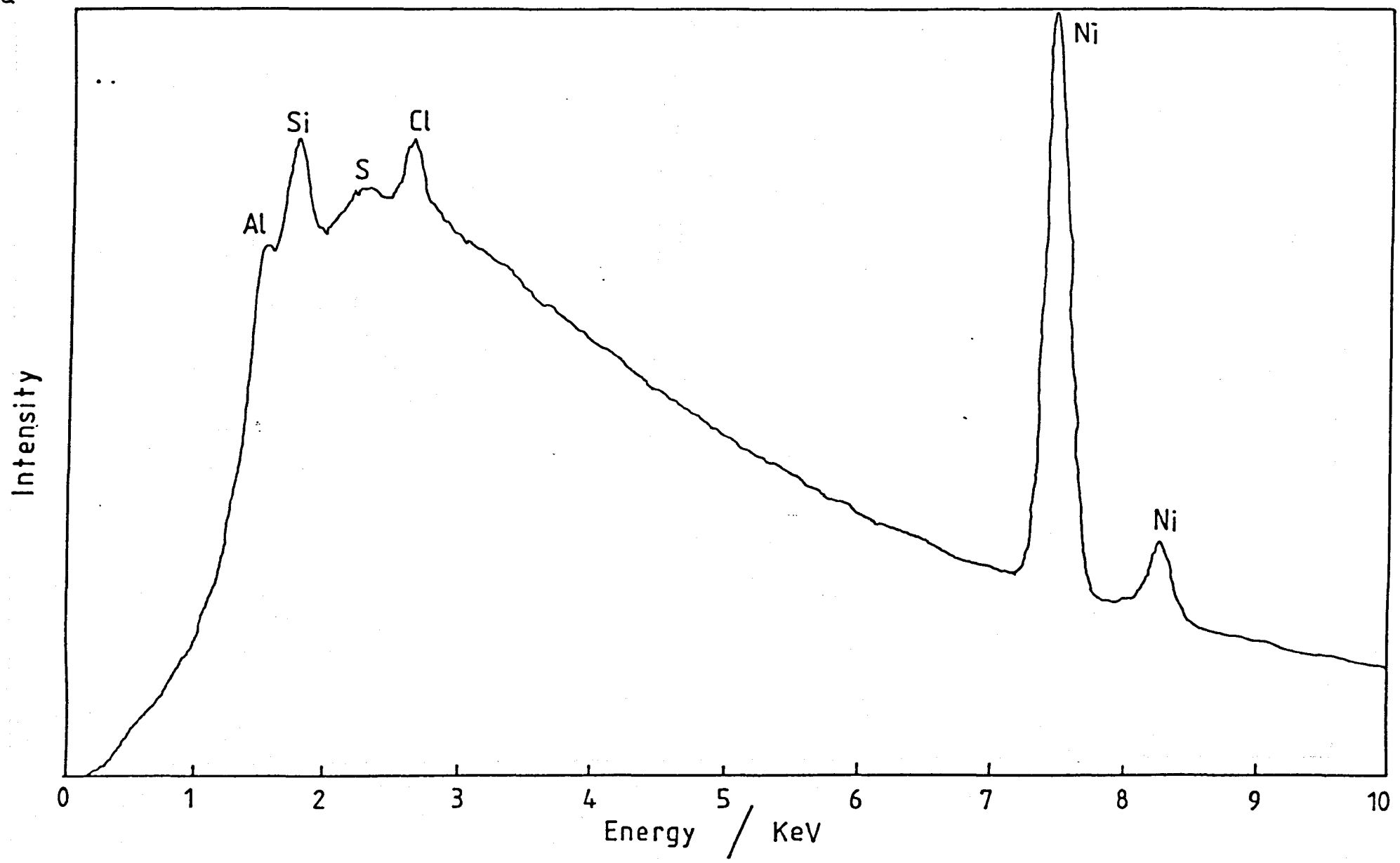

b

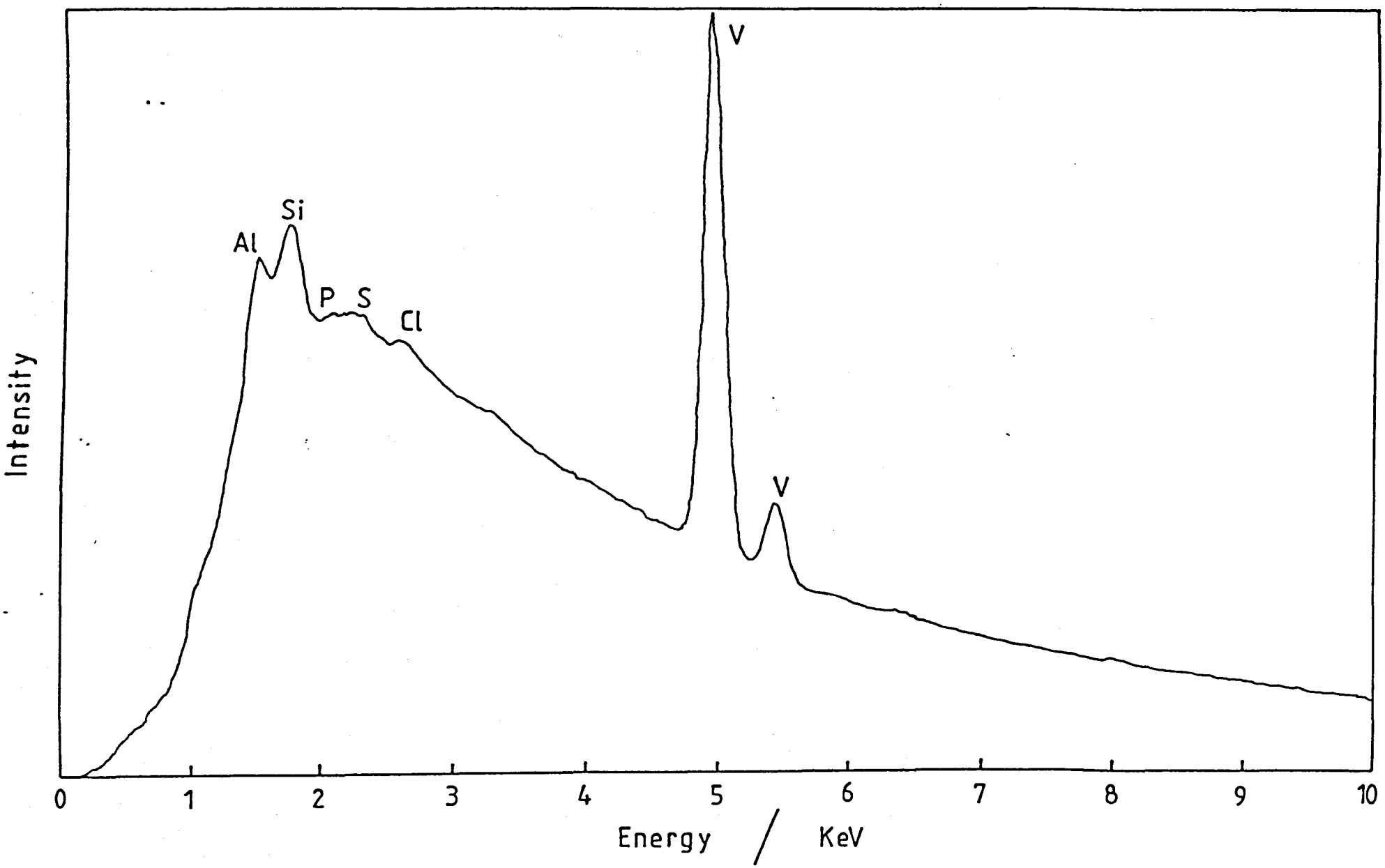

Figure 8.3

X-Ray EDAX spectrum of carbonised polyfurfuryl alcohol containing both nickel and vanadium.

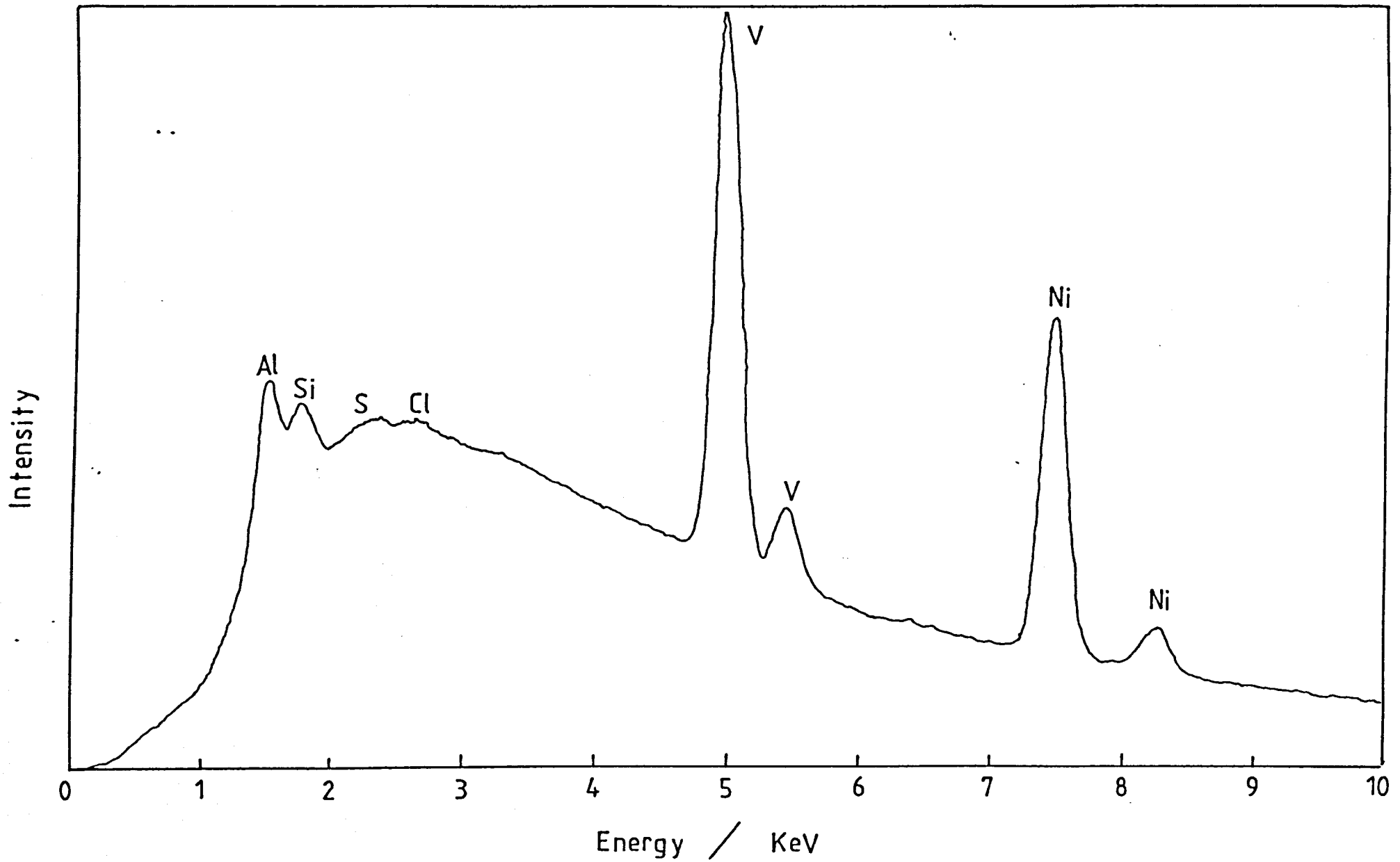
V
Ni
Al
Si
S
Cl
V
Ni
Intensity
0
1
2
3
4
5
6
7
8
9
10
Energy / KeV

Figure 8.4

a) X-Ray EDAX spectrum of carbonised polyfurfuryl alcohol containing nickel after exposure to fluorine evolution.

b) X-Ray EDAX spectrum of carbonised polyfurfuryl alcohol containing vanadium after exposure to fluorine evolution.

c) X-Ray EDAX spectrum of carbonised polyfurfuryl alcohol containing nickel and vanadium after exposure to fluorine evolution.

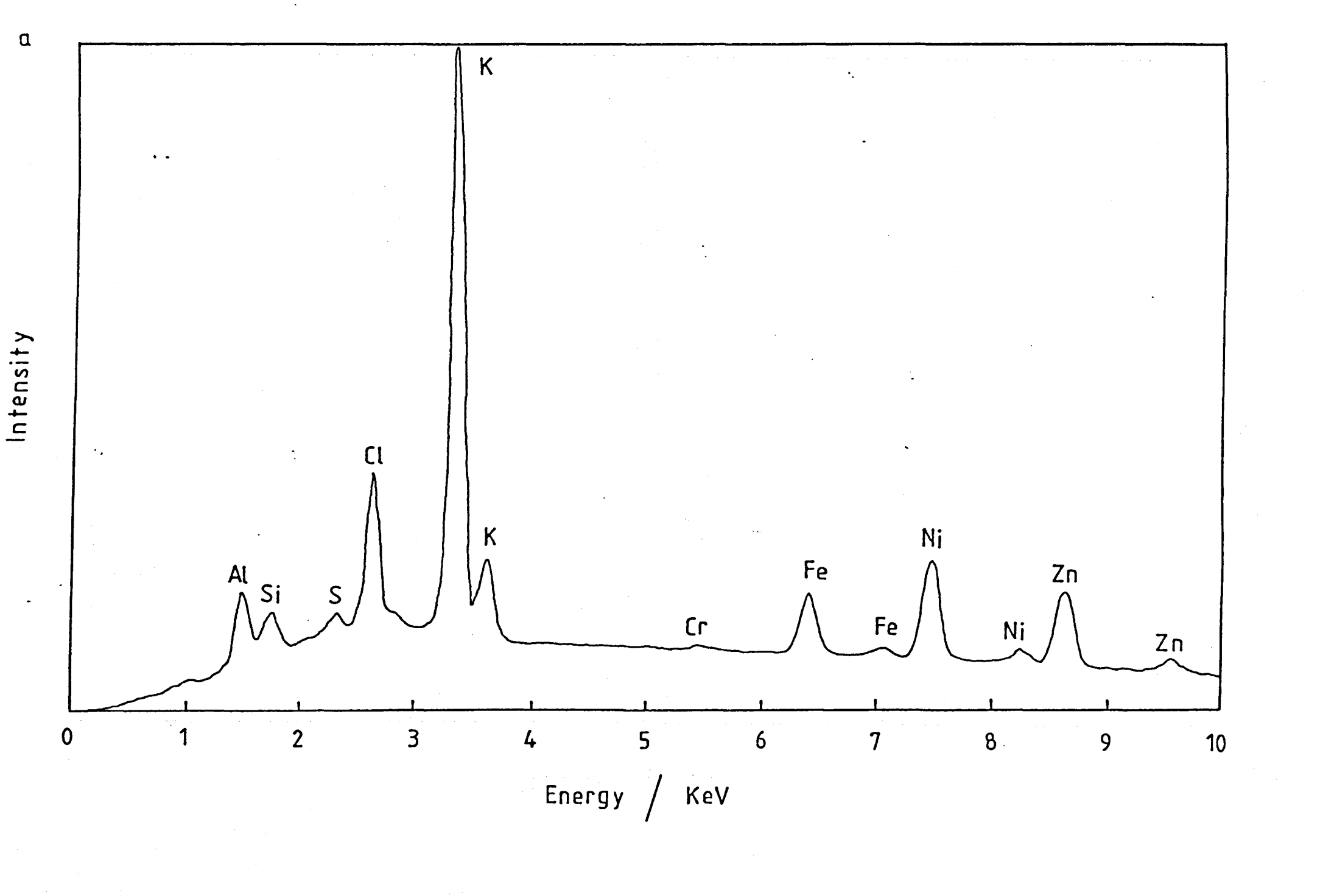
a
Intensity
K
Cl
K
Al
Si
S
Cr
Fe
Fe
Ni
Ni
Zn
Zn
0
1
2
3
4
5
6
7
8
9
10
Energy / KeV

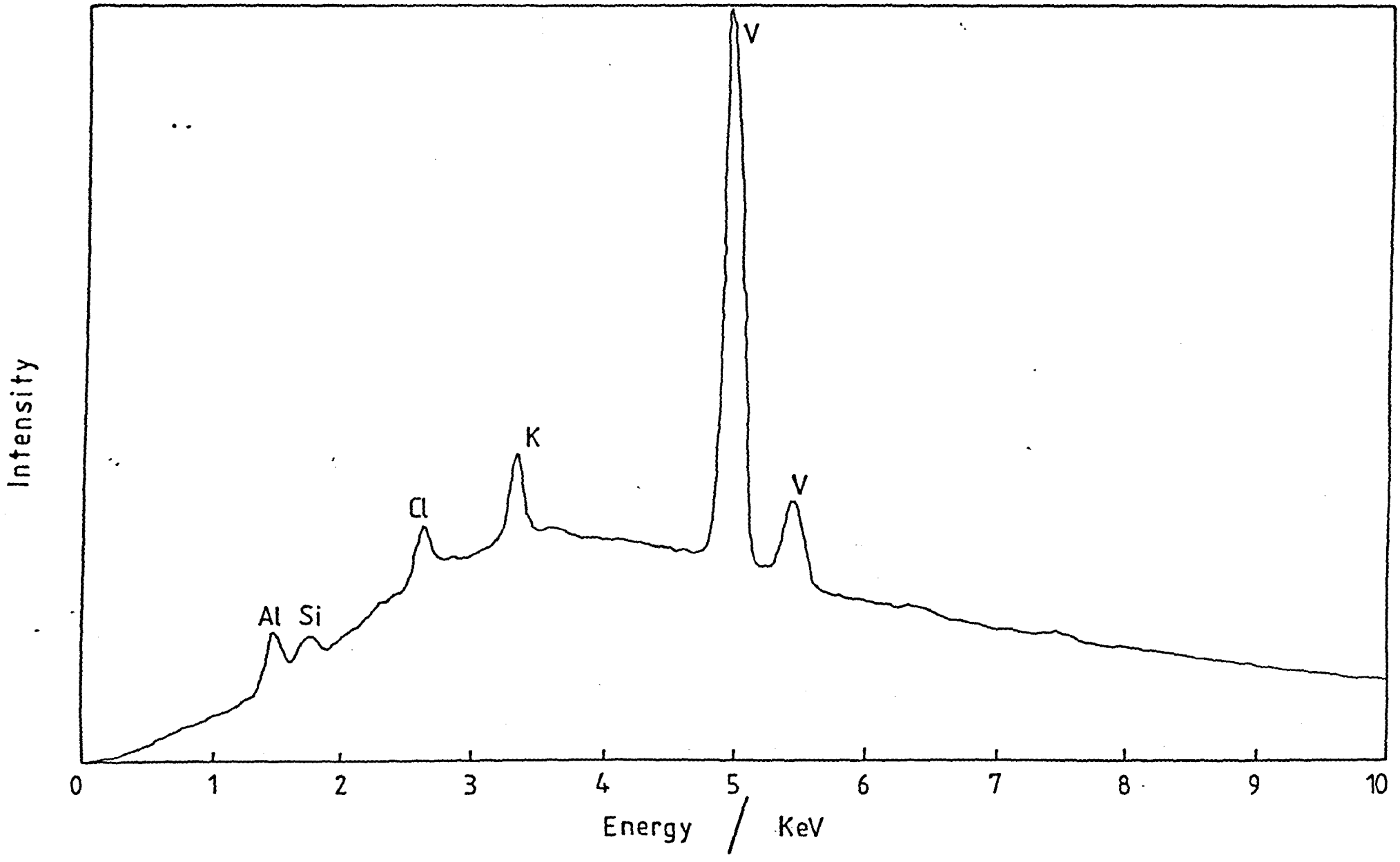
V
K
Cl
V
Al Si
Intensity
0 1 2 3 4 5 6 7 8 9 10
Energy / KeV

c

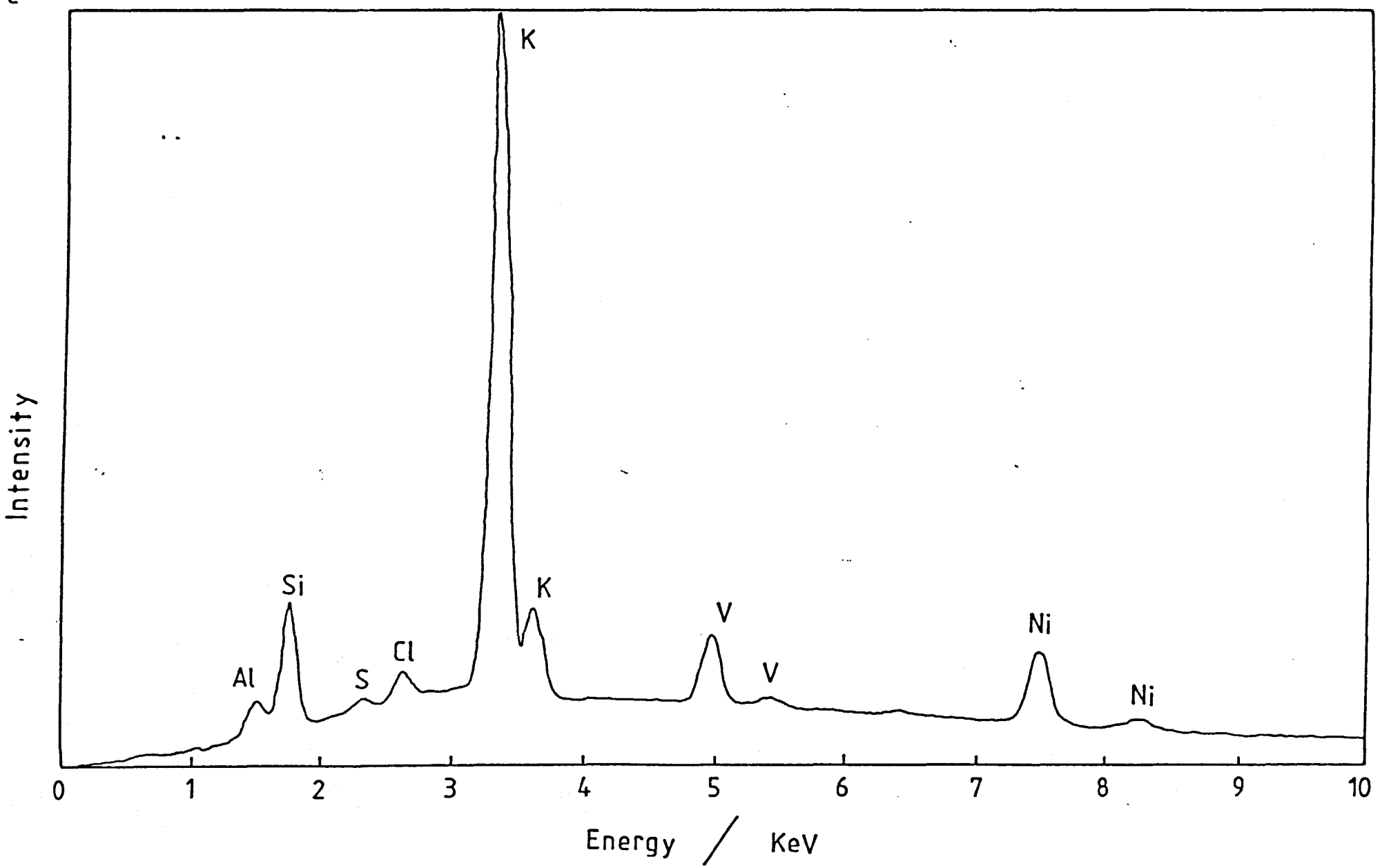

Figure 8.5

Cyclic voltammogram obtained on the first scan at $50Vs^{-1}$ in KF.2HF at an undoped electrode.

Figure 8.6

Cyclic voltammogram obtained on the second scan at $50Vs^{-1}$ in KF.2HF at an undoped electrode.

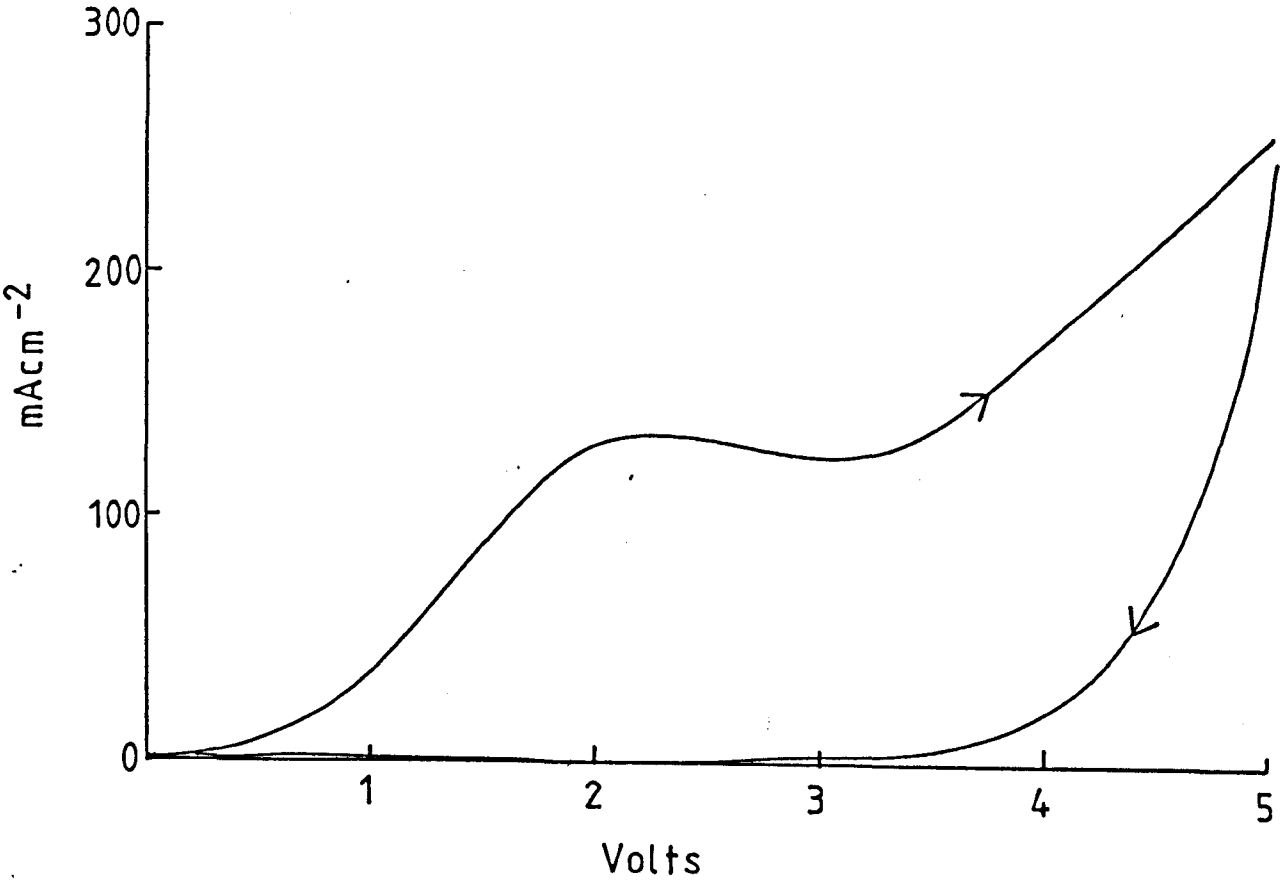
300
200
100
0
mAcm^{-2}
1
2
3
4
5
Volts

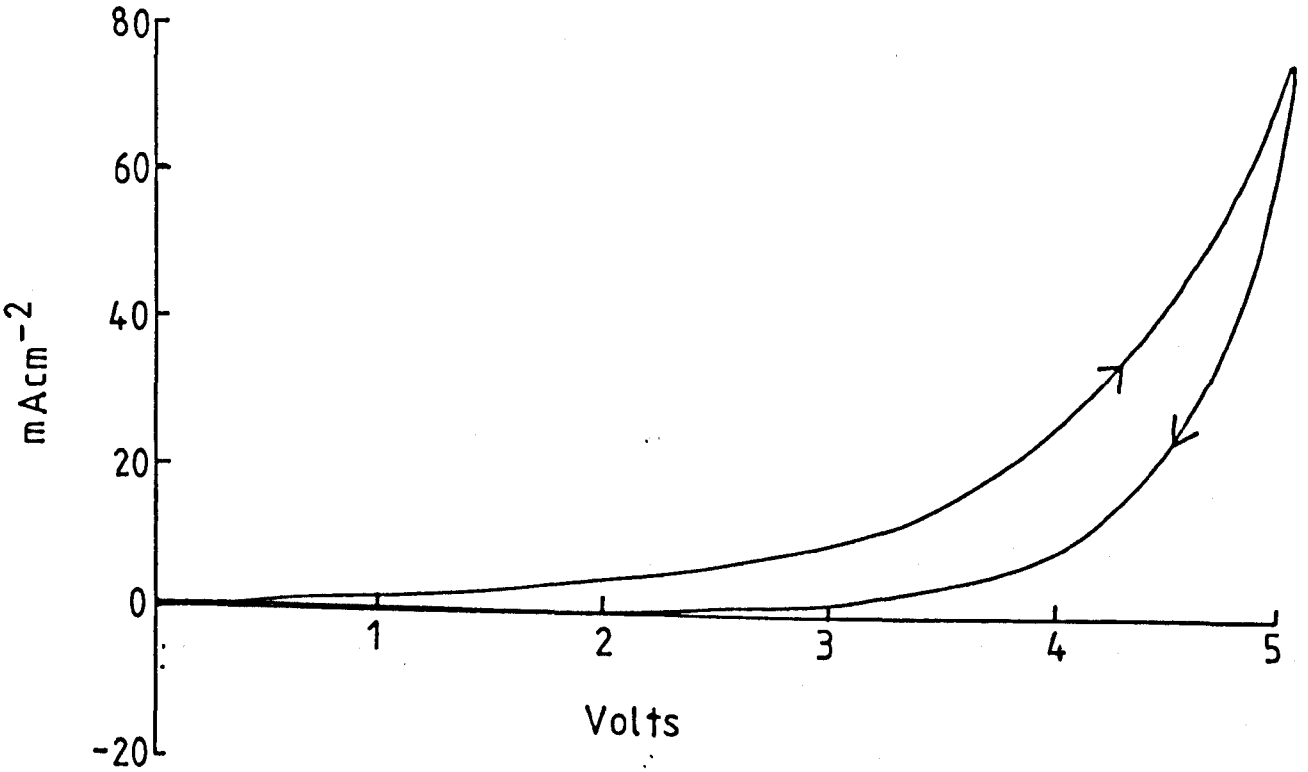
80
60
40
20
0
-20
mAcm^{-2}
1
2
3
4
5
Volts

Figure 8.7

Cyclic voltammogram obtained on the first scan at $50Vs^{-1}$ in KF.2HF at an electrode containing 0.1% Ni.

Figure 8.8

Cyclic voltammogram obtained after six cycles at $50Vs^{-1}$ in KF.2HF at an electrode containing 0.1% Ni. (steady state attained).

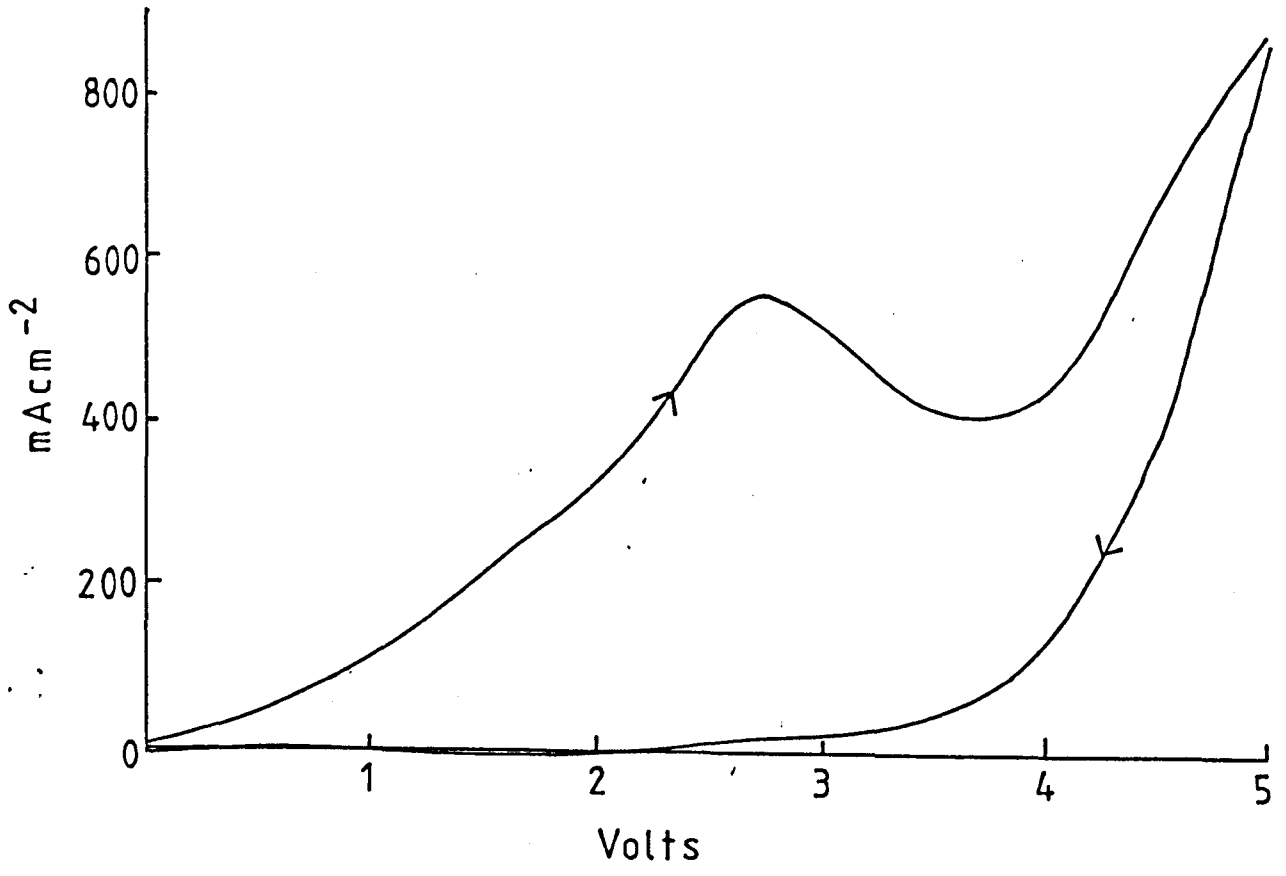
800
600
400
200
0
mAcm -2
1
2
3
4
5
Volts

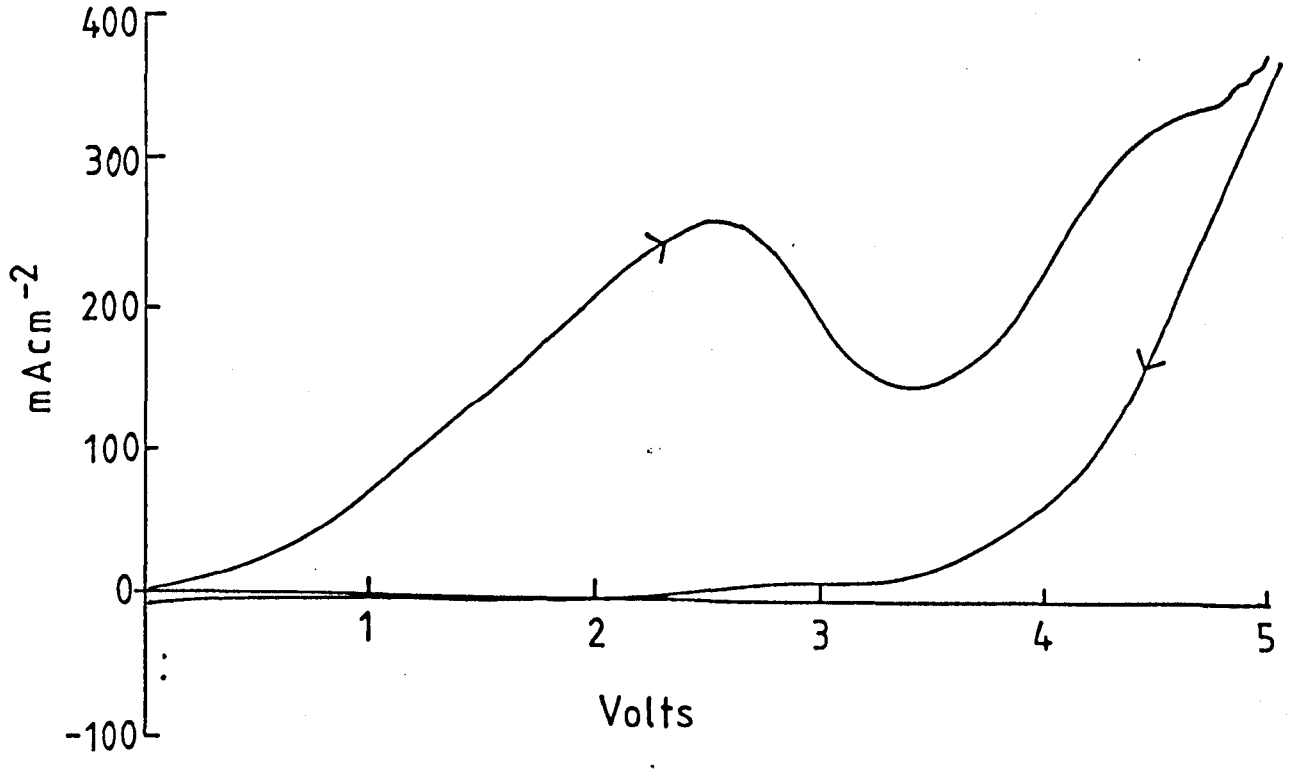
400
300
200
100
0
-100
mAcm -2
1
2
3
4
5
Volts

Figure 8.9

Cyclic voltammogram obtained on the first scan at $50Vs^{-1}$ in KF.2HF at an electrode containing 0.1% vanadium.

Figure 8.10

Cyclic voltammogram obtained after six cycles at $50Vs^{-1}$ in KF.2HF at an electrode containing 0.1% vanadium.

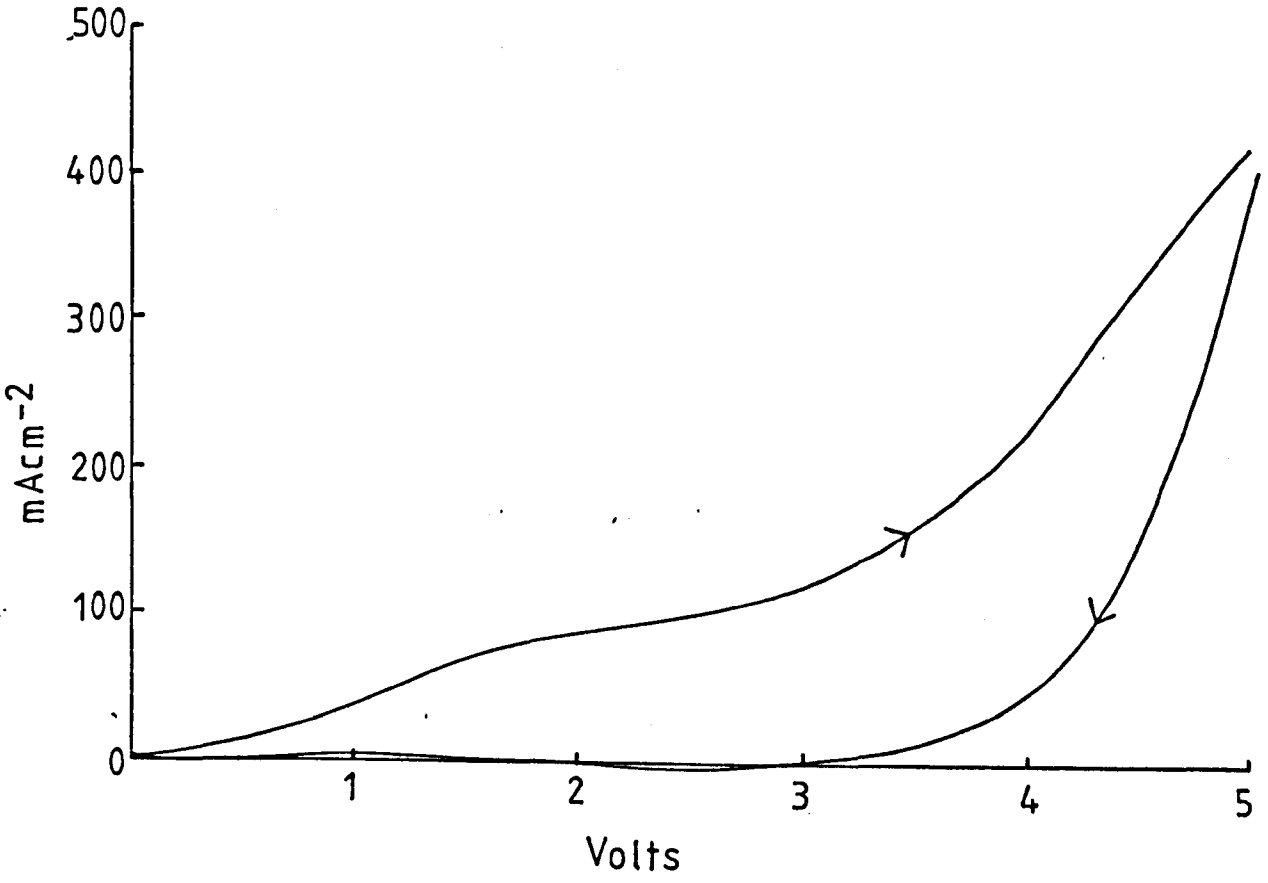
500
400
300
200
100
0
mAcm-2
1
2
3
4
5
Volts

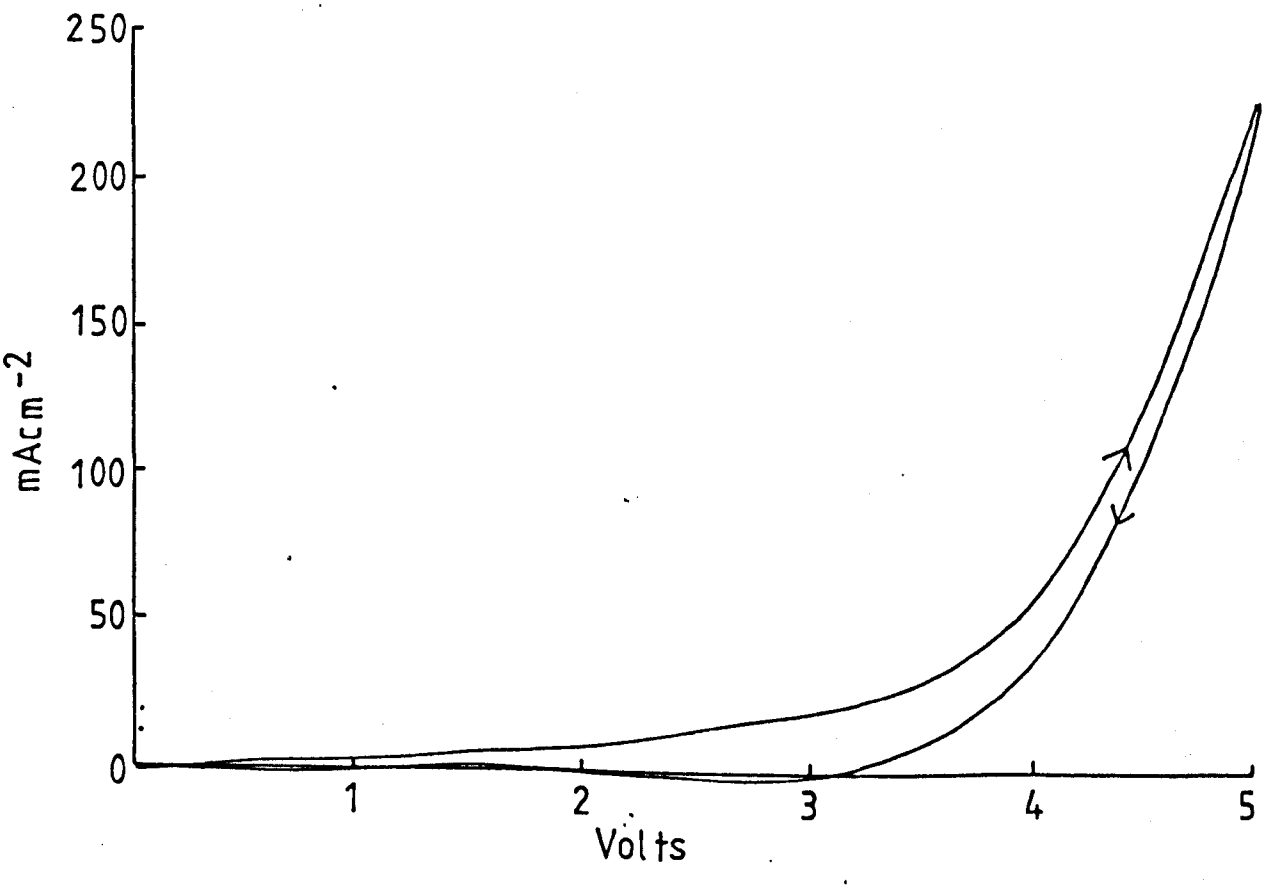
250
200
150
100
50
0
mAcm-2
1
2
3
4
5
Volts

Figure 8.11

Upper Diagram : Cyclic voltammogram obtained on the first scan at $50Vs^{-1}$ in KF.2HF at an electrode containing 0.1% Cr. (Similar results were obtained at electrodes containing Zn, Mn, Cu, and Co.

Lower Diagram : Cyclic voltammogram obtained after six scans at $50Vs^{-1}$ in KF.2HF at an electrode containing 0.1% Cr.

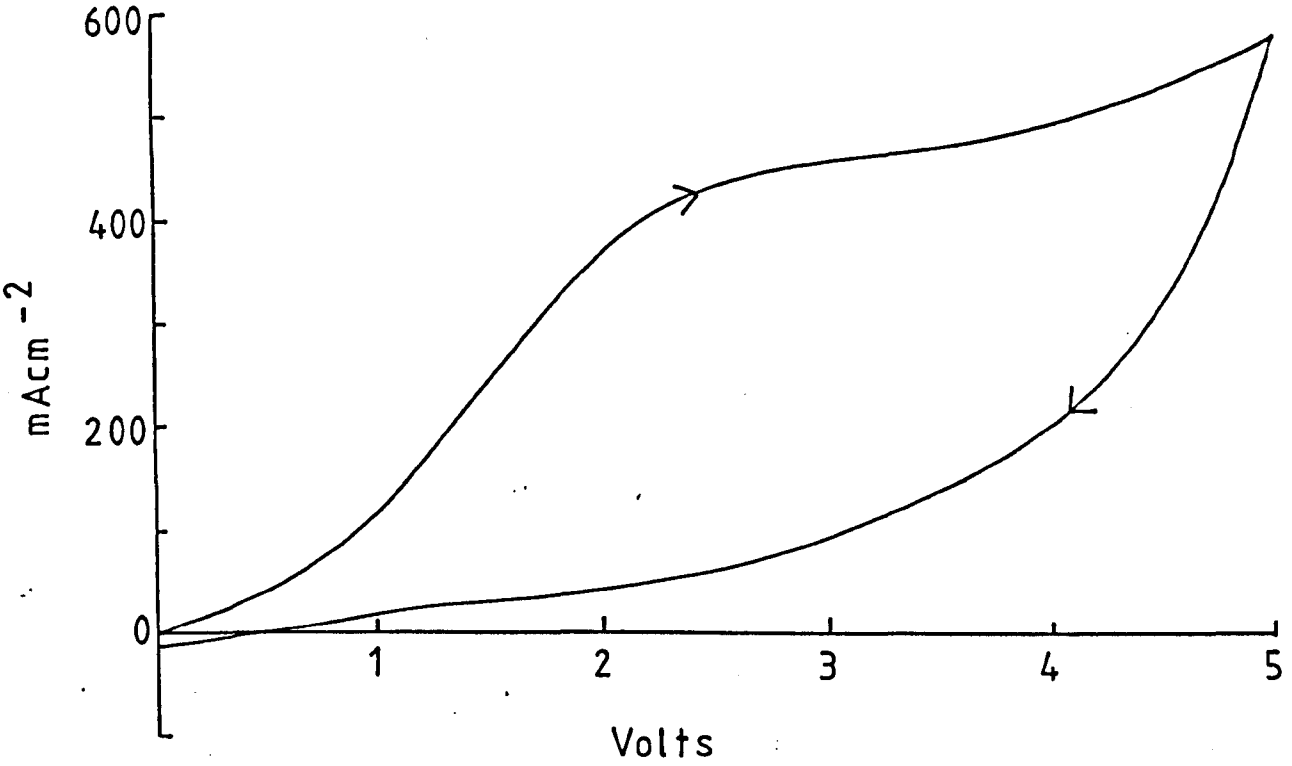
600
400
200
0
mAcm -2
1
2
3
4
5
Volts

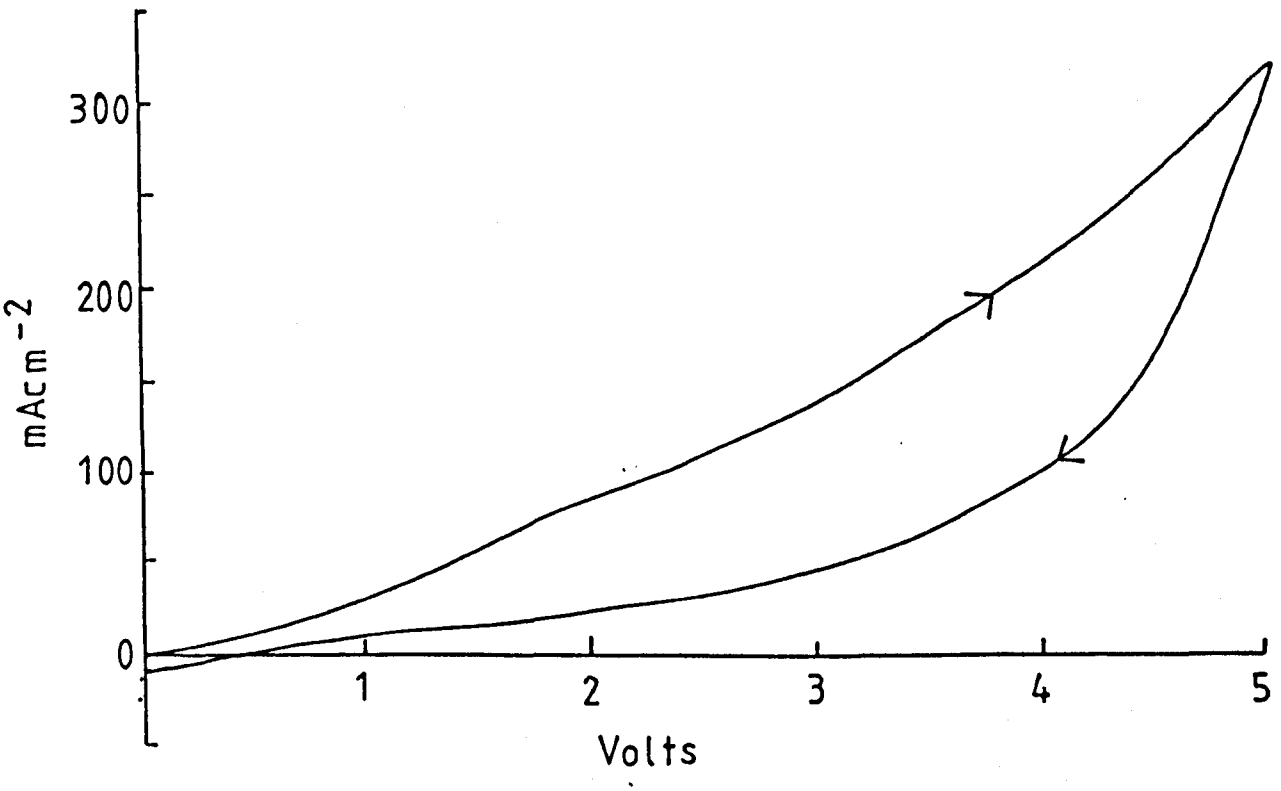
300
200
100
0
mAcm -2
1
2
3
4
5
Volts

Figure 8.12

Upper Diagram : Cyclic voltammogram obtained on the first scan at $50Vs^{-1}$ in KF.2HF at an electrode containing 0.1% Fe (Similar results were obtained at electrodes containing Ti and Mo).

Lower Diagram : Cyclic voltammogram obtained after six scans at $50Vs^{-1}$ in KF.2HF at an electrode containing 0.1% Fe.

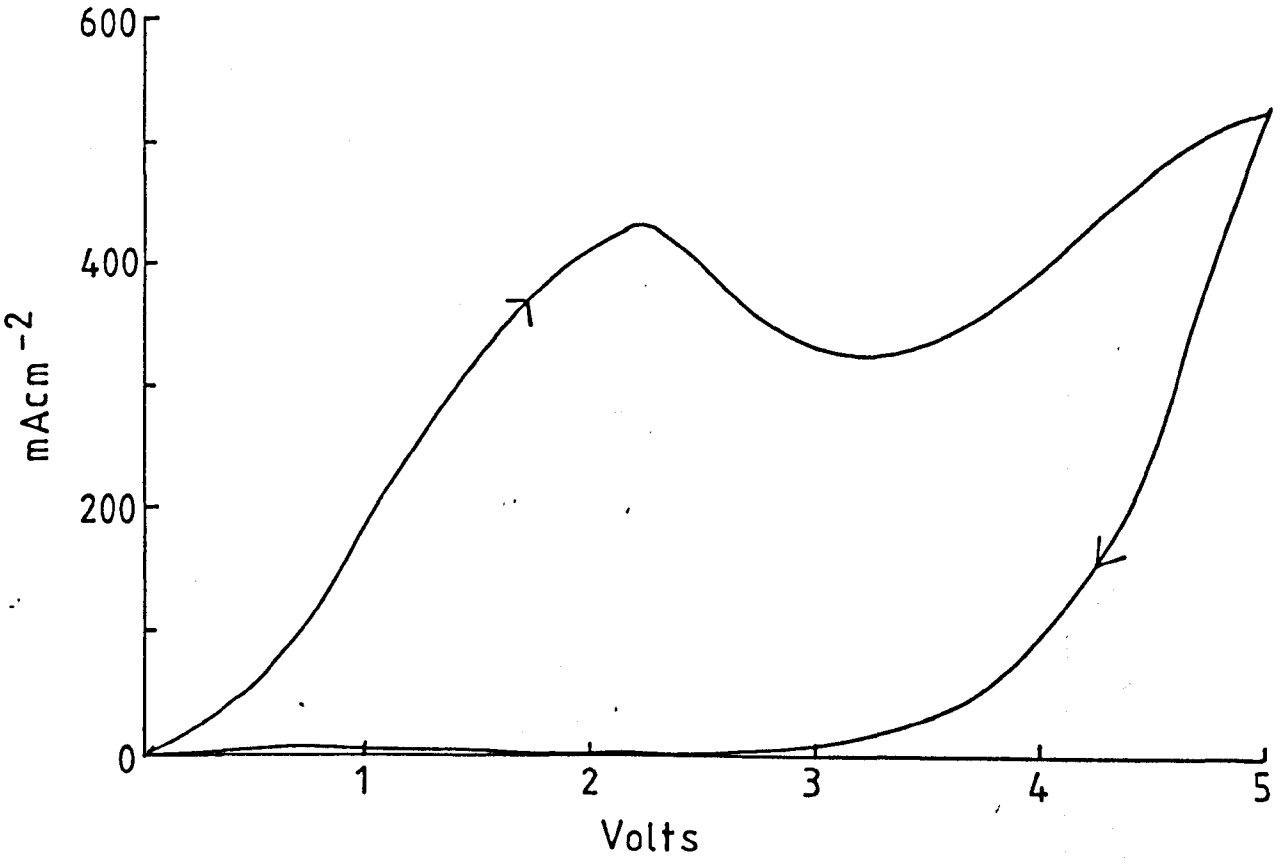
600
400
200
0
mAcm^{-2}
1
2
3
4
5
Volts

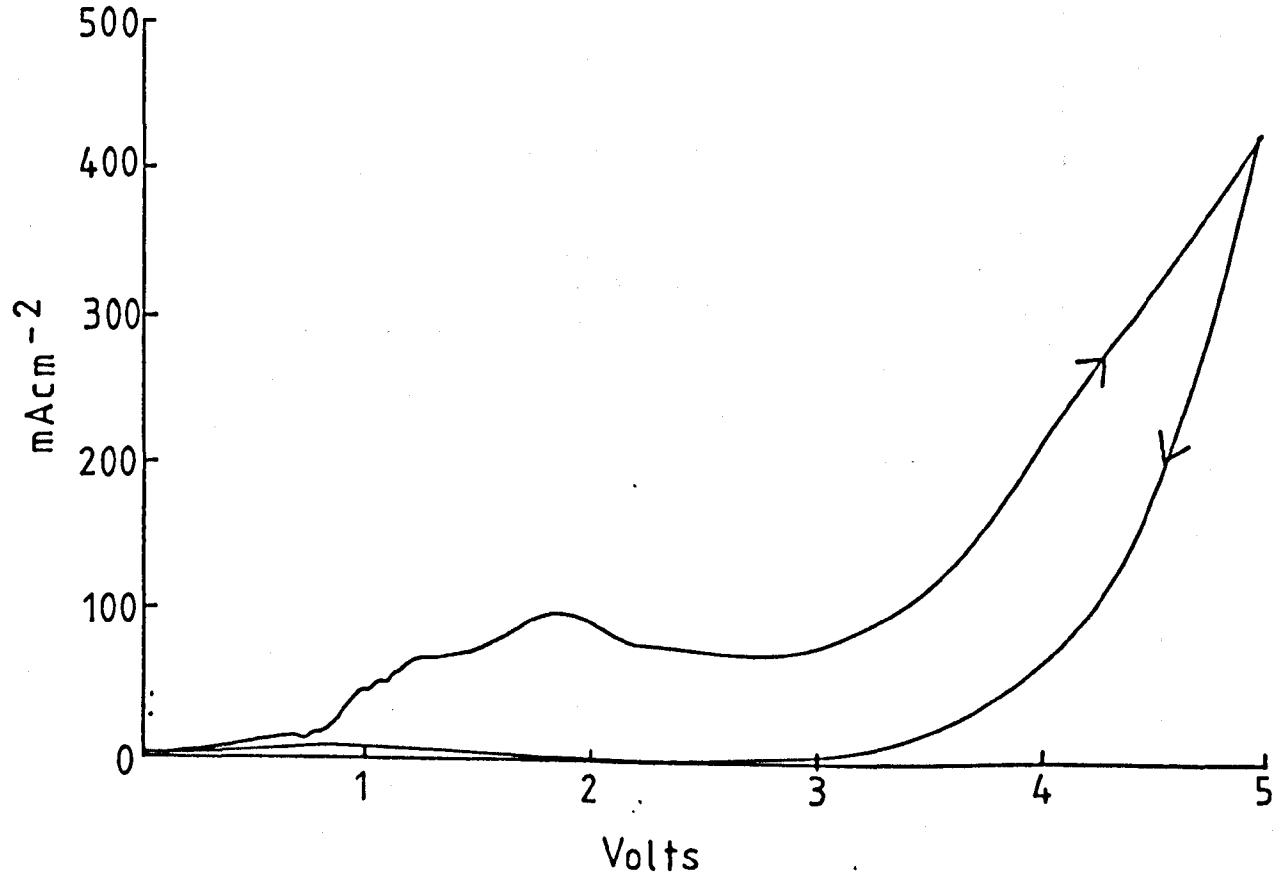
500
400
300
200
100
0
mAcm^{-2}
1
2
3
4
5
Volts

Figure 8.13

Voltage vs. time response obtained at 25mAcm^{-2} at an undoped electrode.

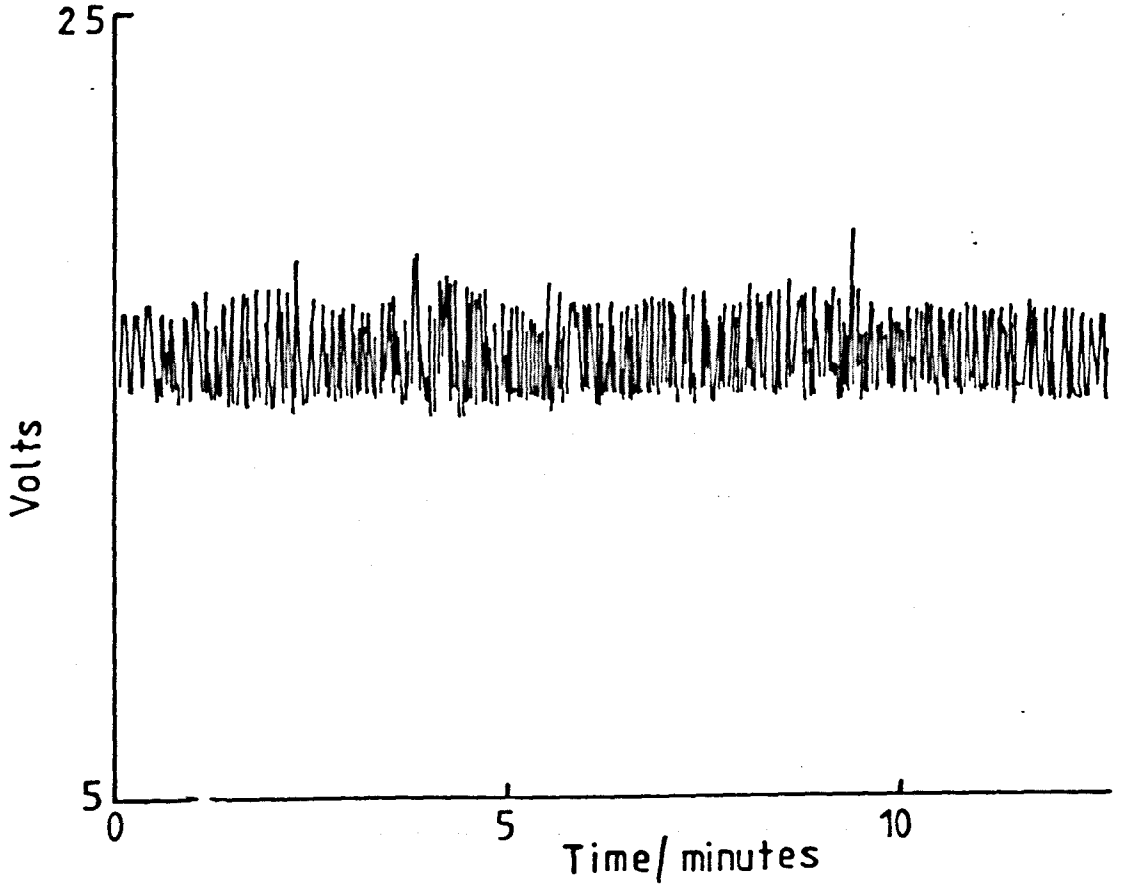

Figure 8.14

Voltage vs. time response obtained at 25mAcm^{-2} at an electrode containing 0.1% Ni.

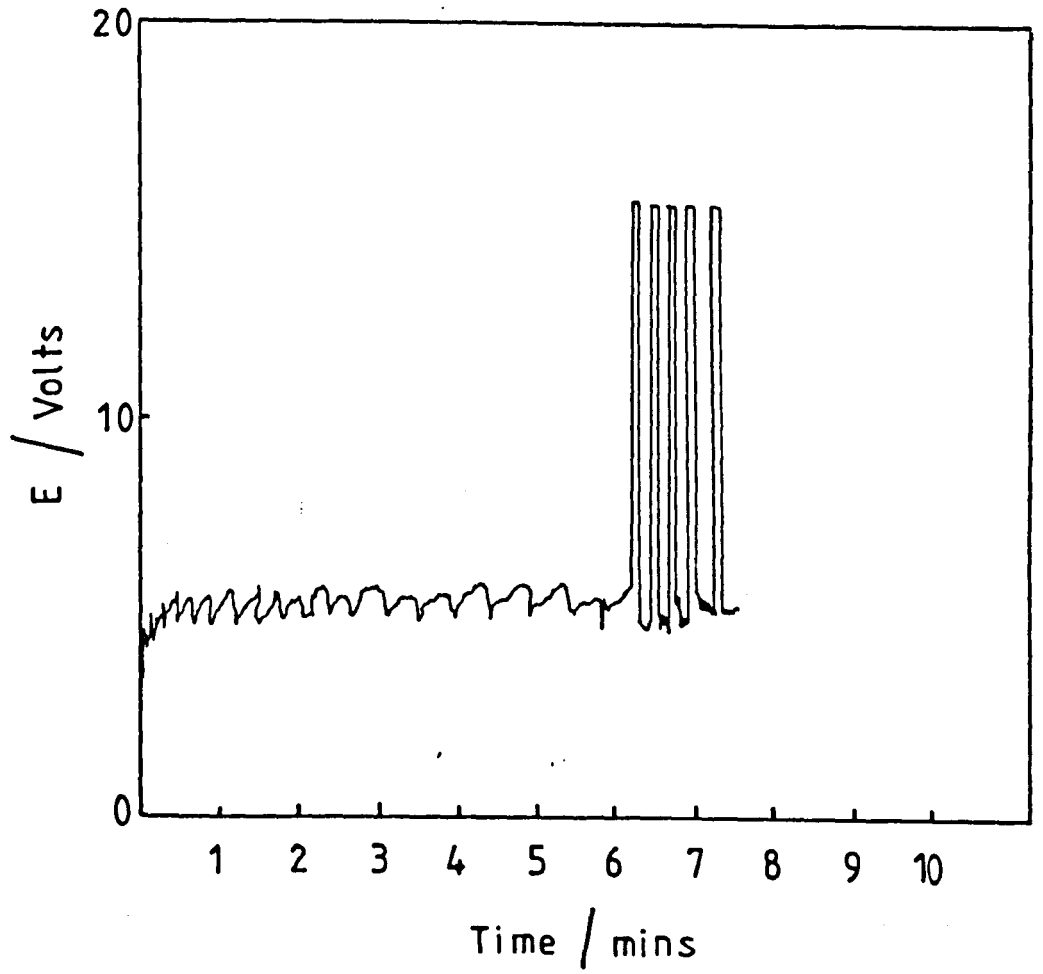

Figure 8.15

a)Voltage vs. time response obtained at 25mAcm^{-2} at an electrode containing 0.1% vanadium. (Times less than 30 minutes).

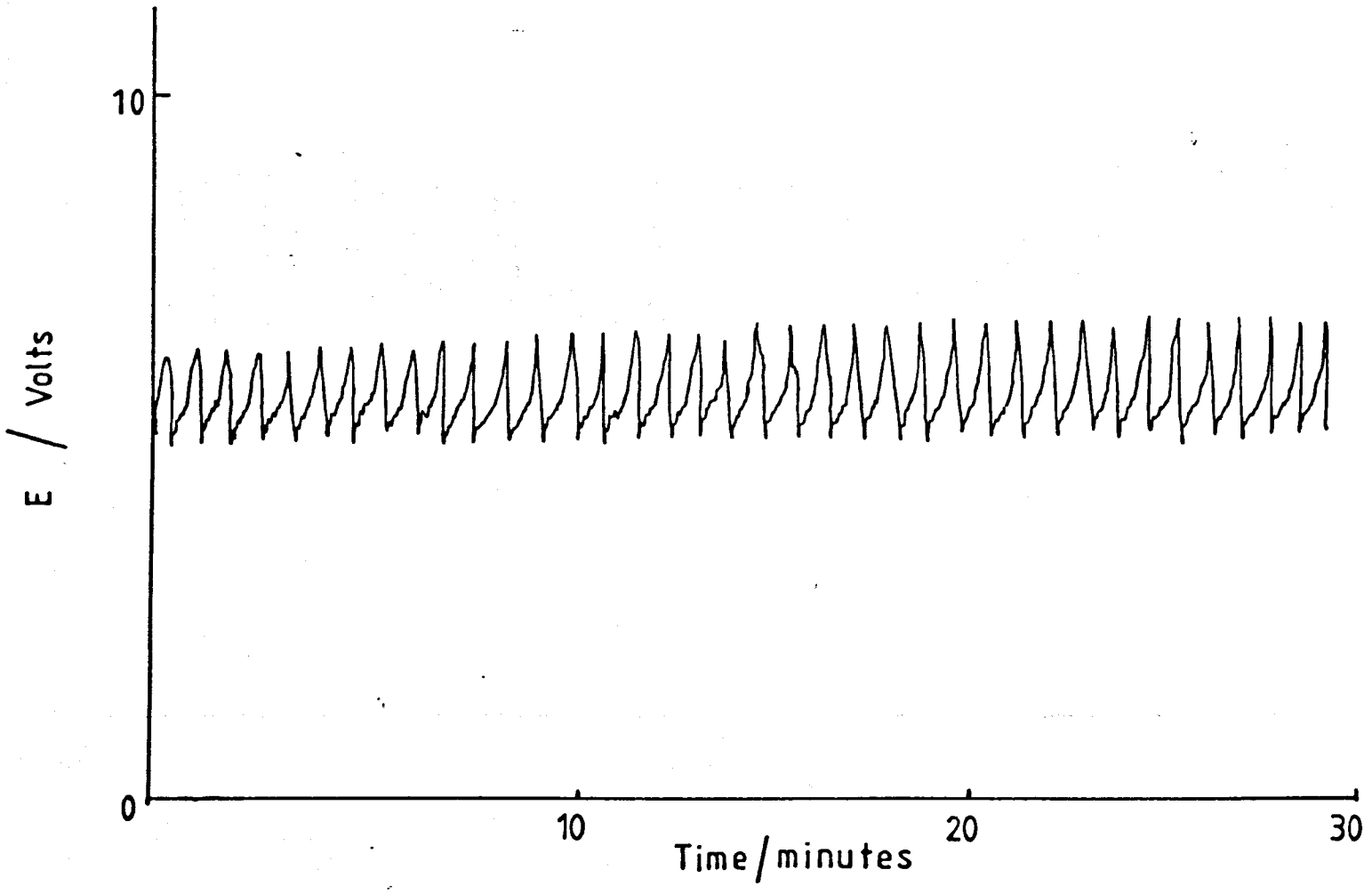

Figure 8.15

b)Voltage vs. time response obtained at 25mAcm^{-2} at an electrode containing 0.1% vanadium. (Times longer than 40 minutes).

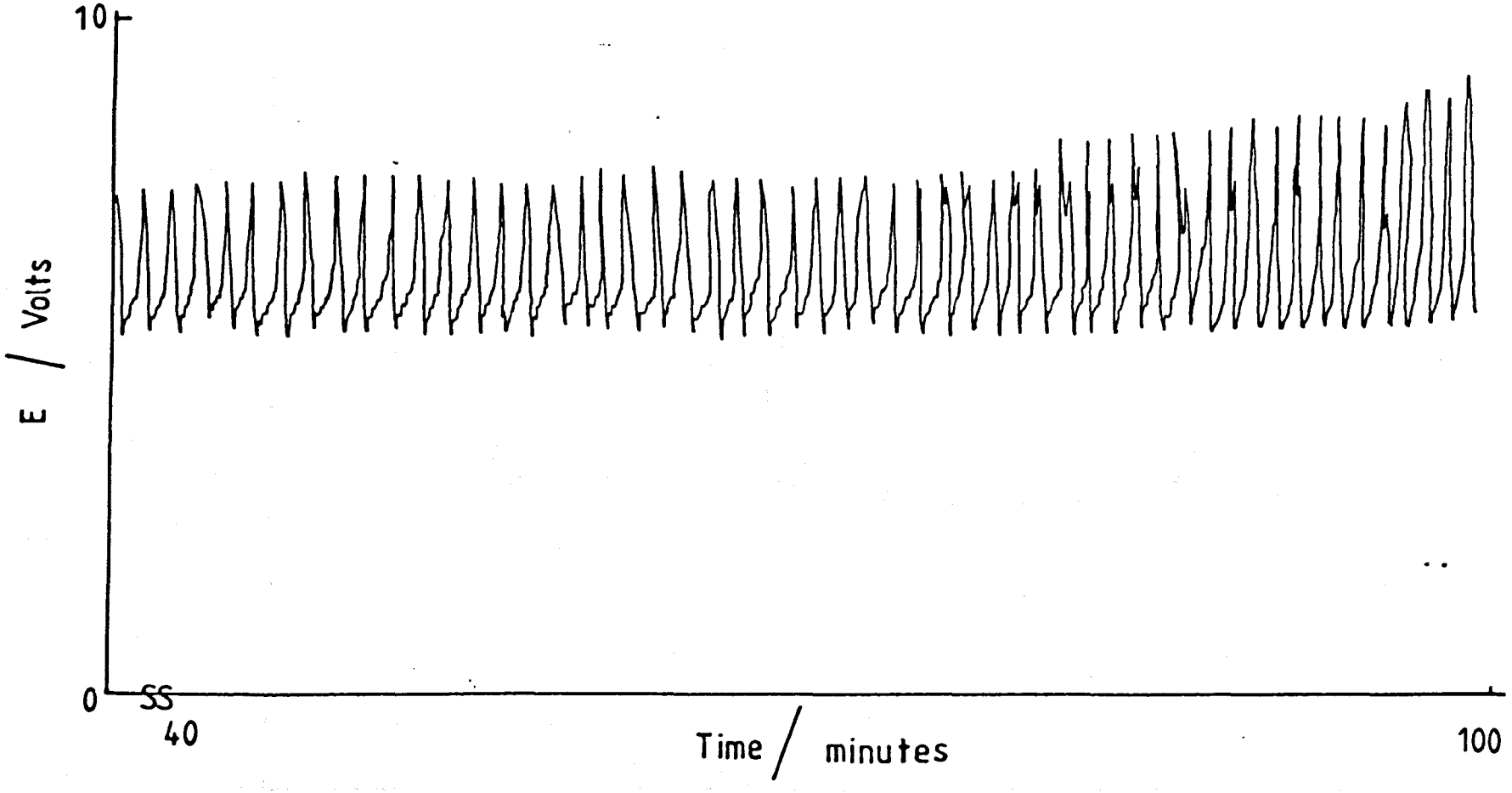

Figure 8.16

Voltage vs. time response obtained at 25mAcm^{-2} at an electrode containing nickel and vanadium.

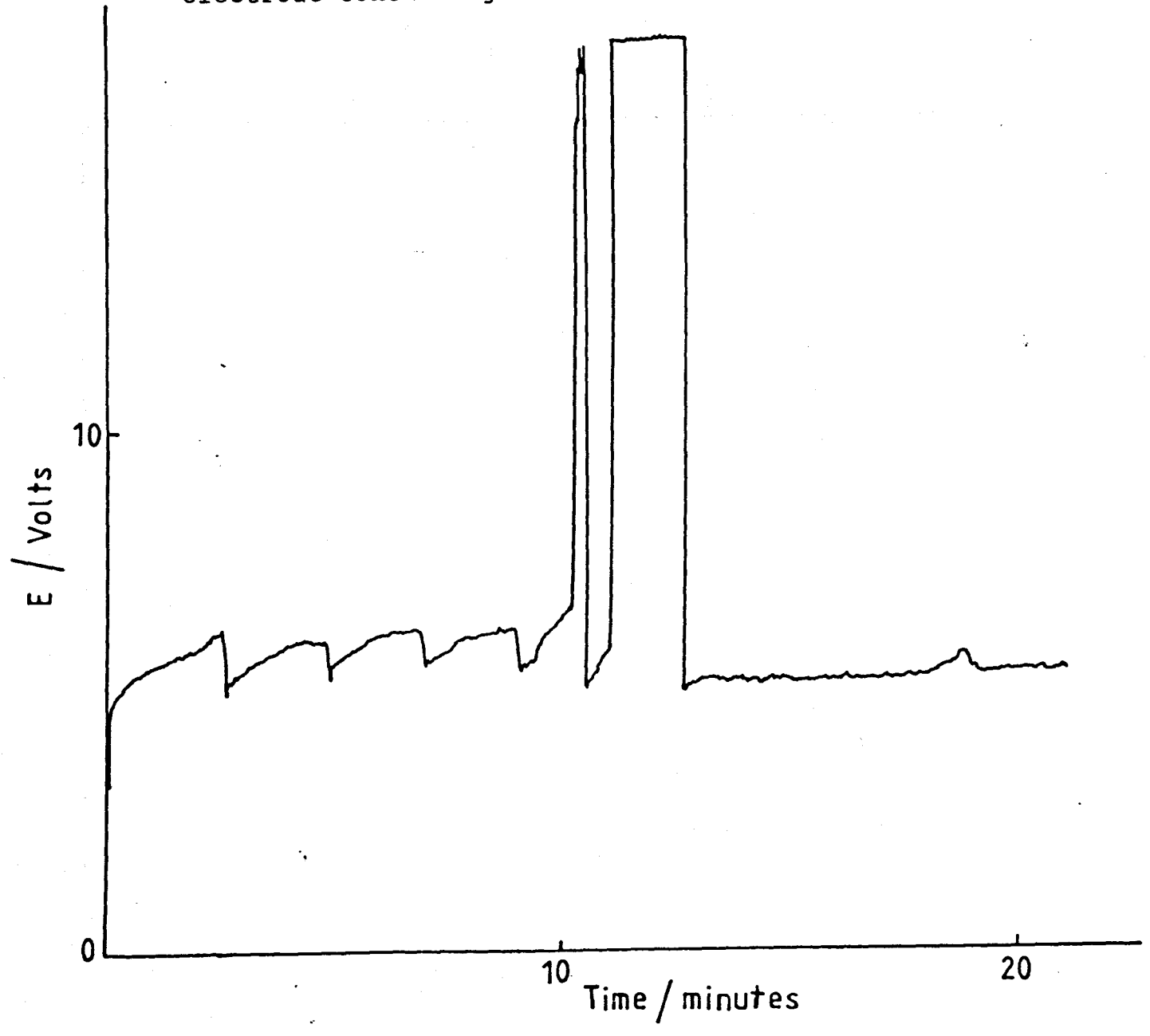

Figure 8.17

Resistance vs. time data obtained from impedance measurements in KF.2HF at 2.4V.

(x) Undoped anode.

(●) 0.1% vanadium.

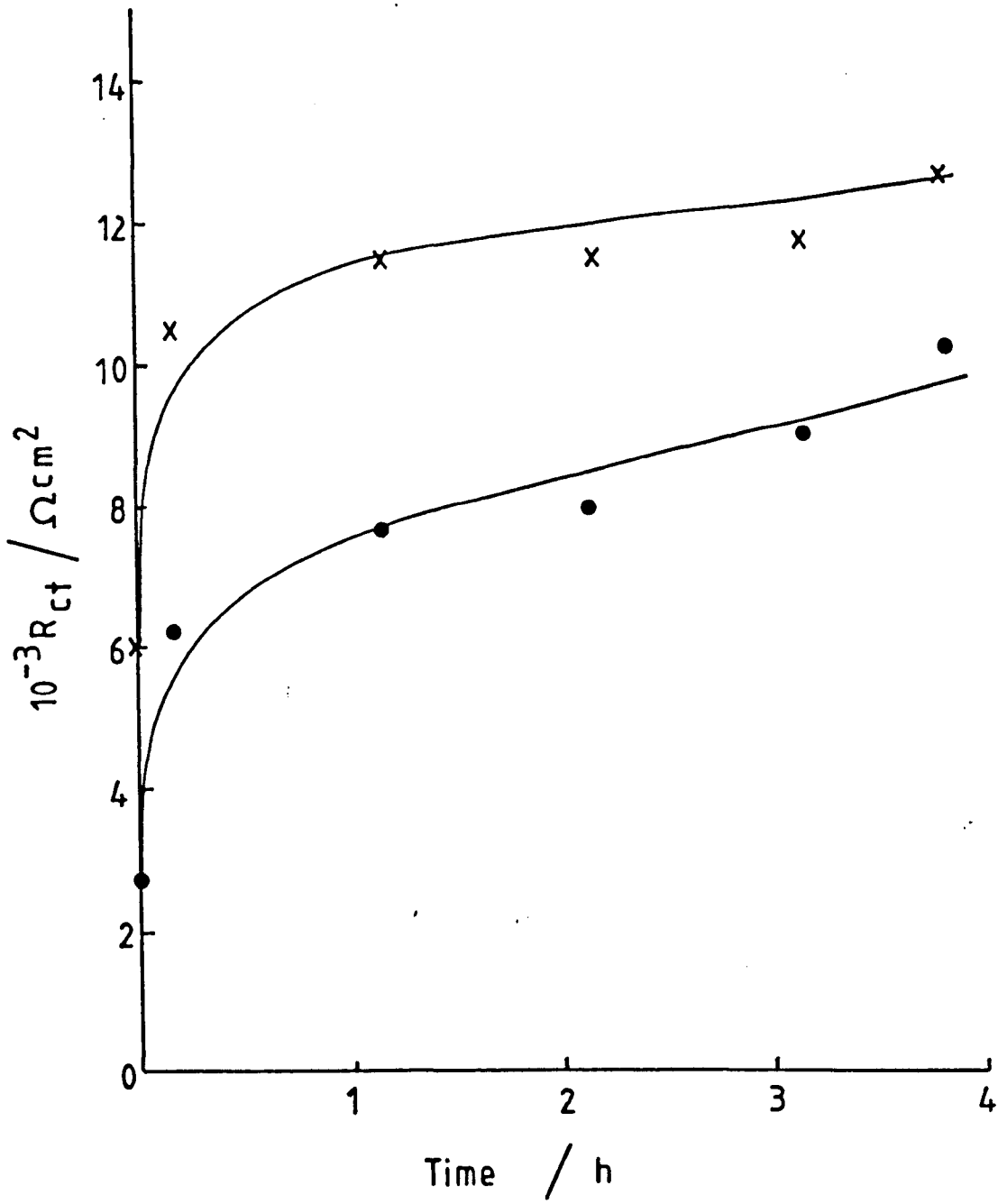

Figure 8.18

Capacitance vs. time data obtained from impedance measurements in KF.2HF at 2.4V.

(X) 0.1% Ni

(●) Ni + V

(▼) 0.1% V

(■) Undoped anode.

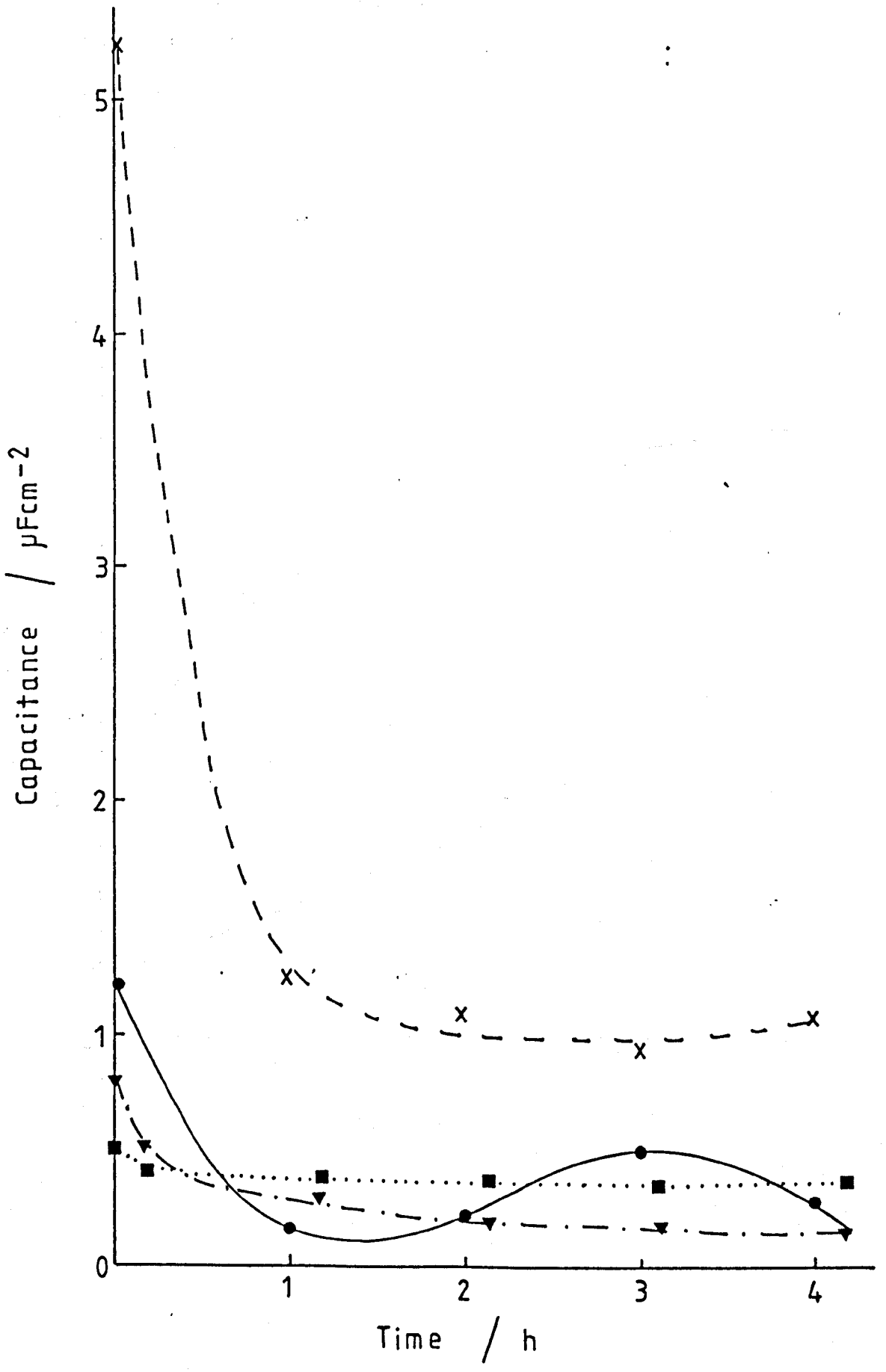
Capacitance / μFcm⁻²
0
1
2
3
4
5
Time / h
1
2
3
4

Figure 8.19

Resistance vs. time data obtained from impedance measurements in KF.2HF at 2.4V.

(●) 0.1% Ni

(x) Ni + V.

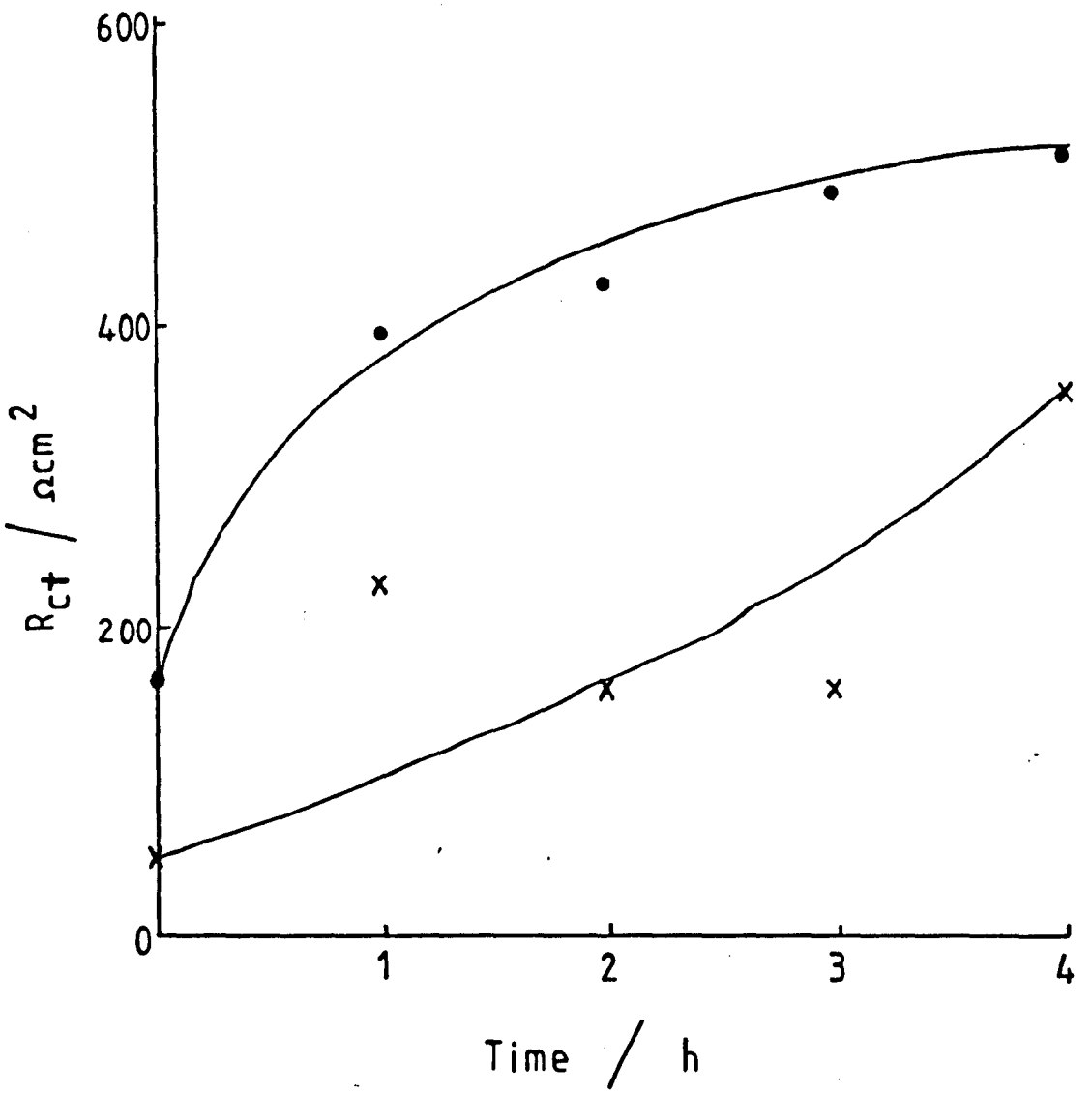

Figure 8.20

Current vs. voltage response obtained during potential pulse measurements in KF.2HF. The current after 100ms of the pulse is plotted against the pulse potential.

(●) Electrode containing 0.1% Ni

(X) Response obtained after evolution of fluorine at 6V for 30 minutes at an electrode containing 0.1% Ni.

(■) Response obtained at an undoped material.

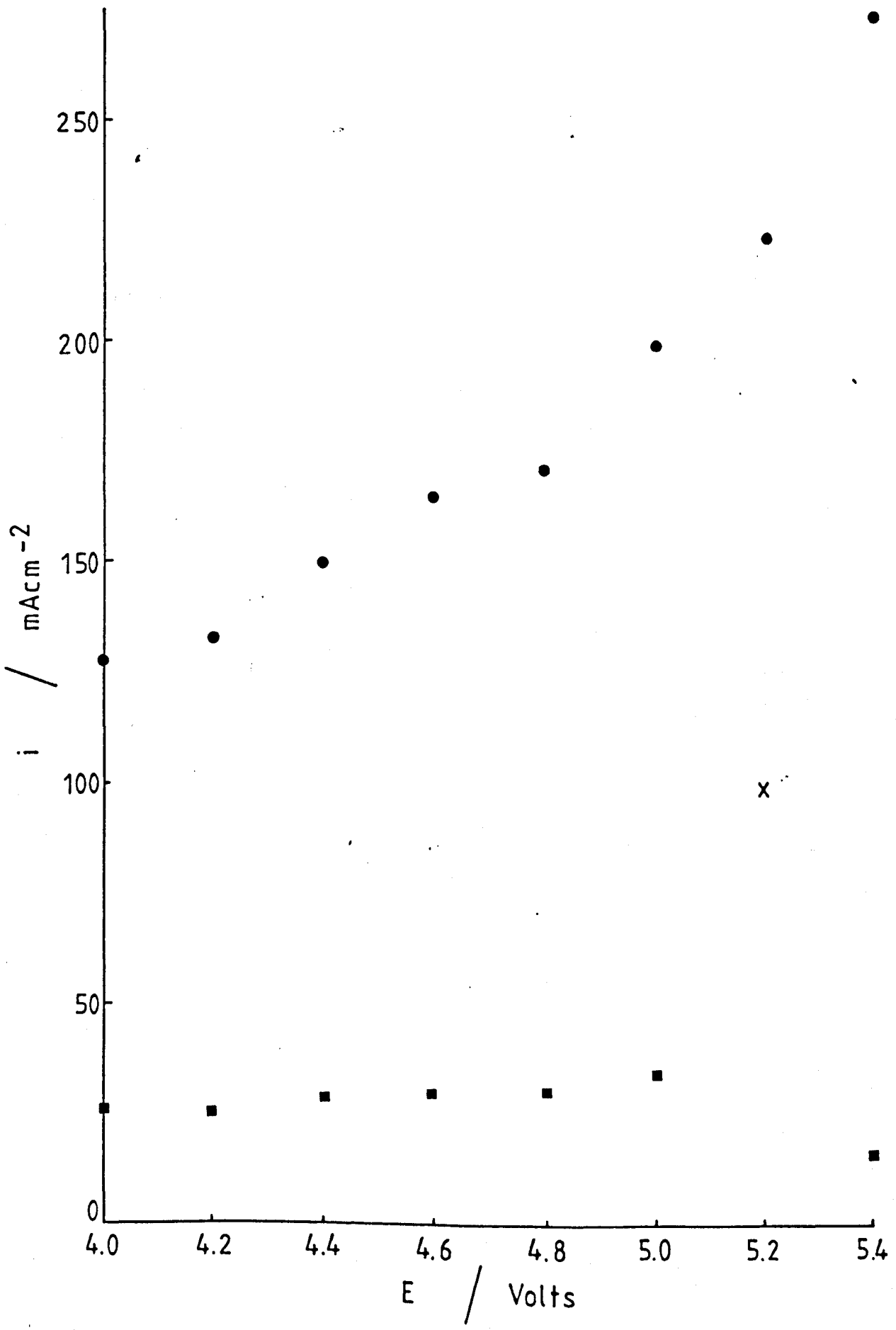
250
200
150
100
50
0
i / mAcm^{-2}
4.0
4.2
4.4
4.6
4.8
5.0
5.2
5.4
E / Volts
x

Figure 8.21

Current vs. voltage response obtained during potential pulse measurements in KF.2HF. The current after 100ms of the pulse is plotted against the pulse potential. Electrode containing 0.1% V% (●) before, and (X) after evolution of fluorine at 6V for 30 minutes.

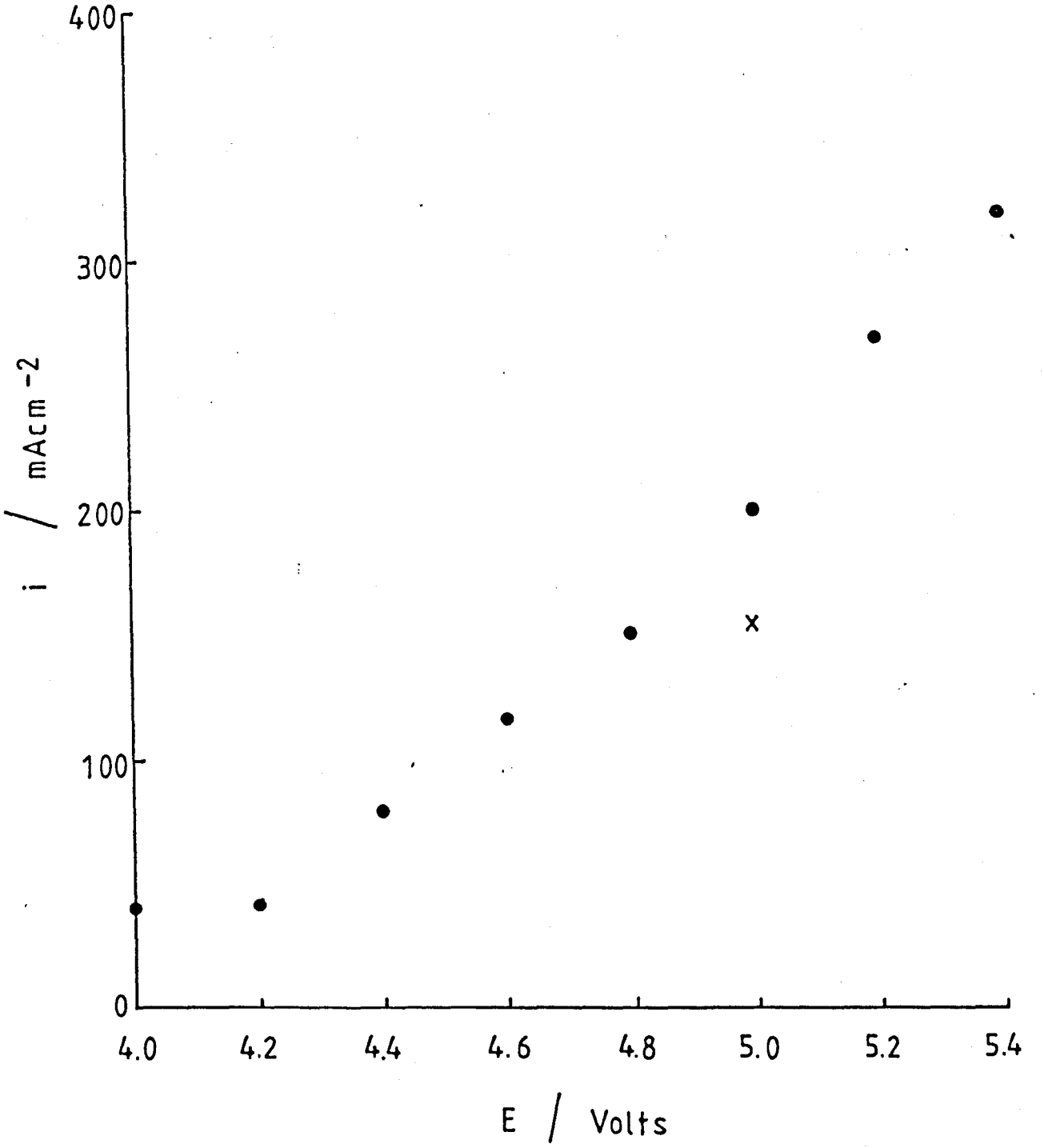
400
300
200
100
0
i / mAcm -2
4.0
4.2
4.4
4.6
4.8
5.0
5.2
5.4
E / Volts

Figure 8.22

Current vs. voltage response obtained during potential pulse measurements in KF.2HF. The current after 100ms of the pulse is plotted against the pulse potential. Electrode containing Ni + V, (●) before, and (x) after evolution of fluorine at 6V for 30 minutes.

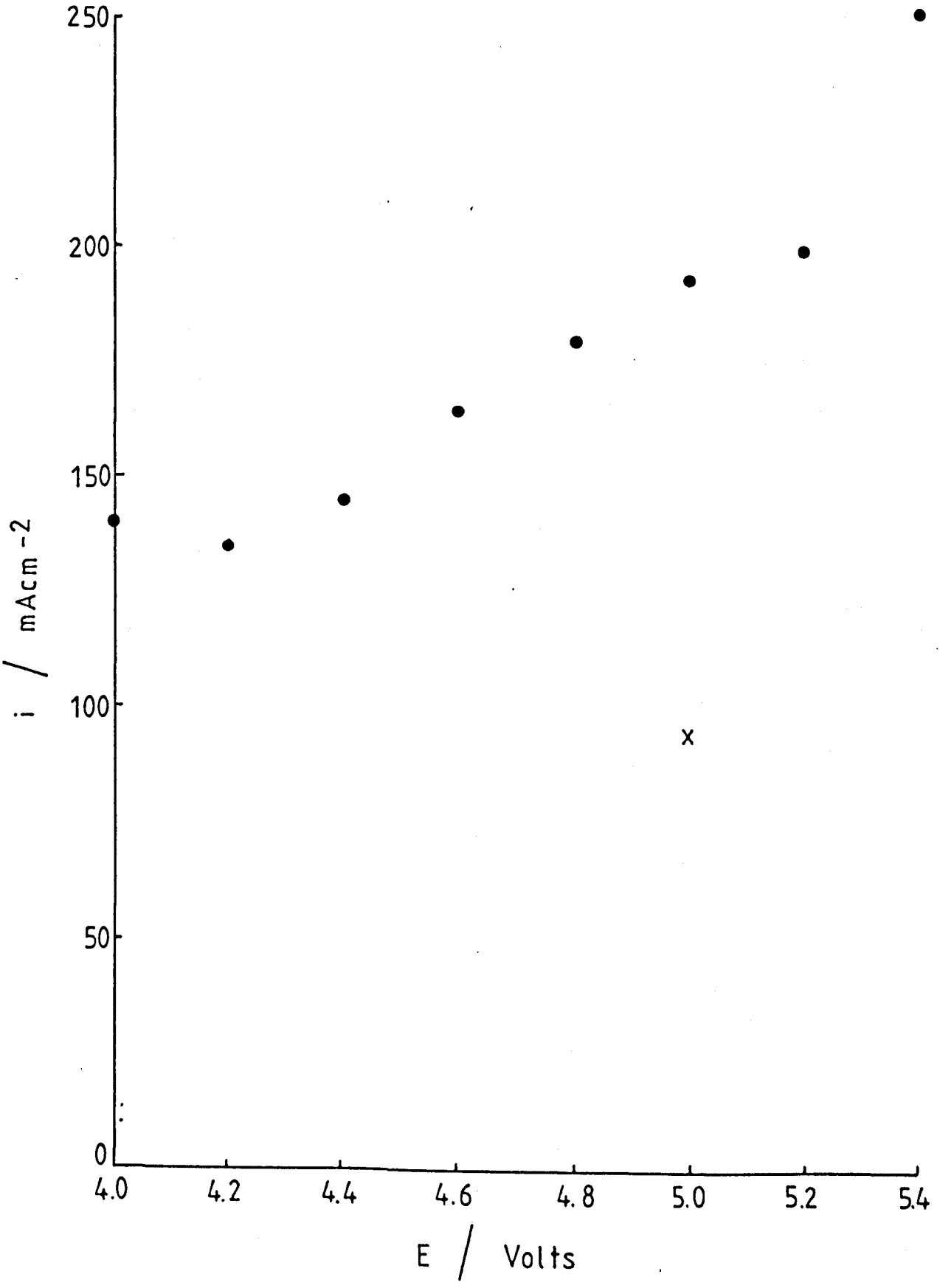
250
200
150
100
50
0
i / mAcm-2
4.0
4.2
4.4
4.6
4.8
5.0
5.2
5.4
E / Volts
x

Figure 8.23

Current vs. voltage response obtained during potential pulse measurements in KF.2HF. The current after 100ms of the pulse is plotted against the pulse potential. Electrode containing 0.1% Fe, (●) before, and (X) after evolution of fluorine at 6V for 30 minutes.

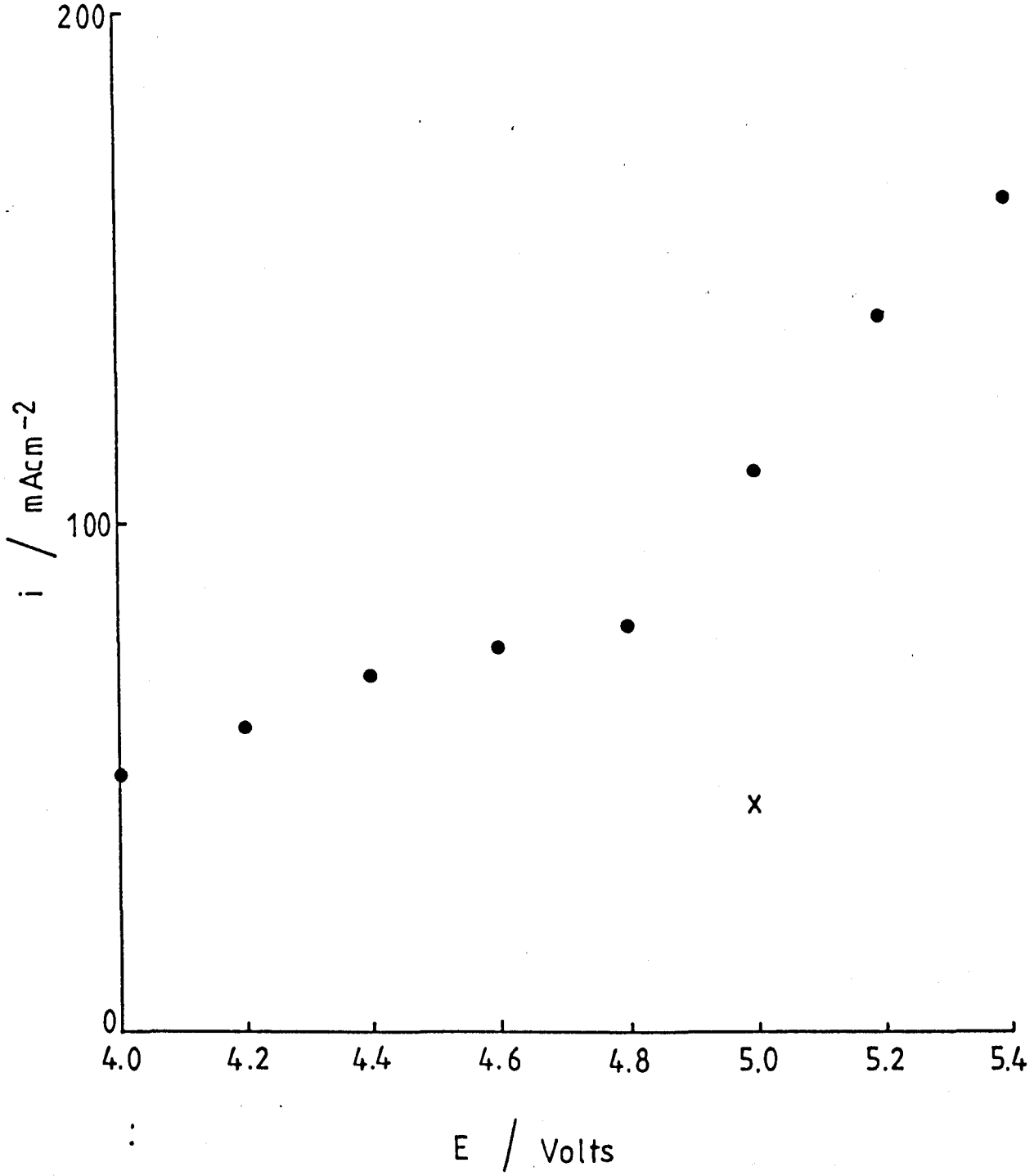
200
100
0
i / mAcm-2
4.0
4.2
4.4
4.6
4.8
5.0
5.2
5.4
E / Volts
x

Figure 8.24

Current vs. voltage response obtained during potential pulse measurements in KF.2HF. The current after 100ms of the pulse is plotted against the pulse potential. Electrode containing 0.1% Cr, (●) before, and (X) after evolution of fluorine at 6V for 30 minutes.

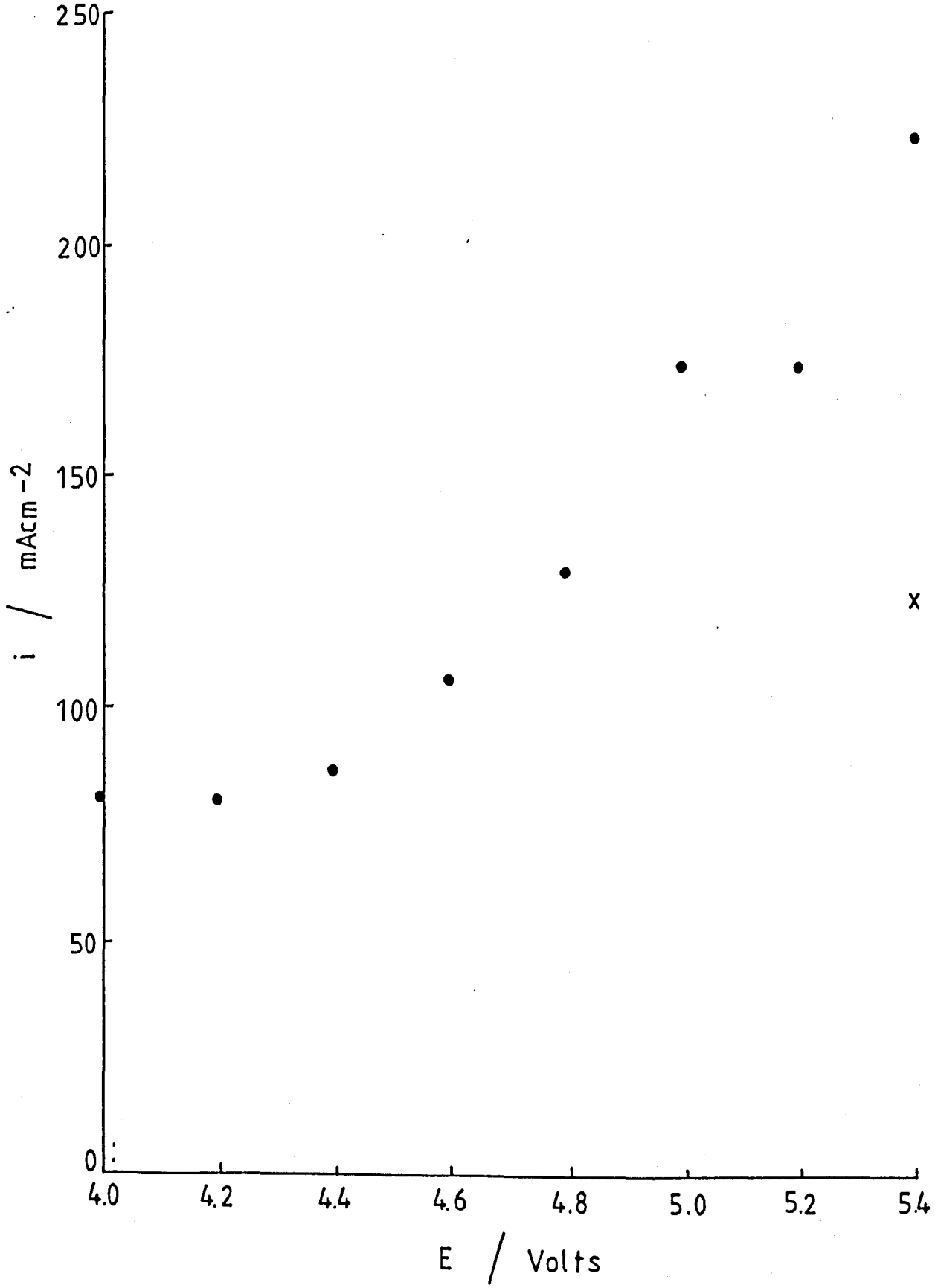
250
200
150
100
50
0
i / mAcm -2
4.0
4.2
4.4
4.6
4.8
5.0
5.2
5.4
E / Volts
x

Figure 8.25

Current vs. voltage response obtained during potential pulse measurements in KF.2HF. The current after 100ms of the pulse is plotted against the pulse potential. Electrode containing 0.1% Co, (●) before, and (X) after evolution of fluorine at 6V for 30 minutes.

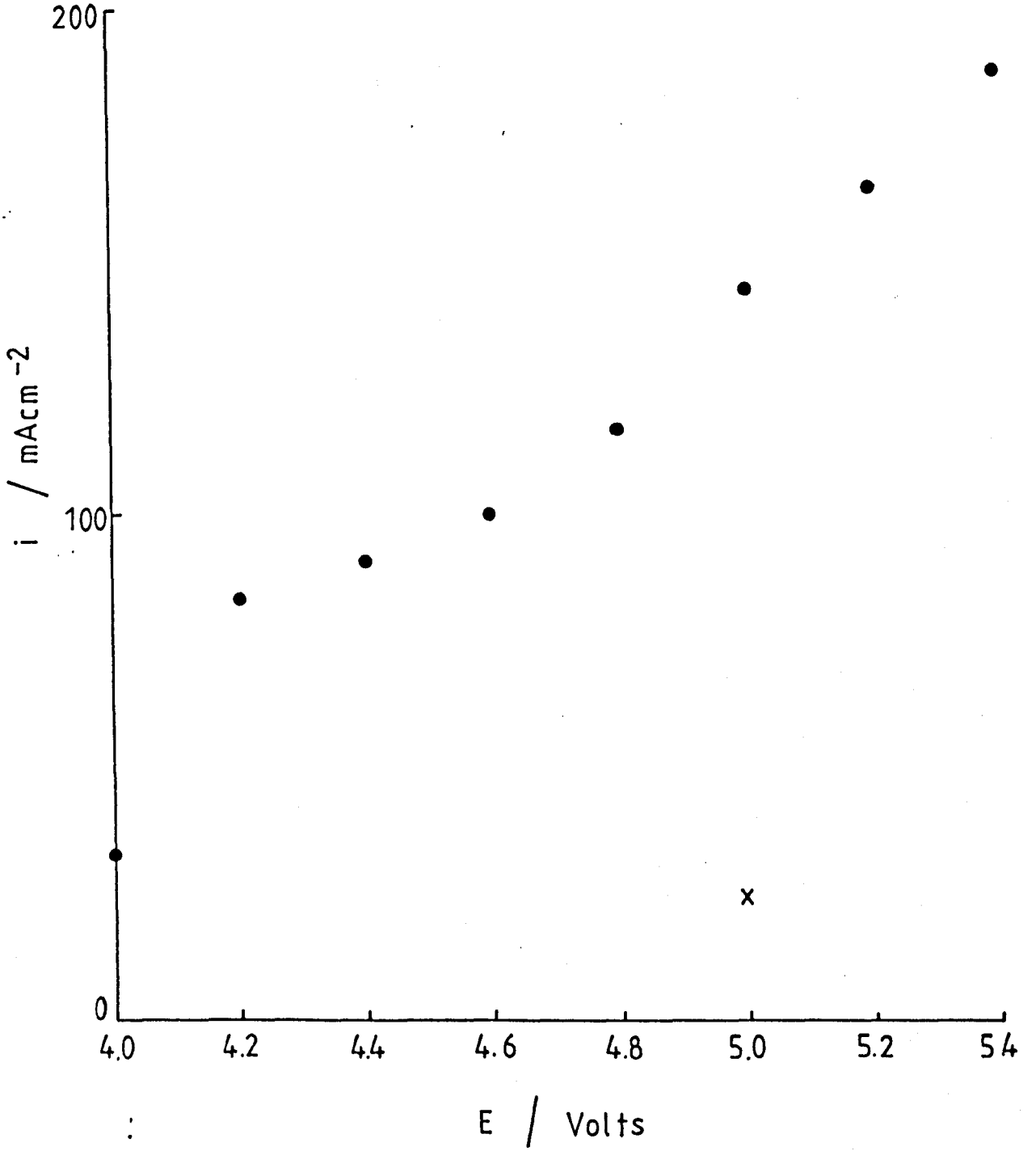
200
100
0
i / mAcm^{-2}
4.0
4.2
4.4
4.6
4.8
5.0
5.2
5.4
E / Volts

Figure 8.26

Current vs. voltage response obtained during potential pulse measurements in KF.2HF. The current after 100ms of the pulse is plotted against the pulse potential. Electrode containing 0.1% Cu, (●) before, and (X) after evolution of fluorine at 6V for 30 minutes.

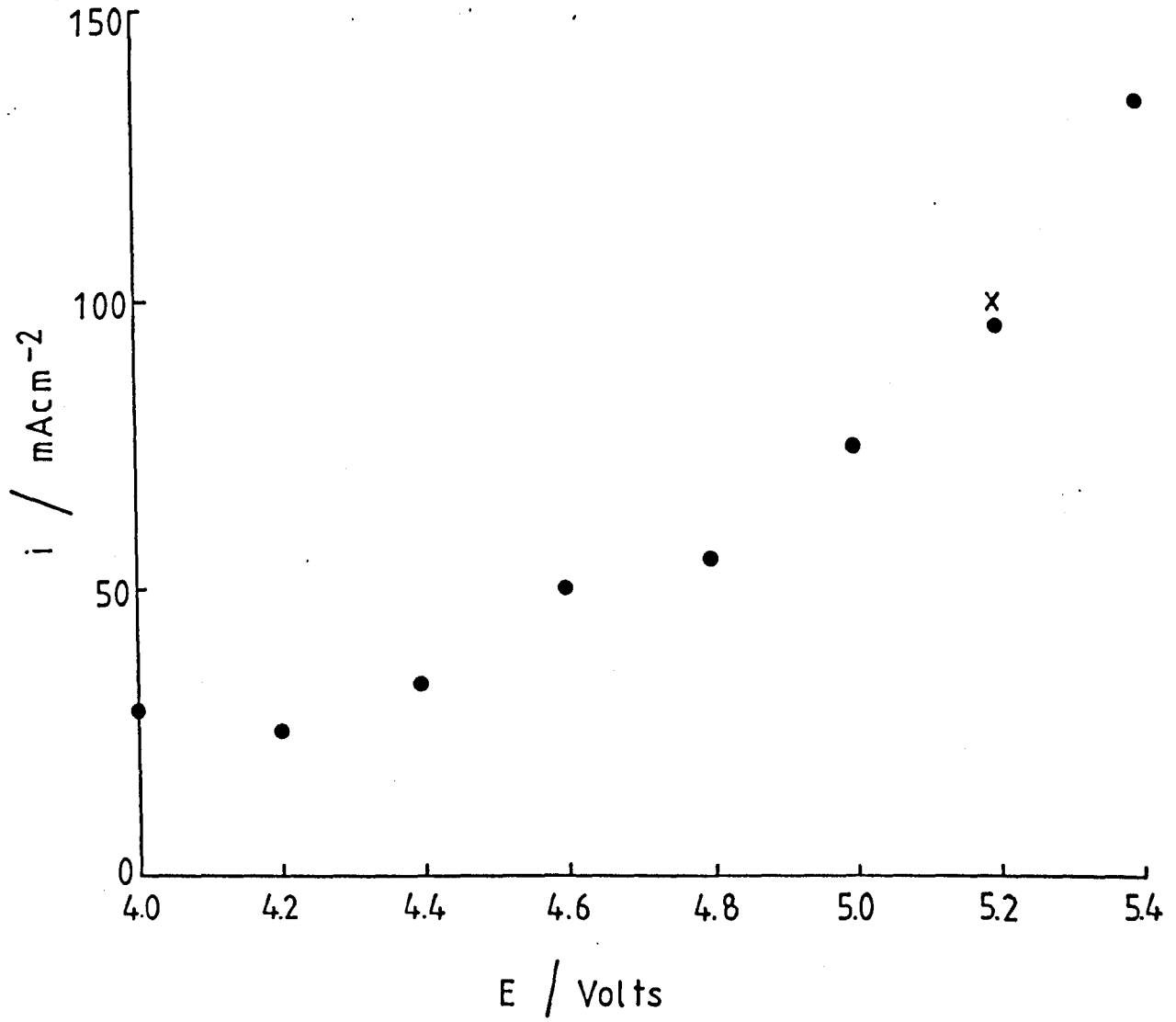
150
100
50
0
i / mAcm^{-2}
4.0
4.2
4.4
4.6
4.8
5.0
5.2
5.4
E / Volts

Figure 8.27

Current vs. voltage response obtained during potential pulse measurements in KF.2HF. The current after 100ms of the pulse is plotted against the pulse potential. Electrode containing 0.1% Ti, (●) before, and (X) after evolution of fluorine at 6V for 30 minutes.

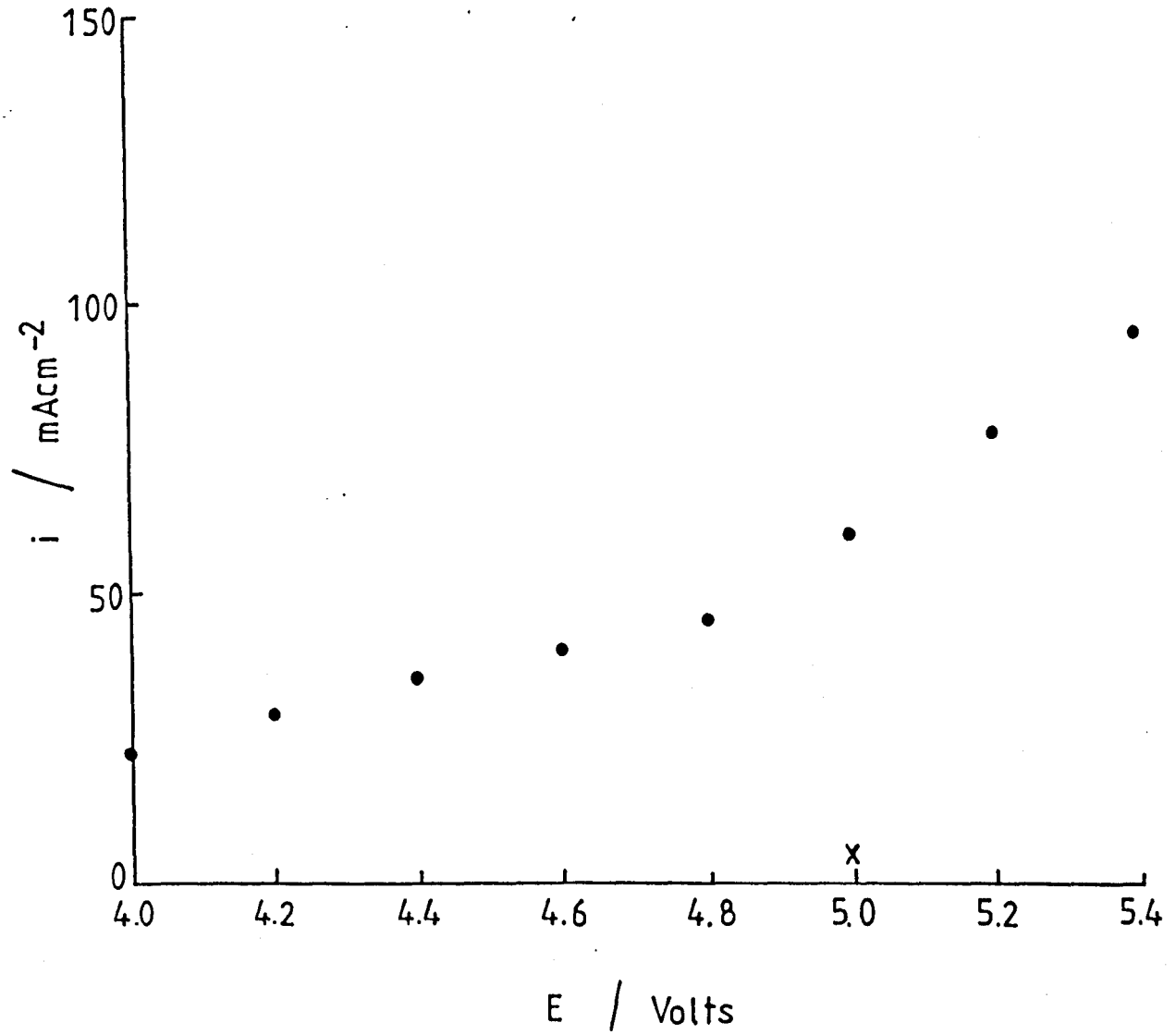
150
100
50
0
i / mAcm-2
4.0
4.2
4.4
4.6
4.8
5.0
5.2
5.4
X
E / Volts

Figure 8.28

Current vs. voltage response obtained during potential pulse measurements in KF.2HF. The current after 100ms of the pulse is plotted against the pulse potential. Electrode containing 0.1% Mo, (●) before, and (X) after evolution of fluorine at 6V for 30 minutes.

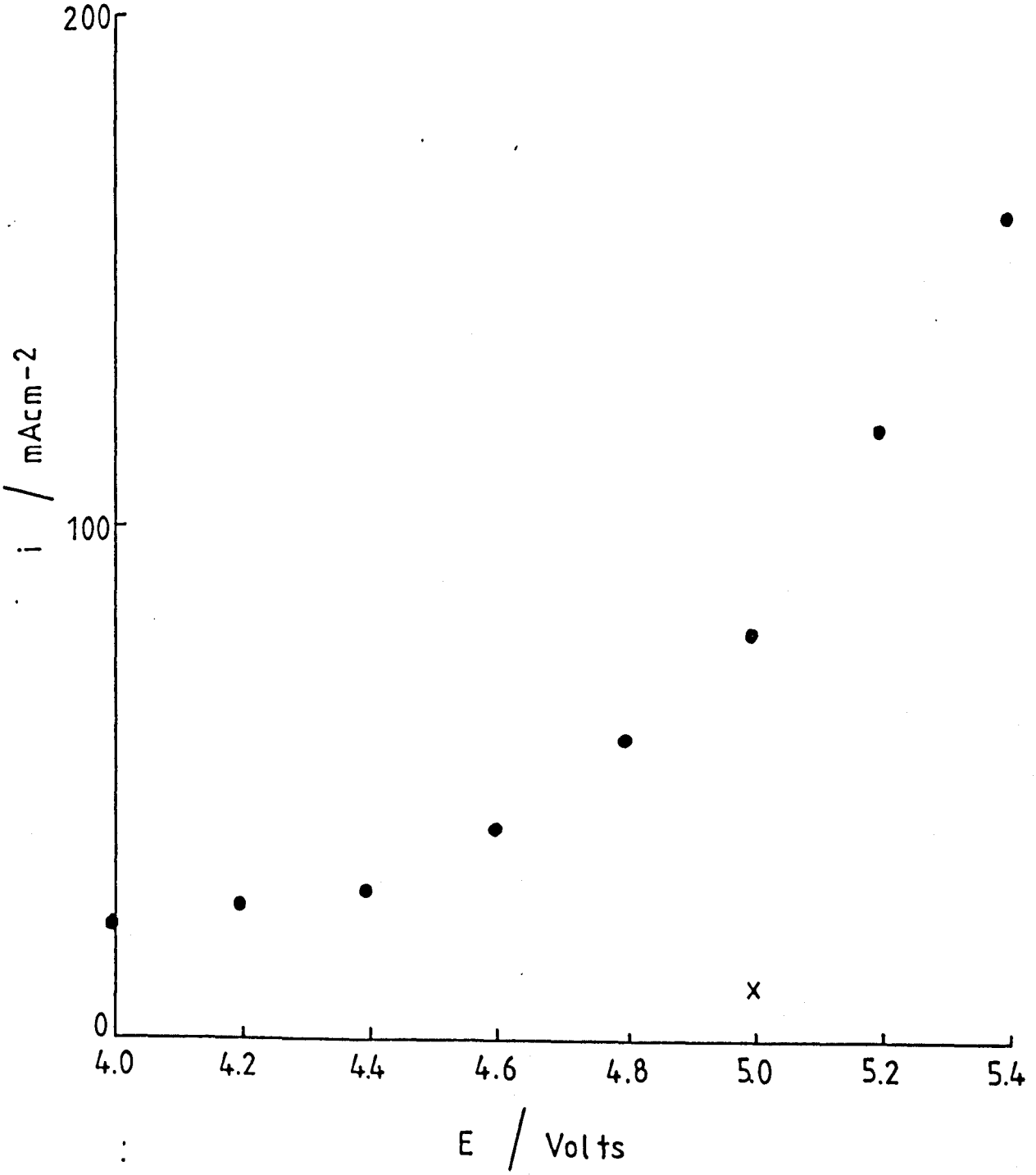
200
100
0
i / mAcm-2
4.0
4.2
4.4
4.6
4.8
5.0
5.2
5.4
E / Volts
x

Figure 8.29

Current vs. voltage response obtained during potential pulse measurements in KF.2HF. The current after 100ms of the pulse is plotted against the pulse potential. Electrode containing 0.1% Mn, (●) before, and (X) after evolution of fluorine at 6V for 30 minutes.

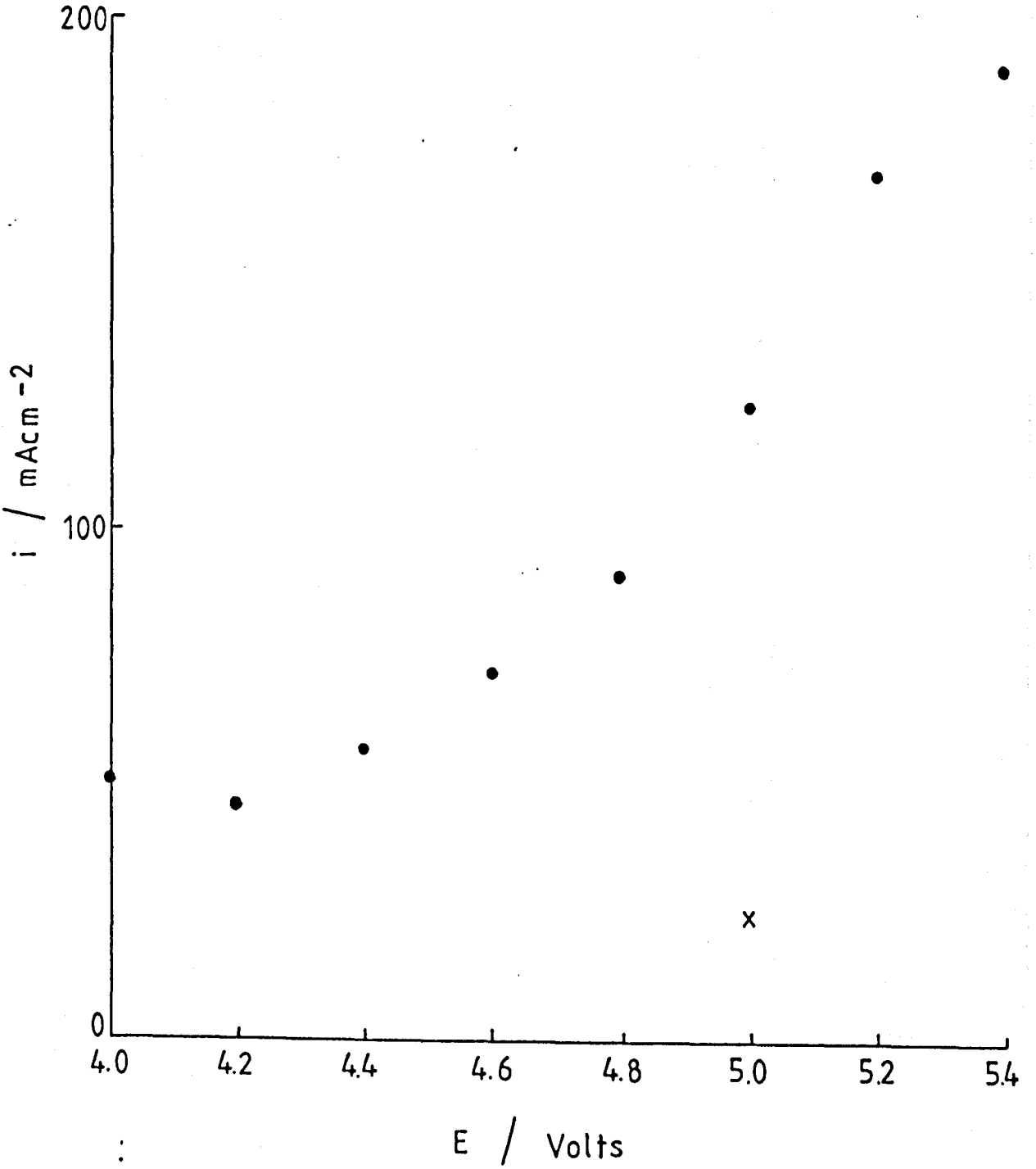
200
100
0
i / mAcm -2
4.0
4.2
4.4
4.6
4.8
5.0
5.2
5.4
E / Volts
x

Figure 8.30

Steady-state electrolysis at 6V in KF.2HF at an electrode containing 0.1% Ni. Current vs. time response.

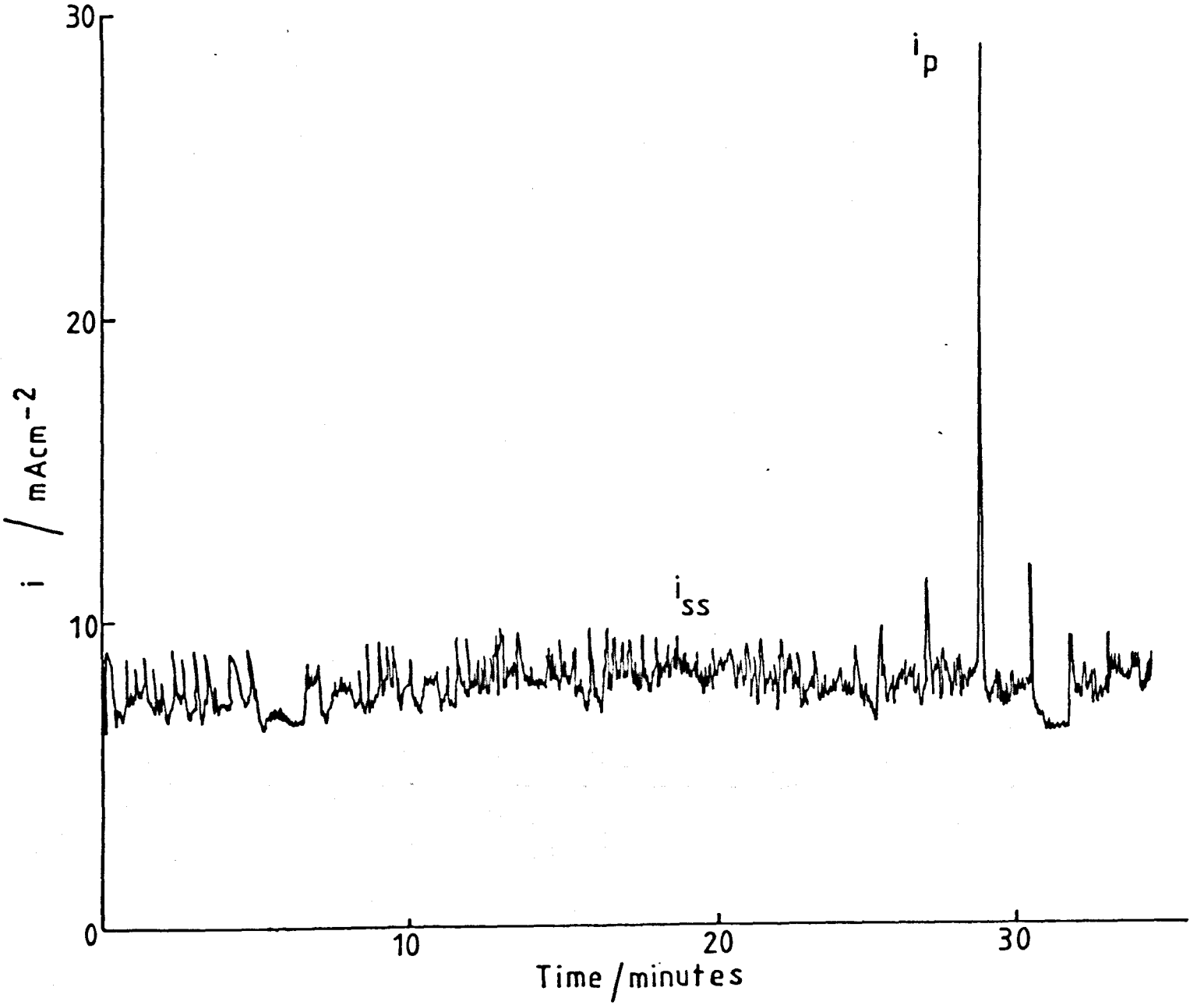

Figure 8.31

Steady-state electrolysis at 6V in KF.2HF at an electrode containing 0.1% V. Current vs. time response.

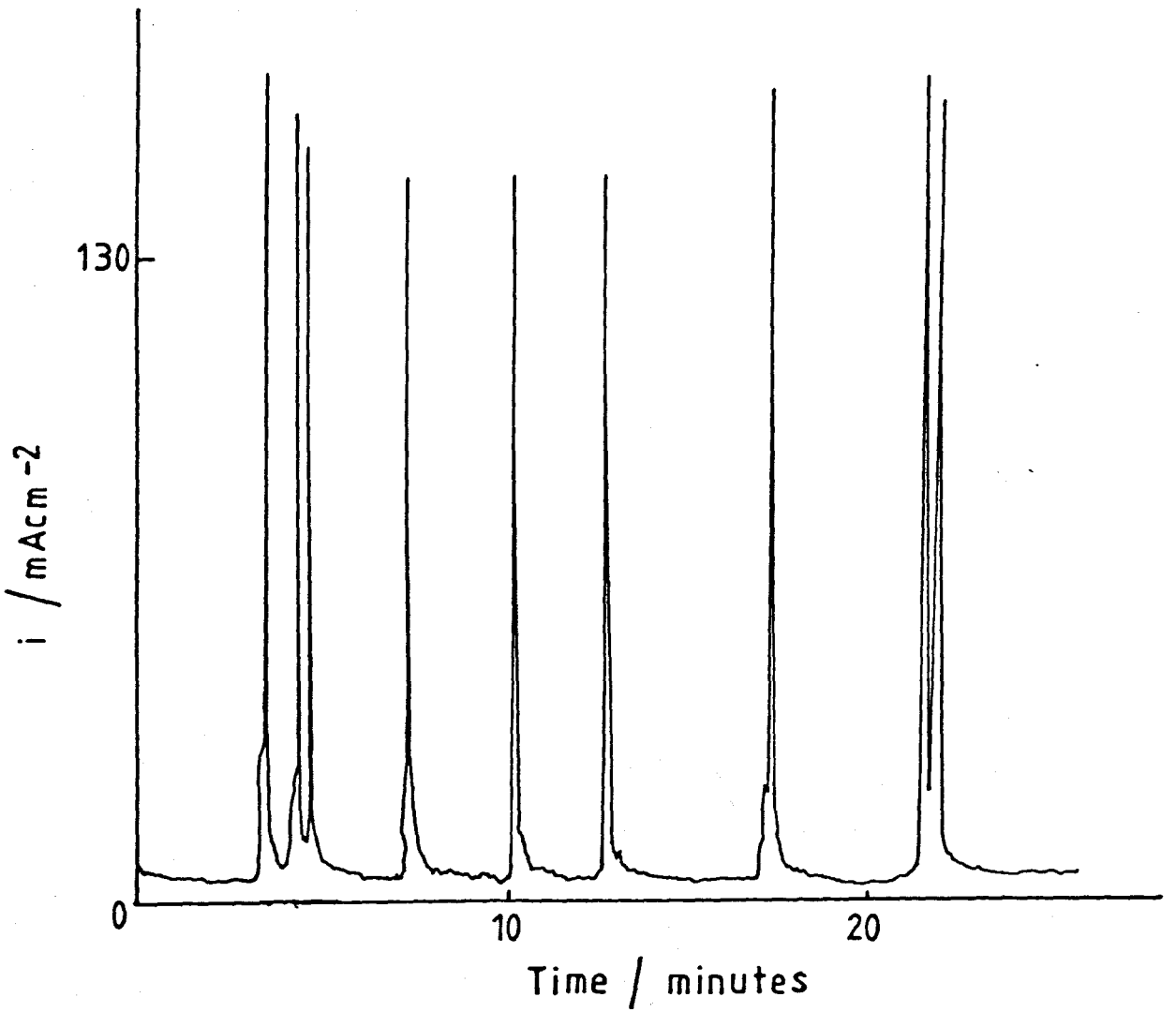

Figure 8.32

Steady-state electrolysis at 6V in KF.2HF at an electrode containing Ni and V. Current vs. time response.

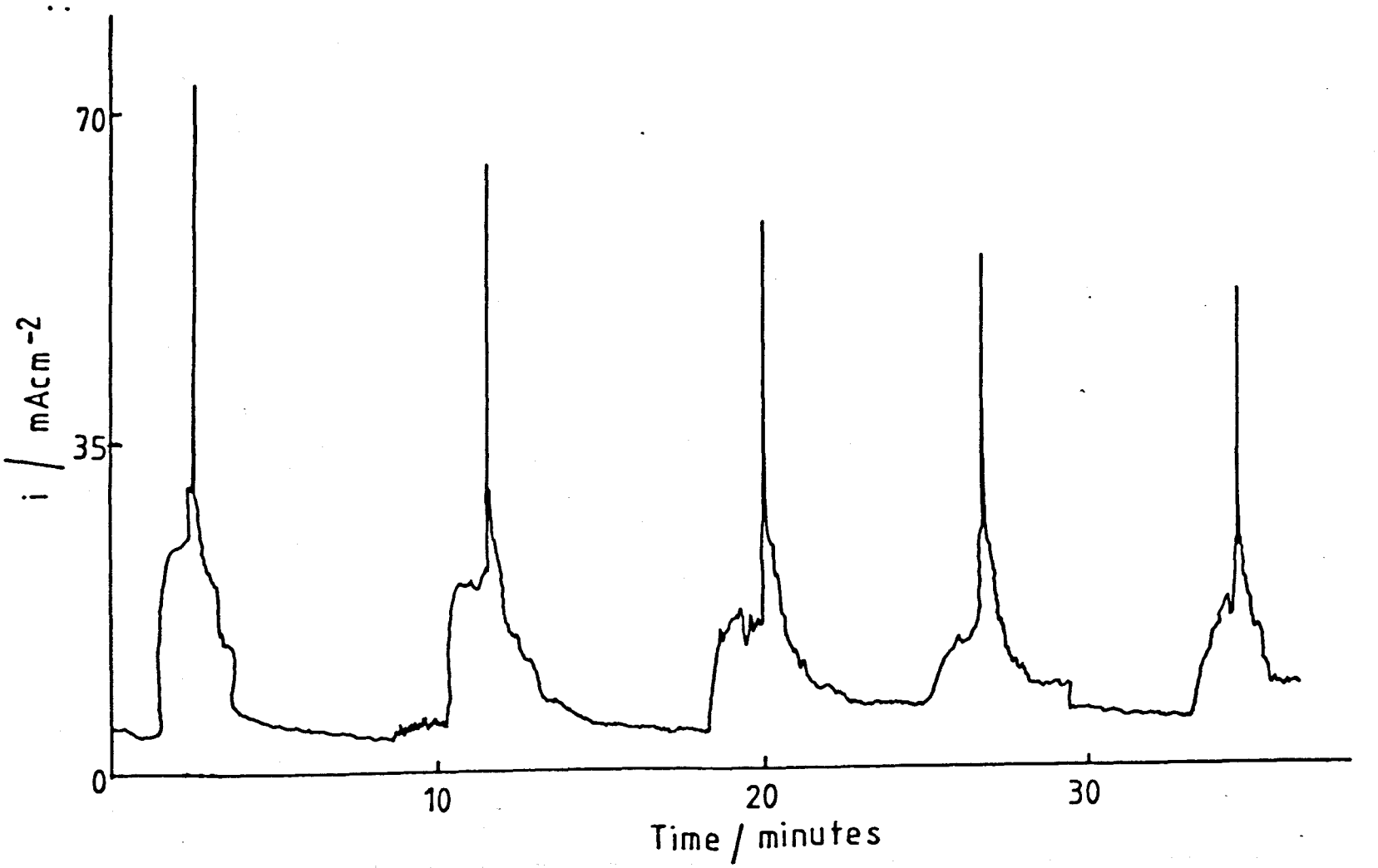

Figure 8.33

Steady-state electrolysis at 6V in KF.2HF at an undoped electrode current vs. time response.

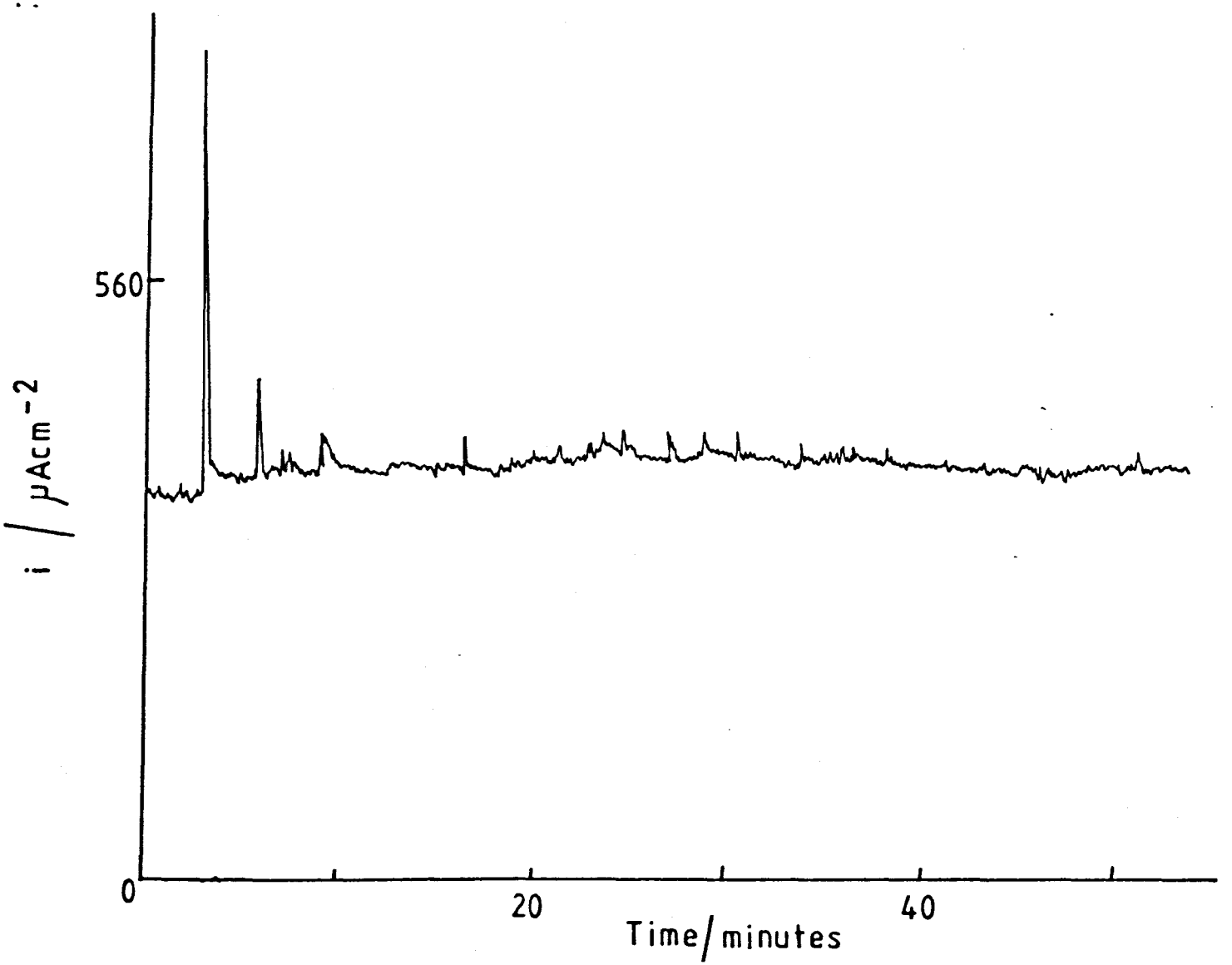

Figure 8.34

Impedance plot for the hexacyanoferrate (II/III) redox couple at an undoped electrode. E = +0.23V (vs.SCE). Electrode area = 0.28cm^2

Figure 8.35

Impedance plot for the hexacyanoferrate (II/III) redox couple at an electrode containing 0.1% Ni. E = +0.23V (vs.SCE). Electrode area = 0.28cm^2

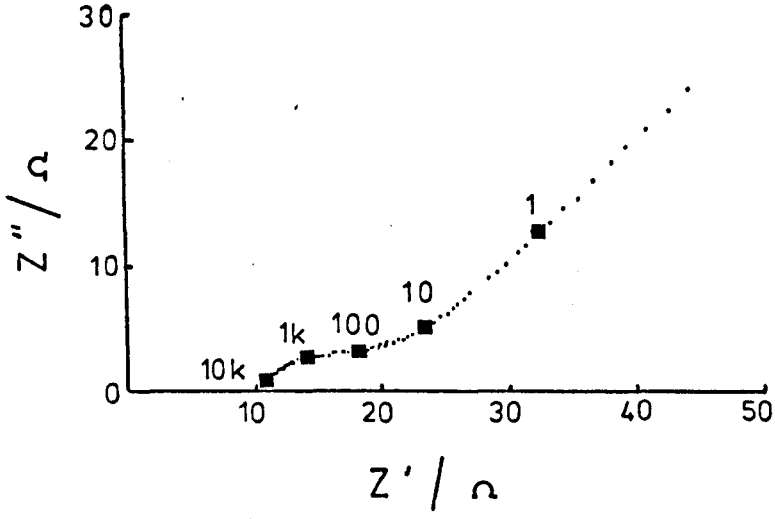
30
20
10
0
Z'' / Ω
10k
1k
100
10
1
10
20
30
40
50
Z' / Ω

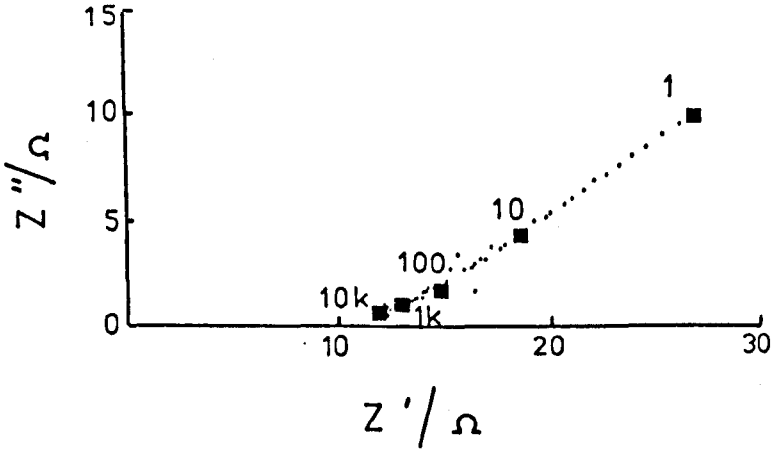
15
10
5
0
Z''/Ω
10k
1k
100
10
1
10
20
30
Z' / Ω

Figure 8.36

Impedance plot obtained in aqueous KCl at an electrode containing 0.1% Ni. E = 0.23V (vs. SCE). Electrode area = 0.28cm^2

Figure 8.37

Impedance plot obtained in aqueous KCl at a YBD porous electrode. E = 0.23V (vs. SCE). Geometric area = 0.5cm^2

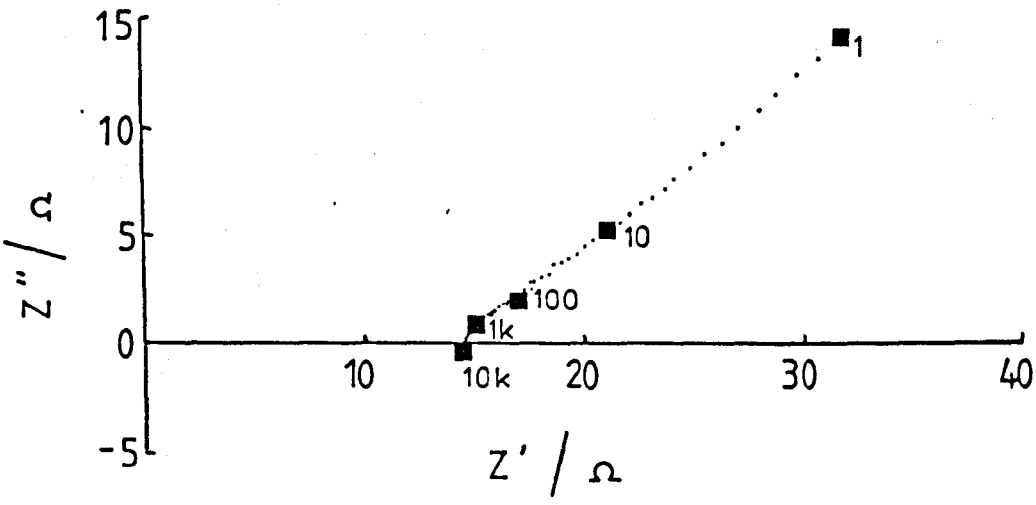
15
10
5
0
-5
Z'' / Ω
10
10k
20
30
40
Z' / Ω
1
10
100
1k

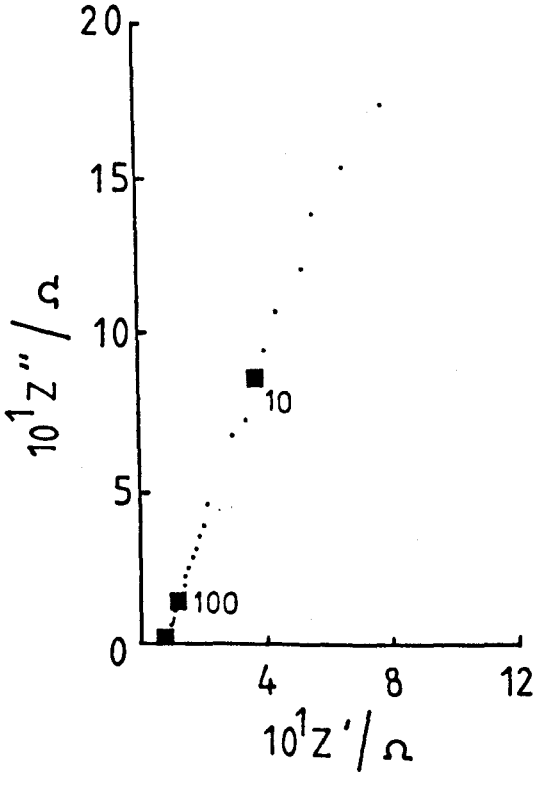
20
15
10
5
0
10¹Z'' / Ω
4
8
12
10¹Z' / Ω
10
100

Figure 8.38

a) Impedance plot obtained at an undoped electrode for the ferrocene/ferricinium redox couple in acetonitrile/$NaClO_4$. E = 0.33V (vs. SCE).

b) Impedance plot obtained at an undoped electrode for the ferrocene/ferricinium redox couple in acetonitrile/$NaClO_4$ after treatment of the electrode at 6V in KF.2HF for 30 minutes. E = 0.33V (vs. SCE). Electrode area = $0.28cm^2$

a

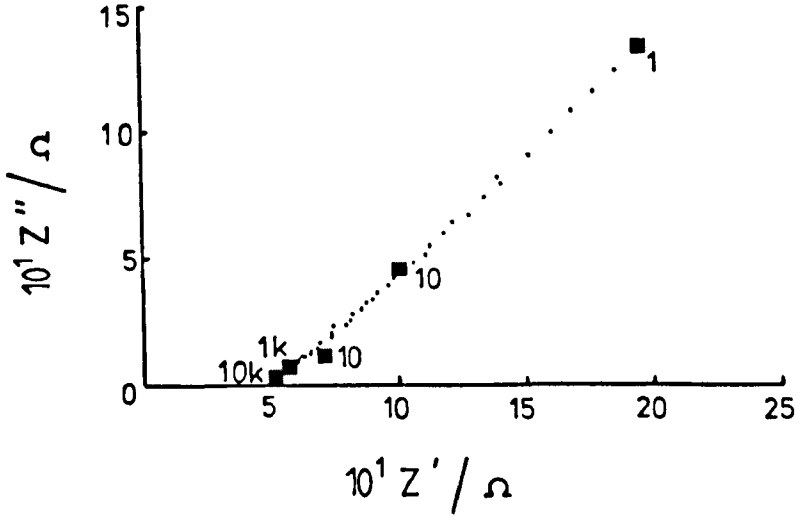

b

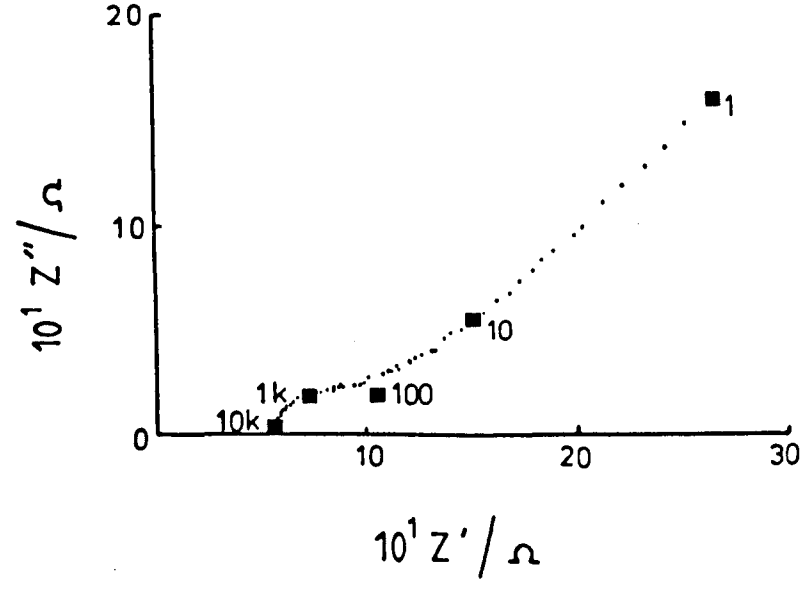

Figure 8.39

Impedance plot obtained at an electrode containing 0.1% Ni in acetonitrile/$NaClO_4$, E = 0.33V (vs. SCE).

a) Fresh electrode no redox couple present.

b) Fresh electrode, electrolyte contains 1 x 10^{-3}M ferrocene.

c) Electrolyte contains 1 x 10^{-3}M ferrocene. Electrode treated at 6V in KF.2HF for 30 minutes. Numbers refer to frequencies in Hz.

Electrode area = $0.28cm^2$

a

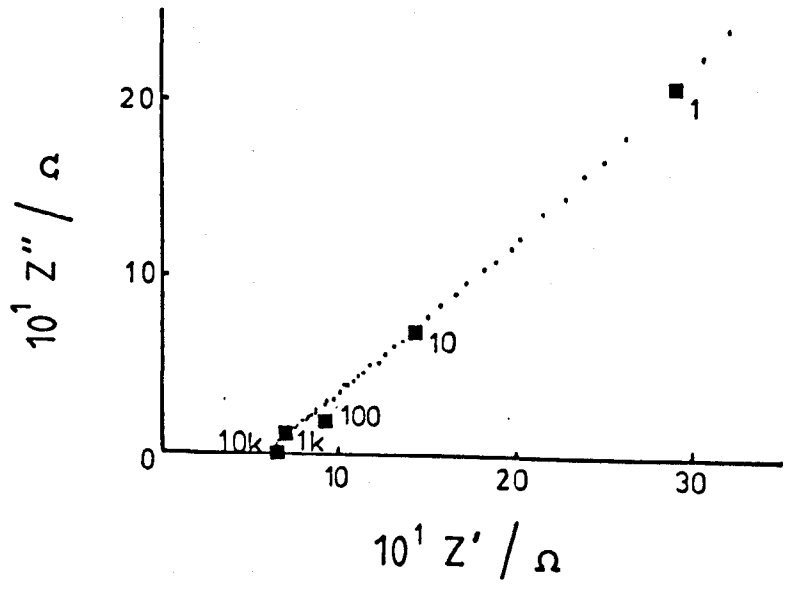
20
10
0
1
10
100
1k
10k
10
20
30
10^1 Z'' / Ω
10^1 Z' / Ω

b

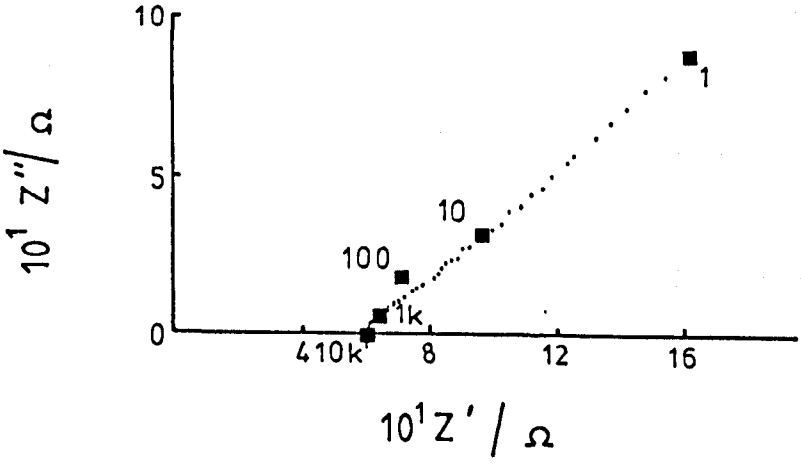
10
5
0
1
10
100
1k
4 10k
8
12
16
10^1 Z'' / Ω
10^1 Z' / Ω

c

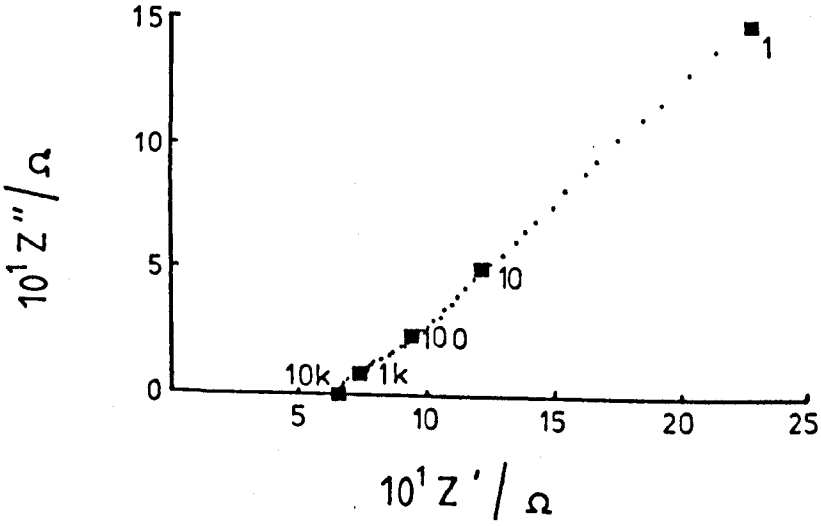
15
10
5
0
1
10
100
1k
10k
5
10
15
20
25
10^1 Z'' / Ω
10^1 Z' / Ω

8.11. REFERENCES

1. W.C. Schumb, R.C. Young and K.J. Radimer, Ind.Eng.Chem. 39, 244, 1947.
2. W.C. Schumb in "Preparation, Properties and Technology of Fluorine and Organic Fluoro-Compounds" C. Slesser and S.R. Schram (Eds) Mcgraw Hill, London, 1st Edn. 1951.
3. R.C. Downing Ibid.
4. J. T. Pinkston Jnr., Ind.Eng.Chem. 39, 255, 1947.
5. N. Watanabe, M. Ishii and S. Yoshizawa, J.Electrochem.Soc.Jpn. 29, E177, 1961.
6. A.J. Rudge, Chem.Ind. (London) 482, 1966.
7. N. Watanabe, M. Aramaki and Y. Kita, UK Pat.Appl. 2054650A, 1981.
8. Japanese Patent 8367877 (1983) (to Asahi Glass Co. Ltd.)
9. D.W. Taylor, Ph.D. Thesis, University of Newcastle upon Tyne, 1978.

CHAPTER 9

CONCLUSIONS AND FURTHER WORK

9.1 CONCLUSIONS

This work has shown that a fluoride film is produced on the carbon anode surface at electrode potentials much below those required for fluorine evolution. This film is stable on vitreous carbon against reduction in the KF.2HF melt above 0V. When fluorine is evolved on a carbon anode several types of CF_x compound (where x varies from 0.4 to 1.1) are produced at different potentials. Films produced above 5V include a layer which acts as a series resistance in the electrode surface and they also have an insulating layer which inhibits electron transfer reactions. At even more positive potentials the degree of fluorination, i.e. the amount of CF_x where x=1.1 is believed to increase. The film is non-homogeneous and consists of an inner conducting lower fluoride with an outer insulating layer of CF_x where x=1.1, but no abrupt boundary exists between these layers. The fluoride film inhibits model electron transfer processes in aqueous and organic systems by a factor of at least 10^2 and it is likely that this factor is a measure of the minimum inhibition factor presented by the film toward fluorine evolution. The fluoride film increases bubble overvoltage because of its non wetting properties. At a vitreous carbon electrode at potentials above 5V, 95% of the anode surface is estimated to be covered by fluorine gas bubbles during fluorine evolution. Thus the film contributes indirectly to the anode overvoltage as well as directly. The actual contribution made to the anode overvoltage by the resistive part of the fluoride film

at the commercial operating current density was calculated to be 2.0V. Bubble overvoltage is estimated to contribute about 1.0V to the cell voltage depending on the nature of the anode material, more porous anodes resulting in lower bubble overvoltages.

The presence of the fluoride film on the carbon anode limits further oxidation of the carbon anode, to a rate set by thermal decomposition of the layer. However, in order to minimise operating cell voltages and hence increase the power efficiency of a fluorine cell it is necessary to modify the properties of this fluoride film. Modification can be approached in two ways :

(i) Alter the non-wetting properties of the film and hence facilitate bubble removal

(II) Enhance the electron transfer properties of the film and hence decrease the overvoltage required for electron transfer from the HF_2^- ion to the electrode.

Addition of certain transition metal ions to the carbon anode appears to improve their properties towards fluorine evolution. However, it is not known if dopants enhance electron transfer, facilitate bubble release or catalyse film decomposition. Certain transition metals notably Ni, V, Co and Ni/V, are more active towards fluorine evolution than others.

9.2 FURTHER WORK

The nature of the film formed at low potentials before fluorine evolution is not fully known. An XPS/SIMS study of the film would indicate the

stoichiometry of the film formed at this potential. Indeed a more detailed study of fluoride film formation should be carried out using XPS/SIMS analysis. This work examined electrodes fluorinated at 5V and 9V (vs Pd/H_2). A systematic study of the films formed at various potentials using commercial carbon electrodes would be informative so that the potential at which the more resistive film is produced could be identified. The stoichiometry of the CF_x compounds could also be determined by comparison with standard CF_x compounds. A similar study of the films formed at doped electrodes might lead to a better understanding of the mechanism of fluorine evolution at doped electrodes and might indicate if there is any difference in the degree of fluorination at doped electrodes in comparison with undoped materials.

Analysis of the gas evolved at the anode using doped electrodes could be performed using either infrared spectroscopy or gas chromatography or mass spectrometry. Monitoring the amount of such species as CF_4 and C_2F_6 would indicate if the role of the transition metal dopants is one of enhancement of thermal decomposition of the fluoride film. Increased amounts of such gases in the anode off-gas would indicate that thermal decomposition of the film was increased.

The home-made electrodes used in this study were non-porous materials and, as a result, suffer from polarisation. The effect of transition metal doping should really be investigated using a more porous anode material. This could be done on the small laboratory

scale by the doping of "Novolak" resin. (It was noted that this produced a porous carbon material). However, it would be best done by fluorine manufacturers themselves, perhaps in conjunction with a carbon manufacturer, rather than by a university.

A more detailed non-electrochemical characterisation of the home-made materials should be performed. Particular emphasis should be placed on the effect of doping on the degree of graphitisation of the carbon samples and on the rate of erosion of the carbon anode. Dopants could cause an increase in the rate of film decomposition and therefore the rate of weight loss. The amount of dopant in the final carbon product should also be determined.

In order to obtain fundamental kinetic parameters for fluorine evolution the fluorine gas film has to be removed from the electrode surface. Use of a suitable rotating electrode in conjunction with conventional impedance measurements would enable kinetic data to be obtained at higher potentials in the absence of a gas film. Such an electrode would also enable the thickness of the fluoride film to be measured in situ directly at potentials of 5, 6, 7V etc. in the absence of the fluorine gas film rather than indirectly at 0.7V as in this work.

Finally it is worth emphasising that the addition of transition metals to the carbon working electrode does appear to have a beneficial effect on fluorine cell voltages. Further study of such electrodes will perhaps lead to the development of a new carbon anode for

fluorine evolution which has a lower operating voltage than those currently used and hence the power efficiency will be improved for the fluorine cell.